Universidade do Porto

Faculdade de Engenharia

FEUP

ADVANCES IN SIMULATED MOVING BED:

NEW OPERATING MODES; NEW DESIGN METHODOLOGIES; AND PRODUCT (FLEXSMB-LSRE®) DEVELOPMENT.

A dissertation presented to the Faculdade de Engenharia da Universidade do Porto for the degree of Doctor in Chemical and Biological Engineering

by

Pedro Sá Gomes

Supervised by Professor Alírio Egídio Rodrigues

and co-supervised by Dr. Mirjana Minceva

Laboratory of Separation and Reaction Engineering, Associate Laboratory LSRE/LCM

Department of Chemical Engineering, Faculty of Engineering, University of Porto, Portugal

September 2009

Pedro Sá Gomes, 2005-2009
Laboratory of Separation and Reaction Engineering, Associate Laboratory LSRE/LCM
Department of Chemical Engineering, Faculty of Engineering, University of Porto
Rua Dr. Roberto Frias
4200-465 Porto
Portugal

Printed by Cromotema, Vilar do Paraíso - V. N. Gaia - Portugal

ACKNOWLEDGEMENTS

First of all, I would like to acknowledge Professor Alírio E. Rodrigues (Universidade do Porto, Portugal) in the condition of director of the Laboratory of Separation and Reaction Engineering (associated lab LSRE/LCM) at the Faculty of Engineering of the University of Porto, and particularly in the condition of my supervisor: Obrigado Professor, por todo apoio e compreensão.

I would also like to thank all the support from Dr. Mirjana Minceva (Universität Erlangen Nürnberg, Germany) my co-supervisor.

I am grateful to the Fundação para a Ciência e Tecnologia from the Ministry of Science and Technology and Higher Education of Portugal for sponsoring my PhD grant (SFRH/BD/22103/2005) and for the financial aid to the research project POCI/EQU/59296/2004.

I would like to thank all my colleagues at LSRE who supported me over these years, especially Michal Zabka, Miriam Zabkova, Nabil Lamia and Eduardo Borges da Silva, thank you all for all those long and productive discussions.

I cannot finish without saying how grateful I am to my family: my parents and my sister. Obrigado, por esse sempre presente alento e inquestionável apoio.

Finally, to Viviana… thank you for all your support, comprehension and affection.

“It would be a great mistake to think of the content of chemical engineering science as permanently fixed. It is likely to alter greatly over the years, in response to the changing requirements of industry and to new scientific discoveries and ideas for their application.”

P.V. Danckwerts

Ao meu avô e padrinho.

Resumo

A tecnologia de Leito Móvel Simulado (LMS) trata-se de um processo que resolveu vários dos problemas associados ao movimento de fase sólida (abrasão entre partículas e com a parede, redistribuição do tamanho de partículas, aumento das quedas de pressão), usuais em métodos de separação cromatográficos de contra corrente, Leito Móvel Verdadeiro. O LMS tem origem nos anos 60 do século passado, tendo como a sua primeira aplicação industrial relevante os processos Sorbex da *Universal Oil Products*. Desde a sua introdução, a tecnologia de LMS foi aplicada com sucesso, primeiro a grandes separações petroquímicas, tais como a separação de *p*-xileno dos seus isómeros C_8, *n*-parafinas de hidrocarbonetos ramificados e cíclicos, na indústria de transformação de açúcares, e mais tarde, na indústria farmacêutica e de química fina. Nas últimas décadas, o advento da tecnologia de LMS tem proporcionado soluções de alto rendimento, eficiente consumo de solvente, seguras e rentáveis. Desde então, um número considerável de artigos, patentes e livros sobre a aplicação do LMS para a separação de compostos relevantes têm sido publicados. Fruto deste interesse, o estudo e investigação da tecnologia de LMS levou à formulação de diferentes modos de operação, as técnicas não-convencionais. Por exemplo, a introdução do movimento de portas assíncrono e a variação de caudais de entrada ou saída, aumentou ainda mais a gama de aplicação do LMS, bem como o seu desempenho. No entanto, e suportado pela forte procura de técnicas eficientes de separação em contínuo, é simples de compreender que o espaço para inovar é ainda considerável. Vários são os aspectos do funcionamento das unidades de LMS que ainda não foram resolvidos. Esta tese, em particular, aborda quatro grandes questões:

(i) Estudo e desenvolvimento de novos modos de operação não-convencionais; Um novo modo de operação é apresentado, o Outlet Streams Swing (OSS). Esta nova técnica, caracterizada por uma colecta periódica de produto (realizada através do fecho das portas de extracto ou refinado durante uma determinada parte do período de comutação de portas, mantendo as secções II e III com caudais constantes, compensados pelo o caudal de eluente), melhora as purezas dos produto finais, ou permite uma maior produtividade (ou menor consumo de eluente), quando comparado com o modo clássico de funcionamento.

(ii) Estudo de unidades de LMS em conta com desactivação do adsorvente; Problemas geralmente associados com a desactivação do adsorvente durante a operação de unidades de LMS foram contabilizados como uma extensão dos modelos matemáticos usuais, resultando em métodos de diagnóstico para mecanismos de envelhecimento, bem como estratégias para a sua compensação.

(iii) Desenvolvimento de um processo industrial de LMS operando em fase gasosa; A concepção de um novo processo industrial para a separação de propano/propileno em fase gasosa por meio de tecnologia de LMS, abordando factores, tais como a geometria de coluna e queda de pressão, é apresentado do zero, proporcionando uma nova aplicação de LMS com um elevado grau de pureza de propileno (> 99.5%), alta recuperação (> 99.0%) e uma produtividade bastante promissora, acima de 1000 kg de propileno por ($m^3_{adsorbente}$h).

(iv) Concepção, construção e operação de uma unidade flexível de LMS; A concepção, construção e operação de uma nova unidade laboratorial de LMS, o FlexSMB-LSRE®, é apresentada. Uma medida de compensação de volumes estagnados é proposta e aplicada na separação de uma mistura racémica de tetralol, bem como uma mistura racémica de guafeinesin, esta última realizada em três diferentes modos de operação: LMS clássico, assíncrona e OSS, mostrando assim a flexibilidade da unidade FlexSMB-LSRE®.

Abstract

The Simulated Moving Bed (SMB) technology is an original mode of operation that solved several problems associated with solid phase motion (particle attrition and wall abrasion, particle size redistribution, increase in pressure drop), usually noted when operating under continuous counter current adsorptive separation processes, the so-called True Moving Bed. The origins of SMB can be tracked back to early 1960s, and its first relevant industrial implementation to the Sorbex processes by Universal Oil Products. Since its introduction, the SMB technology has been successfully applied, firstly to various large petrochemical separations, such as the *p*-xylene separation from its C_8 isomers, *n*-paraffins from branched and cyclic hydrocarbons, sugar processing industry and later, in the pharmaceutical and fine chemical industries. In the past decades, particularly in the area of drug development, the advent of SMB has provided a high throughput, high yield, solvent efficient, safe and cost effective process option. Since then, a considerable number of articles, patents and books on the application of SMB to pharmaceutically important compounds have been published. As consequence of this emergent interest, the study and research on SMB technology led to the formulation of quite singular/different operation modes, the non-conventional SMB techniques. For instance, the introduction of asynchronous port movement and variable inlet or outlet flow rates, were proposed, extending further SMB range of application as well as its performance. Nevertheless, and supported by the strong demand on continuous efficient separation techniques, it is simple to understand that the space to innovate is still considerable. Several are the aspects in the operation of SMB units that were not addressed yet. This thesis, in particular, focus on four major issues:

(i) Study and development of new non-conventional operating modes; A new non-conventional SMB mode of operation was introduced, the Outlet Streams Swing (OSS). This new technique, characterized by a periodical product withdrawal (performed by closing extract or raffinate ports for a given part of the switching time period, keeping sections II and III with constant flow rates by compensating it with the eluent/desorbent flow rate), improves the SMB outlet purities or allow productivity/desorbent increase/reduction, when compared with the classic operating mode.

(ii) Development of design procedures that accounts for SMB units' adsorbent ageing problems; Recurrent problems, usually associated with adsorbent deactivation during the operation of SMB units, were accounted as an extension of the commonly used mathematical models and resulted in some diagnostic methods for the ageing mechanisms as well as short cut strategies for its compensation.

(iii) Development of a design procedure for an industrial gas phase SMB unit; A design procedure for a novel gas phase SMB unit for the industrial propane/propylene separation, addressing factors such as the columns geometry, performance parameters, pressure drop limitations is presented from the scratch, providing high purity propylene (>99.5 %), at high recovery (>99.0 %) and quite promising productivity values, above 1000 kg of propylene per ($m^3_{adsorbent}h$).

(iv) Design, construction and operation of a flexible SMB unit; The design, construction and operation of a new lab-scale flexible SMB unit, the FlexSMB-LSRE®, is addressed. A dead volumes compensation measure is proposed and applied to separate a racemic mixture of tetralol as well as a racemic mixture of guafeinesin, this last performed in three different operating modes: classic SMB, asynchronous SMB and OSS, proving the flexibility of the FlexSMB-LSRE® unit.

Résumé

La technologie du Lit Mobile Simulé (LMS) est un concept original qui permet de résoudre un grand nombre des problèmes induits par le mouvement de la phase solide (abrasion entre les particules et avec les parois de la colonne, redistribution de la taille des particules, augmentation des pertes de charge), habituellement rencontrés avec les méthodes de séparation chromatographique à contre courant, tel que le Lit Mobile Vrai. Le LMS trouve ses origines dans les années 60 du siècle passé, ayant comme première application industrielle significative les procédés Sorbex® de *Universal Oil Products*. La technologie du LMS fut appliquée avec succès, notamment pour les grandes séparations pétrochimiques, dans l'industrie de la transformation du sucre, et plus tard, dans l'industrie pharmaceutique et la chimie fine. Au cours des dernières décennies, l'arrivée du LMS a permis d'obtenir de hauts rendements, une consommation efficace du solvant, et des garanties en termes de sécurité et de coûts. Dès lors, un nombre considérable d'articles, de brevets et de livres sur l'application du LMS pour la séparation de composés importants ont été publiés. Conséquence de cet intérêt croissant, l'étude et la recherche de la technologie LMS se sont portées sur la formulation de différents modes opératoires, généralement désignés comme techniques non conventionnelles. Cependant et compte tenu de la forte demande en techniques efficace de séparation en continue, il paraît évident que l'espace pour innover reste encore considérable. Nombreux sont les aspects de fonctionnement des unités LMS qui n'ont pas encore été résolus. Cette thèse aborde en particulier quatre grands aspects :

(i) Etude et développement de nouveaux modes d'opération non conventionnels; Un nouveau mode d'opération est présenté, le *Outlet Streams Swing* (OSS). Cette nouvelle technique, caractérisée par un soutirage périodique des produits (réalisé en fermant les ports d'extrait ou de raffinat au cours d'un laps de temps de la période de commutation des ports, en maintenant les sections II et III avec des débits constants, en compensant avec le débit de l'éluant/désorbant) améliore ostensiblement les puretés des produits finaux, ou permet une plus grande productivité (ou une plus faible consommation de l'éluant), comparé au mode classique de fonctionnement.

(ii) Développement des procédures de design en tenant compte de la désactivation de l'adsorbant; Les problèmes généralement associés à la désactivation de l'adsorbant durant l'opération des unités LMS ont été pris en compte à travers une extension des modèles mathématiques usuels, résultant des méthodes de diagnostique des mécanismes de vieillissement aussi bien que des procédés de compensation.

(iii) Développement d'un procédé industriel de LMS opérant en phase gaz; La conception d'un nouveau procédé industriel pour la séparation du mélange propane/propylène en phase gaz au moyen de la technologie du LMS répondant à des facteurs tels que la géométrie de la colonne, la limitation des pertes de charge et les paramètres de performance, a ainsi aboutit à une nouvelle application du LMS avec un degré de pureté en propylène élevé (>99.5 %), un taux de récupération élevé (>99.0 %) et une productivité relativement prometteuse au dessus de 1000 kg of propylène par ($m^3_{adsorbent}h$).

(iv) Conception, construction et opération d'une unité de LMS flexible; La conception, la construction et l'opération d'une nouvelle unité de LMS à l'échelle du laboratoire, le FlexSMB-LSRE® est présenté. Une mesure de compensation des volumes stagnants est proposée et appliquée à la séparation aussi bien des mélanges racémiques du tétralol qu'au mélange racémique du guafeinesin, cette dernière étant réalisée en trois différents modes d'opération : LMS classique, asynchrone et OSS, démontrant ainsi la flexibilité du FlexSMB-LSRE®.

Kurzfassung

Die Simulated Moving Bed (SMB) Technologie ist eine Betriebsweise, in welcher die Probleme durch die Feststoffbewegung (Partikel und Wandabrieb, keine gleichmäßige Partikelgrößenverteilung, Zunahme des Druckverlustes), welche normalerweise unter der Gegenstromchromatographie, des sogenannten True Moving Bed, auftreten, gelöst wurden. Die Anfänge des SMB können bis in die frühen 1960er zu der ersten industriellen Umsetzung im Sorbex Prozess durch Universal Oil Products zurückverfolgt werden. Seit ihrer Einführung wurde die SMB Technologie zuerst auf verschiedene petrochemische Trennungen, und in der Zuckerindustrie, später in der pharmazeutischen Industrie und Feinchemie erfolgreich angewendet. In den letzten Jahren, vor allem in der Medikamentenentwicklung, ergab sich durch die Einführung der SMB eine sichere und kostengünstige Prozessalternative mit hohen Durchsätzen, hohen Ausbeuten und ökonomischem Lösungsmittelverbrauch. Seitdem wurde eine beachtliche Anzahl an Artikeln, Patenten und Büchern über die Verwendung von SMB bei der Aufreinigung von pharmazeutisch wichtigen Komponenten veröffentlicht. Infolge des enormen Interesses führen die Beobachtung und Untersuchung der SMB Technologie zu der Entwicklung von verschiedenen Betriebsvarianten, der nicht konventionellen SMB Techniken. Dennoch sind, vor allem durch die hohe Nachfrage nach effizienten kontinuierlichen Trennverfahren, Möglichkeiten für Innovationen gegeben. Verschiedenste Aspekte in der Betriebsweise von SMB Einheiten wurden noch nicht untersucht. Der Schwerpunkt dieser Arbeit liegt auf den folgenden vier Themenbereichen:

(i)Untersuchung und Entwicklung neuer unkonventioneller Betriebsweisen; Eine neue unkonventionelle SMB Betriebsweise, die Outlet Streams Swing (OSS), wurde eingeführt. Die durch einen periodischen Produktabzug (realisiert durch das Schließen von Extrakt- oder Raffinatauslässen für einen Teil der Schaltzeit, wobei die Volumenströme durch Veränderungen des Eluent/Desorbent Volumenstrom in Zone II und III konstant bleiben) charakterisierte neue Technik, verbessert die SMB Outlet Reinheiten oder erlaubt eine höhere Produktivität oder einen geringeren Verbrauch an Eluent im Vergleich zu der klassischen Betriebsweise.

(ii)Entwicklung von Design Verfahren, welche die Adsorbent Alterung von SMB Einheiten berücksichtigen; Probleme, welche üblicherweise mit der Adsorbent Deaktivierung während des Betriebes einer SMB Einheit zusammenhängen, wurden in die üblichen mathematischen Modelle eingefügt und darauf aufbauend Diagnoseverfahren der Alterungsmechanismen sowie ShortCut Methoden zur Kompensation entwickelt.

(iii)Entwicklung eines Design Verfahrens einer industriellen Gasphasen SMB Einheit; Ein Design Verfahren einer neuartigen Gasphasen SMB Einheit für die industrielle Propan/Propylene Trennung, welches sich mit Einflussgrößen wie Kolonnengeometrie, Leistungsparametern, und Druckverlustbegrenzungen befasst, und hohe Reinheit von Propylene (>99.5%), hohe Zurückgewinnung (>99.0%) und eine sehr vielversprechende Produktivität, über 1000kgPropylene per ($m^3_{adsorbent}h$), bietet, wird vorgestellt.

(vi)Design, Konstruktion und Betrieb einer flexiblen SMB Einheit; Design, Konstruktion und Betrieb einer neuen flexiblen SMB Einheit im Labormaßstab, die FlexSMB-LSRE®, wird vorgestellt. Eine Maßnahme, welche das Totvolumen kompensiert, wird vorgeschlagen und auf die Trennung racemischer Mischungen von Tetralol und Guafeinesin angewendet. Letztere wird, zum Beweis der Flexibilität der FlexSMB-LSRE® Einheit, in drei verschiedenen Betriebsweisen durchgeführt: klassischer SMB, asynchronischer SMB und OSS.

Contents

Chapter 1

RELEVANCE AND MOTIVATION, OBJECTIVES AND OUTLINE

Separations' paradigm is changing and factors like energy consumption or process environmental cleanness become more and more major issues. Scientists have now to work closely with members of the financial, manufacturing and marketing departments in order to develop processes which will not only allow economic and feasible scale-up, but also the synthesis and purification of a target compound in the more sustainable way. Following this tendency, and even if in the past chromatographic applications were not seen as competitive, they became important separation techniques in the fine chemicals, pharmaceutical, biotechnological and petrochemical industries, among others.

Over the years, the chromatographic processes passed through a large number of improvements and it is now possible to process a desired separation in many different ways. Among these, the Simulated Moving Bed (SMB) became one of the most promising techniques, based not only in its useful application to various large petrochemical separations (so-called "Old", but still prominent, applications), such as the *p*-xylene separation from its C_8 isomers[*], *n*-parafins from branched and cyclic hydrocarbons[†], olefins separation from parafins; in the

[*] with 88 Parex units licensed by UOP LLC-USA since 1971, ranging from 21 to 1 600 kton.year^{-1}of *p*-xylene; 8 Eluxyl units licensed by Axens (IFP)-France since 1995, with capacities range from 180 to 750 kton.year^{-1}; 2 Aromax units licensed by Toray Industries Inc.-Japan since 1973, with range of about 200 kton.year^{-1};

[†] with 28 Molex units licensed by UOP LLC-USA.

sugar processing industry[*]; and, with the latter developments (by opposition the "New" applications), in the pharmaceutical (biopharmaceutical included) and fine chemicals industries, as in the case of chiral drugs separations[†].

All this interest on the SMB technology, particularly the study and research of its application to the pharmaceutical and fine chemistry industries, led to the formulation of new theories, methodologies and design concepts that resulted in several more applications, as well as, the development of various non-conventional SMB operating modes, that extended further the performance of this technique.

Following this legacy, and supported by the strong demand on continuous efficient separation techniques, it is simple to understand that the space to innovate is still considerable. Several are the aspects in the operation of SMB units that were not addressed yet; nevertheless, just a few can be treated within the time space of a PhD thesis. This thesis, in particular, focus on four major issues:

(i) Study and development of new non-conventional operating modes;

There is a considerable number of different operating modes related with the SMB technology, such as the asynchronous port shift (Varicol), variable feed concentration (ModiCon), variable feed flow rate (Partial Feed or variable internal flow rates as in PowerFeed), operating in different steps as fixed bed and as SMB (Pseudo-SMB, ISMB - Improved SMB), etc. Each of these different modes of operation, or even their combinations, offers more degrees of freedom and thus, the enhancement of purity and/or unit productivity requirements. If each separation has its own particularities, consequently it will mostly require its own "particular operating mode" (a particular combination of the operating modes cited above). In addition, numerous are the possible improvements that can be achieved by the variation of different operating parameters, stating the importance of the study and development of new non-conventional modes of operation and thus, the relevance of this particular objective.

(ii) Development of design procedures that accounts for SMB units' adsorbent ageing problems;

It is from the common wisdom the use of guard beds in the gas processing industry in order to prevent impurities access to the separation process, or more elaborated methods such as online adsorbent removal and innovative fluid distribution apparatus to mitigate fines production. Nevertheless, ageing problems such as "parasite" reactions within the solid or liquid phase, as well as attrition effects (that can lead to fines production and channelling aspects), continue to appear as time goes by during SMB units operation. By treating adsorbent ageing as a system disturbance it is possible to compensate it by applying SMB online controllers. However, the implementation of model predictive control methods could also be improved, if based on robust ageing models as the respective compensating measures. Additionally, when it comes to design and start-up of new SMB units, the analysis of adsorbent ageing factors can have a significant weight on financial and/or management choices

[*] Sarex process by UOP LLC-USA; more than 90 SMB and Improved-SMB plants by FAST - "Finnsugar Applexion Separation Technology", now Novase*p*-France; and Amalgamated Sugar Co.-USA;

[†] with more than 50 units currently installed, mainly by Novase*p*-France, Knauer GmbH-Germany, Bayer BTS-Germany, SepTor Technologies BV-Netherlands part of Outotec Oyj-Finland and ChromaCon AG-Switzerland.

involved in these processes, if not in the main project viability. Nevertheless, the study of adsorbent deactivation during the operation of SMB units is not a recurrent research matter. Therefore, the analysis of ageing effects in the SMB operation, as well as the development of simple compensating measures, is stated as a major objective of this thesis.

(iii) Development of a design procedure for an industrial gas phase SMB unit;

Most of the published works concerning the separation design by means of SMB technology do not address industrial apparatus, and if so, starts already with some considerable background, *i.e.*, are only improvements to established units or most of the operating parameters are just calculated from limitations obtained for a given piece of equipment. The objective hereby enunciated is then to develop a design procedure for an industrial gas phase SMB unit from the scratch, addressing factors such as the columns geometry, performance parameters, pressure drop limitations; making use of the more detailed models and project evaluation criteria.

(iv) Design, construction and operation of a flexible SMB unit.

As mentioned before, the number of non-conventional operating modes concerning the SMB technology is considerable. Therefore, SMB units flexibility becomes an important factor to consider (at least at lab-scale), *i.e.*, the unit's capability for operating different modes, and therefore, to extend its own performance and operability. However, most of the units in the market are limited to one or two types of operation and any changes on the unit layout, or structural changes in mode of operation, dependent on the technology owners. Consequently, the construction of a new and flexible SMB unit is also a major objective of this thesis.

Point (i) refers to the development of new operating modes; points (ii) and (iii) to development of new design methodologies and point (iv) to product (FlexSMB-LSRE®) development, three main aspects when considering the Advances in Simulated Moving Bed technology.

This thesis is constituted by 7 major Chapters, followed by an Annex section, presenting Chapter 1 the Relevance and Motivation, Objectives and Outline of this work.

In Chapter 2, a general introduction is presented, detailing the SMB concept as its development over the years. A special focus is given on SMB non-conventional modes of operation; the modelling, design and operation of SMB units and the more common SMB applications are also cited.

In Chapter 3, a new mode of operation: the Outlet Streams Swing (OSS) is presented. The OSS technique is compared with an optimized (classical) SMB unit for two different chiral separations: a racemic mixture of chiral epoxide enantiomers and a racemic mixture of Guafeinesin. Both separation as regeneration regions are used to compare the OSS *extract-raffinate* and OSS *raffinate-extract* operating strategies with the classical SMB in terms of purity and eluent consumption requirements.

In Chapter 4, the operation of an SMB unit accounting for adsorbent ageing effects is addressed. Three different systems are considered: a classic binary separation with linear adsorption isotherms (fructose/glucose); a Chiral separation, characterized by a linear plus Langmuir adsorption isotherm; and the separation of *p*-xylene from its

C_8 isomers, detailed by a multicomponent nonstoichiometric Langmuir isotherm. Two different consequences of adsorbent deactivation are considered: (i) involving the loss of adsorption equilibrium capacity; and (ii) related with the increase of mass transfer resistance. For each of these cases one direct and straightforward compensation measure is presented: the increase of the solid velocity (decrease of switching time) to compensate the adsorbent capacity decline and the decrease of solid and internal flow rates to compensate the mass transfer resistances increase. Additionally, the asynchronous SMB mode of operation (Varicol) is also tested as a compensating measure.

In Chapter 5, the design of a gas phase SMB for the separation of propane/propylene is presented. The design methodology is based on three major questions: Is it possible?; Is it reasonable? and Is it worth it? For each question, different approaches are used, starting from equilibrium assumptions through more detailed models, accounting for mass transfer resistances, temperature and pressure drops effects, and presenting, in the end, an introductive note to some relevant aspects for the project evaluation stage.

In Chapter 6, the design, construction and operation of a new flexible SMB unit, the FlexSMB-LSRE® is addressed. The design of this lab-scale SMB unit is detailed accounting for flexibility, relevant unit dead volumes and equipment configuration. Four different separations are presented as well: the separation of a racemic mixture of α-tetralol (dilute system, linear adsorption isotherm); and 3 separations of a racemic mixture of guafeinesin (non Langmuir type adsorption isotherm), classical SMB, asynchronous SMB and OSS operation modes. A detailed model accounting for the FlexSMB-LSRE® unit dead volumes and switching time asymmetries is presented and used to determine a dead volumes compensating measure.

The conclusions and suggestions for future work are presented in Chapter 7.

Chapter 2

GENERAL INTRODUCTION

2.1 THE CONCEPT OF SIMULATED MOVING BED (SMB) CHROMATOGRAPHY

Chromatography*, is the general term given to the physical separation method in which the components of a mixture are separated by differences in their distribution between two phases: the stationary phase and a mobile phase (Ettre, 1993). The substances interaction with the stationary phase permits the separation of a given target molecule from other molecules in the mixture, allowing it to be isolated.

Chromatography is usually divided into analytical and preparative. While preparative chromatography searches for the separation of the mixture components for further use (and is thus, a form of purification); analytical chromatography normally operates with smaller amounts of material and seeks for the measurement of the relative proportions of analytes in a mixture. Nevertheless, the two are not mutually exclusive.

According to the physical state of both phases used, the chromatographic techniques can also be classified into: Gas-liquid chromatography (GLC); Gas-solid chromatography (GSC); Liquid-liquid chromatography (LLC); Liquid-solid chromatography (LSC), or simply by relating it only to the mobile phase: Gas chromatography (GC); Liquid Chromatography (LC) or, in the presence of high inlet pressure, High-Performance (or High-Pressure) Liquid Chromatography (HPLC); and Supercritical-Fluid Chromatography (SFC). Chromatography

* from Greek χρώμα: “chroma”, colour and γραφειν: “graphein” to write;

can also be classified according with its mechanism of separation: Adsorption* Chromatography; Partition† Chromatography; Ion-Exchange‡ Chromatography; Exclusion§ Chromatography; Hydrophobic Interaction** and Reverse Phase** Chromatography; or Affinity†† Chromatography.

2.1.1 CHROMATOGRAPHY – A BRIEF HISTORICAL BACKGROUND


M.S. Tswett

It was the Russian botanist Mikhail Semenovich Tswett "Михаил Семенович Цвет" (1872-1919) who invented the first chromatography technique around 1900, during his research on the physico-chemical structure of plants chlorophylls. Using a liquid-adsorption column containing calcium carbonate and carbon disulfide as eluent he was able to separate plant pigments, Xanthophylls and Chlorophylls, Figure 2.1.

The method was described on December 30, 1901 at the 11th Congress of Naturalists and Doctors (XI съезд естествоиспытателей и врачей) in St. Petersburg, and the first printed description in 1903, in the Proceedings of the Warsaw Society of Naturalists, section of Biology. The term chromatography was first used and printed in 1906 in the Tswett two papers about chlorophyll in the German Botanical Journal (Berichte der Deutschen Botanischen Gesellschaft) as an answer to Hans Molisch, professor at the University of Prague and one of the most respected botanists at that period. Tswett discussed his results and described in detail the chromatographic method using the term "Chromatography", (Ettre, 2006a).

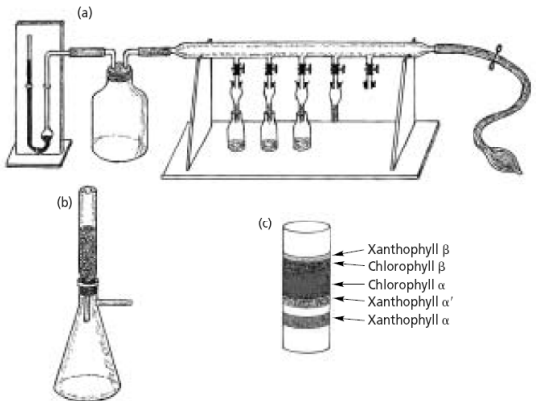

Figure 2.1 – Illustrations on Tswett's 1906 paper. (a) Apparatus for the simultaneous use of as many as five columns. The lower part of the small funnel-like glass pieces (2-3 mm i.d. and 20–30 mm length) served as the packed column. (b) Apparatus for larger samples (1–3 cm i.d., packing length: 5–9 cm). (c) Chromatographic separation of plant pigments as drawn by Tswett. Stationary phase: calcium carbonate; eluent: carbon disulfide – adapted (Ettre, 2003).

---

* process that occurs when a gas or liquid solute accumulates on the surface of a solid or, more rarely a liquid, (adsorbent), forming a molecular or atomic film, the adsorbate;

† process driven by the differences between the solubilities of the components in the mobile and stationary phases;

‡ process based on the charge properties of the molecules;

§ process based on exclusion effects, such as differences in molecular size and/or shape or in charge;

** processes based on interactions between solvent-accessible non-polar groups on the surface of biomolecules and hydrophobic ligands covalently attached to a gel matrix;

†† particular variant of chromatography in which the unique biological specificity of the analyte and ligand interaction is utilized for the separation.

Today, there is not almost any doubt that Tswett was the true inventor of this method. However, there were others who, intentionally or unintentionally, carried out some separation in a moving flow. An example is Runge, that, about one-half a century before Tswett, presented a dynamic separation on filter paper; however, not for separation purposes but to exemplify reactions, (Ettre, 2005). Nonetheless, such isolated applications, with no background methodology, could be tracked back to the old Egyptian Era (Ettre, 2006b); anyhow, various names, in the centre of some disputes to find out who was the really father of chromatography, should be mentioned, in the case, David Talbot Day.

Near to the end of the 19th century, the rapidly developing petroleum production also initiated speculations concerning its origin, and several attempts have been made to explain the reason for the obvious difference in the characteristics of crude oils at different locations. D.T. Day, geologist and engineer at the Mineral Resources of the U.S. Geological Survey, also stated a theory (the "filtration hypothesis") based upon the assumption of migration of the oil in the earth through various strata and selective retardation of certain compounds or compound groups during this migration. To prove the validity of his assumption, Day carried out some model experiments and demonstrated that indeed, some fractionation can be achieved in this way and presented it at the First International Petroleum Congress in Paris (1900) one experiment where "crude oil forced upward through a column packed with limestone changed in colour and composition". This is the basis of PONA* analysis established in 1914 and still used in petroleum industry (Ettre, 2005; Rodrigues and Minceva, 2005). His experiments were repeated in Germany by Carl Engler and their publications also inspired some activities by other petroleum chemists. The technique of Day and Engler somewhat resembled chromatography; however, there was no cross-influence between their work and Tswett's (Ettre, 2005).

R. Kuhn received his Nobel Prize in 1938, but was unable to accept the award until after the end of World War II for the investigations of vitamins and carotenoids that would be impossible without chromatography. These techniques were also widely used in the well-known investigations of the complex protein (and important drug) insulin, adrenocorticotropic and sex hormones, and other substances. In 1952 A.J.P. Martin and R.L.M. Synge were awarded with the Chemistry Nobel Prize for their invention of partition chromatography. Since then, this technology advances have been remarkable (Engelhardt, 2004).

Over the years, the principles underlying Tswett's chromatography were applied in many different ways, giving rise to the different varieties of chromatography and improving further the technical performance of chromatographic processes for the separation of more and more similar molecules.

2.1.2 COLUMN CHROMATOGRAPHY

Column chromatography is the general name given to the chromatographic procedure that uses a column filled with an appropriated adsorbent through which passes a composite mixture. The techniques principle is related to the adsorption affinity of each material in the mixture to the packing material (*e.g.*, adsorbent), which will allow each component to be separated in a different section of the column.

* classification into paraffins (P), olefins (O), naphthenes (N) and aromatics (A).

To perform column chromatography, a liquid/gaseous mixture is poured into a column filled uniformly with the proper amount of adsorbent. Each compound is then adsorbed into the beds at different zones, depending on the component's individual adsorption affinity. However, and at this stage, the sections where each component are retained can not be still not completely separated. To reach a proper separation an appropriate desorbent, or a considerable eluent amount, is poured into the column, which will lead to the dissolution of the components retained on the adsorbent and its subsequent migration downwards in the column. Again the migration rates will differ according to each component's adsorption affinity. The components in the lower layers move faster, and in the end, each component can be clearly separated, process called as "development". In the case of a pigments mixture separation, there will appear coloured zones at different heights in the column filled with adsorbent. When the development stage is over, the adsorbent is pushed out of the column, divided into each coloured zone and the adsorbates are extracted separately, process called as "elution".

Alternately, without removing the adsorbent from the column, a desorbent may be successively poured in from above, and each zone preferentially eluted by the desorbent will dissolve into it and trickle down the column one at a time. The mobile phase can then be collected from the bottom of the column as they drip out. This is the principle of Elution Chromatography*, which was described in detail by Steiger and Reichstein, (this one Nobel laureate in medicine), that used a stepwise series of eluents to elute the components mixture. Later Tiselius (chemistry Nobel laureate) and co-workers, discussed the now mainly used gradient elution with a continuous change of elution strength (Engelhardt, 2004). The basic principle of elution chromatography is illustrated in Figure 2.2.

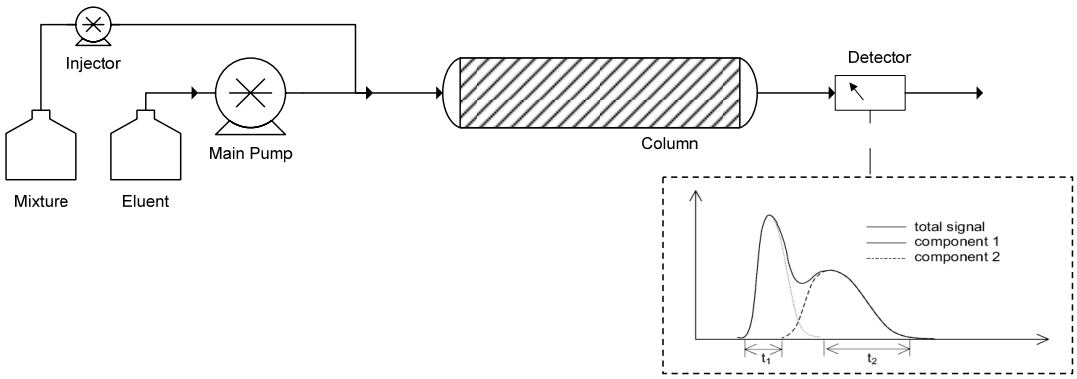

Figure 2.2 - Principle of elution chromatography.

Following Figure 2.2, one can observed how a chromatographic column packed with a solid phase (adsorbent) will be permanently penetrated by a fluid phase (eluent) with a given interstitial velocity. At the time t_0, a well defined amount of the sample mixture is injected into the column. Due to different interaction forces of the mixture components and the adsorbent (different migration velocities), a separation of the mixture into the pure components will take place. At the column outlet the purified components can be detected and collected. The procedure is repeated periodically, eluent, mixture… and therefore called batch chromatography. Among the

* a procedure for chromatographic separation in which the mobile phase is passed through the chromatographic bed after the application of the sample.

established industrial scale separation processes, preparative adsorption chromatography is becoming one of the more used. Some separation tasks (*e.g.*, the separation of enantiomers) can barely be solved by chromatography.

However, as the volume of sample is increased (carrying a fixed concentration of solute) the peak broadens and the height increases until eventually the height remains constant and a rectangular type of peak is formed with a half Gaussian front and a half Gaussian tail. If the column is highly overloaded it will not be sufficient to completely separate the mixture into the pure components and thus, peaks will overlap, Figure 2.3.

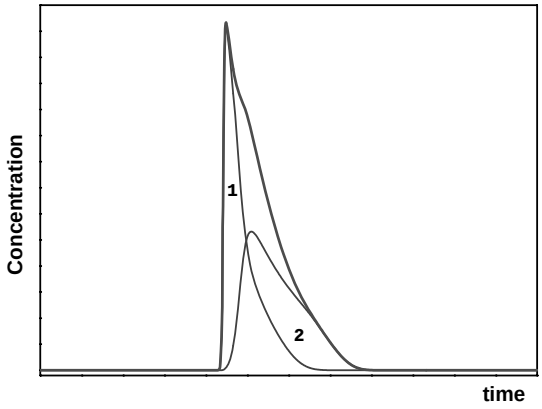

Figure 2.3 - Overlapped bands, consequence of an overloaded column.

In Figure 2.3 is shown a case where separation does not takes place. These parts causes a lower use of the adsorbent capacity, but cannot be avoided in batch chromatography. Consequence of the discontinuous or batch regime of the process, *i.e.*, only discrete amounts of the mixture can be injected. Increasing the scale of the column and by consequence the total amount of adsorbent can help in solving some of these limitations, but it will not change the discontinuous character connected with the lower use of the adsorbent capacity and dilution effects.

2.1.3 CONTINUOUS COUNTER CURRENT CHROMATOGRAPHY

Continuous industrial-scale adsorption processes are usually preferable to batch ones. These processes allow a more "efficient" use of the adsorbent bed. For instance, the Height Equivalent of a Theoretical Plate (HETP) in a batch operation is roughly three times higher than a continuous mode (Gembicki *et al.*, 2002). The use of continuous chromatographic counter current operation in particular, maximizes the mass transfer driving force providing a better utilization of the adsorbent, which may have a lower selectivity (Ruthven and Ching, 1989). This technique is also known for other relevant advantages, including reduction of solvent consumption, the increase in productivity as purity rates and less diluted product streams, when compared to conventional batch chromatography.

The counter-current movement of the solid, with respect to the fluid phase, allows continuous regeneration of the adsorbent with reduced eluent requirements, followed by enhanced mass transfer. These aspects become critical when one desires to achieve products with an high-purity and only low selectivity adsorbents are available.

It is easier to understand the concept of continuous counter current chromatography by examining the concept of batch elution chromatography, as mentioned before, in a continuous fashion (Figure 2.4a).

Let us consider a single chromatographic column and just two species: component *A* and component *B,* and establish that the affinity of *A* with the stationary phase is higher than in the case of *B*. A discrete amount of a diluted solution of both components is then fed to a column (packed with a suitable adsorbent, the stationary phase). Both components will travel in the mobile phase direction; however, since *A* has an higher affinity with the stationary phase, it will take longer to get out from the column. If there is enough column length, all *B* product fed to the column will be collected in the end of the column before *A* starts to getting out. Now, let us imagine that *A* product is a snail, the Snail, and B a jolly Fox, running a race on a straight track, "The Fixed Bed", Figure 2.4a. In normal conditions the Fox will come out first, and then the Snail. Consider that they are running on a moving belt (Figure 2.4b), if the belt is moving slower than the Snail, both will be retarded, and the result the same as in case a), and *vice-versa* if the belt is moving faster than the Fox. However, there is a region of plausible belt velocities, faster than the Snail but slower than the Fox, that will move the Snail to the left-hand side and the fox to the right-hand one, Figure 2.4c.

With this principle in mind, a device can be constructed that can separate Snails and Foxes, fed continuously to the centre of the moving belt.

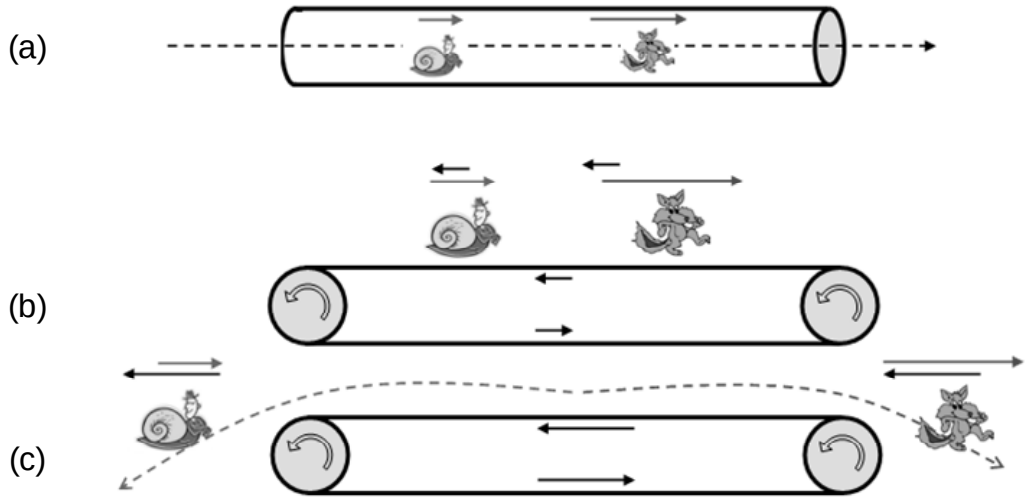

Figure 2.4 - (a) Metaphor to a single chromatographic column where the more-retained species A is represented by a Snail and less retained species B by a Fox. The continuous Snail–Fox separator (b) – when the belt velocity has no effect, therefore any separation, (c) - the efficient belt velocity.

The same principle can be applied to chromatography in the counter current column illustrated in Figure 2.5, the arrangements in which, there is actually flow of solid are known as *moving beds* or True Moving Bed (TMB).

The moving bed allows the achievement of high purity even if the resolution of the two peaks is not excellent, since only the purity at the two tails of the concentration profiles, where the withdrawal ports are located, is of interest. This is contrary to batch chromatography where high resolution is vital in order to achieve high purity.

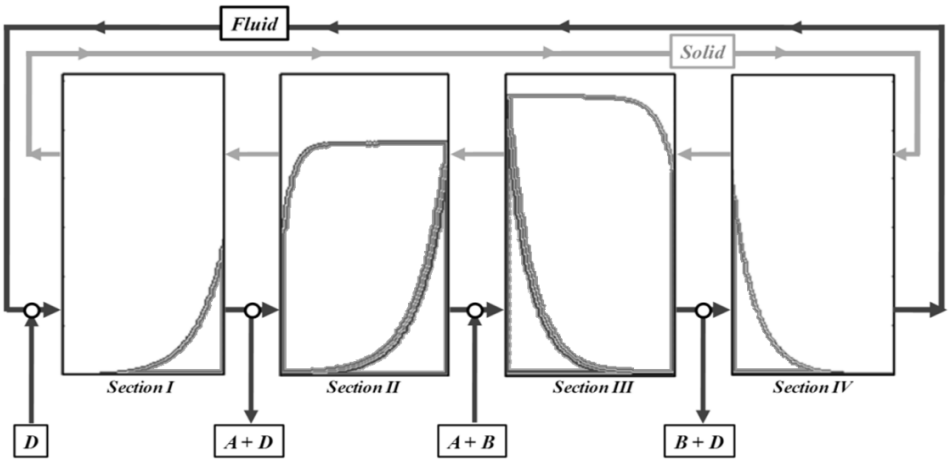

Figure 2.5 - A four section True Moving Bed (TMB) unit for the separation of A and B with D as eluent/desorbent (Fructose/Glucose separation).

If we define *section* as the part of the TMB unit where the fluid flow rate is approximately constant (section limited by inlet/outlet streams), then, it is possible to find four different sections with different roles:

Section *I:* Regeneration of the adsorbent (desorption of *A* from the solid);

Section *II:* Desorption of *B* (so that, the extract is not contaminated by the less retained component);

Section *III:* Adsorption of *A* (raffinate clean from the more adsorbed species);

Section *IV:* Regeneration of the eluent/desorbent (adsorption of *B* from the fluid phase).

Nevertheless, with this counter current mode of operation is necessary to circulate not only the fluid phase but also the solid. The solid motion inside of the column and the consequent recycle presents some technical problems, namely: equipment abrasion, mechanical erosion of adsorbent and difficulties in maintaining plug flow for the solid (especially in beds with large diameter). From a technical point of view, this clearly limits the implementation of such technologies.

In order to avoid this issue, a sequence of fixed bed columns was conceived (Broughton and Gerhold, 1961) in which the solid phase is at rest in relation to a fixed referential, but where a relative movement between both phases is experienced by switching the inlet and outlet fluid streams to and from the columns from time to time (in the direction of the fluid flow). In the simplest operating mode, the period that a certain operating configuration prevails is called the switching time, t_s. Since the solid flow is avoided, although a kind of counter-current movement is created relatively to the fluid, this technology is called **Simulated Moving Bed (SMB)**.


Donald B. Broughton

Consider that at certain moment in the operation of an SMB, the positions for the inlet of feed and desorbent and outlet of products is represented by Figure 2.6a. Assume also the simplest operating mode (synchronous advance of all streams) and one column per section. After a period of time equal to the switching time, the injection and withdrawn points all move one column in the direction of the fluid flow (Figure 2.6b). When the initial location of injection/collection of all the streams is reencountered, we have completed one cycle (in a four equally zoned SMB, it takes $4n_j t_s$ to complete one cycle, where n_j is the number of columns in each one of the four sections). As it is possible to see in Figure 2.6, during one cycle the same column is in different sections, assuming therefore different roles in the separation process.

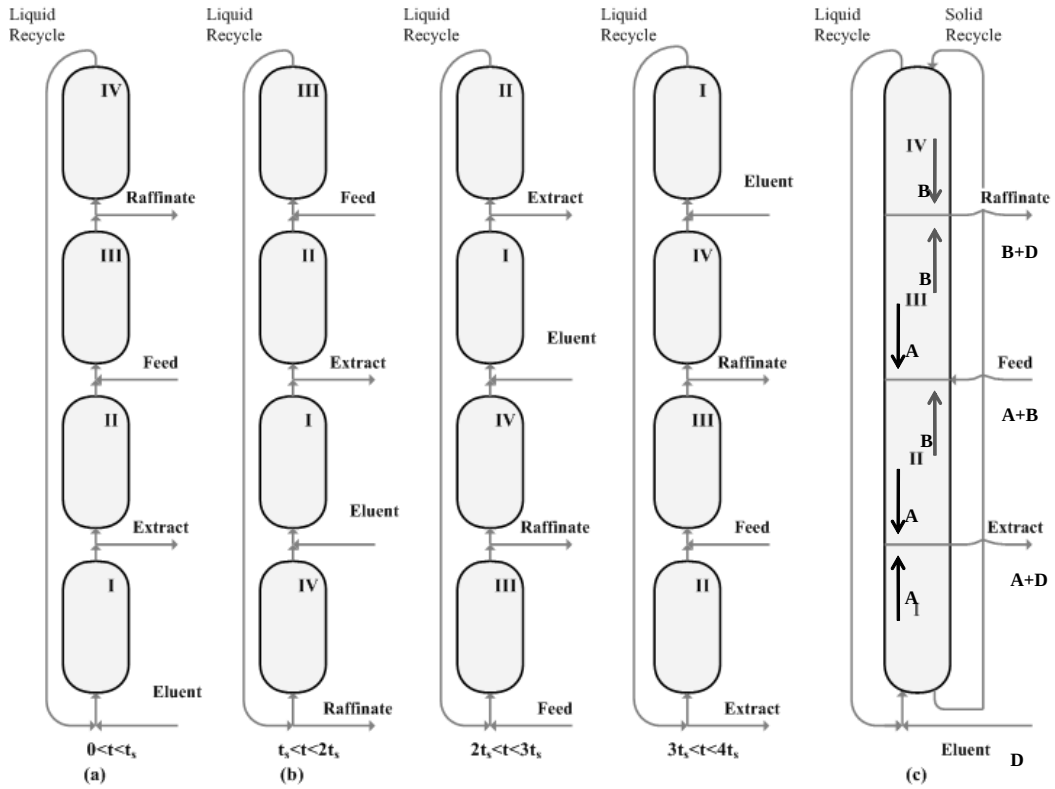

Figure 2.6 - Schematic representation of a 4 columns SMB unit operating over a complete cycle, from 0 to $4t_s$ (with t_s representing the ports switching time); (a) period of the first switch; (b) period of the second switch and (c) a TMB unit.

As mentioned before, the continuous movement of inlet and outlet lines into and from the column is almost impractical, therefore discreet jumps (with the length of one bed, during t_s) have to be applied. Several are the valves schemes used to minimize the discontinuities associated with theses jumps, such as the use of a rotary valve or by a system of on-off valves (Chin and Wang, 2004). The construction and design of SMB units will be detailed later in Chapter 6.

The analogy between SMB and the TMB is then possible by the introduction of the relative velocity concept, where $u_j^* = u_j + u_s$, with u_j the fluid interstitial velocity in each section j in the TMB, u_j^* the interstitial velocity in the SMB unit and u_s the solid interstitial velocity in the TMB. The solid velocity is evaluated from the switching time interval value t_s in the SMB as $u_s = \frac{L_c}{t_s}$, being L_c the column length. As consequence, The internal flow rates in both apparatus are not the same, but related by $Q_j^* = Q_j + \frac{\varepsilon_b V_c}{t_s}$, where Q_j^* and Q_j represent

the internal liquid flow-rates in the SMB and TMB, respectively, ε_b is the bulk porosity and V_c the column volume.

2.2 SMB MODES OF OPERATION

So far, only the hereby called as "classical" SMB mode of operation has been considered, which indeed means that each section has a fixed number of columns and there is no variation on the pre-established inlet/outlet flow rates or the switching time value.

However, in the last decades some "non-conventional" SMB operating modes were proposed, developing the range of the applications of SMB technology and extending further its potential. Some of these operating modes, worthy of note, are listened in the following sections.

2.2.1 ASYNCHRONOUS SHIFTING SMB (THE VARICOL® PROCESS)

The asynchronous shifting SMB or Varicol® process (Adam *et al.,* 2000; Bailly *et al.,* 2000; Ludemann-Hombourger *et al.,* 2000; Ludemann-Hombourger *et al.,* 2002) commercialized by Novasep (Pompey, France), became one of the most studied and used processes of the so-called non-conventional SMB modes of operation. Instead of a fixed unit configuration with constant section length, the Varicol® operating mode is performed by the implementation of an asynchronous inlet/outlet ports shift, providing a flexible use of each section length, Figure 2.7.

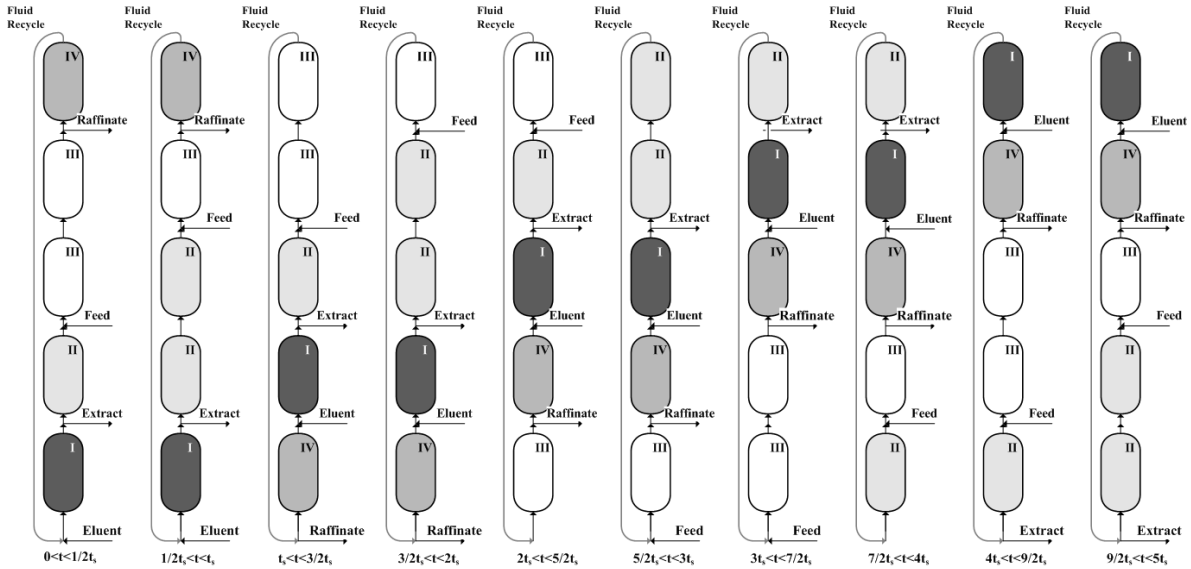

Figure 2.7 – [1 1.5 1.5 1] Asynchronous SMB for a complete cycle; section II has 1 column during the first half of the switching time and 2 columns in the remain time (within a switching time period), thus 1.5 columns; the opposite happens to section III.

By means of Varicol® mode of operation it is possible to increase the productivity value up to 30 % more than the classical SMB apparatus, principally when operating under a reduced number of columns (Toumi *et al.*, 2002; Zhang *et al.*, 2002b; Pais and Rodrigues, 2003; Subramani *et al.*, 2003b, 2003a; Toumi *et al.*, 2003; Yu *et al.*, 2003b; Sá Gomes *et al.*, 2006c; Mota *et al.*, 2007b; Rodrigues *et al.*, 2007a; Sá Gomes *et al.*, 2007b; Zhang *et al.*, 2007).

2.2.2 PARTIAL-FEED, PARTIAL-DISCARD

With the Partial-Feed mode of operation two additional degrees of freedom are introduced: the feed length and the feed time (Zang and Wankat, 2002a; Zang and Wankat, 2002b). The SMB unit is just fed during a given feed length period that consequently influences the raffinate and extract flow rates along the time. Also referred in the literature is the Partial-Discard (or partial withdraw) operating mode, where just a part of the outlet products is used in order to improve the overall purity (Zang and Wankat, 2002b; Bae and Lee, 2006), or with the partial recirculation of the outlet products back to the feed (Kessler and Seidel-Morgenstern, 2008; Seidel-Morgenstern *et al.*, 2008).

The ISMB (Improved SMB) mode of operating (Yoritomi *et al.,* 1981, 1983), commercialized by the Nippon Rensui Co. (Tokyo, Japan) and FAST - "Finnsugar Applexion Separation Technology", now Novasep-France, is also well known. In ISMB process, during a first step the unit is operated as a conventional SMB but without any flow in section IV; in the second step the inlet and outlet ports are closed and the internal flow through the four sections allowing the concentration profiles to move to adjust their relative position with respect to the outlet ports (Rajendran *et al.*, 2009).

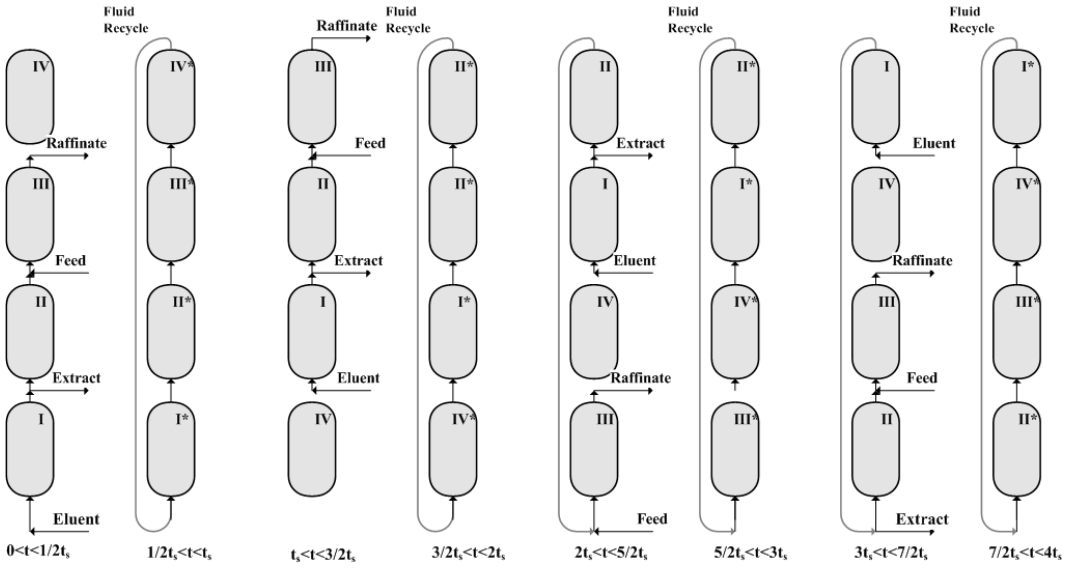

Figure 2.8 – 4 columns ISMB, with the first length (time step is equal to the second step $(1/2\, t_s)$;

A novel non-conventional mode of operation, the Outlet Swing Stream-SMB (OSS) (Sá Gomes and Rodrigues, 2007), was developed under the framework of this thesis and is latter detailed in Chapter 3.

2.2.3 POWERFEED AND MODICON

The modulation of the section flow rates (PowerFeed) was originally proposed by Kearney and Hieb (1992) and later studied in detail by other authors (Kloppenburg and Gilles, 1999b; Zhang *et al.*, 2003b; Zhang *et al.*, 2004b; Kawajiri and Biegler, 2006b). Another SMB operating concept, based on the feed concentration variation within one switching interval, was suggested by Schramm *et al.*, (2002; 2003b) known as the ModiCon. The use of auxiliary feed tanks, where section flow rate flows into a tank to dissolve solid raw materials and fed into section III, has also been studied (Wei and Zhao, 2008). The cross combination of PowerFeed, Modicon and Varicol

modes of operation is also a recurrent research matter, principally of optimization studies (Zhang *et al.*, 2004a; Araüjo *et al.*, 2006a; Rodrigues *et al.*, 2007b), providing more degrees of freedom and allowing better performance values.

2.2.4 TWO FEED OR MULTIFEED SMB AND SIDE STREAM SMB

Recently, the introduction of multi feed streams in the SMB area, by analogy with distillation columns, led to the formulation of the Two Feed SMB, or MultiFeed, operating mode presented by Kim (2005) and later studied by Sá Gomes and Rodrigues (Sá Gomes *et al.*, 2007b; Sá Gomes and Rodrigues, 2007). Also multi extract/raffinate are referred in the literature (Mun, 2006), known as side stream SMB (Beste and Arlt, 2002). These techniques, combined with the distillation know-how for the optimum location of multiple feeds, can allow the development of more efficient SMB processes.

2.2.5 SEMI-CONTINUOUS, TWO AND THREE ZONES SMB

There are several semi-continuous SMB apparatus that operate with two-zone, two or one-column chromatograph, with/without recycle, analogous to a four-zone SMB (Abunasser *et al.*, 2003; Abunasser and Wankat, 2004; Araüjo *et al.*, 2005a; Araüjo *et al.*, 2005b; Jin and Wankat, 2005b; Mota and Araüjo, 2005; Araüjo *et al.*, 2006b; Araüjo *et al.*, 2007; Rodrigues *et al.*, 2008b), that allow a reasonable separation, some allowing centre cut for ternary or quaternary separations (Hur and Wankat, 2005b, 2005a, 2006a, 2006b; Hur *et al.*, 2007), under reduced equipment usage.

The discontinuous injection in a system with 2 or more columns, based on the concept of simulated adsorbent movement, as also been applied by Novasep under the denomination of Cyclojet®, Hipersep®, Supersep™ (Supersep MAX™ with Super Critical CO_2) and Hipersep®, (Grill, 1998; Valery and Ludemann-Hombourger, 2007).

2.2.6 GRADIENT SMB

As a further possibility for increasing the productivity, the introduction of gradients in the different separation sections of the SMB process is also described in literature. The gradient mode was suggested firstly for the SMB-SFC (SMB-supercritical fluid chromatography) process, where the elution strength can be influenced by a pressure gradient (Clavier and Nicoud, 1995; Clavier *et al.*, 1996). Nowadays, there are more gradient-variants that allows the variation solvent elution strength by changing the temperature, the pH-value, the content of salt or the modifier concentration (Jensen *et al.*, 2000; Antos and Seidel-Morgenstern, 2001; Migliorini *et al.*, 2001; Abel *et al.*, 2002; Antos and Seidel-Morgenstern, 2002; Abel *et al.*, 2004; Ziomek and Antos, 2005; Mun and Wang, 2008a), or as in Rodrigues's group with the purification of proteins by Ion Exchange-SMB (IE-SMB) (Li *et al.*, 2007; Li *et al.*, 2008). Also worth of note is the MCSGP (Multicolumn Counter-current Solvent Gradient Purification) process (Aumann and Morbidelli, 2006; Strohlein *et al.*, 2006; Aumann and Morbidelli, 2007; Aumann *et al.*, 2007; Aumann and Morbidelli, 2008; Müller-Späth *et al.*, 2008), commercialized by ChromaCon AG (Zürich, Switzerland), which combines two chromatographic separation techniques, the solvent gradient batch and continuous counter-current SMB for the separation of multicomponent mixtures of biomolecules.

2.2.7 HYBRID-SMB: SMB COMBINED WITH OTHER PROCESSES

It is possible to improve the performance of SMB units by integrating it with other different separation techniques. The more simple application of this approach is to combine in series the two different processes and then recycle back the outlets between (or within) the different units (Lorenz *et al.*, 2001; Amanullah *et al.*, 2005; Kaspereit *et al.*, 2005; Amanullah and Mazzotti, 2006; Gedicke *et al.*, 2007). Among these, an interesting hybrid SMB was presented (M. Bailly *et al.*, 2005; Abdelmoumen *et al.*, 2006), the M3C process; or the similar process Enriched Extract operation (EE-SMB) (Paredes *et al.*, 2006), in which a portion of the extract product is concentrated and then re-injected into the SMB at the same, or near to, the collection point. The use of SMB-PSA apparatus is also referred in the literature for gas phase separations, (Rao *et al.*, 2005; Sivakumar, 2007; Kostroski and Wankat, 2008). The use of two SMB units with concentration steps between, for the separation of binary mixtures, was also developed under the denomination of hybrid SMB-SMB process (Jin and Wankat, 2007a).

2.2.8 THE SMBR MULTIFUNCTIONAL REACTOR

The integration of reaction and separation steps in one single unit has the obvious economical advantage of reducing the cost of unit operations for downstream purification steps. Besides reactive distillation, reactive extraction or membrane reactors, the combination of (bio)chemical reaction with SMB chromatographic separator has been subject of considerable attention in the last 15 years. This integrated reaction-separation technology adopts the name Simulated Moving Bed Reactor (SMBR). Several applications have been published considering the SMBR: the enzymatic reaction for higher-fructose syrup production (Hashimoto *et al.*, 1983; Azevedo and Rodrigues, 2001; Borges da Silva *et al.*, 2006; Sá Gomes *et al.*, 2007a); the esterification from acetic acid and β-phenethyl alcohol and subsequent separation of the product β-phenetyl acetate (Kawase *et al.*, 1996), or methyl acetate ester (Lode *et al.*, 2001; Yu *et al.*, 2003a); the synthesis and separation of the methanol from syngas (Kruglov, 1994); the esterification of acetic acid with ethanol (Mazzotti *et al.*, 1996b); the lactosucrose production (Kawase *et al.*, 2001); the MTBE synthesis (Zhang *et al.*, 2001); the diethylacetal (and dimethylacetal) synthesis (Silva, 2003; Rodrigues and Silva, 2005; Silva and Rodrigues, 2005a; Pereira *et al.*, 2008); the ethyl lactate synthesis from lactic acid and ethanol (Pereira *et al.*, 2009a; Pereira *et al.*, 2009b); the biodiesel synthesis (Geier and Soper, 2007); or the isomerization and separation of *p*-xylene (Minceva *et al.*, 2008), are examples that prove the promising potential of this technique. Depending on the reactive system some interesting arrangements of the general SMBR setup can be found in the literature, a more detailed review of several SMBR applications can be found elsewhere (Minceva *et al.*, 2008).

2.2.9 MULTICOMPONENT SEPARATIONS

The application of SMB technology to multicomponent separations has also been an important research topic in the last years. The common wisdom for such multicomponent process is the simple application of SMB cascades (Nicolaos *et al.*, 2001a, 2001b; Wankatt, 2001; Kim *et al.*, 2003; Kim and Wankat, 2004); nevertheless, there are some non-conventional operation modes that proved to have interesting performance, as the one introduced by the Japan Organo Co. (www.organo.co.jp), called JO process (or Pseudo-SMB); this process was discussed in detail (Mata and Rodrigues, 2001; Borges da Silva and Rodrigues, 2006, 2008) and (Kurup *et al.*, 2006a). The

process is characterized by a 2-steps operation: (a) in the first step the feed is introduced while the intermediary product is recovered with the whole unit working as a fixed bed; (b) during the second step the feed stopped, the unit works as a standard SMB and the less and more retained products are collected, see Annex I for details. The use of two different adsorbents (Hashimoto *et al.*, 1993), two different solvents (Ballanec and Hotier, 1992), or a variation of the working flow rates during the switching period (Kearney and Hieb, 1992), were also proposed.

2.2.10 SMB – GAS AND SUPER CRITICAL PHASES

Most of the industrial applications of SMB technology operate in the liquid phase; nevertheless, SMBs can also be operated under supercritical conditions; where a supercritical fluid, typically CO_2, is used as eluent offering a number of advantages namely reduction of eluent consumption, favourable physicochemical properties and lower pressure drop and higher column efficiency (Clavier and Nicoud, 1995; Clavier *et al.*, 1996; Denet and Nicoud, 1999; Depta *et al.*, 1999; Denet *et al.*, 2001; Johannsen *et al.*, 2002; Peper *et al.*, 2002; Peper *et al.*, 2007). Also in the gas phase, the recent developments have been remarkable (Storti *et al.*, 1992; Mazzotti *et al.*, 1996a; Juza *et al.*, 1998; Biressi *et al.*, 2000; Cheng and Wilson, 2001; Biressi *et al.*, 2002; Rao *et al.*, 2005; Lamia *et al.*, 2007; Mota *et al.*, 2007b; Sivakumar, 2007; Kostroski and Wankat, 2008).

The design of gas-phase SMB for the separation of propane/propylene was developed in the framework of this thesis and will be detailed in Chapter 5.

2.3 SMB MODELLING, DESIGN AND OPERATION

In the last 50 years, modelling, design and optimization of chromatographic separation processes have been frequent research subjects. As consequence, several modelling methods, strategies and approaches have been developed and can now be applied to solve the same problem in many different ways. In the field of SMB separations, there is no exception and several are the possible procedures to provide the proper operating specifications to run a separation by means of an SMB unit.

2.3.1 MODELLING STRATEGIES

Generally, one can model a chromatographic separation process, and consequently an SMB unit, by means of two major approaches: by a cascade of mixing cells; or a continuous flow model (plug flow or axial dispersed plug flow, making use of partial differential equations derived from mass, energy and momentum balances to a differential volume element $A_c dz$), (Rodrigues and Beira, 1979; Ruthven and Ching, 1989; Tondeur, 1995; Pais *et al.*, 1998). Each of these approaches can include mass transfer resistances, thermal, and/or pressure drop effects. Nevertheless, most of the recent literature concerning SMB processes just makes use of the continuous approach, detailing the particle diffusion and/or film mass transfer (the Detailed Particle Model), or using approximations to the intraparticle mass transfer rate in a similar way as the Linear Driving Force (LDF) approach presented by Glueckauf (1955), (Guiochon, 2002).

One can argue that an SMB unit is no more than the practical implementation of the continuous counter current TMB process, Figure 2.6. Consequently, the equivalence between the TMB and a hypothetical SMB with an infinite number of columns can be used in the modelling and design of real SMB units. Therefore, two main approaches are possible when modelling SMB units: the TMB and SMB modelling strategies.

a) TMB model approach

By using the first approach (TMB), it is possible to solve the problem's steady state case, reducing the model equations to a simple set determined for each section j. Considering the global nodes balances:

Eluent (E) node: $u_I = u_{IV} + u_E$ (2.1)

Extract (X) node: $u_{II} = u_I - u_X$ (2.2)

Feed (F) node: $u_{III} = u_{II} + u_F$ (2.3)

Raffinate (R) node: $u_{IV} = u_{III} - u_R$ (2.4)

It is possible to obtain the concentration of i species in the beginning of each section j, $C^0_{b\,i,j}$, from the node mass balances as follows:

$$j = I: \quad C_{b\,i,IV}\Big|_{z=L_{IV}} = \frac{u_I}{u_{IV}} C^0_{b\,i,I} - \frac{u_E}{u_{IV}} C^E_i \tag{2.5}$$

$$j = II, IV: \quad C_{b\,i,(j-1)}\Big|_{z=L_{(j-1)}} = C^0_{b\,i,j} \tag{2.6 a,b}$$

$$j = III: \quad C_{b\,i,II}\Big|_{z=L_{II}} = \frac{u_{III}}{u_{II}} C^0_{b\,i,III} + \frac{u_F}{u_{II}} C^F_i \tag{2.7}$$

where z is the axial coordinate, $L_j = L_c n_j$, the length of section j, with n_j the number of columns in section j; $C_{b_{i,j}}$ the bulk fluid concentration of species i in section j; C^F_i and C^E_i the species i feed and eluent concentrations, respectively.

One can now detail the mass transfer phenomena at different levels, for instance the Detailed Particle Model or LDF approach, as follows.

i. Detailed Particle Model

Two sets of transient mass balances are performed to each species i in each section j, becoming for a volume element in the bulk fluid phase:

$$\frac{\partial C_{b_{i,j}}}{\partial t} = D_{b\,j} \frac{\partial^2 C_{b_{i,j}}}{\partial z^2} - u_j \frac{\partial C_{b_{i,j}}}{\partial z} - \frac{(1-\varepsilon_b)}{\varepsilon_b} \frac{3 k f_i}{r_p} \left(C_{b\,i,j} - C_{p\,i,j}\Big|_{r=r_p} \right) \tag{2.8}$$

and in a volume element of the spherical particle, considering constant particle diffusivity:

$$\left\{ \frac{\partial C_{s_{i,j}}}{\partial t} - u_s \frac{\partial C_{s_{i,j}}}{\partial z} \right\} + \varepsilon_p \left\{ \frac{\partial C_{p_{i,j}}}{\partial t} - u_s \frac{\partial C_{p_{i,j}}}{\partial z} \right\} = D_{pe\,i} \frac{1}{r^2} \frac{\partial}{\partial r} \left(r^2 \frac{\partial C_{p_{i,j}}}{\partial r} \right) \tag{2.9}$$

with the respective initial:

$$t = 0: \quad C_{b\,i,j}(z,0) = C_{p_{i,j}}(z,r,0) = 0 \tag{2.10 a,b}$$

and the boundary conditions, for the bulk concentration, based in Danckwerts (1953):

$$z = 0: \quad C^0_{b\,i,j} = C_{b\,i,j}\Big|_{z=0} - \frac{D_{b\,j}}{u_j}\frac{\partial C_{b\,i,j}}{\partial z}\Big|_{z=0} \tag{2.11}$$

$$z = L_j: \quad \frac{\partial C_{b\,i,j}}{\partial z}\Big|_{z=L_j} = 0 \tag{2.12}$$

$$\begin{cases} C_{p_{i,j}}\Big|_{z=L_j} = C_{p_{i,(j+1)}}\Big|_{z=0} \quad , \quad j = I, II, III \\ C_{p_{i,IV}}\Big|_{z=L_{IV}} = C_{p_{i,I}}\Big|_{z=0} \end{cases} \tag{2.13 a,b}$$

$$\begin{cases} C_{s_{i,j}}\Big|_{z=L_j} = C_{s_{i,(j+1)}}\Big|_{z=0} \quad , \quad j = I, II, III \\ C_{s_{i,IV}}\Big|_{z=L_{IV}} = C_{s_{i,I}}\Big|_{z=0} \end{cases} \tag{2.14 a,b}$$

$$r = 0: \quad \frac{\partial C_{p_{i,j}}}{\partial r}\Big|_{r=0} = 0 \tag{2.15}$$

$$r = r_p: \quad \frac{\partial C_{p_{i,j}}}{\partial r}\Big|_{r=r_p} = \frac{k_{f_i}}{D_{pe_i}}\left(C_{b\,i,j} - C_{p_{i,j}}\Big|_{r=r_p}\right) \tag{2.16}$$

plus the adsorption equilibrium isotherms,

$$C_{s_{i,j}} = f\left(C_{p_{i,j}}\right) \tag{2.17}$$

where t is the time; r the particle radial coordinate; r_p the particle radius, $C_{p_{i,j}}$ the particle pore concentration; $C_{s_{i,j}}$ the adsorbed phase concentration; the ratio between fluid and solid interstitial velocities; D_{b_j} the axial dispersion coefficient in section j; k_{f_i} the film mass transfer coefficient and D_{pe_i} the i species effective diffusion coefficient, obtained from $D_{pe_i} = D_{m_i}\frac{\varepsilon_p}{\tau}$, with D_{m_i} the molecular diffusivity coefficient, τ the particle porosity and ε_p the particle porosity.

Introducing: $x = \frac{z}{L_j}$, the dimensionless axial coordinate with respect to L_j; $\theta = \frac{t}{t_s}$, the dimensionless time normalised by the SMB switching time; and $\rho = \frac{r}{r_p}$, the dimensionless particle radial coordinate, the node mass balances become:

$$j = I: \quad C_{b\,i,IV}\Big|_{x=1} = \frac{u_I}{u_{IV}}C^0_{b\,i,I} - \frac{u_E}{u_{IV}}C^E_i \tag{2.18}$$

$$j = II, IV: \quad C_{b\,i,(j-1)}\Big|_{x=1} = C^0_{b\,i,j} \tag{2.19 a,b}$$

$$j = III: \quad C_{b\,i,II}\Big|_{x=1} = \frac{u_{III}}{u_{II}} C^0_{b\,i,III} + \frac{u_F}{u_{II}} C^F_i \tag{2.20}$$

For the balance in a volume element in the bulk fluid:

$$\frac{\partial C_{b\,i,j}}{\partial \theta} = \frac{\gamma_j}{n_j}\left\{\frac{1}{Pe_j}\frac{\partial^2 C_{b\,i,j}}{\partial x^2} - \frac{\partial C_{b\,i,j}}{\partial x} - \frac{(1-\varepsilon_b)}{\varepsilon_b} N_{f\,i,j}\left(C_{b\,i,j} - C_{p\,i,j}\Big|_{\rho=1}\right)\right\} \tag{2.21}$$

And for the mass balance in a volume element of the spherical particle,

$$\left\{\frac{\partial C_{s\,i,j}}{\partial \theta} - \frac{1}{n_j}\frac{\partial C_{s\,i,j}}{\partial x}\right\} + \varepsilon_p\left\{\frac{\partial C_{p\,i,j}}{\partial \theta} - \frac{1}{n_j}\frac{\partial C_{p\,i,j}}{\partial x}\right\} = \frac{\gamma_j}{n_j}\left\{N_{p\,i,j}\frac{1}{\rho^2}\frac{\partial}{\partial \rho}\left(\rho^2\frac{\partial C_{p\,i,j}}{\partial \rho}\right)\right\} \tag{2.22}$$

with the respective initial conditions :

$$\theta = 0: \quad C_{b\,i,j}(x,0) = C_{p\,i,j}(x,\rho,0) = 0 \tag{2.23 a,b}$$

and the boundary conditions, for the mass balance in the fluid phase:

$$x = 0: \quad C^0_{b\,i,j} = C_{b\,i,j}\Big|_{x=0} - \frac{1}{Pe_j}\frac{\partial C_{b\,i,j}}{\partial x}\Big|_{x=0} \tag{2.24}$$

$$x = 1: \quad \frac{\partial C_{b\,i,j}}{\partial x}\Big|_{x=1} = 0 \tag{2.25}$$

$$\begin{cases} C_{p\,i,j}\Big|_{x=1} = C_{p\,i,(j+1)}\Big|_{x=0} & , \quad j = I, II, III \\ C_{p\,i,IV}\Big|_{x=1} = C_{p\,i,I}\Big|_{x=0} \end{cases} \tag{2.26 a,b}$$

$$\begin{cases} C_{s\,i,j}\Big|_{x=1} = C_{s\,i,(j+1)}\Big|_{x=0} & , \quad j = I, II, III \\ C_{s\,i,IV}\Big|_{x=1} = C_{s\,i,I}\Big|_{x=0} \end{cases} \tag{2.27 a,b}$$

$$\rho = 0: \quad \frac{\partial C_{p\,i,j}}{\partial \rho}\Big|_{\rho=0} = 0 \tag{2.28}$$

$$\rho = 1: \quad \frac{\partial C_{p\,i,j}}{\partial \rho}\Big|_{\rho=1} = Bi_{mi,j}\left(C_{b\,i,j} - C_{p\,i,j}\Big|_{\rho=1}\right) \tag{2.29}$$

with $\gamma_j = \frac{u_j}{u_s}$, the ratio between fluid and solid interstitial velocities, $Pe_j = \frac{u_j L_j}{D_{b_j}}$, the section j Peclet number; $N_{f_{i,j}} = \frac{3k_{f_i}}{r_p} t_j$, the number of film mass transfer units, with $t_j = \frac{L_j}{u_j}$, the fluid phase space time; $N_{p_{i,j}} = \frac{D_{pe_i}}{{r_p}^2} t_j$ the number of intraparticle mass transfer units and $Bi_{mi,j} = \frac{k_{f_i} r_p}{D_{pe_i}} = \frac{1}{3}\frac{N_{f_{i,j}}}{N_{p_{i,j}}}$ the Biot number.

It should be noted the inclusion of the substantial time derivative (Bird *et al.*, 2002; Sá Gomes *et al.*, 2007a) on pore and at pore surface concentration,

$$\frac{D}{D\theta}\left(C_{s_{i,j}} + \varepsilon_p C_{p_{i,j}}\right) = \left\{\frac{\partial C_{s_{i,j}}}{\partial \theta} + \varepsilon_p \frac{\partial C_{p_{i,j}}}{\partial \theta}\right\} - \frac{1}{n_j}\left\{\frac{\partial C_{s_{i,j}}}{\partial x} + \varepsilon_p \frac{\partial C_{p_{i,j}}}{\partial x}\right\} \tag{2.30}$$

representing the particle accumulation as well as the solid counter-current movement by means of its interstitial velocity u_s.

ii. Linear Driving Force (LDF) Approach

Considering the dimensionless form presented before, the LDF approximation can be obtained from $\alpha_{i,j} = \left(\frac{r_p}{3k_{f_i}} + \frac{{r_p}^2}{\varphi D_{pe_i} H_i}\right)^{-1} t_j = k_{LDF} t_j$, with φ a coefficient between 10 and 15, and thus obtaining for the bulk fluid mass balance:

$$\frac{\partial C_{b_{i,j}}}{\partial \theta} = \frac{\gamma_j}{n_j}\left\{\frac{1}{Pe_j}\frac{\partial^2 C_{b_{i,j}}}{\partial x^2} - \frac{\partial C_{b_{i,j}}}{\partial x} - \frac{(1-\varepsilon_b)}{\varepsilon_b}\alpha_{i,j}\left(q_{i,j}^{eq} - \langle q_{i,j}\rangle\right)\right\} \tag{2.31}$$

and for mass balance in the particle,

$$\frac{\partial \langle q_{i,j}\rangle}{\partial \theta} = \frac{1}{n_j}\frac{\partial \langle q_{i,j}\rangle}{\partial x} + \frac{\gamma_j}{n_j}\alpha_{i,j}\left(q_{i,j}^{eq} - \langle q_{i,j}\rangle\right) \tag{2.32}$$

with the respective initial:

$$\theta = 0: \quad C_{b_{i,j}}(x,0) = \langle q_{i,j}(x,0)\rangle = 0 \tag{2.33 a,b}$$

and boundary conditions:

$$x = 0: \quad C_{b_{i,j}}^0 = C_{b_{i,j}}\Big|_{x=0} - \frac{1}{Pe_j}\frac{\partial C_{b_{i,j}}}{\partial x}\Big|_{x=0} \tag{2.34}$$

$$x = 1: \quad \frac{\partial C_{b_{i,j}}}{\partial x}\Big|_{x=1} = 0 \tag{2.35}$$

$$\begin{cases} \langle q_{i,j}\rangle\big|_{x=1} = \langle q_{i,(j+1)}\rangle\big|_{x=0} \quad , \quad j = I, II, III \\ \langle q_{i,IV}\rangle\big|_{x=1} = \langle q_{i,I}\rangle\big|_{x=0} \end{cases} \tag{2.36 a,b}$$

where the adsorption equilibrium isotherm is:

$$q_{i,j}^{eq} = f\left(C_{b\,i,j}\right) \tag{2.37}$$

and $\langle q_{i,j} \rangle$, represents the average solid concentration $\langle q_{i,j} \rangle = \frac{\int_0^1 \left(C_{s_{i,j}} + \varepsilon_p C_{p_{i,j}}\right) \rho^2 d\rho}{\int_0^1 \rho^2 d\rho}$.

The steady state solution can be obtained by setting the time derivatives to zero, resulting in a Partial Differential Equations (PDE) system for the Detail Particle Model and a set of Ordinary Differential Equations (ODE) for the LDF approach.

Applying both these approaches for the separation of a racemic mixture of chiral epoxide (from Sandoz Pharma; Basel, Switzerland), in a stationary phase constituted by microcrystalline cellulose triacetate (Merck, Darmstadt-Germany) with an average particle diameter of 45 μm and pure methanol as eluent, characterized by Pais (1999; Rodrigues and Pais, 2004b) with a linear + Langmuir competitive adsorption isotherm at 25 ºC, and represented as follows:

$$C_{s_{A,j}} = 0.90 C_{p_{A,j}} + \frac{7.32 \cdot 0.163 C_{p_{A,j}}}{1 + 0.163 C_{p_{A,j}} + 0.087 C_{p_{B,j}}} \tag{2.38}$$

$$C_{s_{B,j}} = 0.90 C_{p_{B,j}} + \frac{7.32 \cdot 0.087 C_{p_{B,j}}}{1 + 0.163 C_{p_{A,j}} + 0.087 C_{p_{B,j}}} \tag{2.39}$$

or in terms of retained concentration in the particles:

$$q_{A,j}^{eq} = 1.35 C_{b_{A,j}} + \frac{7.32 \cdot 0.163 C_{b_{A,j}}}{1 + 0.163 C_{b_{A,j}} + 0.087 C_{b_{B,j}}} \tag{2.40}$$

$$q_{B,j}^{eq} = 1.35 C_{b_{B,j}} + \frac{7.32 \cdot 0.087 C_{b_{B,j}}}{1 + 0.163 C_{b_{A,j}} + 0.087 C_{b_{B,j}}} \tag{2.41}$$

one can now obtain the steady state (SS) concentration profiles* here stated for an SMB unit of 5 columns detailed in Table 2.1, and the operating conditions presented in Table 2.2, Figure 2.9.

* The different model equations presented in this Chapter were numerically solved using the gPROMS v2.3.6 a commercial package from Process Systems Enterprise (www.psenterprise.com), by applying the OCFEM (Orthogonal Collocation on Finite Elements) with 2 collocation points per element, 50 elements in each column for the axial coordinate and 3 collocation points and 5 elements for the radial discretization (when applied). After the axial and/or radial discretization step, the time integration is performed by the ordinary differential equation solver SRADAU a fully-implicit Runge-Kutta method that implements a variable time step, the resulting system is then solved by the gPROMS BDNSOL (Block decomposition NonLinear SOLver). An absolute and relative tolerance value was set to 10^{-5}.

Table 2.1 - SMB unit characteristics and parameters.

Model Parameters	SMB Columns
Pe_j=1600	$n_j = [1\ 1\ 2\ 1]$
ε_b=0.4; ε_p=0.45	L_c=15.84 cm
r_p=22.5 μm	d_c=2.6 cm
	SMB Operating Conditions
D_{pe_i}=4.5x10^{-7} cm^2.s^{-1}	C_i^F=5 g.l^{-1}
k_{f_i}=4.3x10^{-4} cm.s^{-1}	t_s=317 s; Q_s=9.54 ml.min^{-1}
	Q_E=25.02 ml.min^{-1}; Q_X=17.34 ml.min^{-1};
	Q_F=0.66 ml.min^{-1}; Q_R=8.34 ml.min^{-1};
	Q_{IV}^*=17.76 ml.min^{-1}.

Table 2.2 - SMB and equivalent TMB operating parameters (Sá Gomes *et al.*, 2007b).

SMB Model approach	TMB Model approach
γ_j^*=[6.72 4.00 4.10 2.79]	γ_j =[5.72 3.00 3.10 1.79]
Q_j^*=[42.78 25.44 26.10 17.76] ml.min^{-1}	Q_j =[36.42 19.08 19.74 11.40] ml.min^{-1}

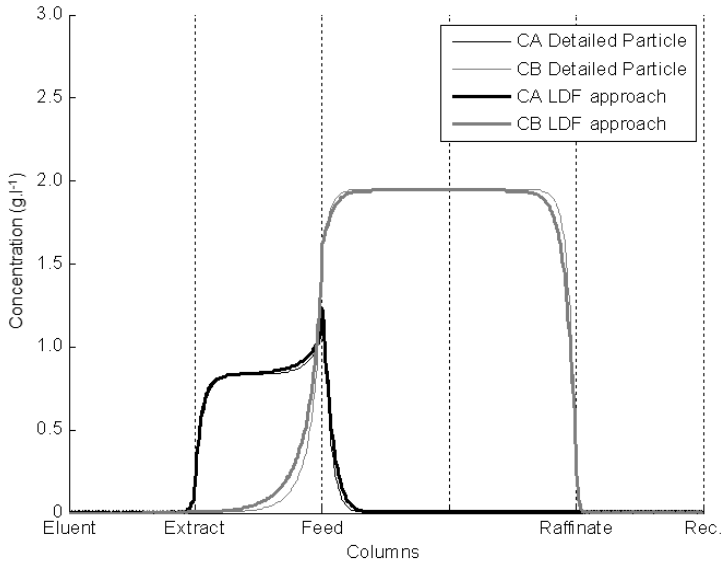

Figure 2.9 – Steady State bulk concentration profiles for the separation of a racemic mixture of chiral epoxide, simulated with detailed particle and LDF methodologies, both by means of the TMB model approach; adapted from Sá Gomes *et al.,* (2007b).

From Figure 2.9, it is possible to note that the Detailed Particle and LDF approaches gave similar concentration profiles; however, the second methodology provided faster calculations.

Nevertheless, the TMB model approach just presents a reasonable agreement with the real SMB unit when a large number of columns per section is considered.

b) SMB model approach

The SMB model approach represents an SMB unit as a sequence of columns described by the usual system equations for an adsorptive fixed bed (each column k), thus represented by a PDE system. Nevertheless, the nodes equations can be stated to each section j^*, making use of the equivalence between the interstitial velocity in the TMB and SMB, and thus:

Eluent (E) node: $u_I^* = u_{IV}^* + u_E$ (2.42)

Extract (X) node: $u_{II}^* = u_I^* - u_X$ (2.43)

Feed (F) node: $u_{III}^* = u_{II}^* + u_F$ (2.44)

Raffinate (R) node: $u_{IV}^* = u_{III}^* - u_R$ (2.45)

The issue here is that, due to the switch of inlet and outlet lines, the boundary conditions to a certain column are not constant during a whole cycle but change after a period equal to the switching time.

Since the model equations are set to each column k, one will obtain the concentration of i species in the begin of each section k, $C_{b\,i,k}^0$, from the following node mass balances:

$\theta = 0\ to\ 1$:

$$k = 1:\ \ C_{b\,i,\left(\sum_{j=I}^{IV} n_j\right)}\Big|_{x^*=1} = \frac{u_I^*}{u_{IV}^*} C_{b\,i,1}^0 - \frac{u_E}{u_{IV}^*} C_i^E \quad (2.46)$$

$$k = 2\ to\ (n_I + n_{II}):\ \ C_{b\,i,(k-1)}\Big|_{x^*=1} = C_{b\,i,k}^0 \quad (2.47)$$

$$k = (n_I + n_{II} + 1):\ \ C_{b\,i,(n_I+n_{II})}\Big|_{x^*=1} = \frac{u_{III}^*}{u_{II}^*} C_{b\,i,(n_I+n_{II}+1)}^0 - \frac{u_F}{u_{II}^*} C_i^F \quad (2.48)$$

$$k = (n_I + n_{II} + 2)\ to\ \left(\sum_{j=I}^{IV} n_j\right):\ \ C_{b\,i,(k-1)}\Big|_{x^*=1} = C_{b\,i,k}^0 \quad (2.49)$$

* in the SMB approach, one can state the global node equations to each section j if there is no variation in the volumetric flow rate (interstitial velocity) within a section, which generally happens in dilute systems (tracer separations). In other cases (bulk separations), one should consider a axial distributed volumetric flow rate (interstitial velocity), and by consequence discretized for each column k. This aspect will later be detailed in Chapter 4 and 5 for a liquid and a gas phase separation, respectively; and for the case of an SMBR unit in Annex II.

$\theta = 1\ to\ 2$:

$$k = 1:\ \ C_{b\,i,\left(\sum_{j=I}^{IV} n_j\right)}\Big|_{x^*=1} = C^0_{b\,i,1} \tag{2.50}$$

$$k = 2:\ \ C_{b\,i,1}\Big|_{x^*=1} = \frac{u_I^*}{u_{IV}^*} C^0_{b\,i,2} - \frac{u_E}{u_{IV}^*} C_i^E \tag{2.51}$$

$$k = 3\ to\ (n_I + n_{II} + 1):\ \ C_{b\,i,(k-1)}\Big|_{x^*=1} = C^0_{b\,i,k} \tag{2.52}$$

$$k = (n_I + n_{II} + 2):\ \ C_{b\,i,(n_I+n_{II}+1)}\Big|_{x^*=1} = \frac{u_{III}^*}{u_{II}^*} C^0_{b\,i,(n_I+n_{II}+2)} - \frac{u_F}{u_{II}^*} C_i^F \tag{2.53}$$

$$k = (n_I + n_{II} + 3)\ to\ \left(\sum_{j=I}^{IV} n_j\right):\ \ C_{b_{i,(k-1)}}\Big|_{x^*=1} = C^0_{b\,i,k} \tag{2.54}$$

Considering now $x^* = \frac{z}{L_c}$. This set of equations continues to progress in a similar way (shifting one column per t_s), until $\theta = \sum_{j=I}^{IV} n_j$, repeating then from the first switch.

As for the TMB model approach, also the Detailed Particle Model and LDF approach can be used in this modelling strategy, and thus becoming:

i. Detailed Particle Model

The two sets of transient mass balances are now performed to each species i in each column k, and thus for a volume element in the bulk fluid becomes:

$$\frac{\partial C_{b\,i,k}}{\partial \theta} = \gamma_j^* \left\{ \frac{1}{Pe_k^*} \frac{\partial^2 C_{b\,i,k}}{\partial x^{*2}} - \frac{\partial C_{b\,i,k}}{\partial x^*} - \frac{(1-\varepsilon_b)}{\varepsilon_b} N^*{}_{f\,i,k} \left(C_{b\,i,k} - C_{p\,i,k}\Big|_{\rho=1} \right) \right\} \tag{2.55}$$

to a volume element of the spherical particle:

$$\frac{\partial C_{s\,i,k}}{\partial \theta} + \varepsilon_p \frac{\partial C_{p\,i,k}}{\partial \theta} = \gamma_j^* \left\{ N_{p\,i,k} \frac{1}{\rho^2} \frac{\partial}{\partial \rho} \left(\rho^2 \frac{\partial C_{p\,i,k}}{\partial \rho} \right) \right\} \tag{2.56}$$

with the respective initial conditions:

$$\theta = 0:\ \ C_{b\,i,k}(x^*, 0) = C_{p\,i,k}(x^*, \rho, 0) = 0 \tag{2.57 a,b}$$

and boundary conditions:

$$x^* = 0:\ \ C^0_{b\,i,k} = C_{b\,i,k}\Big|_{x^*=0} - \frac{1}{Pe_k^*} \frac{\partial C_{b\,i,k}}{\partial x^*}\Big|_{x^*=0} \tag{2.58}$$

$$x^* = 1:\ \ \frac{\partial C_{b\,i,k}}{\partial x^*}\Big|_{x^*=1} = 0 \tag{2.59}$$

$$\rho = 0: \quad \left.\frac{\partial C_{p_{i,k}}}{\partial \rho}\right|_{\rho=0} = 0 \tag{2.60}$$

$$\rho = 1: \quad \left.\frac{\partial C_{p_{i,k}}}{\partial \rho}\right|_{\rho=1} = Bi_{mi,k}{}^{*}\left(C_{b\,i,k} - \left.C_{p_{i,k}}\right|_{\rho=1}\right) \tag{2.61}$$

plus the adsorption equilibrium isotherms,

$$C_{s_{i,k}} = f\left(C_{p_{i,k}}\right) \tag{2.62}$$

where $\gamma_j^* = \frac{u_j^*}{u_s}$ the ratio between SMB fluid and the TMB solid interstitial velocities, $Pe_k^* = \frac{u_j^* L_c}{D_{b_k}}$ the column k Peclet number; $N_{f_{i,k}} = \frac{3k_{f_{i,k}}}{r_p} t_k$ the number of film mass transfer units and $t_k = \frac{L_c}{u_j^*}$ the fluid phase space time; $N_{p_{i,k}} = \frac{D_{pe_i}}{{r_p}^2} t_k$ the number of intraparticle mass transfer units, with D_{pe_i} the i species effective diffusion coefficient and $Bi_{mi,k} = \frac{k_{f_i} r_p}{D_{pe_i}} = \frac{1}{3}\frac{N_{f_{i,k}}}{N_{p_{i,k}}}$ the Biot number.

ii. Linear Driving Force (LDF) Approach

The LDF approximation can be obtained from $\alpha_{i,k} = \left(\frac{r_p}{3k_{f_i}} + \frac{{r_p}^2}{\varphi D_{pe_i} H_i}\right)^{-1} t_k = k_{LDF} t_k$, with φ a coefficient between 10 and 15, and thus obtaining for the bulk fluid mass balance:

$$\frac{\partial C_{b_{i,k}}}{\partial \theta} = \gamma_j^* \left\{\frac{1}{Pe_k^*}\frac{\partial^2 C_{b_{i,k}}}{\partial {x^*}^2} - \frac{\partial C_{b_{i,k}}}{\partial x^*} - \frac{(1-\varepsilon_b)}{\varepsilon_b}\alpha_{i,k}\left(q_{i,k}^{eq} - \langle q_{i,k}\rangle\right)\right\} \tag{2.63}$$

and for the mass balance in the particle,

$$\frac{\partial \langle q_{i,k}\rangle}{\partial \theta} = \gamma_j^* \alpha_{i,k}\left(q_{i,k}^{eq} - \langle q_{i,k}\rangle\right) \tag{2.64}$$

with the respective initial:

$$\theta = 0: \quad C_{b\,i,k}(x^*, 0) = \langle q_{i,k}(x^*, 0)\rangle = 0 \tag{2.65 a,b}$$

and boundary conditions:

$$x^* = 0: \quad C_{b\,i,k}^0 = \left.C_{b\,i,k}\right|_{x^*=0} - \frac{1}{Pe_j}\left.\frac{\partial C_{b_{i,k}}}{\partial x^*}\right|_{x^*=0} \tag{2.66}$$

$$x^* = 1: \quad \left.\frac{\partial C_{b_{i,k}}}{\partial x^*}\right|_{x^*=1} = 0 \tag{2.67}$$

where the adsorption equilibrium isotherm is:

$$q_{i,k}^{eq} = f\left(C_{b\,i,k}\right) \tag{2.68}$$

As a consequence one obtains discontinuous solutions, reaching not a continuous Steady State (SS) but a Cyclic Steady State (CSS).

By applying the SMB model approach, both the Detailed Particle as LDF strategies, to the system described by eqs. (2.38-2.41), and the SMB unit and operating conditions presented in Table 2.1 and Table 2.2, one obtains the CSS concentration profiles over a complete switching time, Figure 2.10.

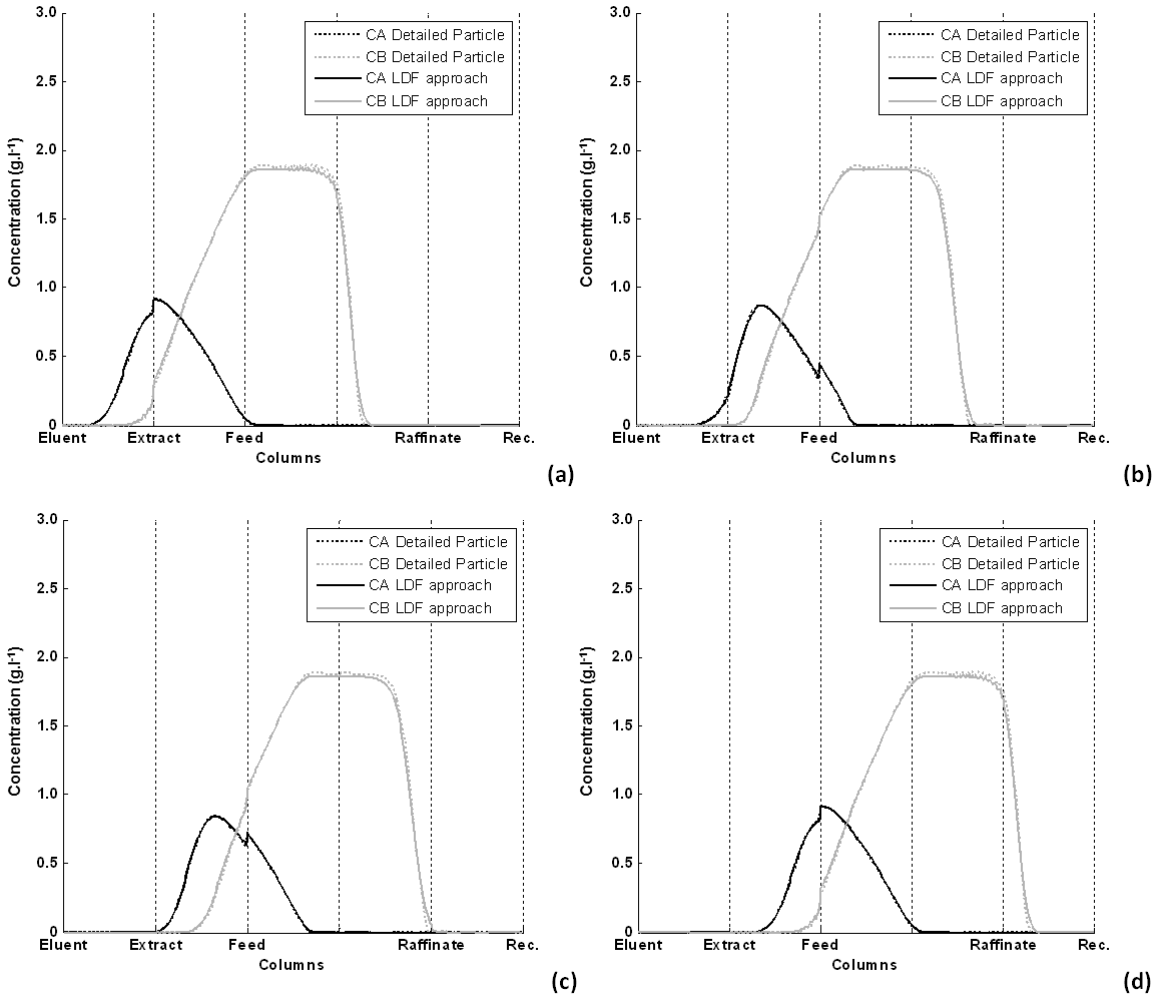

Figure 2.10 - Evolution of the bulk concentration profiles for the separation of a racemic mixture of chiral epoxide at the beginning (a), at one third (b), two thirds (c) and at the end of a switching time period (d); obtained for detailed particle and LDF approaches by means of the SMB model strategy at the Cyclic Steady State, adapted from Sá Gomes *et al.*, (2007b).

Once again, and for this system, the difference from the Detailed Particle and LDF approaches is negligible. The concentration history in the extract and raffinate outlets until the CSS is shown in Figure 2.11.

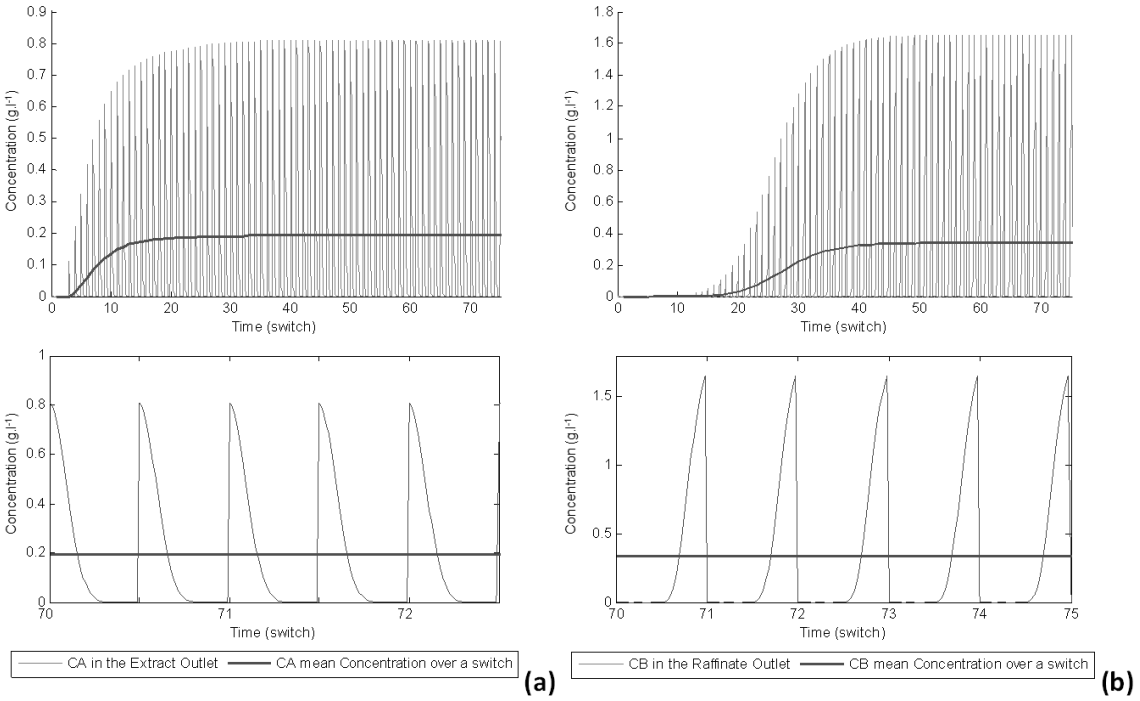

Figure 2.11 - Evolution of the bulk concentration profiles for [1 1 2 1] real SMB (a) C_{b_A} in the extract and (b) C_{b_B} in the raffinate outlet currents.

Comparing the average concentration in the extract and raffinate ports, at the CSS, from the SMB and the extract and raffinate SS concentration from the TMB model approach, Figure 2.12.

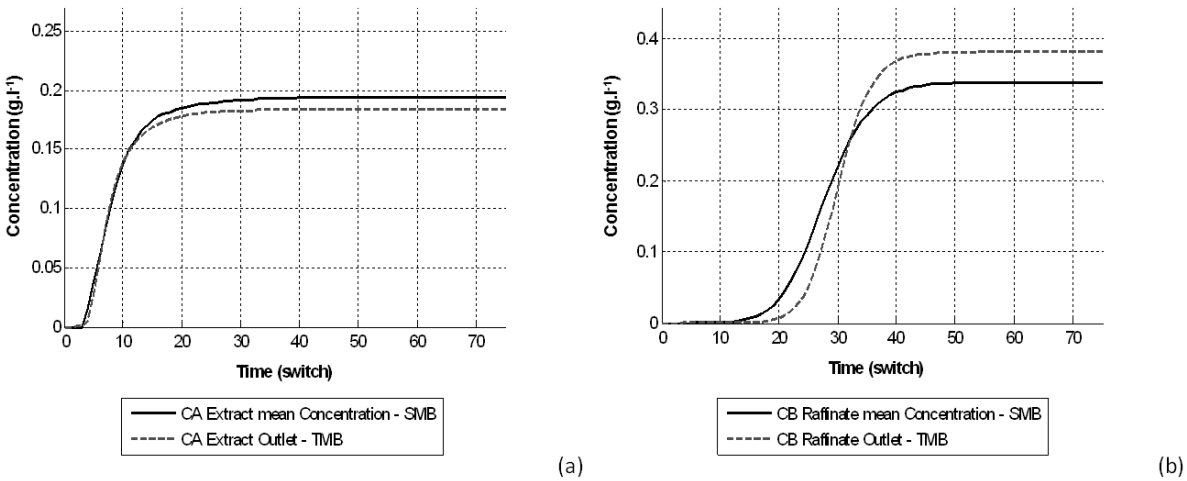

Figure 2.12 - Concentration profiles in the extract (a) and raffinate (b) outlets, SMB versus TMB, both LDF approach.

From Figure 2.11 and 2.12, it can be justified the observation stated before, that even thought being faster (computational calculation time), the TMB model approach will just give reasonable results if a considerable number of columns per section is present. In this thesis scope, the influence of TMB and SMB modelling

approach was also detailed for the multicomponent separations by means of the Pseudo-SMB mode of operation. In this particular case, it is shown that, and apart from the TMB and SMB model differences noted in the case cited before, the TMB model approach can lead to confusing results related with the cleavage of the switching time period that can be observed in the Pseudo-SMB mode of operation, *i.e.*, when the ratio between the Step 2 period and the switching time period is not an integer. These aspects are detailed in Annex I.

2.3.2 PERFORMANCE PARAMETERS

The performance of the SMB unit for a given separation is usually characterized by the following parameters: purity, recovery, productivity per the amount adsorbent volume and eluent/desorbent consumption per mass of treated product. The definitions of all these performance parameters, for the case of a binary mixture, are given bellow:

Purity (%) of the more retained (A) species in extract and the less retained one (B) in the raffinate stream, over a complete cycle (from θ to $\theta + \sum_{j=I}^{IV} n_j$):

$$PU_X = \frac{\int_{\theta}^{\theta+\sum_{j=I}^{IV} n_j} C_A^X d\theta}{\int_{\theta}^{\theta+\sum_{j=I}^{IV} n_j} C_A^X d\theta + \int_{\theta}^{\theta+\sum_{j=I}^{IV} n_j} C_B^X d\theta} \tag{2.69}$$

$$PU_R = \frac{\int_{t}^{\theta+\sum_{j=I}^{IV} n_j} C_B^R d\theta}{\int_{\theta}^{\theta+\sum_{j=I}^{IV} n_j} C_A^R d\theta + \int_{\theta}^{\theta+\sum_{j=I}^{IV} n_j} C_B^R d\theta} \tag{2.70}$$

Recovery (%) of more retained (A) species in extract and the less retained one (B) in raffinate stream, again over a complete cycle:

$$RE_X = \frac{\int_{\theta}^{\theta+\sum_{j=I}^{IV} n_j} C_A^X d\theta . Q_X}{\sum_{j=I}^{IV} n_j Q_F C_A^F} \tag{2.71}$$

$$RE_R = \frac{\int_{\theta}^{\theta+\sum_{j=I}^{IV} n_j} C_B^R d\theta . Q_R}{\sum_{j=I}^{IV} n_j Q_F C_B^F} \tag{2.72}$$

the productivity per total volume of adsorbent $\left(\frac{\text{g}}{\text{l}_{adsorbent}\text{day}}\right)$:

$$PR_X = \frac{\int_{\theta}^{\theta+\sum_{j=I}^{IV} n_j} C_A^X d\theta . Q_X}{\left(\sum_{j=I}^{IV} n_j\right)^2 V_c(1-\varepsilon_b)} = \frac{RE_X Q_F C_A^F}{V_c(1-\varepsilon_b)\sum_{j=I}^{IV} n_j} \tag{2.73}$$

$$PR_R = \frac{\int_{\theta}^{\theta+\sum_{j=I}^{IV} n_j} C_B^R d\theta . Q_X}{\left(\sum_{j=I}^{IV} n_j\right)^2 V_c(1-\varepsilon_b)} = \frac{RE_R Q_F C_B^F}{V_c(1-\varepsilon_b)\sum_{j=I}^{IV} n_j} \tag{2.74}$$

the eluent/desorbent consumption $\left(\frac{l_{Eluent/Desorbent}}{g_{pure\ product}}\right)$:

$$EC = \frac{Q_E + Q_F}{Q_F\left(C_A^F + C_B^F\right)} \tag{2.75}$$

These parameters hold for both SMB and TMB model approaches; nevertheless, one can simplify: in the SMB model strategy the same equations can be stated for a switching time period (from θ to $\theta + 1$) if the unit is symmetrical, *i.e.*, there are no differences between each switching time period (either due to the implementation of non conventional modes of operation, or to the use of more detailed models accounting for dead volumes or switching time asymmetries); in the TMB model approach there is no need of the integral calculation, since the solutions from this model strategy are continuous and thus, the performance parameters constant over the time (at the steady state).

2.3.3 DESIGN STRATEGIES

The design of an SMB separation involves taking decisions at many levels, from the configuration of the unit (number of columns per section, column and particle size) to operating conditions (feed concentration, switching time, internal flow rates). Although simulation work can be exhaustively done until the right combination of parameters is found for the expected performance, it is useful to have a design method that will provide a preliminary estimation of the optimum operating point, followed by simulation and/or optimization, (Sá Gomes *et al.*, 2009a).

Once again, the equivalence between TMB and SMB can be quite useful. Recalling the role of each section, one can write some constraints that will limit the feasible region and allow a complete separation (recover of the more retained species (A) in the extract stream and the less retained one (B) in the raffinate port, Figure 2.6c). Consequently, one can set net fluxes for each component in every of the four sections so that: the more retained species is directed upwards in section I (providing the solid regeneration); in sections II and III the species movement is downwards for the more retained and upwards for the less retained; and in section IV the species movement is with the solid, *i.e.*, downwards for the less retained species, cleaning the eluent to be recycled. These conditions will lead to a set of flow rates constraints that will identify the separation region (section II and III) as well as the regeneration one (section I and IV).

$$\frac{Q_I}{Q_s} > \frac{\langle q_{A,I}\rangle}{C_{b_{A,I}}} \tag{2.76}$$

$$\frac{\langle q_{A,II}\rangle}{C_{b_{A,II}}} > \frac{Q_{II}}{Q_s} > \frac{\langle q_{B,II}\rangle}{C_{b_{B,II}}} \tag{2.77}$$

$$\frac{\langle q_{A,III}\rangle}{C_{b_{A,III}}} > \frac{Q_{III}}{Q_s} > \frac{\langle q_{B,III}\rangle}{C_{b_{B,III}}} \tag{2.78}$$

$$\frac{Q_{IV}}{Q_s} < \frac{\langle q_{B,IV}\rangle}{C_{b_{B,IV}}} \tag{2.79}$$

Where Q_s represents the solid flow rate, $\langle q_{i,j} \rangle$ the average solid concentration of species i in section j and $C_{b_{i,j}}$ the bulk fluid concentration of species i in section j.

Usually the fluid and solid velocities in each section are combined into one only operating parameter, such as the $m_j = \frac{Q_j}{Q_s}$ from Morbidelli and his co-workers or the $\gamma_j = \frac{(1-\varepsilon_b)}{\varepsilon_b}\frac{Q_j}{Q_s}$, as used by Ruthven (1989). The identification of constraints, eq. (2.76) to eq. (2.79), led to the appearance of several design methods, which are usually approximated and/or graphical, providing a better insight into the possible operating regions. From the plates theory and McCabe-Thiele diagrams (Ruthven and Ching, 1989); analytical solutions for a linear adsorption isotherms system in presence of mass transfer resistances (Silva *et al.*, 2004); to the determination of waves velocities as in the Standing Wave Design (SWD) methodology* (Ma and Wang, 1997; Mallmann *et al.*, 1998; Xie *et al.*, 2000; Xie *et al.*, 2002; Lee *et al.*, 2005). A particular emphasis should be given to the strategy developed for binary and multicomponent separations modelled by linear and non linear isotherms as in (Storti *et al.*, 1989b; Storti *et al.*, 1993; Mazzotti *et al.*, 1994; Storti *et al.*, 1995; Mazzotti *et al.*, 1996c; Mazzotti *et al.*, 1997b; Chiang, 1998; Migliorini *et al.*, 2000; Mazzotti, 2006b), the so-called "Triangle Theory", where the term $\frac{\langle q_{i,j} \rangle}{C_{b_{i,j}}}$ is treated by assuming that the adsorption equilibrium is established everywhere at every time (Equilibrium Theory†, (Helfferich, 1967; Klein *et al.*, 1967; Tondeur and Klein, 1967; Helfferich and Klein, 1970), resulting in a feasible separation region formed by the above constraints (2.77) and (2.78), which in the case of linear isotherms takes the shape of a right triangle in the $(\gamma_{II} \times \gamma_{III})$ plane, Figure 2.13, (or a triangle shaped form with rounded lines in non linear isotherms case), and a rectangular shape in the $(\gamma_I \times \gamma_{IV})$ plane.

Recently, this methodology was also extended for the design of SMB units under reduced purity requirements, in which the separation triangle boundaries are stretched to account for different extract and/or raffinate purities (Kaspereit *et al.*, 2007; Rajendran, 2008).

Nevertheless, the inclusion of mass transfer resistances and non-linear equilibrium can deeply affect the result of the design. By taking into account all mass transfer resistances, and running successive simulations, it is possible obtain more detailed separation/regeneration regions, as well as the separation study carried out for three different sections (II, III and I) or (II, III and IV) allowing the analysis of solvent consumption or solid recycling, as proposed in the "Separation Volume" methodology, (Azevedo and Rodrigues, 1999; Rodrigues and Pais, 2004a), or the influence of the solid flow rate in the separation region (Zabka *et al.*, 2008a).

* SWD, where the flow rate in a given zone is chosen so that a given key concentration wave (boundary of a solute band) in a given zone migrates at the same speed as the ports, as result, all band boundaries, or waves, remain stopped (standing) with respect to the ports;

† the "Equilibrium Theory", in fact, is based on the assumptions of local equilibrium at any time and at all points of the exchanger bed; absence of hydrodynamic mixing and diffusion in the flow direction; homogeneity of the bed; and absence of secondary processes, such as neutralization, weak acid or weak-base formation in the fluid phase, complex formation, or precipitation, (Klein *et al.*, 1967).

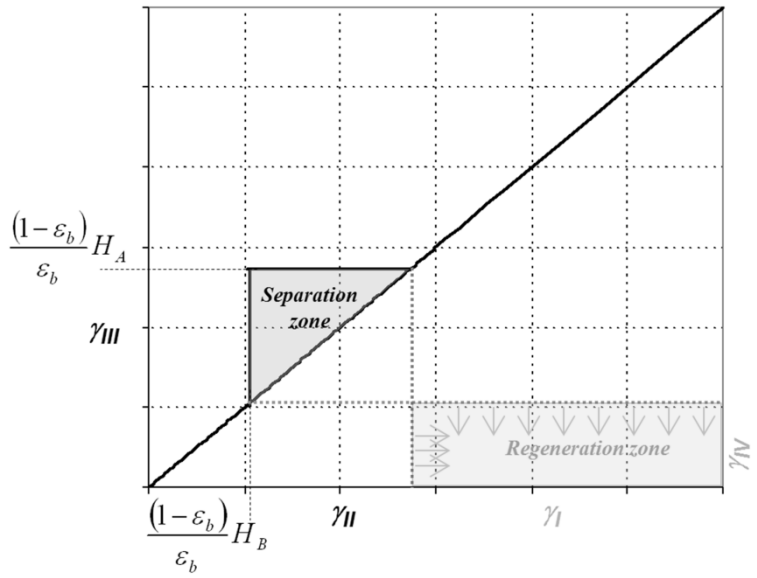

Figure 2.13 – "Triangle Theory", separation and regeneration regions for linear isotherms, where H_i represents the Henry constant for linear adsorptions isotherms (A: the more retained and B: the less retained species), (Sá Gomes *et al.*, 2006c).

The same procedure (methodical simulation of several operating conditions accounting for mass transfer resistances), can also be used to obtain a separation region surface for different purity requirements, accounting for mass transfer resistances as well, Figure 2.14.

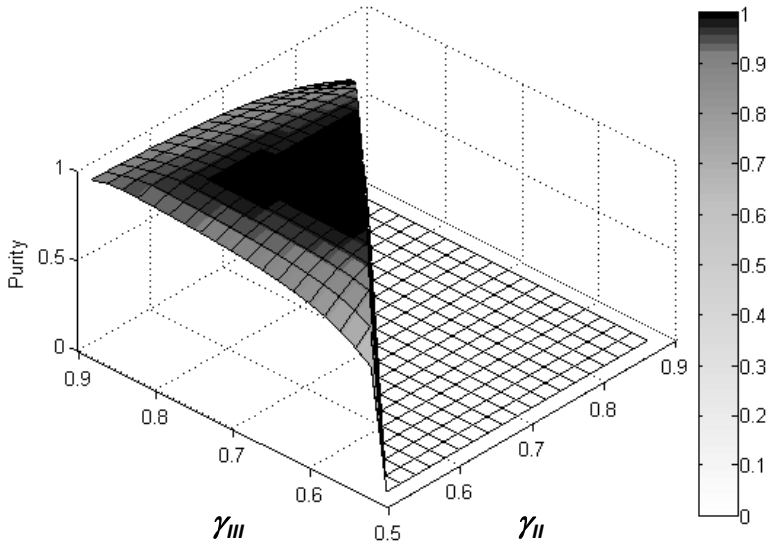

Figure 2.14 – Separation region for linear isotherms in presence of mass transfer resistances, (Sá Gomes *et al.*, 2006c).

Similar to what is presented by the equilibrium based assumptions for the design of SMB under reduce purity requirements, also this approach demonstrates larger triangles for reduced purity values.

2.3.4 OPTIMIZATION

The design strategies mentioned before can be quite useful for *a priori* selection of the SMB operating conditions, as well as good starting points for more extensive optimization procedures.

Usually one can classify the optimization of SMB units according to 3 different criteria: (i) the number of objective functions; (ii) the type of the objective functions; (iii) optimization of a new or an already existing SMB unit (only optimization of the operating parameters). Taking into account the number of objective functions, the optimization problems can be considered as single-objective or multiple-objective. In the case of multiple-objective optimization a global optimum may not exist; there is a possibility of an entire set of optimal solutions that are equally good, the so-called Pareto Optimal Solutions. As for the type of the objective functions two main cases can be considered: (i) performance parameters (productivity, adsorbent requirements or desorbent/eluent consumption for given purities and/or recovery requirements); (ii) based on the separation cost. In the case (i) each objective function can lead to a different optimum solution; therefore a multi-objective functions procedure should be considered as in Minceva and Rodrigues (2005); in the second case (ii) all those different performance parameters can be homogenized/normalized by the separation cost, where separation independent costs (wages, labour, maintenance, among others) and the separation dependent costs (adsorbent, plant, desorbent/eluent consumption, desorbent/eluent recycling, feed losses...) are taken into account and weighted by cost factors, which some times are quite difficult to characterize (Jupke *et al.*, 2002; Chan *et al.*, 2008).

To solve these problems, the use of powerful optimization algorithms, such as: IPOPT (Interior Point OPTimizer, (Wachter and Biegler, 2006), employed for liquid as gas phase SMB separations (Kawajiri and Biegler, 2006b, 2006a; Mota *et al.*, 2007a; Mota and Esteves, 2007; Rodrigues *et al.*, 2007b; Kawajiri and Biegler, 2008a, 2008b); the commercial package gOPT from gPROMS (Process System Enterprise, London, UK) with a Single (or Multiple) Shooting-Control Vector Parameterisation, used in the two level optimization of a existing Parex® unit (Minceva and Rodrigues, 2005), for ageing analysis (Sá Gomes *et al.*, 2008b) and gas phase separation of propane/propylene (Sá Gomes *et al.*, 2009a) or for optimal economic design (Chan *et al.*, 2008); the Non-dominated Sorting Genetic Algorithm (NSGA) or the Jumping Gene based algorithms (Deb, 2001), such as NSGA-II-JG, applied by several groups to optimize SMB units, from *p*-xylene to chiral separations (Zhang *et al.*, ; Zhang *et al.*, 2002a; Subramani *et al.*, 2003b; Zhang *et al.*, 2003a; Wongso *et al.*, 2004; Kurup *et al.*, 2005; Wongso *et al.*, 2005; Kurup *et al.*, 2006b; Paredes and Mazzotti, 2007; Lee *et al.*, 2008; Mun and Wang, 2008b), is recurrent, either in the refinement of the design strategies mentioned before, or as a diagnosis method (such as the use of superstructures SMB considering several hypothetic inlet/outlet recycles), allowing the identification of new SMB configurations or modes of operation.

2.3.5 OPERATION

There are several common deviations that "real" SMB units present when compared with ones described by the more commonly used models. Among these deviation one can list: uncertainty in the equilibrium isotherm data, kinetic data (diffusion and axial dispersion coefficients) and bed voidage (packing asymmetries), as well as, extra column dead volumes (tubing, equipment, asymmetries); variation in port velocity (solid velocity,

asymmetries); fluctuations in pump flow rates (fluid inlets, outlets and internal) (Azevedo *et al.*, 1998; Mun *et al.*, 2006).

At the industrial-scale SMB units, the relative volume of the connection lines is not as significant as for pilot or lab-scale units; nevertheless, it has been studied in detail and different techniques are applied to overcome the associated negative impacts. For instance, the UOP technique for flushing of the transfer lines before withdrawing the extract, applied in Parex process/(industrial scale SMB unit for *p*-xylene separation), was previously analyzed (Minceva and Rodrigues, 2003). In pilot or lab-scale SMB units, the relative volume associated with equipment and transfer lines is indeed an issue and therefore it has to be taken into account even before unit's design and construction, as well as along its operation. Usually this type of units are designed to account for it in its own operation mode, and thus compensating it (Hotier and Nicoud, 1996; Blehaut and Nicoud, 1998), or extended design methodologies are used to account for it during the design procedure (Migliorini *et al.*, 1999b; Mun *et al.*, 2003b). Nevertheless, these are still proxies to the use of more detailed models and some differences are noted. A detailed model accounting for equipment dead volumes, tubing connections and switching time asymmetries or delays, was developed to model a lab-scale (FlexSMB-LSRE®) and a pilot-scale (Licosep 12-26) units and then used to compare dead volumes design and compensating strategies (Zabka *et al.*, 2008b; Sá Gomes *et al.*, 2009b), and will be later referred in Chapter 6.

Adsorbent/Catalyst deactivation (or ageing) has been subject of several studies in the reactive/separation engineering field. However, regarding the SMB technology, this issue remains restricted to the plant operators and technology owners and usually is only treated as a disturbance and compensated applying SMB online controllers. In SMBs separations the adsorbent decline also takes place in different time scales; for example a chiral separation is known to work at reasonable efficiency for 3 to 5 years while in *p*-xylene separation a 20-30% adsorbent capacity decline occurs during a 10 to 20 years period (Minceva and Rodrigues, 2002). The idea of working near to the best operation point (near to the vertex and to the Lower Solvent Consumption point) and adjust this location with the adsorbent deactivation, trying to keep it at the same relative distance, is attractive as an adsorbent ageing corrective action. This aspect was studied by Sá Gomes *et al.*, (Sá Gomes *et al.*, 2007d, 2008b) and will be detailed later in Chapter 4.

In recent years the control of SMB units has also been wide investigated (Erdem *et al.*, 2004b; Engell, 2007; Grossmann *et al.*, 2008a; Grossmann *et al.*, 2008b). Several reports on dynamic control strategies include nonlinear control strategies such as: the input-output linearizing control, where the controller action is based on a nonlinear state estimator using the TMB model (Kloppenburg and Gilles, 1999a); and model predictive control (MPC) (Natarajan and Lee, 2000; Erdem *et al.*, 2004a; Dietz and Corriou, 2008); or design on the basis of neural networks (Wang *et al.*, 2003). Also a model based SMB control where an optimal trajectory is calculated off-line was proposed by (Klatt *et al.*, 2000; Klatt *et al.*, 2002) and from wave reconstruction (Kleinert and Lunze, 2008). A more recent strategy based on the nonlinear wave propagation phenomena aims to control the central sections of the SMB unit by controlling the position of the concentration fronts (Schramm *et al.*, 2003a). The control of chromatographic processes (SMB included) by means of the standard control procedures (P, PI or PID

controllers*), but detecting characteristic points of the unit where the history of a specific variable of the fractions of the mixture to be separated will be representative for the control action was also addressed (Valery and Morey, 2009).

2.4 SMB APPLICATIONS: "OLD" AND "NEW"

Industrially, SMB applications can be regarded as "Old" and "New", associated with petrochemical and pharmaceutical/fine chemistry fields, respectively (Sá Gomes *et al.*, 2006c). Among the first applications of SMB technology (back to 1960s) are the ones implemented by the UOP Inc. (Des Plaines, IL-USA) with the Sorbex® processes (Figure 2.15), such as: the Parex® unit for separation of *p*-xylene from mixtures with its C_8-isomers (Broughton *et al.*, 1970), separation also performed by the Aromax® process from Toray Industries (Tokyo, Japan) (Otani *et al.*, 1973) and the Eluxyl® process by Axens/IFP (Institut Français du Pétrole, France) (Ash *et al.*, 1994); the Ebex® for the separation of EthylBenzene (EB) from a mixed of C_8-aromatic isomers (Broughton, 1981); the Molex® for the separation of *n*-paraffins from branched and cyclic hydrocarbons; and the Olex® process to separate olefins from parafins; the Cresex® and Cymex® for the separation of *p*-cresol and *p*-cymene from its isomers, respectively.

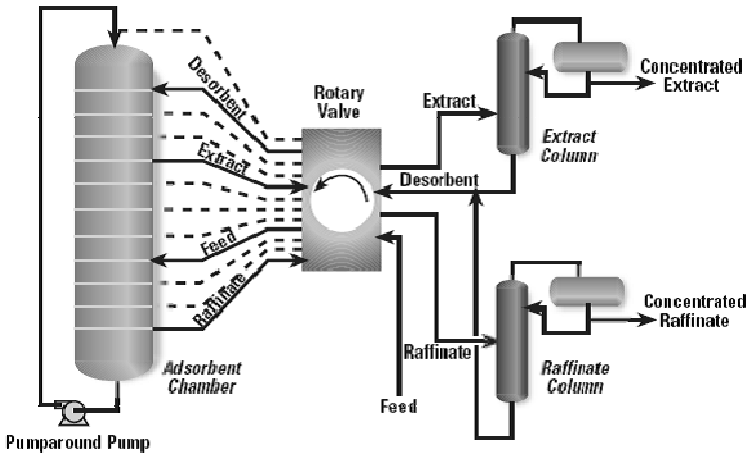

Figure 2.15 – The Sorbex® process (adapted from www.uop.com, 2006).

The application of SMBs in the sugar industry is also substantial, with the Sarex® process, for the separation of fructose from the corn syrup with dextrose and polysaccharides on polystyrene-divinylbenzene resins in calcium form (Broughton, 1983); or as patented by Japan Organo Co. (Japan), (Heikkilä *et al.*, 1989); by Amalgamated Sugar Company LLC, also known as the Snake River Sugar Company (Boise, ID-USA), (Kearney and Mumm, 1990).

With the development of HPLC processes for the preparative separation of fine chemicals in the earlier 70s, smaller stationary phase particles (10 to 40 m), shorter columns operating at higher pressure started to be used. Consequently, chromatographic processes became an interesting form to the pharmaceutical industry meet the product purities constraints imposed by the pharmaceutical and food regulatory organizations. However, and as

* P: proportional; I: integral and D: derivative controllers.

mentioned before, the batch preparative chromatography presents considerable limitations of dilution and thus achieves quite low productivity values.

In the last decade, particularly in the area of drug development, the advent of SMB has provided a high throughput, high yield, solvent efficient, safe and cost effective process option. Although it had long been established as a viable, practical, and cost-effective liquid-phase adsorptive separation technique, the pharmaceutical and biomolecule separations community did not show considerable interest in SMB technology until the mid-1990s. The application of the SMB concept to the fine chemical separations in the earlier 90s, led to the second "boom" on the SMB technology (Negawa and Shoji, 1992; Nicoud *et al.*, 1993; Kusters *et al.*, 1995; Rodrigues *et al.*, 1995; Cavoy *et al.*, 1997; Francotte and Richert, 1997; Guest, 1997; Pais *et al.*, 1997a; Pais *et al.*, 1997b; Francotte *et al.*, 1998; Grill and Miller, 1998; Lehoucq *et al.*, 1998; Pais *et al.*, 1998; Dapremont *et al.*, 1999; Miller *et al.*, 1999; Nagamatsu *et al.*, 1999; Nicoud, 1999a, 1999b; Pedeferri *et al.*, 1999; Strube *et al.*, 1999; Juza *et al.*, 2000; Kniep *et al.*, 2000; Wang *et al.*, 2001), as shown by the number of publications concerning chiral separations, Figure 2.16.

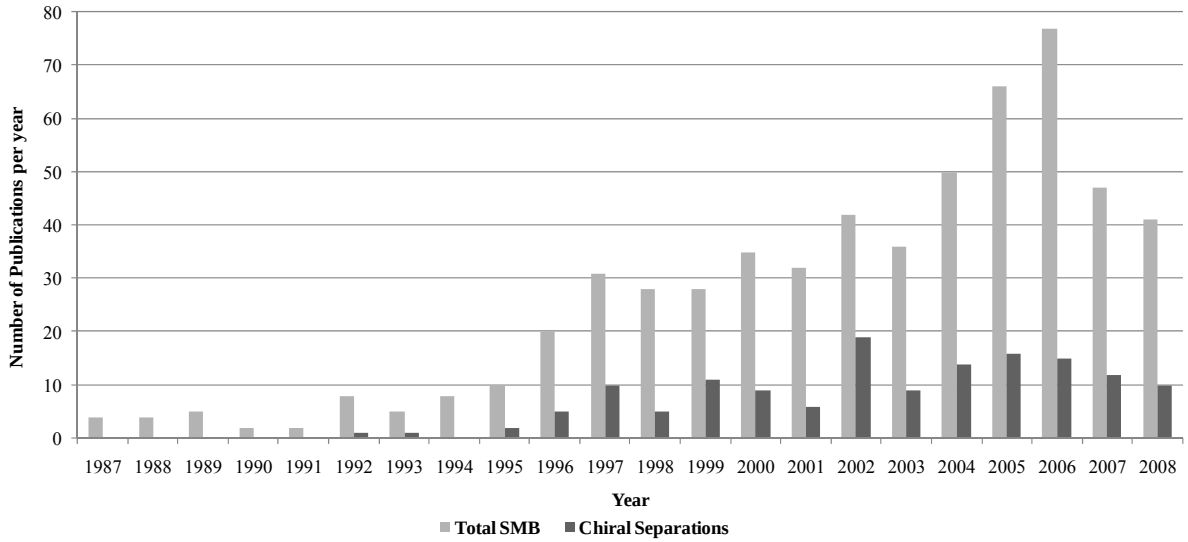

Figure 2.16 - Publications regarding SMB applications over the past 20 years (2008 incomplete).

In 1992, Daicel Chemical Industries, Ltd (Japan) first published the resolution of optical isomers through SMB (Negawa and Shoji, 1992). Since that time, a considerable number of articles, patents and books on the application of SMB to pharmaceutically important compounds have been published, and already approved by the Food and Drug Administration (FDA) for some Active Principle Ingredient (API) production. Several are the separations already running including renowned products such as: Biltricide (Praziquantel) Cipralex/Lexapro (Escitalopram), Keppra (Levetiracetam), Modafinil/Provigil, Taxol (Paclitaxel), Xyzal (Levocetirizine), Zoloft (Sertraline), Zyrtec (Cetirizine), Celexa/Citrol/Cipram (Citalopram), Prozac (Fluoxetine hydrochloride) and insulin among others (Abel and Juza, 2007); which shows how important SMB technology is for the fine chemical field.

From the drugs cited above, most are chiral. Many chiral drugs are produced as a 50-50 % mixture of the two enantiomers, the racemate. The problem is that those two enantiomers can often have different biological activity. Therefore, it becomes important the separation of the target isomer from the other that can be inactive or

have an adverse effect. There are two different approaches to obtain pure enantiomers compounds: (a) preparing the racemic material and then the separation or (b) asymmetric synthesis of the target enantiomer. The second approach has been widely used; nevertheless, the number of stages and the cost of all enantiomeric reagents needed would decrease the economical benefits and therefore the separation of racemate performed by SMB technology is attractive. The first approach will take months while the second 2-5 years, if not more. But SMB is not limited to chiral separations. Any separation that can be turned into a binary separation is potentially an excellent candidate for SMB. Removal of troublesome impurities by SMB is a good example. Troublesome impurities are closely related to the main product or are dimers or trimers of the product and are very difficult to remove. Sometimes multiple crystallizations are required to meet the final product specifications. Ron Bates from Bristol-Myers Squibb states in 2004 that when HPLC separation costs 100 USD.kg^{-1} to 5000 USD.kg^{-1} the SMB makes it from 50 USD.kg^{-1} to 200 USD.kg^{-1}. Novasep S.A. and Knauer GmbH (Berlin, Germany) are among the more prominent equipment suppliers for SMB separation of fine chemical. Novasep equiped various renowned companies such as UCB Pharma (Belgium), Lundbeck Pharmaceuticals Limited, (UK subsidiary of H. Lundbeck A/S of Denmark), AMPAC Fine Chemicals (USA) and Merck KGaA (Darmstadt, Germany) among others. Knauer claims to have installed at least 16 units since 1998 in various Universities, institutes and companies around the world[*].

The scale is much smaller than that used in the petrochemical field. Some of the design as performance parameters are presented in Table 2.3, where it is interesting to note that some design parameters relations are the same in the "Old" and "New" SMB applications; for example the aspect ratio between column diameter and column high is roughly 10 (Sá Gomes *et al.*, 2006c), Table 2.3.

Table 2.3 - Comparison of "Old" and "New" SMB units, (Rodrigues, 2004).

	p-xylene Separation[†]	Chiral Separations
Number of columns N_c	24	6
Column length L_c (m)	1.0	0.1
Maximum column internal diameter d_c (m)	9.5	1.0
Particle radius r_p (x10^{-3} m)	0.30	0.01
Aspect ratio d_c/L_c	≈10	≈10
Productivity $\left(\frac{kg}{m^3_{adsorbent}h}\right)$	120	1-10
Adsorbent capacity $\left(\frac{kg}{m^3_{adsorbent}}\right)$	200	10

[*] Other companies that provides SMB units, or services related with SMB separations, should also be cited: the Semba Octave™ Chromatography System (www.sembabio.com); the MCSG*P*-process from ChromaCon AG (www.chromacon.biz); Organo Corp. (www.organo.co.jp); ISS-Integrated Separation Solutions (www.isepsol.com); www.xendo.nl; www.outotec.com, among others.

[†] The largest SMB single train plant in the world, installed in South Korea; an Eluxyl® unit constituted by 24 columns with 9.0 m of i.d., i.d., higher than 1 m and processing over 650 kton.year^{-1} of 99.9 % *p*-xylene purity.

It seems that there is still space to improve, the *p*-xylene separation units have about 10 to 100 times more productivity than the chiral drugs ones, reflect of 40 years of continuous development when compared with the "New" applications.

2.5 CONCLUSIONS

The use of continuous chromatographic counter current operation maximizes the mass transfer driving force, providing a better utilization of the adsorbent, which may have a rather low selectivity. In addition, the continuous counter current apparatus allows the reduction of solvent consumption, increases productivity and purity and provides less diluted product streams, when compared to conventional batch chromatography. This is contrary to batch chromatography where high resolution is vital in order to achieve high purity. Nevertheless, the actual circulation of the solid phase inside the column and the consequent recycle, presents some technical problems, namely: equipment abrasion, mechanical erosion of adsorbent, difficulties in maintaining plug flow for the solid. This clearly limits the implementation of such technologies. In order to avoid those issues, a sequence of fixed bed columns was conceived in which the solid phase does not move in relation to a fixed referential, but the relative movement between both fluid and solid streams is created by switching all the inlet and outlet fluid streams from time to time in the direction of the fluid flow, the Simulated Moving Bed (SMB) technology.

Industrially, SMB applications can be regarded as "Old" and "New", associated with petrochemical and pharmaceutical/fine chemistry fields, respectively. In the last decade, particularly in the area of drug development, the advent of SMB has provided a high throughput, high yield, solvent efficient, safe and cost effective process option. Since that time, a considerable number of articles, patents and books have been published referring new modelling design and operation techniques (new "non-conventional" SMB operating modes, such as asynchronous port movement and variable inlet or outlet flow rates) that extended further the potential of this technique.

After more than 40 years of developments and a new age in the last decade, the SMB appears as a key technology for chromatographic separations, applied in different fields as from the separation of sugars, desalting, chiral and proteins purification to the separation of important commodities.[*]

[*] A significant part of Chapter 2 was published on: Sá Gomes, P., M. Minceva and A. E. Rodrigues, "Simulated moving bed technology: Old and new." Adsorption 12(5-6), 375-392, (2006c).; Sá Gomes, P., M. Minceva, L. S. Pais and A. E. Rodrigues, "Advances in Simulated Moving Bed Chromatographic Separations." Chiral Separation Techniques (Third Edition). S. Dr. Ganapathy: 181-202, (2007a).; and presented in: Sá Gomes, P., M. Minceva and A. E. Rodrigues Modelling, Simulation and Optimisation of Cyclic Separation Processes. PSE annual meeting 2006. London, U.K., (2006a). and Sá Gomes, P., M. Zabka, V. M. T. Silva and A. E. Rodrigues Separation of Fine Chemical Species by Means of Continuous Chromatography: The Simulated Moving Bed Technology. AIChE Annual Meeting. Philadelphia – Pennsylvania USA, (2008d).

Chapter 3

OUTLET STREAMS SWING (OSS) SMB

3.1 INTRODUCTION

As mentioned in Chapter 2, the Simulated Moving Bed (SMB) technology experienced an emergent interest in the last decade, mainly related with its successful application to drugs resolution in the pharmaceutical, biotechnological and other fine chemical separation industries. This late demand on the SMB technique, directly linked to a considerable research effort, led to the formulation of quite different operation modes since the original patent. From these so-called non conventional operating strategies, which have been reviewed in detail in the previous Chapter, one will just emphasize those based in the periodic modulation of inlet/outlet streams flow rates, such as:

- the Partial-Feed, (Zang and Wankat, 2002a; Zang and Wankat, 2002b), in which the inlet feed flow rate varies along the time compensated by the raffinate flow rate; or in the limit, by varying all internal flow rates, the PowerFeed, (Kloppenburg and Gilles, 1999b; Zhang *et al.*, 2003b; Zhang *et al.*, 2004b; Kawajiri and Biegler, 2006b);
- the Partial-Discard (or partial Withdraw) (Zang and Wankat, 2002b; Bae and Lee, 2006), performed by a partial collection in the extract and/or raffinate streams; the fraction that has not been "collected" can be recycled back to the feed after a possible concentration step (Kessler and Seidel-Morgenstern, 2008; Seidel-Morgenstern *et al.*, 2008);
- the ISMB (Improved SMB) mode of operating, commercialized by the Nippon Rensui Co. (Tokyo, Japan), (Yoritome *et al.*, 1981, 1983), with two different stages: a first step, where the unit is operated as a

conventional SMB but without any flow in section IV; and in the second step, where the inlet and outlet ports are closed and the internal flow through the four sections allowing the concentration profiles to move to adjust their relative position with respect to the outlet ports (Rajendran *et al.*, 2009).

Considerable performances improvements have been noted by the application of such techniques; however, any refers to the possibility of varying the eluent/desorbent flow rate. While the partial feed strategy has been considerably studied over the time, resulting in significant productivity improvements, the analysis of a similar eluent/desorbent flow rate variation has not been so much addressed. Based in this statement, and also on the partial discard as ISMB techniques, a new operation technique was introduced under the scope of this thesis: the Outlet Streams Swing (OSS).

3.2 THE OSS *MODUS OPERANDI*

The SMB OSS mode of operation assumes that both extract and raffinate flow rates can vary over the time, but keeping the same operating parameters (for instance the SMB ratio between the interstitial fluid and solid velocities, $\gamma_j^* = \frac{(1-\varepsilon_b)}{\varepsilon_b}\frac{Q_j^*}{Q_s}$ or in the TMB model approach, $\gamma_j = \frac{(1-\varepsilon_b)}{\varepsilon_b}\frac{Q_j}{Q_s}$, with ε_b the bulk porosity), *i.e.*, the average section flow rates over a switching time period are the same as in a classic SMB. Section II and III do not suffer any changes over the time (are maintained at constant flow rates) and thus, the eluent/desorbent flow rate fluctuate to amortize the effect of extract or raffinate flow rate variations, a sort of "partial eluent" strategy.

To better explain the development of this new technique one should remind the equilibrium design constraints mentioned before ("Triangle Theory"), now in terms of the ratio between the interstitial fluid and solid velocities, as follows,

$$\gamma_I > \frac{(1-\varepsilon_b)}{\varepsilon_b}\frac{\langle n_{A,I}\rangle}{C_{b_{A,I}}} \tag{3.1}$$

$$\frac{(1-\varepsilon_b)}{\varepsilon_b}\frac{\langle n_{A,II}\rangle}{C_{b_{A,II}}} > \gamma_{II} > \frac{(1-\varepsilon_b)}{\varepsilon_b}\frac{\langle n_{B,II}\rangle}{C_{b_{B,II}}} \tag{3.2}$$

$$\frac{(1-\varepsilon_b)}{\varepsilon_b}\frac{\langle n_{A,III}\rangle}{C_{b_{A,III}}} > \gamma_{III} > \frac{(1-\varepsilon_b)}{\varepsilon_b}\frac{\langle n_{B,III}\rangle}{C_{b_{B,III}}} \tag{3.3}$$

$$\gamma_{IV} < \frac{(1-\varepsilon_b)}{\varepsilon_b}\frac{\langle n_{B,IV}\rangle}{C_{b_{B,IV}}} \tag{3.4}$$

where $\langle n_{i,j}\rangle$ the species i average solid concentration in section j and $C_{b_{i,j}}$ the species i fluid concentration in section j.

Considering the chromatographic resolution of a racemic mixture of chiral epoxide enantiomers (Sandoz Pharma, Basel, Switzerland), over microcrystalline cellulose triacetate (Merck, Darmstadt, Germany) with an average particle diameter of 45 μm, as chiral stationary phase and pure methanol as eluent.

The adsorption equilibrium isotherms were measured at 25 ºC and represented by the linear plus Langmuir competitive model in terms of retained concentration in the particles by Pais (1999; Rodrigues and Pais, 2004b), the same system as presented in Chapter 2:

$$q_{A,j}^{eq} = 1.35C_{b\,A,j} + \frac{7.32 \cdot 0.163 C_{b\,A,j}}{1+0.163C_{b\,A,j}+0.087C_{b\,B,j}} \tag{3.5}$$

$$q_{B,j}^{eq} = 1.35C_{b\,B,j} + \frac{7.32 \cdot 0.087 C_{b\,B,j}}{1+0.163C_{b\,A,j}+0.087C_{b\,B,j}} \tag{3.6}$$

with $q_{i,j}^{eq}$ in g.$\mathrm{l}^{-1}_{\mathrm{adsorbent}}$ and $C_{b\,i,j}$ in g.l^{-1}.

The model parameters and operating conditions were taken from Rodrigues and Pais (2004b), where the classic interstitial velocity ratios values for SMB or TMB model approaches (γ_j^* or γ_j) for sections I and IV were kept constant and far from the critical values for total solid and eluent regeneration ($\gamma_I > \gamma_I^{min} = 3.815$ and $\gamma_{IV} < \gamma_{IV}^{max} = 2.714$, according to the equilibrium theory).

For sections II and III, the interstitial velocity ratios values were obtained for the best purity values in extract and raffinate streams for a constant 1.5 ml.min^{-1} feed inlet, Figure 3.1, considering the mass transfer coefficient of k_{LDF} =0.33 s^{-1} and constant flow rates in section I and section IV, as in Table 3.1.

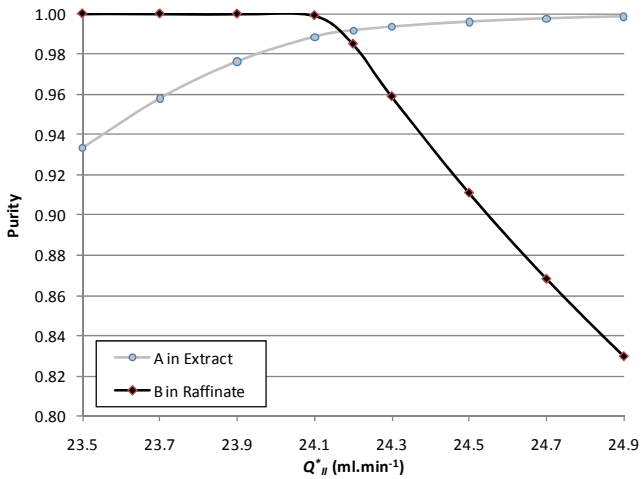

Figure 3.1 – Optimum operating point for t_S=198 s, Q_I^*=33.84 ml.min^{-1}, Q_{IV}^*=21.80 ml.min^{-1} and Q_F=1.50 ml.min^{-1}; values obtained using the SMB model with LDF approach, as mentioned in Chapter 2*.

By operating at higher or lower eluent consumption values it was found that, for the same feed flow rate, the purity value in both extract and raffinate streams was not improved. The full optimized unit, maximum purity,

* Again, the different model equations were numerically solved using the gPROMS v2.3.6 from Process Systems Enterprise (www.psenterprise.com), by applying the OCFEM (Orthogonal Collocation on Finite Elements) with 2 collocation points per element, 50 elements in each column for the axial coordinate. After the axial discretization step, the time integration is performed by the ordinary differential equation solver SRADAU a fully-implicit Runge-Kutta method that implements a variable time step, the resulting system is then solved by the gPROMS BDNSOL (Block decomposition NonLinear SOLver). An absolute and relative tolerance was set to 10^{-5}.

minimum solvent consumption (Q_E=8.37 ml.min^{-1}) for a given feed flow-rate (Q_F=1.50 ml.min^{-1}) presented similar purity values in both extract and raffinate streams as the hereafter called as classic SMB (PU_X=99.1% of A and PU_R=98.5 % of B). A summary of these operating conditions and model parameters is presented in Table 3.1 and Table 3.2.

Table 3.1 – SMB unit characteristics and model parameters.

Model Parameters	SMB Columns
Pe_c=1000	n_j=[2 2 2 2]
ε_b=0.4;	L_c=9.9 cm
r_p=2.25x10^{-5} m	d_c=2.6 cm
	Classic SMB Operating Conditions
k_{LDF}=0.33 s^{-1}	C_i^F=5 g.l^{-1}
	t_s=198 s;
	Q_E =12.04 ml.min^{-1}; Q_X =9.64 ml.min^{-1};
	Q_F =1.50 ml.min^{-1}; Q_R =3.90 ml.min^{-1};
	Q_{IV}^*=21.80 ml.min^{-1}.

Table 3.2 – Classic SMB and equivalent TMB section operating conditions.

Real SMB	Equivalent TMB
γ_j^*=[5.31 3.80 4.03 3.42]	γ_j =[4.31 2.80 3.03 2.42]
Q_j^*=[33.84 24.20 25.70 21.80] ml.min^{-1}	Q_j =[27.47 17.83 19.33 15.43] ml.min^{-1}
	Q_s =9.56 ml.min^{-1}

The OSS strategy will now be employed to extract and raffinate flow rates (altering section I and IV) at same time, in two different steps (within each switching time period): in the first step, while the A front in section I is expanding the B front in section IV is being contracted; during the second step when the B front in section IV is expanding the A front in section I is being contracted and *vice-versa*.

To induce the violation of constraint (3.4) and thus, B front expansion in section IV, the flux of the raffinate is decreased (at the same time the flow rate of extract is increased), leading to an increase of recycle flow at the end of section IV, recycled to section I (where the contraction of A front is happening). With the decrease of the extract flow rate (at the same time increase of the raffinate flow rate), the opposite movements are observed, with the contraction of the B front in section IV (and expansion of A front in section I).

For linear or quasi linear adsorption isotherms, with products having the same or similar mass transfer rates, the complementary of A and B fronts expansion/contraction movements will be higher as the selectivity value is near one, *i.e.*, difficult separations. For non linear isotherms, one should have in mind the Solute Movement Theory and thus, concentration waves velocities must be also taken into account in addition to the other effects mentioned above, selectivity and mass transfer rates.

Moving the collection fronts will not change almost anything in the solution of the TMB model. Averaging the concentration variation occurred in the collection port, extract or raffinate nodes, will result in the same value as if a constant average flow rate was used, in both sections I and IV. But, when these types of movements are simulated by means of the SMB model approach, the results are quite different. The collection fronts are stretched or compressed depending on the strategy adopted, *i.e.*, if the more retained product is being mainly collected in the extract stream during the first step or in the second step and *vice-versa* for the less retained product in the raffinate.

As it has been mentioned so far, the OSS operation mode involves two different steps. If the low extract flow rate and high raffinate flow rate occurs during the first step, *i.e.*, expansion of A front in section I and contraction of B front in section II, the canonical "*OSS raffinate-extract*" name is given; otherwise "*OSS extract-raffinate*".

This expansion or contraction of the collection fronts is quite important since the contamination fronts will not suffer these movements with the same intensity, leading to a length decrease or increase between them, Figure 3.2.

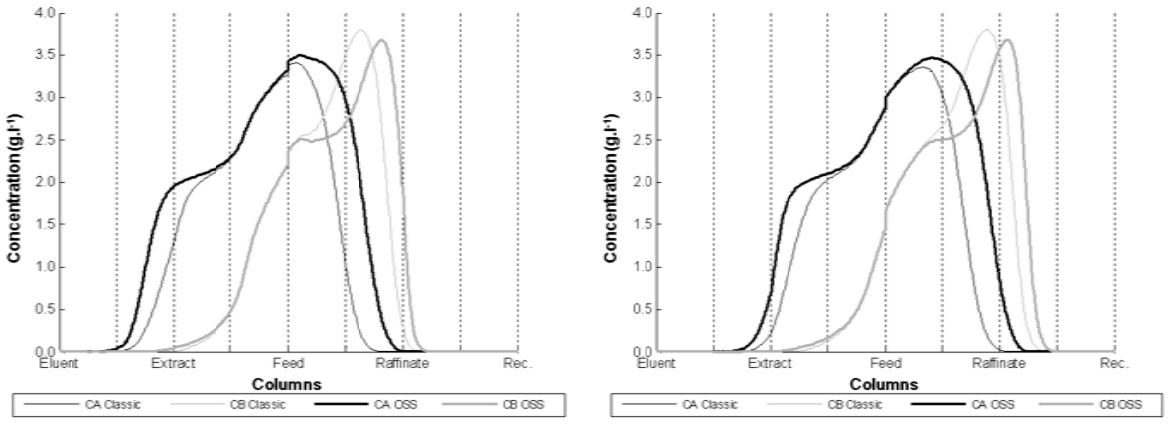

Figure 3.2 - Expansion movements at cyclic steady state (CSS): (a) at θ=0.25 and (b) at θ=0.75.

Figure 3.2 illustrates the type of induced movements aimed in the two collection fronts, simulated by an SMB model with LDF approach (similar to one present in Chapter 2). The strategy presented in Figure 3.2 was obtained by collecting the more retained product (A) in the extract during the second step while the less retained (B) in the raffinate during the first step. In this study each step is performed by half of the time switch (50-50%) not optimized and thus, the canonical form 50-50% OSS *raffinate-extract* is given.

It should be noted that for the full line in Figure 3.2, the classic SMB case, the products are always being collected at the end of column 2 (extract point) and at the end of column 6 (raffinate point), while the OSS technique only collects periodically as already mentioned. As it can be observed, the collection point in Figure 3.2 (a) is now for product B in the raffinate node while the extract port is closed; the difference between the collection front and the contamination one is quite larger than the one observed in the classic approach. A similar observation holds for Figure 3.2(b) in the extract point. The strategy is dynamic and discontinuous, the expansion either in section I or IV is obtained by the violation of the respective constraints in each section during a part of the switching time period ((3.1) in section I and (3.4) in section IV). In Figure 3.2, the expansion action is performed to the left of the extract point and to right of the raffinate node. The average of first plus second step flow rates in both sections I and IV fulfil the constraints set by the design techniques, eqs. (3.1) and (3.4), since are the same as the classic SMB flow rates. To calculate the possible collection fronts expansion on the real SMB unit, it is useful to simulate the dynamic front with its equivalent TMB model, by setting the fluxes to operate the expansion and contraction movements. In the limit, once the expansion time reaches the "point of no return" the fluxes are set to contraction so that no contamination would be noted at the end of section IV or the beginning of section I.

A first consequence can be easily noted: for this type of front movements it is necessary some column space, length of column in sections I and IV free of products A or B, the more column space is available more extensive the expansion action can perform. As a consequence, higher purity of the collected product is obtained, till the limit where the front occupies all of the column available space.

The OSS is limited by the complete closing of extract and/or raffinate ports. Considering that each step is performed for 50 % of the switching time, in the left extreme we have the 50-50% OSS-*extract-raffinate* strategy, where in the first step a complete closure of the raffinate port is performed and the same in step 2 for the extract port; in the middle the classic operation and in the right limit the 50-50% OSS-*raffinate-extract*, as in Figure 3.3. One will now focus only in the analysis on these pure strategies and compare it with the classic SMB operating mode.

3.2.1 OSS EXTRACT-RAFFINATE STRATEGY

The case of *50-50% OSS extract-raffinate* strategy, is considered when A or B front expansion movement in section I or IV is obtained by closing the extract outlet leaving the raffinate flow rate higher than the estimated by the classic approach, during the first half of the switch time; and closing the raffinate outlet while leaving the extract flow rate higher than estimated by the classic approach during the other half of the switching time, respectively. This operating strategy is presented in Figure 3.4, the operating values shown in Table 3.3 and the flow rates of outlet and inlet streams detailed in Figure 3.5.

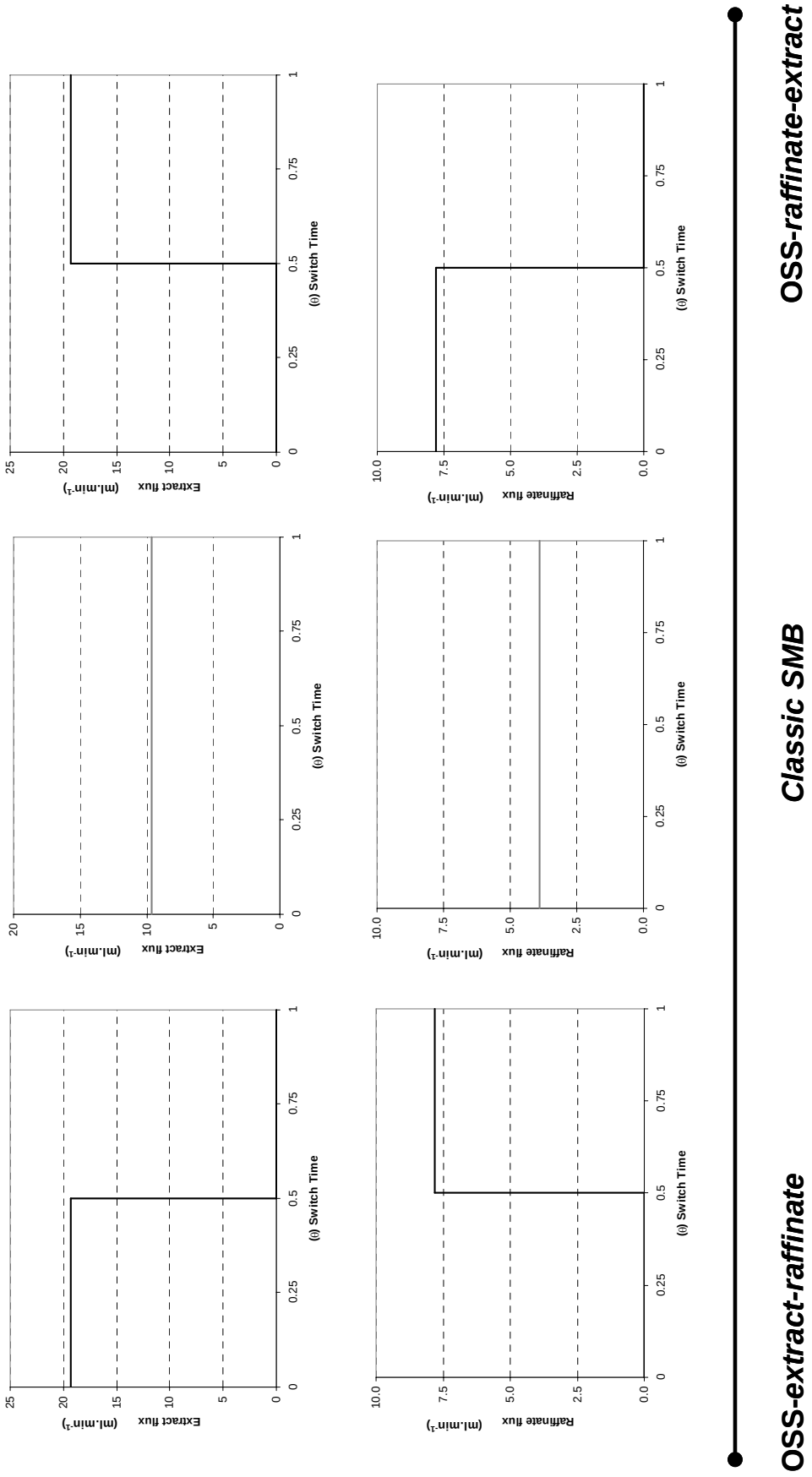

Figure 3.3 – OSS range of application, the 50%-50% OSS strategies.

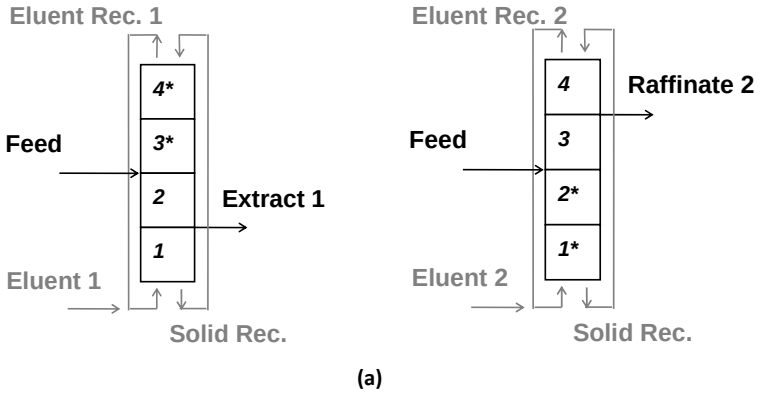

Figure 3.4 – OSS strategy for the test case, (a) the first half of the switch time, (b) the second half of the switch time, equivalent TMB scheme.

Table 3.3 – 50-50% OSS *extract-raffinate* SMB and equivalent TMB section operating conditions

SMB 1st half of a θ	TMB 1st half of a θ
γ_j^*=[6.82 3.80 4.03 4.03]	γ_j =[5.82 2.80 3.03 3.03]
Q_j^*=[43.48 24.20 25.70 25.70] ml.min^{-1}	Q_j =[37.11 17.83 19.33 19.33] ml.min^{-1} Q_s =9.56 ml.min^{-1}
SMB 2nd half of a θ	**TMB 2nd half of a θ**
γ_j^*=[3.80 3.80 4.03 2.81]	γ_j =[2.80 2.80 3.03 1.81]
Q_j^*=[24.20 24.20 25.70 17.90] ml.min^{-1}	Q_j =[17.83 17.83 19.33 11.53] ml.min^{-1} Q_s =9.56 ml.min^{-1}

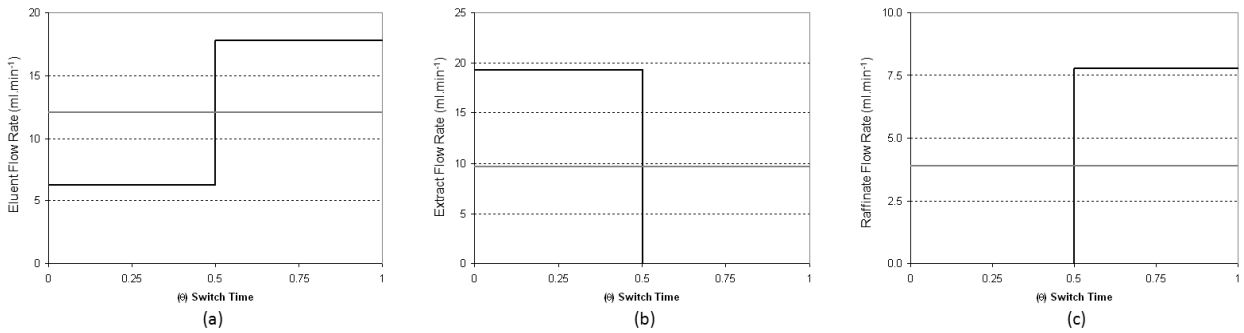

Figure 3.5 – Eluent (a), Extract (b) and Raffinate (c) currents during the pure 50-50% OSS *extract-raffinate* SMB strategy.

With the operating parameters mentioned above, the stretched profiles are obtained as mentioned before, simulated by means of the SMB model with LDF approach, as shown in Figure 3.6, and the purity and recovery presented in Table 3.4.

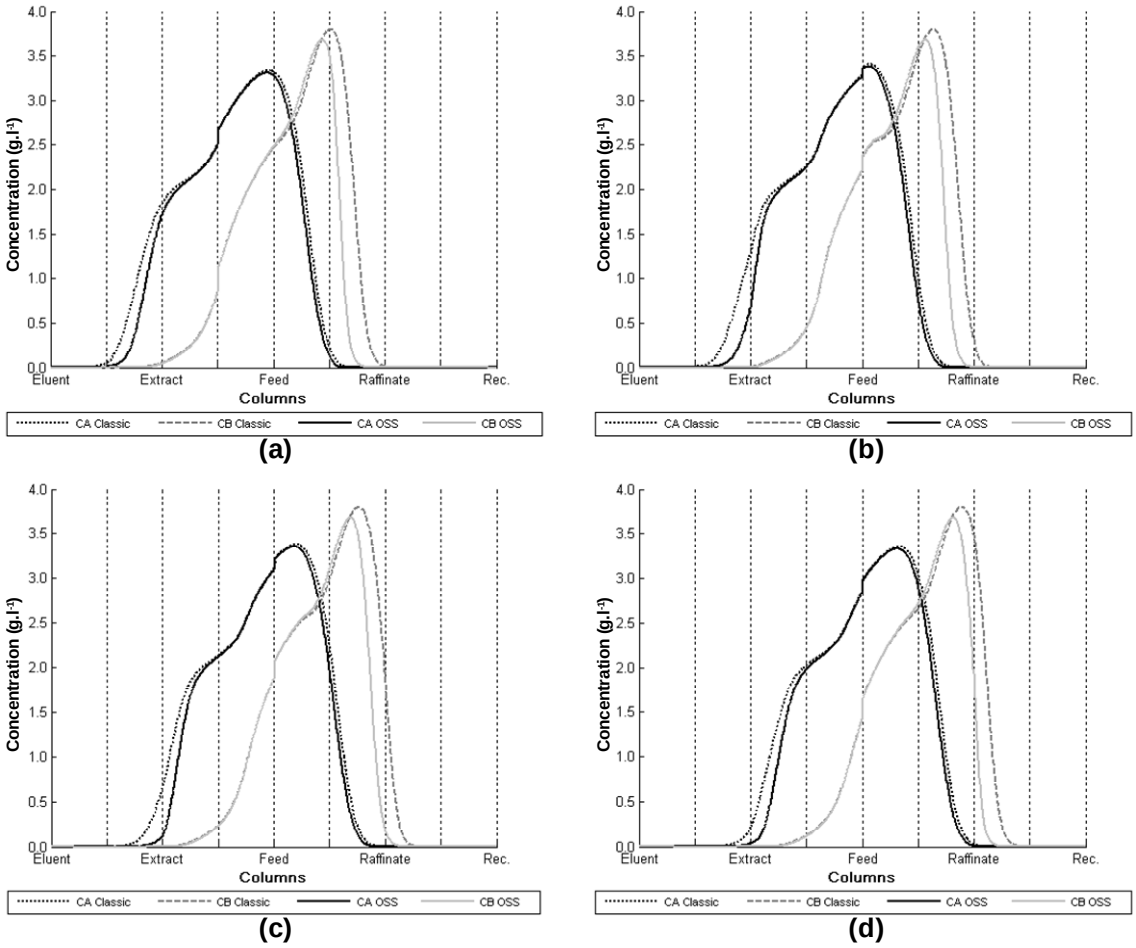

Figure 3.6 – Concentration profiles for the pure OSS 50-50% *extract-raffinate* strategy, (a) at θ=0, (b) θ=0.25, (c) θ=0.50 and (d) at θ=0.75, at the CSS.

Table 3.4 – Values for extract and raffinate purity and recovery for the 50-50% OSS *extract-raffinate* technique and the classical SMB separation.

	Classic SMB		OSS	
	Extract	Raffinate	Extract	Raffinate
Purity	99.1 % of *A*	98.5 % of *B*	99.0 % of *A*	98.5 % of *B*
Recovery	98.5 % of *A*	99.1 % of *B*	98.5 % of *A*	99.0 % of *B*

From Figure 3.6 it can be observed that the contraction of both A front in section I as B front in section IV resulted in almost the same purity, as recovery, values for both the *50-50% OSS raffinate-extract* as the Classical SMB strategy; nevertheless, it is noted that the OSS strategy provided a difference of 0.1 % lower purity in the extract than the classic SMB, as well as in the recovery of B species in the raffinate.

3.2.2 OSS RAFFINATE-EXTRACT STRATEGY

The other possible configuration, working with the same flow-rates and the same step time (50% of the real switching time), is performed when the collection on the extract is occurring during the second stage (step 2) and the collection of the less retained product in the raffinate during the first stage (step 1), Figure 3.7.

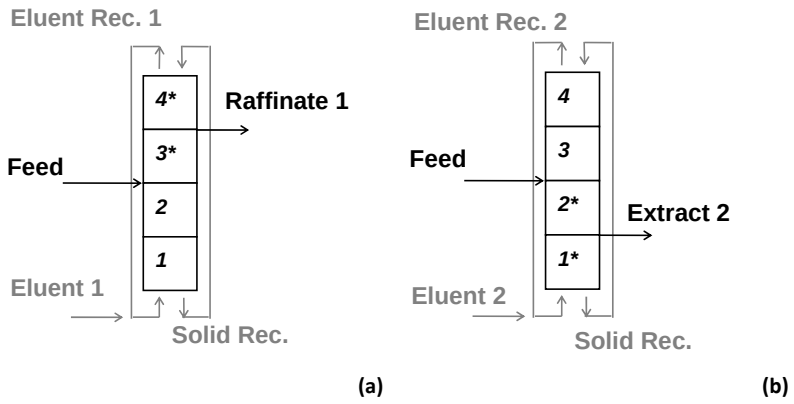

Figure 3.7 – OSS strategy for the test case, (a) the first half of the switch time, (b) the second half of the switch time, equivalent TMB scheme.

The operating values for this strategy are presented in Table 3.5, the simulation results for the bulk concentration profiles are CSS shown in Figure 3.8 and the performance parameters for this strategy shown in Table 3.6.

Table 3.5 – 50-50% OSS *raffinate-extract* SMB and equivalent TMB section operating conditions

SMB 1st half of a θ	TMB 1st half of a θ
γ_j^*=[3.80 3.80 4.03 2.81]	γ_j =[2.80 2.80 3.03 1.81]
Q_j^*=[24.20 24.20 25.70 17.90] ml.min^{-1}	Q_j =[17.83 17.83 19.33 11.53] ml.min^{-1} Q_s =9.56 ml.min^{-1}
SMB 2nd half of a θ	**TMB 2nd half of a θ**
γ_j^*=[6.82 3.80 4.03 4.03]	γ_j =[5.82 2.80 3.03 3.03]
Q_j^*=[43.48 24.20 25.70 25.70] ml.min^{-1}	Q_j =[37.11 17.83 19.33 19.33] ml.min^{-1} Q_s =9.56 ml.min^{-1}

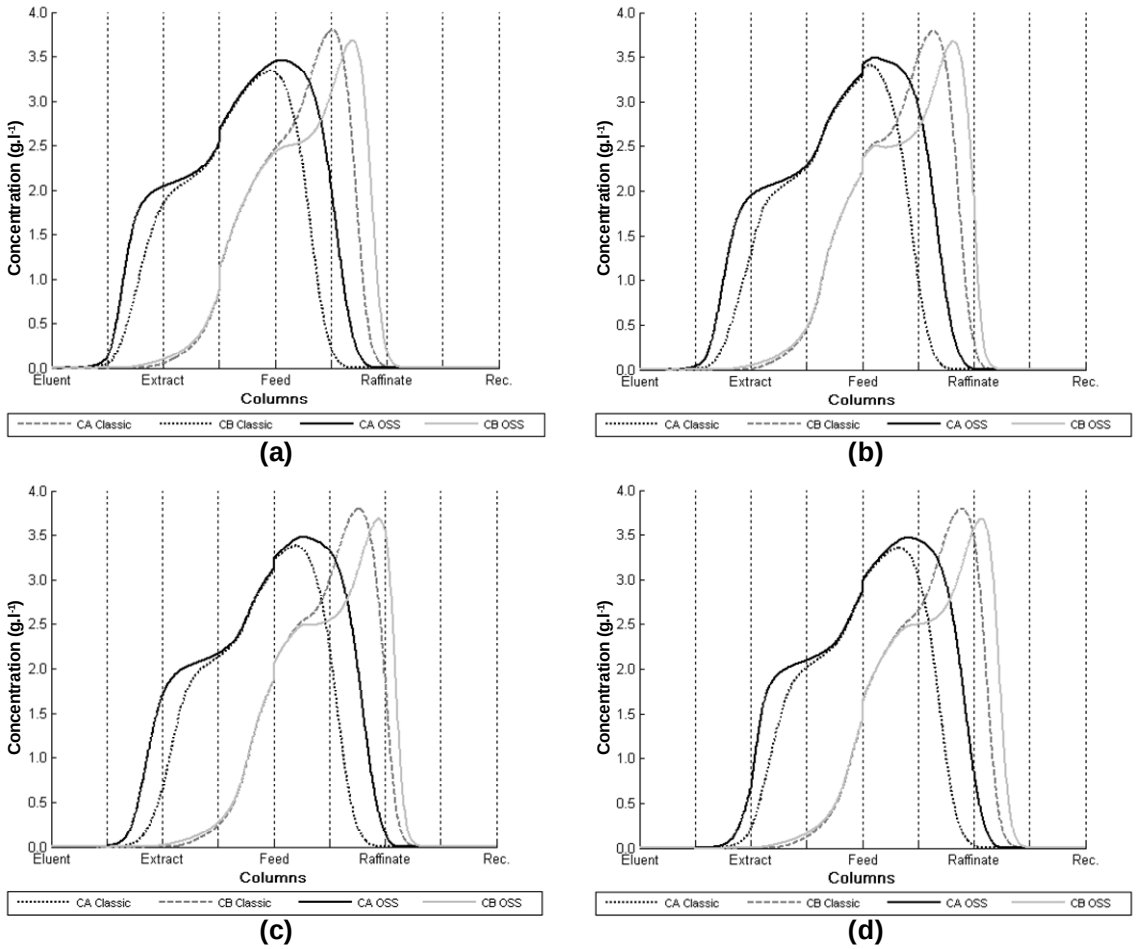

Figure 3.8 – Concentration profiles for the pure OSS 50-50% *raffinate-extract* strategy, (a) at θ=0, (b) θ=0.25, (c) θ=0.50 and (d) at θ=0.75, at the CSS.

Table 3.6 – Values for extract and raffinate purity and recovery for the 50-50% OSS *raffinate-extract* technique and the classical SMB separation.

	Classic SMB		OSS	
	Extract	Raffinate	Extract	Raffinate
Purity	99.1 % of *A*	98.5 % of *B*	99.7 % of *A*	98.6 % of *B*
Recovery	98.5 % of *A*	99.1 % of *B*	98.6 % of *A*	99.7 % of *B*

As can be observed the second strategy (50-50% OSS *raffinate-extract*), is quite better than the classic SMB unit and the other OSS strategy. A good presentation of the technique performance is achieved with the species recovering in outlet streams here exemplified by the concentration history in the extract for both species analysed, Figure 3.9.

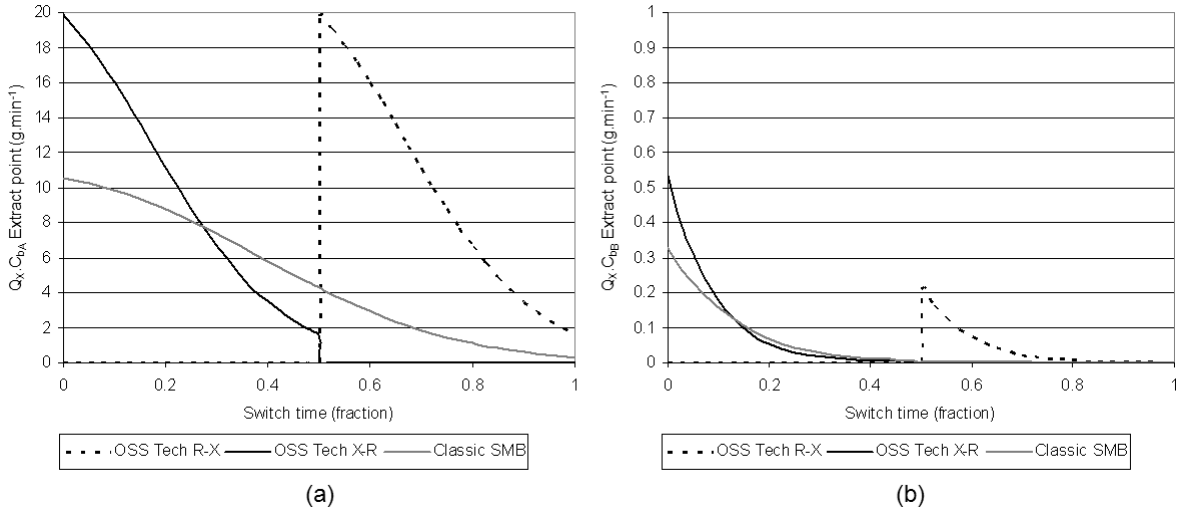

Figure 3.9 – Concentration history in the extract stream (a) A species and (b) B species.

As can be noted, the amount of species A is similar in both OSS strategies and in the classical approach; nevertheless, there are important differences in the B species (the contamination front), as can be seen in Figure 3.9(b), where the 50-50% OSS *raffinate-extract* technique justifies why the values of purities in the extract have been improved.

The eluent consumption in the classic approach is 12.04 ml.min^{-1} and with the 50-50% OSS *extract -raffinate* approach also 12.04 ml.min^{-1} of eluent not constantly but periodically, during the first step 17.78 ml.min^{-1} and the second half time (step 2) 6.30 ml.min^{-1}; in the 50-50% OSS *raffinate-extract* strategy also the eluent consumption is 12.04 ml.min^{-1} periodically spent: in the first step is 6.30 ml.min^{-1} and the second half time (step 2) 17.78 ml.min^{-1}.

3.3 SEPARATION OF A RACEMIC MIXTURE OF GUAFEINESIN

The study of the non-conventional OSS operating strategy will now be extended to the separation of a racemic mixture of guafeinesin[*], which will also serve as a preliminary analysis for further studies presented latter in Chapter 6.

The adsorption equilibrium of guafeinesin enantiomers in Chiralpak AD[†] (particle diameter, d_p, 20 μm), with a n-heptane/ethanol mixture at 85/15 in volumetric percentage as mobile phase (Table 3.7), was determined by the adsorption/desorption and fitted with Langmuir adsorption equilibrium isotherm,

$$q_{i,k} = \frac{q_m K_i C_{p_{i,k}}}{1+\sum_{l=1}^{2} K_l C_{p_{l,k}}} \tag{3.7}$$

[*] guaiacol glyceryl ether;

[†] amylose tris-(3,5 dimethylphenylcarbamate coated onto 20 μm silica-gel), provided by Chiral Technologies Europe (France).

by frontal analysis at the preparative scale by Dr. Miriam Zabkova (Sá Gomes *et al.*, 2009b), the fitting parameters are presented in Table 3.8.

Table 3.7 - Geometrical and physical particle parameters and mobile phase density (ρ) and viscosity (μ).

Parameters	Chiralpak AD	n-heptane/Ethanol (85/15)	
d_p [m]	20×10^{-6}	ρ_f [g.l^{-1}]	μ [cP]
ε_p	0.33	0.702	0.512

Table 3.8 - Multicomponent adsorption isotherm parameters.

q_m [g.l^{-1}]	K_A [l.g^{-1}]	K_B [l.g^{-1}]	H_A	H_B
106.759	0.065	0.056	6.939	5.978

With $H_i = q_m K_i$.

In this case, the mass transfer resistances are represented by the internal mass transfer coefficient, k_{int_i}, calculated by means of the LDF approximation suggested by Glueckauf (1955) $k_{int_i} = \frac{5\varepsilon_p D_{m_i}}{\tau r_p}$; where D_{m_i} is the free molecular diffusivity and τ is the particle tortuosity factor, estimated by $\tau = \frac{(2-\varepsilon_p)^2}{\varepsilon_p}$. The molecular diffusivity of the solute guaifenesin enantiomers was calculated by the Wilke – Chang (1955) equation extended to mixed solvents by Perkins and Geankoplis (1969) $D_{m_i} = 7.4\times10^{-8} T \frac{\sqrt{\phi M}}{\mu V_{m_i}^{0.6}}$; where T is the absolute temperature, μ is the mobile phase viscosity, calculated according to Teja and Rice (1981) method for liquid mixture; V_{m_i} (ml. mol^{-1}) is the molar volume of the adsorbate at its normal boiling temperature estimated by the Le Bas method; and ϕM obtained from $\phi M = x_A \phi_A M_A + x_B \phi_B M_B$ where x_i are the molar fractions, M_i the molar masses and ϕ_i are the association factors constants which account for solute-solvent interactions. The molecular diffusivity of each enantiomer is similar and therefore the internal mass transfer coefficient k_{int_i} identical for both enantiomers $\left(k_{int_i} = 0.20 \text{ cm. min}^{-1}\right)$.

3.3.1 MODELLING AND DESIGN STRATEGIES

The SMB model approach used to simulate this particular separation is similar to the one applied in the previous case study (See Chapter 2 and Section 3.2); however, the LDF approximation is now set in terms fluid phase concentration $\left(C_{b\,i,k} - \overline{C_{p_{i,k}}}\right)$ and thus presented bellow.

By performing a mass balance to a volume element of the column k,

$$\frac{\partial C_{b_{i,k}}}{\partial t} = D_{b\,k} \frac{\partial^2 C_{b_{i,k}}}{\partial z^2} - u_j^* \frac{\partial C_{b_{i,k}}}{\partial z} - \frac{(1-\varepsilon_b)}{\varepsilon_b} \frac{3}{r_p} k_{int_i} \left(C_{b\,i,k} - \overline{C_{p_{i,k}}}\right) \tag{3.8}$$

and similarly the particle mass balance,

$$\varepsilon_p \frac{\partial C_{p_{i,k}}}{\partial t} + \left(1-\varepsilon_p\right)\frac{\partial q_{i,k}^{eq}}{\partial t} = \frac{3}{r_p} k_{int_i}\left(C_{b\,i,k} - \overline{C_{p_{i,k}}}\right) \tag{3.9}$$

with the initial conditions:

$$t = 0 \;:\quad C_{b\,i,k}(z,0) = \overline{C_{p_{i,k}}}(z,0) = 0 \tag{3.10 a,b}$$

The Danckwerts boundary conditions at the inlet of column $(z = 0)$ and column exit $(z = L_k)$ for $(t > 0)$ are set to each column k,

$$z = 0 \;:\quad D_{b\,k}\frac{\partial C_{b\,i,k}}{\partial z}\Big|_{z=0} = u_j^*\left(C_{b\,i,k}\Big|_{z=0} - C_{b\,i,k}^0\right) \tag{3.11}$$

$$z = L_k \;:\quad \frac{\partial C_{b\,i,k}}{\partial z}\Big|_{z=L_k} = 0 \tag{3.12}$$

The fluid velocities and inlet concentrations in each section *j* are calculated from the inlet and outlet nodes balances as presented before (eqs. 2.42-2.54).

Recalling the constraints mentioned before (eqs. 3.1 to 3.4), now considering that $\langle n_{i,j}\rangle$ will represent the total average solid concentration of species *i* in section *j*, with $\langle n_{i,j}\rangle = \left(1-\varepsilon_p\right)q_{i,j} + \varepsilon_p C_{p_{i,j}}$, and simplifying the term $\frac{\langle n_{i,j}\rangle}{C_{i,j}}$ by assuming that the adsorption equilibrium is established everywhere at every time (from the Equilibrium Theory assumptions), it is possible to obtain a preliminary calculation of the operating conditions in section I and IV as well as for the separation region $(\gamma_{II} \times \gamma_{III})$ plan.

For the separation hereby analyzed, the maximum flow rate in section I was set at 41 ml.min^{-1} (a compromise between the hardware limitation and pressure drop restriction, around 45 ml.min^{-1}, in the FlexSMB-LSRE® unit). According to the Equilibrium Theory for a complete regeneration of the solid phase in section I, the following condition must be fulfilled,

$$\gamma_I > \gamma_{I_{min}} = \frac{1-\varepsilon_b}{\varepsilon_b}\left(H_A\left(1-\varepsilon_p\right) + \varepsilon_p\right) = 7.47 \tag{3.13}$$

Where $H_A = 6.94$ is the initial slope of the isotherm of the more retained compound and by consequence the switching time (t_s) that will fulfil this condition can be 2.57 min.

As explained before, the purpose of section IV is to regenerate the liquid phase, thus the less retained compound must move towards the raffinate port. The SMB flow rate in the section IV was calculated according the following equation:

$$Q_{IV}^* = \frac{\varepsilon_b V_c}{t_s}\left(1 + \frac{1-\varepsilon_b}{\varepsilon_b}\varepsilon_p + \frac{1-\varepsilon_b}{\varepsilon_b}\left(1-\varepsilon_p\right)\frac{\Delta q_B^F}{\Delta C_B^F}\right) \tag{3.14}$$

where $\frac{\Delta q_B^F}{\Delta C_B^F}$ is the slope of the less retained compound and $V_c = 31.4$ ml (FlexSMB-LSRE® columns). Considering that the concentration of the less retained compound in the feed is 2.0 g.l^{-1} then, the term $\frac{\Delta q_B^F}{\Delta C_B^F}$ is equal to 5.38 and consequently, the flow rate in the section IV 33.75 ml.min^{-1}. For this recycle flow rate value and selected switching time, the condition for complete eluent regeneration in section IV by equilibrium theory is also fulfilled: $\gamma_{IV} < \gamma_{IV\,max} = \frac{1-\varepsilon_b}{\varepsilon_b}\left(H_B\left(1-\varepsilon_p\right)+\varepsilon_p\right) = 6.50$.

The separation region based Equilibrium Theory assumptions can be obtained by the procedure suggested by Mazzotti *et al.* (1994), and presented in Figure 3.10.

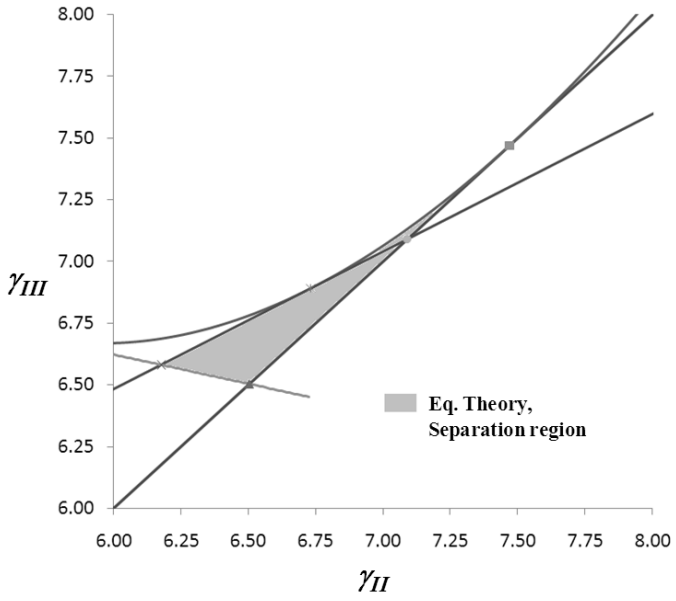

Figure 3.10 – Separation region according to the Equilibrium Theory assumptions (Triangle Theory).

As can be observed in Figure 3.10, the separation region for guafeinesin enantiomers has a triangular shape in $(\gamma_{II} \times \gamma_{III})$ plan characteristic of the systems with a weak desorbent (eluent). According to the equilibrium theory assumptions, an operating point within this separation region will provide a complete separation (pure extract and raffinate).

Nevertheless, real SMB units generally do not fulfil the Equilibrium theory assumptions and factors such as mass transfer resistances or units particularities (*i.e.*, tubing and equipment dead volumes, switching time asymmetries and delays, pumps flow rates variations and equipment limitations, discussed latter in Chapter 6) are in fact issues. As a consequence, and to better detail this study, one should consider at least the mass transfer resistances when drawing both separation as regeneration regions (Azevedo and Rodrigues, 1999).

3.3.2 SEPARATION REGION ANALYSIS

To account for the mass transfer resistances when drawing the separation region, one can make use of the SMB model stated in the previous section and run successive simulations of different $(\gamma_{II} \times \gamma_{III})$ pairs, considering significantly higher values for γ_I and lower values for γ_{IV} than the ones predicted by the Triangle Theory to guarantee assuring that the flow rates in the regeneration region do not influence the shape and size of the separation region, as stated by the Separation Volume concept (Azevedo and Rodrigues, 1999). This procedure was in fact used to perform the separation region analysis for the pure 50-50% OSS *raffinate-extract* and *extract-raffinate* running successive simulations for different $(Q_{II}^* \times Q_{III}^*)$ pairs with constant Q_I^* =44.0 ml.min^{-1}, Q_{IV}^* =32.0 ml.min^{-1} and t_s =2.57 min and the SMB unit parameters considered from the FlexSMB-LSRE® unit presented in Table 3.9.

Table 3.9 - Experimental operating conditions of the SMB experiment.

n_j= [1 2 2 1]	ε_b= 0.4
L_c= 10 cm;	C_i^F= 2.0 g.l^{-1}
d_c= 2.0 cm	d_p= 20 μm

The separation regions obtained are shown in Figure 3.11.

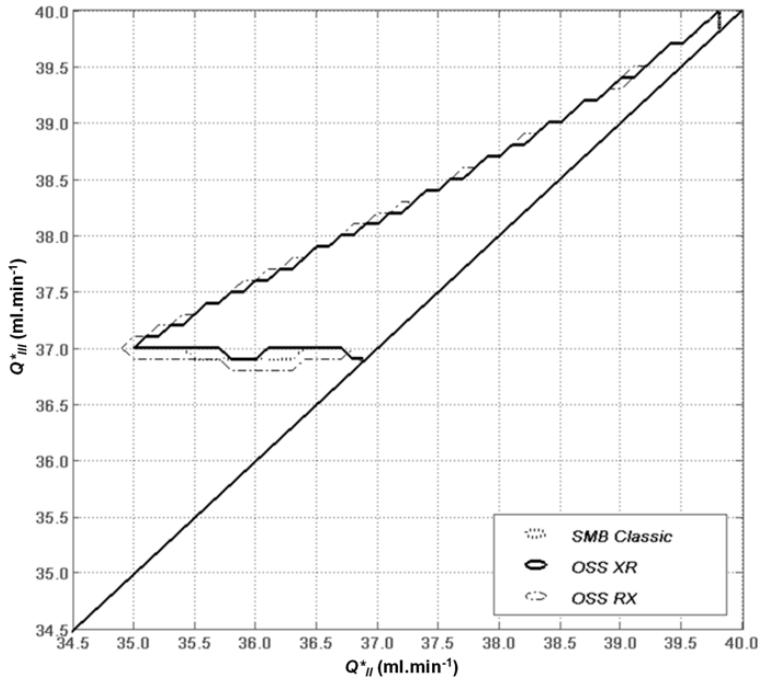

Figure 3.11 - Separation region for classic SMB and 50-50% OSS strategies: *extract-raffinate* (OSS *XR*) and *raffinate-extract* (OSS *RX*), step of 0.100 ml.min^{-1} for both Q_{II}^* and Q_{III}^*[*]; minimum purity in both extract and raffinate streams of 99.75 %.

[*] Both the separation as regeneration regions, for the guafeinesin resolution by OSS, were obtained by solving the mathematical model with gPROMS software package (version 3.0.4) from Process System Enterprise (UK). The numerical method used was based on the Orthogonal Collocation in Finite Elements (OCFEM) with an axial discretization in 40 finite elements, with two interior collocation points. An absolute and relative tolerance of 10^{-5} was set.

While the SMB classic and the OSS *extract-raffinate* (OSS *XR*) strategy separation regions are almost superposed the separation region of the OSS *raffinate-extract* (OSS *RX*) appears to be larger as observed before.

3.3.3 REGENERATION REGION ANALYSIS

In the case of the regeneration region analysis for the pure 50-50% OSS *raffinate-extract* and *extract-raffinate* the analysis was performed again by running successive simulations for different $(Q_I^* \times Q_{IV}^*)$ pairs with constant Q_{II}^* =36.2 ml.min^{-1}, Q_{III}^* =37.1 ml.min^{-1} and t_s =2.57 min, Figure 3.12.

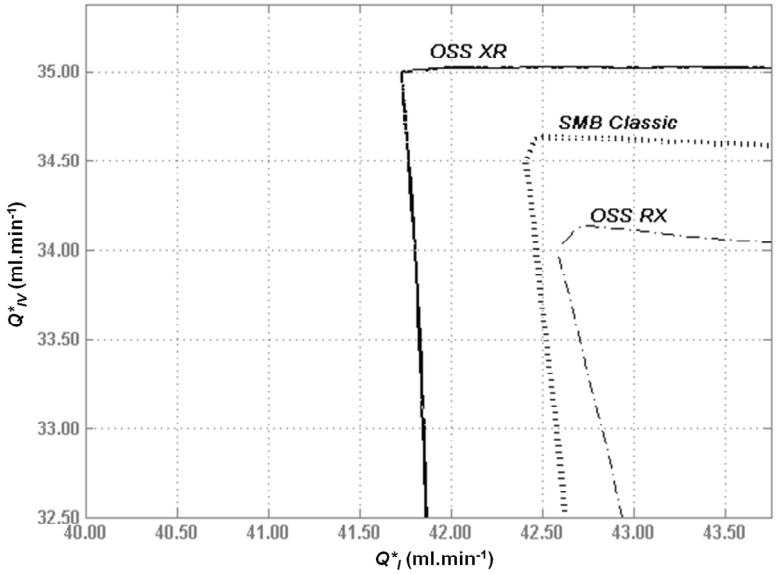

Figure 3.12 - Regeneration region for classic SMB and 50-50% OSS strategies: *extract-raffinate* (OSS *XR*) and *raffinate-extract* (OSS *RX*) step of 0.125 ml.min^{-1} and 0.250 ml.min^{-1} for Q_I^* and Q_{IV}^*, respectively; minimum purity in both extract and raffinate streams of 99.75 %.

From Figure 3.12, it can be observed that the OSS *extract-raffinate* operating strategy is now considerable better than SMB classic and quite better than the OSS *raffinate-extract*, an opposite conclusion than the one obtained from the separation region analysis. However, the differences between both OSS strategies and the classic operating SMB mode observed in Figure 3.12 (regeneration region analysis) are quite larger than the ones observed in Figure 3.11 (separation region analysis) and thus, stating the OSS operating mode as a sort of partial eluent strategy (by opposition with the partial feed strategy). In fact, one expects that the OSS mode of operation will play a more relevant role in eluent consumption (or eluent recovery duties) studies than productivity optimization ones.

If the objective is to improve the productivity values (for instance by increasing the feed flow rate), the OSS *raffinate-extract* strategy will better suit the purpose. It is interesting to note that a similar conclusion was achieved by Biegler and co-workers (Kawajiri and Biegler, 2006b) when performing the maximization of feed flow rate, keeping constant the section flow rates ("Constant zone velocities") and variable inlet and outlets streams. These authors performed what can be named as a sort of partial feed coupled with a free OSS technique

(where the flow rates of extract and raffinate do not need to be zero during a given period within the switching time period) and by optimization found the basics of a sort of 40%-60% OSS *raffinate-extract* operating strategy.

In the other hand if the objective is to decrease the eluent consumption (or eluent recovery duty), then the OSS *extract-raffinate* strategy seems to be the more indicated, since it will not affect too much the separation region but will in fact improve the efficiency of both sections I and IV.

3.4 VARIANTS OF OSS TECHNIQUE

As mentioned before, the canonical name of 50-50% OSS *raffinate-extract* was given to describe a technique where the extract port is closed during the first half of the switching time and the less retained product is being collected on raffinate stream and the rest of the switching time period the raffinate port is closed and the more retained species being collected don the extract stream, and *vice-versa* for the or 50-50% OSS *extract-raffinate* mode of operation. However, and for example in the case of the OSS *extract-raffinate* mode of operation, one could operate it during the initial 30 % of the switching time period collecting the more retained product in the extract and last 30 % period of the switching time withdrawing the less retained species in the raffinate (in the remaining time both ports are closed), what would be the 30-30% OSS *extract-raffinate* strategy; in the same way one could just operate the OSS strategy in the extract port closing the extract port for the final 50% of the switching time period (50% OSS *extract-0*) or closing it in the initial 50% period (50% OSS *0-extract*), and similarly for the raffinate port (50% OSS *raffinate-0*…). One will now study these variants in particular and thus detailing the influence of the closing period as well as extract or raffinate influence *per se*.

For the sake of simplicity just the OSS *extract-raffinate* technique, which presented better results in term of eluent consumption, will now be studied and in particular OSS *extract-0* and OSS *0-raffinate* variants.

3.4.1 OSS *EXTRACT-0*

Under the scope of the OSS operating technique, closing and opening the extract port means that only the flow rate in section I will suffer variations thus, the influence of this variant technique (OSS *extract-0*) versus Q_I^* and the collecting time is now analysed by means of successive simulations on the case of Guafeinesin separation with $Q_{II}^* = 36.2\ \text{ml.min}^{-1}$, $Q_{III}^* = 37.1\ \text{ml.min}^{-1}$, $Q_{IV}^* = 32.5\ \text{ml.min}^{-1}$ and $t_s = 2.57\ \text{min}$, Table 3.10.

As can be observed from Table 3.10, when comparing OSS *extract-0* with the classic SMB operating modes, the difference in the extract purity is almost insignificant (but better in the classic SMB mode of operation); however, the raffinate purity values obtained by the classic SMB mode of operation are always lower than the ones obtained when running with the OSS *extract-0* operating mode, independently of the collecting time period. Within the OSS *extract-0* operating strategy and for a given Q_I^* flow rate value, the extract purity values increases with the collecting period, but in a minor extension to what it is observed in the raffinate purities, where the higher purity values are observed for the lower collecting periods. However, one should remind that the shorter the collecting period is, the higher will be the extract flow rate during this period and thus the perturbations in the system, which can play a relevant role in the practical implementation of OSS technique.

Table 3.10 - OSS *extract-0* analysis: collecting time and Q_I^*, for $Q_{II}^* = 36.2$ ml. min^{-1}, $Q_{III}^* = 37.1$ ml. min^{-1}, $Q_{IV}^* = 32.5$ ml. min^{-1} and $t_s = 2.57$ min.

				Extract Purity		
Q_I^*	Classic	30% OSS *X0*	40% OSS *X0*	50% OSS *X0*	60% OSS *X0*	70% OSS *X0*
40.5	*100.00%*	99.98%	99.99%	100.00%	100.00%	100.00%
41.0	*100.00%*	99.96%	99.97%	99.98%	99.99%	99.99%
41.5	*100.00%*	99.95%	99.96%	99.97%	99.98%	99.98%
42.0	*99.99%*	99.95%	99.95%	99.96%	99.97%	99.97%
42.5	*99.98%*	99.94%	99.95%	99.96%	99.97%	99.97%
43.0	*99.98%*	99.94%	99.95%	99.96%	99.96%	99.97%
				Raffinate Purity		
Q_I^*	Classic	30% OSS *X0*	40% OSS *X0*	50% OSS *X0*	60% OSS *X0*	70% OSS *X0*
40.5	*92.42%*	94.95%	94.80%	94.60%	94.36%	94.04%
41.0	*95.33%*	97.61%	97.48%	97.31%	97.09%	96.81%
41.5	*97.44%*	99.14%	99.05%	98.93%	98.78%	98.57%
42.0	*98.78%*	99.79%	99.74%	99.69%	99.61%	99.49%
42.5	*99.51%*	99.96%	99.95%	99.93%	99.90%	99.86%
43.0	*99.83%*	100.00%	99.99%	99.99%	99.98%	99.97%

As mentioned before, OSS *extract-0* operating strategy mainly influences the fronts section I. By operating in OSS *extract-0*, the more retained species front in section I will suffer a contraction and thus avoiding this product to move with the solid to section IV when the ports switching operation is performed. It is then possible to achieve higher raffinate purities operating under OSS *extract-0* or, reduce the eluent consumption for a given raffinate purity requirement, as shown in Figure 3.13.

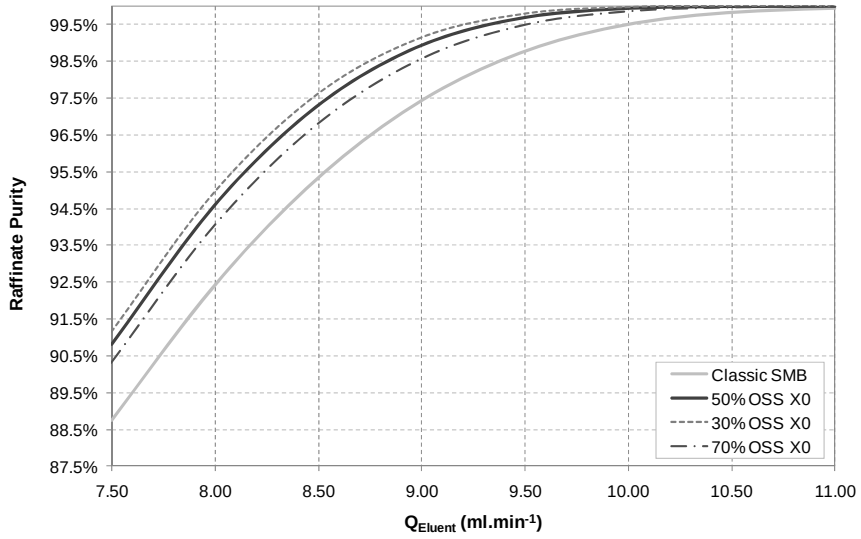

Figure 3.13 – Eluent consumption *vs.* raffinate purity for Classic SMB and OSS *X0* operating modes.

The shorter the collecting time period is, the higher will be the front compression and thus, the potential of the operating technique.

3.4.2 OSS *0-RAFFINATE*

In opposition to what happens with the OSS *extract-0* strategy, by closing and opening the raffinate port it will only affect the flow rate in section IV since the eluent flow rate compensates the remaining flow rates (namely in section I and by consequence sections II and III). Thus, the influence of OSS *0-raffinate* variant technique versus Q_{IV}^* and the collecting time is now analysed, again by running successive simulations on the case of guafeinesin separation by keeping constants: $Q_{II}^* = 36.2\ \text{ml.min}^{-1}$, $Q_{III}^* = 37.1\ \text{ml.min}^{-1}$, $Q_I^* = 42.5\ \text{ml.min}^{-1}$ and $t_s = 2.57$ min, Table 3.11.

Table 3.11 - OSS *0-raffinate* analysis: collecting time and Q_{IV}^*, for $Q_{II}^* = 36.2\ \text{ml.min}^{-1}$, $Q_{III}^* = 37.1\ \text{ml.min}^{-1}$, $Q_I^* = 42.5\ \text{ml.min}^{-1}$ and $t_s = 2.57$ min.

				Extract Purity		
Q_{IV}^*	Classic	30% OSS *0R*	40% OSS *0R*	50% OSS *0R*	60% OSS *0R*	70% OSS *0R*
34.625	*99.77%*	99.98%	99.98%	99.98%	99.98%	99.98%
34.750	*99.55%*	99.98%	99.98%	99.98%	99.97%	99.95%
34.875	*99.10%*	99.98%	99.98%	99.97%	99.95%	99.90%
35.000	*98.18%*	99.97%	99.96%	99.94%	99.89%	99.79%
35.125	*96.39%*	99.94%	99.90%	99.83%	99.68%	99.39%
35.250	*93.45%*	97.54%	97.53%	97.51%	97.41%	97.11%
				Raffinate Purity		
Q_{IV}^*	Classic	30% OSS *0R*	40% OSS *0R*	50% OSS *0R*	60% OSS *0R*	70% OSS *0R*
34.625	*99.68%*	99.80%	99.80%	99.79%	99.79%	99.68%
34.750	*99.70%*	99.81%	99.80%	99.80%	99.79%	99.78%
34.875	*99.71%*	99.81%	99.81%	99.80%	99.80%	99.79%
35.000	*99.72%*	99.82%	99.81%	99.81%	99.80%	99.79%
35.125	*99.73%*	99.82%	99.82%	99.81%	99.81%	99.80%
35.250	*99.75%*	99.83%	99.83%	99.82%	99.82%	99.81%

From Table 3.11, it can be observed that the difference in the raffinate purities between the OSS *0-raffinate* and the classic SMB operating modes is small, but worse in the classic SMB mode of operation case; nevertheless, the extract purities in the classic SMB mode of operation are always lower than the ones obtained when running with the OSS *0-raffinate* operating mode, independently of the collecting time period.

Within the OSS *0-raffinate* operating strategy, and for a given Q_{IV}^* flow rate value, the purity values (extract and raffinate) increases as the collecting period decreases. Again, one should remind the practical consequences of operating at low collecting periods mentioned before.

The same justification given to the front contraction in section I when operating under the OSS *extract-0* operating strategy can now be applied to section IV, where the less retained species front is compressed by

operating under the OSS *0-raffinate* technique. Once again it is possible to either improve extract purities or reduce the eluent consumption for a given extract purity requirement, Figure 3.14.

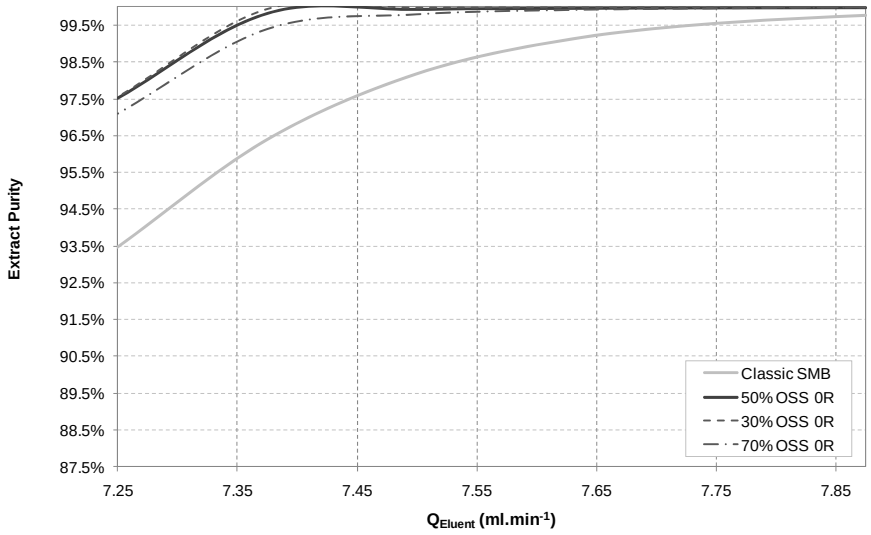

Figure 3.14 - Eluent consumption *vs.* extract purity for Classic SMB and OSS *0R* operating modes.

Compressing both fronts (the more retained species in section I and the less retained species in section IV) is then possible to experience the OSS technique at its complete potential.

3.5 CONCLUSIONS

A new non-conventional SMB technique, the Outlet Streams Swing (OSS), was introduced, modelled and simulated. This technique is based on a periodical outlet collection procedure. It can be performed in the extract, raffinate or even extract and raffinate ports at the same time. It was proved that, by means of these actions, it is possible to perform compression or expansion movements in both the less retained species front in section IV and the more retained component in section I. These movements can be adjusted either to increase the separation region and thus improving the unit productivity for given purity requirements (achieved when operating under OSS *raffinate-extract* strategy), or to decrease the eluent consumption (possible by operating under OSS *extract-raffinate* strategy).

Throughout a methodical analysis, it was possible to understand the basics of eluent, extract and raffinate streams flow rates variation, giving stated answers to results obtained before by some optimization procedures.

By coupling the OSS technique with the partial feed operating strategy, it will be possible to extend further the potentialities of this kind of operating modes and to better understand generalist techniques such as PowerFeed.[*]

[*] A significant part of Chapter 3 was published on: Sá Gomes, P. and A. E. Rodrigues, "Outlet Streams Swing (OSS) and MultiFeed operation of simulated moving beds." Separation Science and Technology 42(2), 223-252, (2007).

Chapter 4

OPERATION STRATEGIES FOR SMB UNITS IN PRESENCE OF ADSORBENT AGEING

4.1 INTRODUCTION

Adsorbent/Catalyst deactivation (or ageing) has been subject of several studies in the reaction/separation engineering field. Ageing mechanisms can generally be divided into six major groups (Bartholomew, 2001): (i) Poisoning, caused by irreversible or "pseudo-irreversible" adsorption of some species in the adsorbent active sites; (ii) Fouling, physical (mechanical) deposition of species from the fluid phase onto the solid one, resulting in activity losses due to sites and/or pores obstruction; (iii) Thermally-induced deactivation (sintering, among others); (iv) Vapour compound formation accompanied by transport; (v) Vapour-solid and/or solid-solid reactions; and (vi) Attrition/Crushing, mechanical failure (quite usual in moving bed and fluidized-bed systems). Literature addressing catalyst/adsorbent deactivation and possible solutions has been published and expanded considerably over the past three decades (Bartholomew, 2001).

Nevertheless, regarding the Simulated Moving Bed (SMB) technology, the work published on catalyst/adsorbent ageing is almost inexistent as reported elsewhere (Minceva and Rodrigues, 2002; Sá Gomes *et al.*, 2006b). Modelling-based research is required to define the ageing problem consequences and indicate strategies that can be used to mitigate capacity loss or other deactivation effects (Aida and Silveston, 2005). However, the information considering this issue remains restricted to the plant operators and technology owners and mainly particle size re-distribution and capacity decline are mentioned as a result of adsorbent ageing leading to process performance decrease.

Guard beds are normally used in the gas processing industry in order to prevent the impurities access into the separation process, or more elaborated methods such as online adsorbent removal (Pilliod *et al.*, 2006b, 2006a) and innovative fluid distribution apparatus (Frey *et al.*, 2006), to mitigate fines production. Nevertheless, ageing problems such as "parasite" reactions within the solid or liquid phase, and other attrition effects, leading to fine and channelling still occur during operation of industrial SMB units.

By treating adsorbent ageing as a system disturbance it is possible to compensate it by applying SMB online controllers, as pointed out in recent studies (Natarajan and Lee, 2000; Amanullah *et al.*, 2007; Engell, 2007; Grossmann *et al.*, 2008b). However, the implementation of model predictive control methods should also be based on robust ageing models as compensative measures. Additionally, when it comes to design and start-up of a new SMB unit, the analysis of adsorbent ageing factors can have a significant weight on financial and/or management choices involved in these projects. In fact, the "time life" of the adsorbent, a predominant economical factor in the SMB units design as adsorbent cost, has considerable influence on the complete unit design, if not in the main project viability.

Time scales of catalyst/adsorbent deactivation vary in a wide range from few seconds in the case of catalyst cracking, up to 5 to 10 years, as for example in ammonia synthesis with iron catalyst (Bartholomew, 2001). In SMBs separations the adsorbent decline also takes place in different time scales. Chiral separations are known to work at a reasonable efficiency just for 3 to 5 years while in *p*-xylene separation a 20-30% adsorbent capacity decline occurs during a 10 to 20 years period (Minceva and Rodrigues, 2002). These are slow mechanisms, when compared to the dynamic characteristics of the SMB process (the dynamics of attainment of the unit cyclic steady state after some perturbation), but common in the operation of almost every SMB units, and therefore, the ones detailed in this work*.

As mentioned before, a productive SMB unit depends on the calculation of optimal operating parameters (ratio between fluid and the simulated solid interstitial velocities) obtained from the separation region (see section 2.3.3). The optimal unit performance is obtained when working near the vertex of this "triangle", and therefore a slight change in the operating point will lead to the violation of one or more of the separation conditions ruining all the operation (Minceva and Rodrigues, 2005). This slight movement of the operating point could result from the adsorbent ageing problem, even if the operating parameters (internal flows, columns arrangements etc.), are kept at constant optimum values as the ones calculated for the initial unit design.

The idea of working near to the best operation point (near to the vertex and to the Lower Solvent Consumption point), and adjust this location with the adsorbent deactivation, trying to keep it at the same relative distance, is attractive as an adsorbent ageing corrective action.

Therefore, in this Chapter, it is studied the effect of adsorbent ageing on the performance parameters of an SMB unit and some operating strategies to overcome this problem are proposed. The same methodology here-by presented, can also be used to compare adsorbents with different properties, as well as for the tuning of SMB units after complete/partial fresh or improved adsorbent changes.

---

* Rapid perturbations involving dramatic changes on the inlet concentrations, for example, the entrance of heavy impurities results on considerable ageing problems, but is not the purpose of this work to address these unpredicted aspects.

Two different consequences of the above stated adsorbent deactivation mechanisms are considered in this Chapter: the adsorbent capacity decrease and the increase of mass transfer resistances. For each case, different compensating strategies are presented: (i) the decrease of switching time (solid flow rate increase), as a continuous corrective strategy for the adsorbent capacity decrease; and (ii) the decrease of internal flow rates and increase of switching time to compensate the mass transfer resistances increase. The compensation strategies are not similar or compatible and therefore it is important to understand which is the most significant cause for adsorbent deactivation (the solid capacity decrease or the mass transfer resistances increase). A simple diagnosis method is also suggested to simplify this task. A non continuous strategy is presented: the unit rearrangement, different number of columns per section (performed by means of asynchronous shift SMB, Varicol)with the ageing evolution. These procedures are applied to 3 different systems: sugar, chiral and *p*-xylene separation.

These corrective operational strategies of adsorbent ageing could lead to the extension of the sieve life, keeping similar performance parameters (productivity, recovery and product purities), as the ones established with the initial SMB unit design.

4.2 ADSORBENT AGEING PROBLEM

Adsorbent/catalyst deactivation is generally the result of a number of unwanted chemical and physical changes (Bartholomew, 2001). The causes of deactivation can be divided in three major categories: chemical, thermal and mechanical. In this work the thermal effects, generally associated with high amplitude changes of the operating temperature, will not be considered.

The mechanical deactivation, as a result of physical breakage, attrition or crushing of the adsorbent particle is an important deactivation phenomenon in the SMB separation field. Associated with particle size changes during the SMB unit operation are: the increased columns packing heterogeneity; the formation of preferential paths (channelling); the stagnant zones problems; the increase of pressure drop and dispersion, which lead to substantial drop of columns efficiency. Nevertheless, in terms of consequences, the establishment of preferential paths or dead volumes can be associated with a "global adsorbent capacity" decline (and treated as adsorbent capacity decline), and particle size redistribution associated with the LDF mass transfer coefficient.

Chemical and mechanical deactivation mechanisms may affect both the adsorbent capacity as the intraparticle kinetics. Therefore, instead of studying each adsorbent ageing mechanism separately, the definition of compensation strategies for the two major consequences of the adsorbent deactivation (loss of adsorbent capacity or increase of the mass transfer resistances), is taken as the principal objective of this work. First of all, one needs to study the impact of both adsorbent deactivation consequences on the operation of a regular SMB unit. Secondly, on the basis of the conclusions from these studies, some compensation procedures to overcome ageing problems are proposed.

4.2.1 ADSORBENT CAPACITY DECLINE DUE TO ADSORBENT DEACTIVATION

Under the assumptions of the "Triangle Theory", by consequence the Equilibrium Theory, one can state that each SMB design problem is based on its own adsorption isotherms. In this section, one considers that the only adsorbent ageing consequence is represented by the adsorption capacity decline. Changing the adsorption capacity will change the adsorption equilibrium isotherms and thus the SMB design problem. To maintain the

same, or similar, SMB performance parameters one needs to recalculate new operating parameters. In this way, it is important to study the influence of the adsorbent capacity decline on the separation region, as well as the rectangular regeneration region (Figure 4.1), in order to formulate corrective strategies that will change the operating parameters, overcoming the ageing problem and maintaining the SMB performance parameters the closest possible to the initial ones.

a) Linear isotherms case

Considering the following linear adsorption isotherms as general case,

$$q_i^{eq} = H_i C_{b_i} \tag{4.1}$$

The separation, as the regeneration, can be easily drawn under the "Triangle Theory" assumptions,

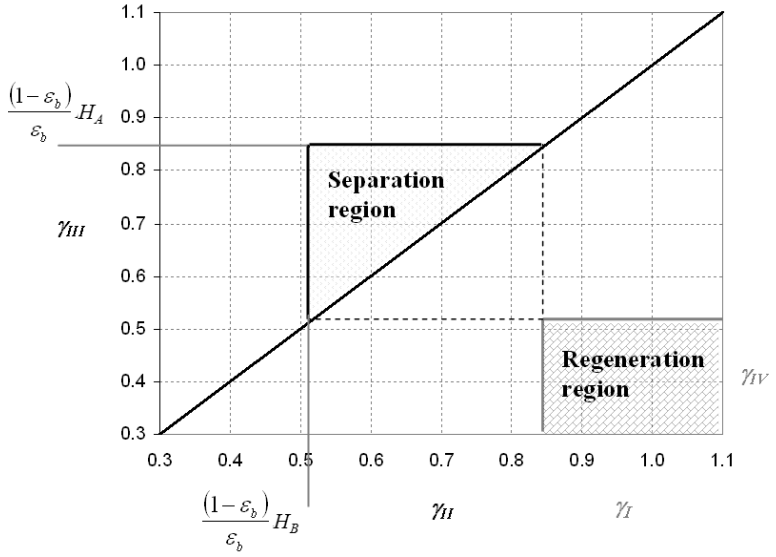

Figure 4.1 - Separation region for linear adsorption isotherms case, under the Triangle Theory assumptions.

It can be assumed that, for a constant feed concentration, the adsorbed capacity decline due to the adsorbent ageing mechanisms can be represented by the decrease of the Henry adsorption constant value H_i, as follows:

$$H_i = H_i^0 f(t) \tag{4.2}$$

where H_i^0 represents the initial value of the Henry adsorption constant and $f(t)$ a general adsorbent ageing law as a function of time.

With the adsorbent capacity decline due to ageing problems, in the case of a binary separation, three general scenarios can happen:

- the deactivation is the same for the different species;
- it is higher for the more adsorbed species (A);
- it is higher for the less adsorbed species (B).

For the deactivation of one species, case ii or iii, it is simple to understand that the separation triangle will be reduced by the upper limit $\frac{1-\varepsilon_b}{\varepsilon_b} H_A$ due to the decrease of H_A value, in the case of species A deactivation only, or will augment by the lower limit $\frac{1-\varepsilon_b}{\varepsilon_b} H_B$ due to the decrease of H_B value, if there is only B species deactivation. These cases are quite specific and almost theoretical, since the more common ageing problems are consequence from adsorbent deactivation of both species. Therefore, in this study only the case (i) will be considered, where both species have the same deactivation rates and thus maintaining constant selectivity[*]. In this case, the decrease of adsorbent capacity for both species results in migration of the separation region downwards to lower values of γ_{II} and γ_{III}, well represented by the change of the vertex point position, where $(\gamma_{II}, \gamma_{III}) = \left(\frac{1-\varepsilon_b}{\varepsilon_b} H_B, \frac{1-\varepsilon_b}{\varepsilon_b} H_A\right)$, as shown in Figure 4.2.

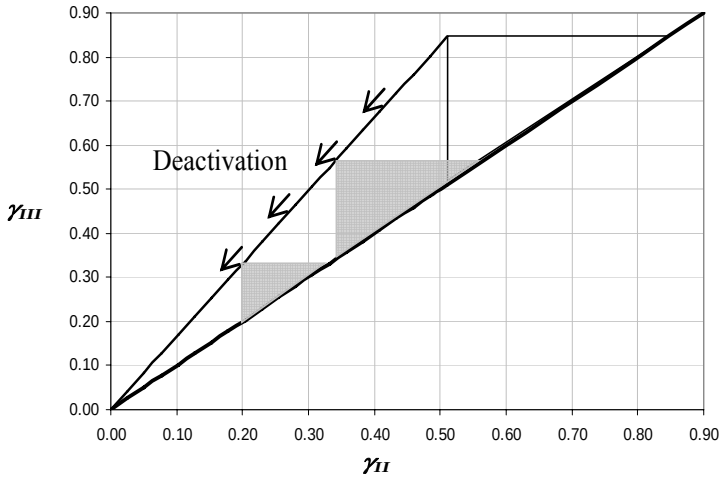

Figure 4.2 – Triangle Theory applied to an SMB design problem: new adsorbent (black) and the capacity decline effect due to aged adsorbent (gray), considering the case (i).

A classic SMB binary separation with linear adsorption isotherms, as the one presented by Leão and Rodrigues (2004) for the separation of a mixture with Fructose (*A*) and Glucose (*B*), characterized by the model parameters and optimized operating conditions presented in Table 4.1 and Table 4.2, was considered as case study.

In this study, the film mass transfer coefficient was considered to be negligible and all mass transfer resistances for both species represented by the k_{LDF}.

The linear adsorption isotherms are as follows:

$$q_A^{eq} = 0.5634 C_{b_A} \tag{4.3}$$

$$q_B^{eq} = 0.3401 C_{b_B} \tag{4.4}$$

with C_{b_i} in g.l^{-1} and q_i^{eq} in g.l$^{-1}_{\text{adsorbent}}$.

[*] This case can be related with the poisoning of the same active sites, used for both species, the increase of dead volumes and channeling aspects that can be considered as a general adsorbent capacity decline phenomena.

By applying the same SMB model with LDF approach as the one described in Chapter 2, it is possible to observe the effect of adsorbent capacity decline on the SMB concentration profiles. Therefore, let us now assume various levels of adsorbent ageing effect by reducing the Henry constant for both fructose and glucose by 2, 4, 6 and 8 %, keeping the same operating conditions as those presented in Table 4.1 and Table 4.2.

Table 4.1 –SMB unit characteristic parameters for the linear adsorption isotherm case, (Leão and Rodrigues, 2004).

Model Parameters	SMB Columns
Pe_j=2000	n_j = [3 3 3 3]
ε_b=0.4	L_c=11.5 cm
	d_c=2.6 cm
k_{LDF}=0.1 s^{-1}	SMB Operating Conditions
	C_i^F=30 $g.l^{-1}$
	t_s=105 s;
	Q_E =8.23 $ml.min^{-1}$; Q_X =5.62 $ml.min^{-1}$;
	Q_F =1.28 $ml.min^{-1}$; Q_R =3.89 $ml.min^{-1}$;
	Q_{IV}^*=19.89 $ml.min^{-1}$.

Table 4.2 – The SMB and equivalent TMB section operating conditions for the linear adsorption isotherm case (Leão and Rodrigues, 2004).

SMB model approach	TMB model approach
γ_j^* =[2.01 1.61 1.70 1.43]	γ_j =[1.01 0.61 0.70 0.43]
Q_j^*=[28.12 22.50 23.78 19.89] $ml.min^{-1}$	Q_j =[14.16 8.54 9.82 5.93] $ml.min^{-1}$

The concentration profiles at half switching time in the Cyclic Steady state (CSS) and SMB performances at different levels of adsorbent deactivation (percentage of adsorbent capacity lost) are presented in Figure 4.3 and Table 4.3, respectively.

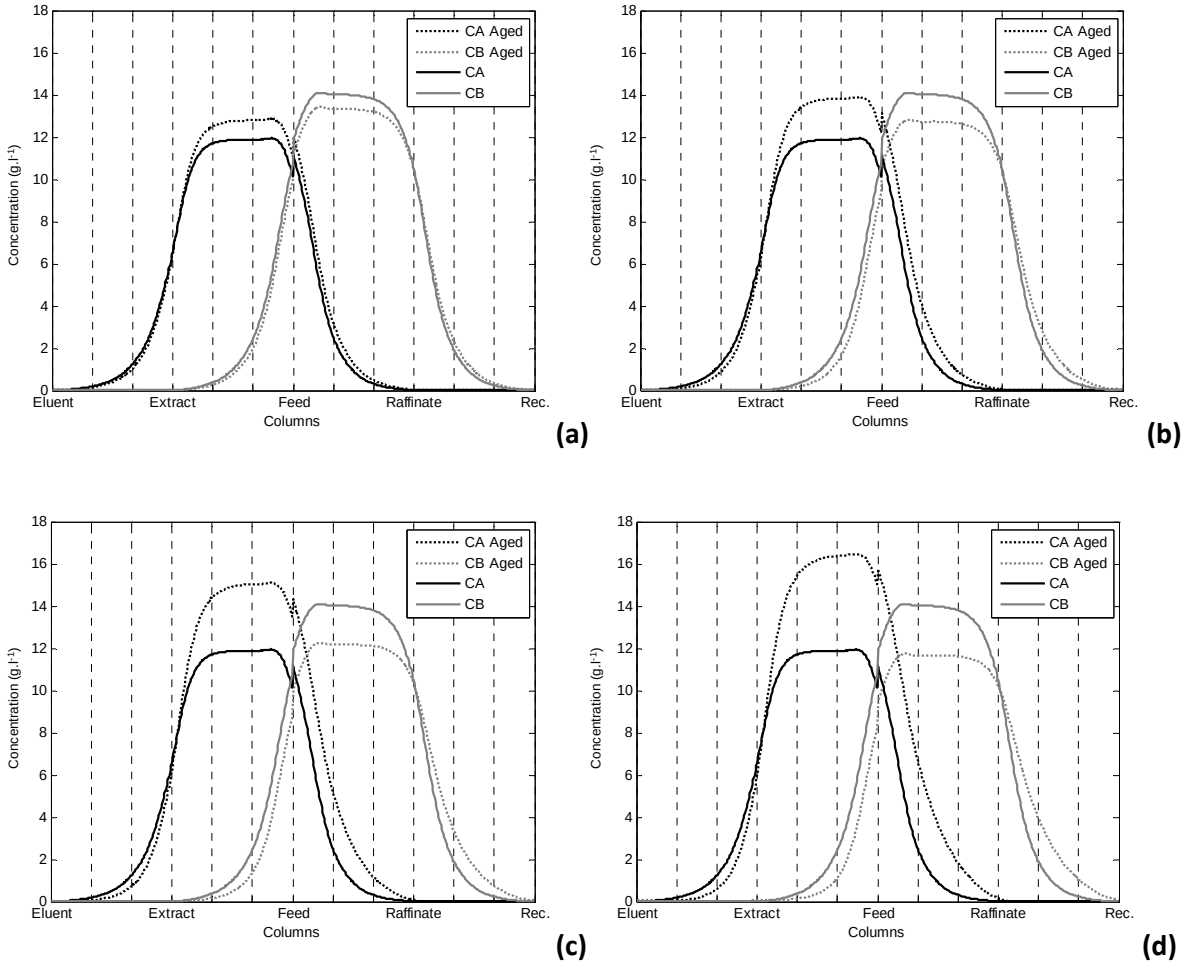

Figure 4.3 – SMB bulk concentration profiles of fructose (A) and glucose (B) as result of adsorbent capacity decline (a) H_A=0.5521 and H_B=0.3333 (less 2%), (b) H_A=0.5409 and H_B=0.3265 (less 4%), (c) H_A=0.5296 and H_B=0.3197 (less 6%) and (d) H_A=0.5183 and H_B=0.3129 (less 8%), at half of the swicthing time in the CSS.

Table 4.3 – SMB performance parameters values for different levels of adsorbent deactivation: 2, 4, 6 and 8 % (adsorbent capacity decrease: H_A=0.5521 and H_B=0.3333, H_A=0.5409 and H_B=0.3265, H_A=0.5296 and H_B=0.3197 and H_A=0.5183 and H_B=0.3129, respectively).

Deactivation (%)	PU_X (%)	PU_R (%)	RE_X (%)	RE_R (%)
0	99.5	99.6	99.6	99.5
2	99.6	99.5	99.5	99.6
4	99.5	99.2	99.2	99.5
6	99.4	98.7	98.7	99.4
8	99.2	97.7	97.7	99.2

As can be observed in Figure 4.3, the tendency of concentration profiles change is not the same in each section, even if the adsorbent capacity decline is the same for both species. With the adsorbent capacity decline, the bulk

concentration fronts moved from left to the right. It is also interesting to observe that when the solute is essentially "moving" with the solid (from section IV to section I direction) in sections III and IV, the fluid bulk concentration have increased, while when the solute is being transported in the direction of the fluid phase (section I and II) the bulk concentration decreased. This tendency is noted both in the plateaus zone (section II and II) and in the regeneration region I and IV. This behaviour can be related with the distance between the operating point (represented by the set $(\gamma_{II} \times \gamma_{III})$ and $(\gamma_I \times \gamma_{IV})$) to its respective constraints, which changed as a result for adsorbent capacity decline.

From Table 4.3, it can be noted that by increasing the deactivation level, the raffinate became more polluted than the extract; consequence of the fronts movement from left to right, as shown before by Figure 4.3. From Figure 4.3, it can be noted that the concentration plateau value, for the more adsorbed species (A) in section II, was lower than the one for the less adsorbed species (B) in section III. However, at a certain adsorbent capacity decline level, the concentration plateaus ratio was reversed, becoming the A plateau in section II higher than the B plateau in section III. This behaviour can be justified by the following analysis based on the Equilibrium Theory and the TMB model approach.

Assuming that A product fed to the SMB unit is recovered in the extract and all product B is recovered in the raffinate and that the solid adsorbed concentration is in equilibrium with the corresponding fluid flow concentration, species A will only be present in section II and species B in section III, and thus:

$$\begin{cases} Q_s H_A C_{b\,A,II} - Q_{II} C_{b\,A,II} = Q_X C_{b\,A}^X = Q_F C_{b\,A}^F \\ Q_{III} C_{b\,B,III} - Q_s H_B C_{b\,B,III} = Q_R C_{b\,B}^R = Q_F C_{b\,B}^F \end{cases} \tag{4.5}$$

which means that:

$$\frac{C_{b\,A,II}}{C_{b\,B,III}} = \frac{C_{b\,A}^F}{C_{b\,B}^F} \frac{(Q_{III} - Q_s H_B)}{(Q_s H_A - Q_{II})} \tag{4.6}$$

For the same operating conditions the ratio $\frac{C_{b\,A,II}}{C_{b\,B,III}}$, as a function of adsorbent capacity loss (deactivation %), is shown Figure 4.4.

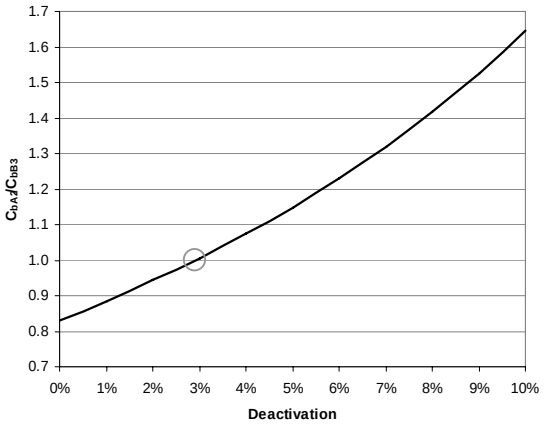

Figure 4.4 – Concentration ratio in plateaus $\frac{C_{b\,A,II}}{C_{b\,B,III}}$, as a function of adsorbent deactivation (%), assuming the equilibrium theory.

In Figure 4.4, it can be observed that for adsorbent capacity decline higher than 3 % the species A concentration plateau in section II is higher than the concentration plateau of species B in section III and *vice-versa*.

b) Non-linear isotherm case

The influence of the adsorbent capacity decline on the SMB performances in the case of non-linear isotherm was also studied. Therefore, the case of a chiral separation characterized by a linear + Langmuir adsorption equilibrium isotherm, represented by eq. (4.7) was considered.

$$q_i^{eq} = m_i C_{b_i} + \frac{q_{m_i} K_i C_{b_i}}{1+\sum_{l=1}^{NC} K_l C_{b_l}} \tag{4.7}$$

For a constant feed concentration, the adsorbed capacity decline was simulated by means of the maximum adsorption capacity (q_{m_i}). Of course ageing can also affect the particle porosity and diffusivity. Nevertheless, only the reduction of the maximum adsorption capacity will be considered in this study. Similarly to what was performed for the linear adsorption isotherm case, eq. (4.8):

$$q_{m_i} = q_{m_i}^0 f(t) \tag{4.8}$$

where $q_{m_i}^0$ represents the initial maximum adsorption capacity and *f(t)* is a law of the adsorbent ageing as a function of time.

The enantiomer separation presented by Rodrigues and Pais (2004b) was considered as case study for the analysis of the capacity decline influence on the binary separations characterized by non-linear adsorption isotherms. The interstitial velocity ratios values (γ_j^* or γ_j) for sections I and IV were kept constants and far from the critical values calculated by the Triangle Theory design methodology for complete solid and eluent regeneration in section I and IV, respectively. For the sections II and III the interstitial velocity ratios were taken from the analysis presented by Rodrigues and Pais based on the ($\gamma_{II} \times \gamma_{III}$) separation region for a 99.0 % purity criterion with a mass transfer coefficient of k_{LDF}=0.33 s^{-1}. The summary of all operating conditions and model parameters is presented in Table 4.4 and Table 4.5.

The linear plus Langmuir isotherms in terms of retained concentration in the particles for both species represented by eqs. (4.9-4.10):

$$q_A^{eq} = 1.35 C_{b_A} + \frac{7.32 \cdot 0.163 C_{b_A}}{1+0.163 C_{b_A}+0.087 C_{b_B}} \tag{4.9}$$

$$q_B^{eq} = 1.35 C_{b_B} + \frac{7.32 \cdot 0.087 C_{b_B}}{1+0.163 C_{b_A}+0.087 C_{b_B}} \tag{4.10}$$

considering C_{b_i} in g.l^{-1} and q_i^{eq} in g.$l_{\text{adsorbent}}^{-1}$.

Table 4.4 – SMB unit characteristic parameters for the non linear adsorption isotherm case, (Rodrigues and Pais, 2004b).

Model Parameters	SMB Columns
Pe_j=1000	n_j=[2 2 2 2]
ε_b=0.4	L_c=9.9 cm
r_p=2.25x10^{-5} m	d_c=2.6 cm
	Classic SMB Operating Conditions
k_{LDF}=0.33 s^{-1}	C_i^F=5 g.l^{-1}
	t_s=198 s
	Q_E =25.04 ml.min^{-1}; Q_X =17.98 ml.min^{-1};
	Q_F =0.95 ml.min^{-1}; Q_R =8.01 ml.min^{-1};
	Q_{IV}^*=17.79 ml.min^{-1}.

Table 4.5 - The SMB and equivalent TMB sections operating conditions non linear adsorption isotherm case, (Rodrigues and Pais, 2004b).

SMB model approach	TMB model approach
γ_j^*=[6.72 3.90 4.05 2.79]	γ_j =[5.72 2.90 3.05 1.79]
Q_j^*=[42.83 24.85 25.80 17.79] ml.min^{-1}	Q_j =[36.46 18.48 19.43 11.42] ml.min^{-1}

The mathematical strategy used was again the SMB model with LDF approach presented in Chapter 2. By keeping the same operating parameters it was possible simulate different adsorbent ageing rates (adsorbent capacity decline percentage) and thus, observe how the bulk concentration profiles (Figure 4.5) and SMB performance parameters (Table 4.6) are affected by the adsorbent capacity decline.

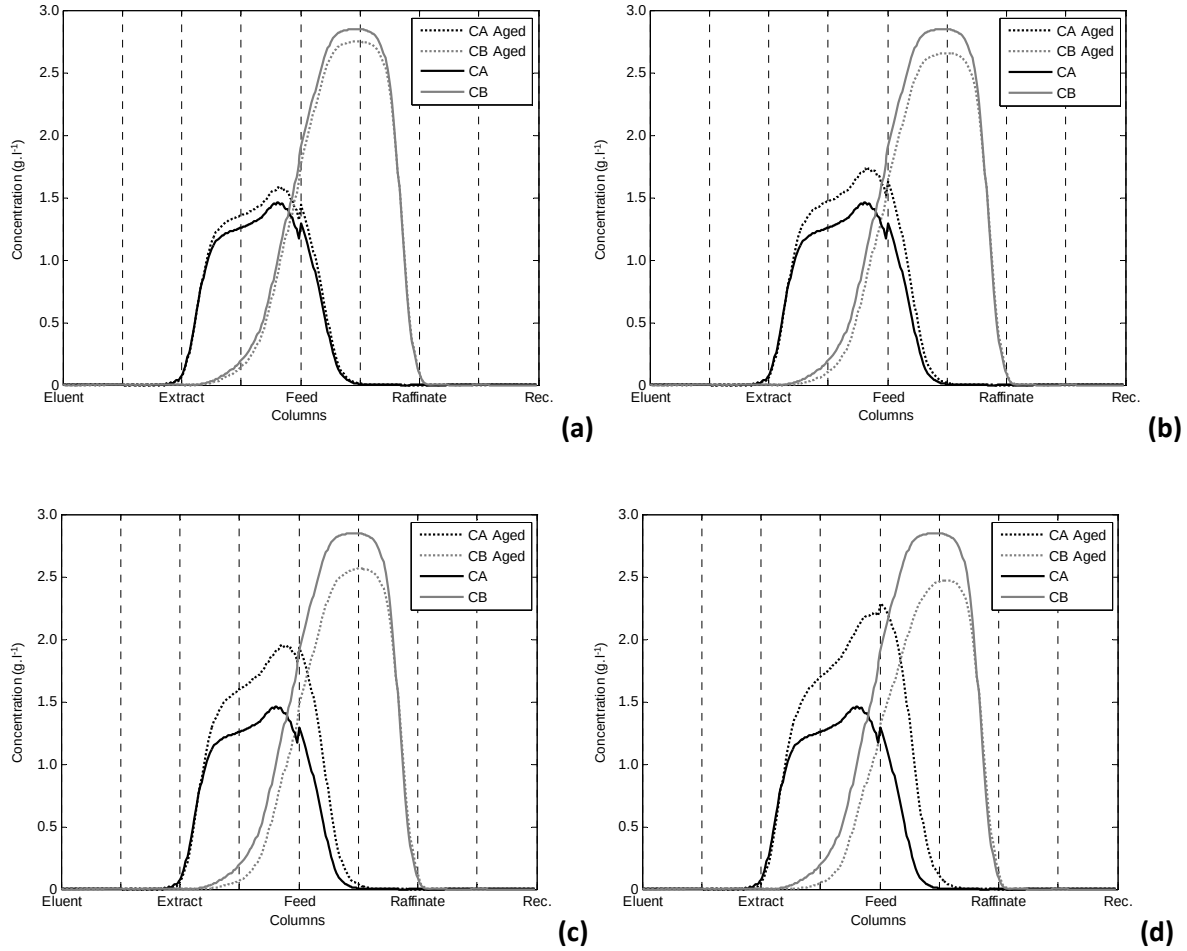

Figure 4.5 – SMB bulk concentration profiles of the as result of aged adsorbent (a) q_{m_i}=7.17 (less 2 %), (b) q_{m_i}=7.03 (less 4 %), (c) q_{m_i}=6.88 (less 6 %) and (d) q_{m_i}=6.73 (less 8 %), at half switching time in the CSS.

Table 4.6 – SMB performance parameters values for different levels of adsorbent deactivation: 2, 4, 6 and 8 % (adsorbent capacity decrease: q_{m_i}=7.17, q_{m_i}=7.03, q_{m_i}=6.88 and q_{m_i}=6.73, respectively).

Deactivation (%)	PU_X (%)	PU_R (%)	RE_X (%)	RE_R (%)
0	99.0	100.0	100.0	99.0
2	99.4	100.0	100.0	99.4
4	99.6	100.0	100.0	99.7
6	99.8	99.7	99.6	99.9
8	99.9	99.8	99.4	100.0

From Figure 4.5, it can be observe that the concentration profiles moved to the right as already noted for the case of linear adsorption isotherms. Again the raffinate purity will decrease for higher adsorbent capacity decrease.

Considering the "Triangle Theory" for non-linear systems it must be taken into account that the separation region is no longer a rectangular triangle, as for the linear case, but has a "triangle shaped form" calculated from (Mazzotti *et al.*, 1994), here, and for sake of simplicity, without the curved lines, Figure 4.6.

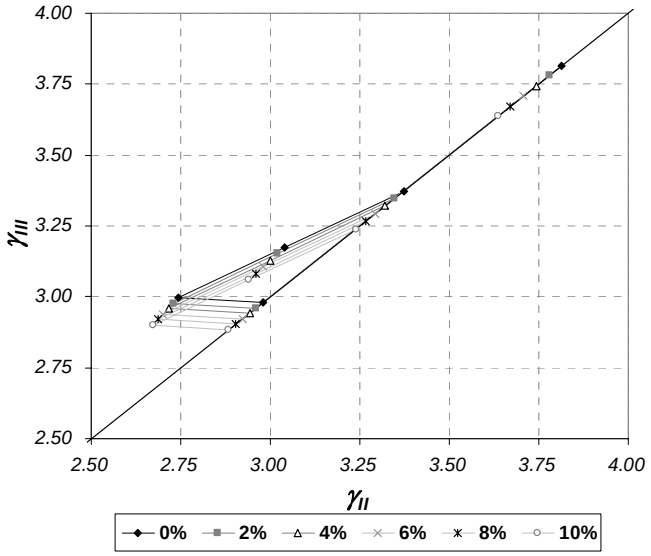

Figure 4.6 - Nonlinear separation region for the studied enantiomer separation, different ageing adsorbent rates (0 %, 2 %, 4 %, 6 %, 8 % and 10 % adsorbent capacity decline rate).

As can be perceived from Figure 4.6, and as observed before for the linear adsorption isotherm case, the separation region moves downwards in the $(\gamma_{II} \times \gamma_{III})$ plan as the adsorbent capacity decline increases.

4.2.2 INCREASE OF MASS TRANSFER RESISTANCES DUE TO ADSORBENT AGEING PROBLEMS

The influence of the increase of mass transfer resistances on the SMB performance will be studied by analysing the consequences of k_{LDF} value decrease:

$$k_{LDF} = k_{LDF}^{0} g(t) \tag{4.11}$$

where k_{LDF}^{0} represents the initial mass transfer coefficient and $g(t)$ a general law of the mass transfer resistance increase due to adsorbent ageing problem as a function of time.

a) Linear isotherms case

Various adsorbent ageing levels, due to the increase of the mass transfer limitation, have been simulated (once more by means of the SMB with LDF approach) by reducing the mass transfer coefficient values for both fructose and glucose by 10, 20, 30 and 40 % of its initial value, keeping the same operating conditions as those presented in Table 4.1 and Table 4.2. The bulk concentration profiles at half switching time in the CSS and SMB performance parameters are presented in Figure 4.7 and Table 4.7, respectively.

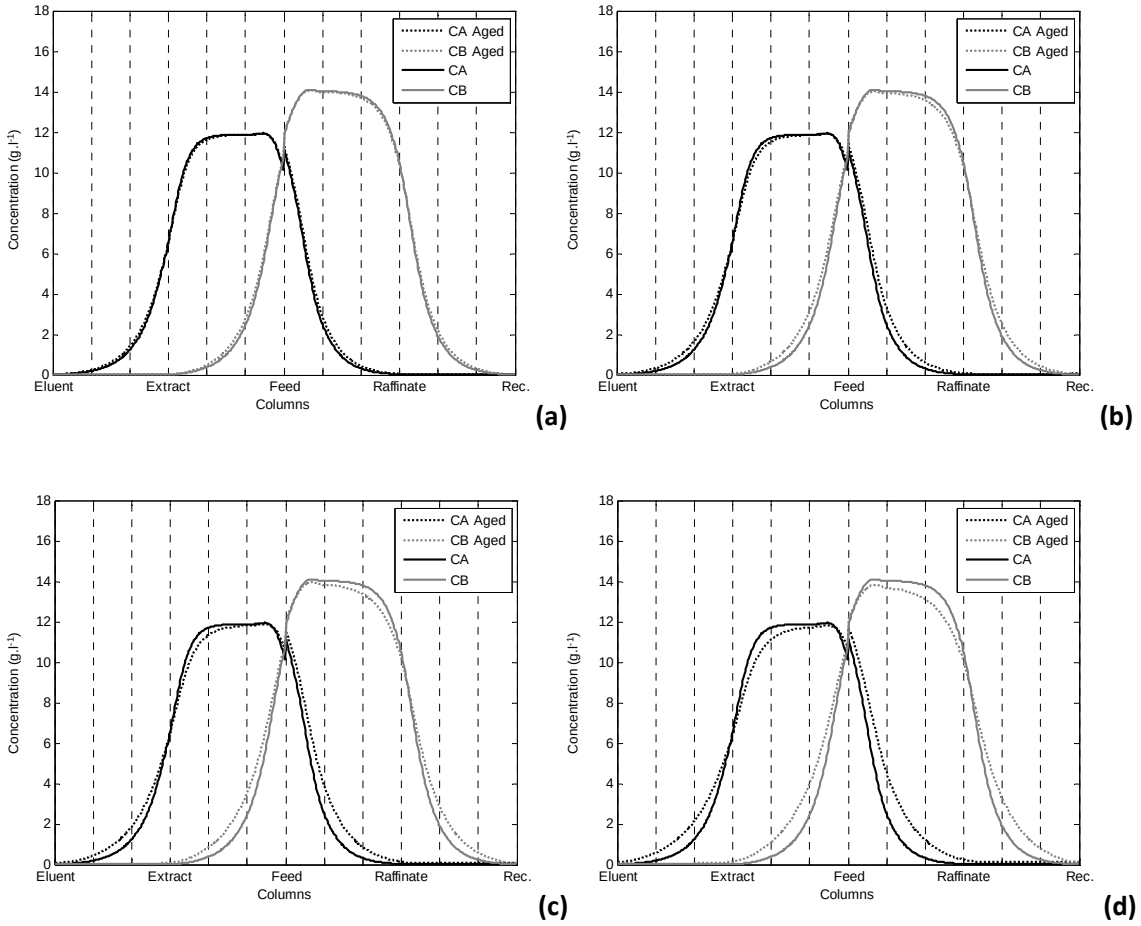

Figure 4.7 –SMB concentration profiles of fructose (*A*) and glucose (*B*) as result of mass transfer coefficient decrease: (a) k_{LDF}=0.09 s^{-1} (less 10 %), (b) k_{LDF}=0.08 s^{-1} (less 20 %), (c) k_{LDF}=0.07 s^{-1} (less 30 %) and (d) k_{LDF}=0.06 s^{-1} (less 40 %), at half switching time in the CSS.

Table 4.7 – SMB performance for different levels of adsorbent deactivation: 10, 20, 30 and 40 % (adsorbent mass transfer resistance increase: k_{LDF}=0.09 s^{-1}, k_{LDF}=0.08 s^{-1}, k_{LDF}=0.07 s^{-1} and k_{LDF}=0.06 s^{-1}, respectively).

Deactivation (%)	PU_X (%)	PU_R (%)	RE_X (%)	RE_R (%)
0	99.5	99.6	99.6	99.5
10	99.3	99.4	99.4	99.3
20	98.9	99.0	99.0	98.9
30	98.2	98.4	98.4	98.2
40	97.2	97.3	97.3	97.2

As can be observed from Figure 4.7, with the increase of mass transfer limitation the concentration plateaus of both species remain unchanged, but the concentration profiles become more dispersed, leading to SMB products contamination and decline of the product purities and recoveries (see Table 4.7).

b) Non-Linear isotherms case

The same procedure will now be applied for the non-linear isotherm case, considering 10, 20, 30 and 40 % decrease of k_{LDF} for both species; the remaining operating conditions are kept constant as those presented in Table 4.4 and Table 4.5.

The effect of different levels of mass transfer resistance increase on the enantiomers concentration profiles at half switching time in the CSS and SMB performances are presented in Figure 4.8 and Table 4.8, respectively.

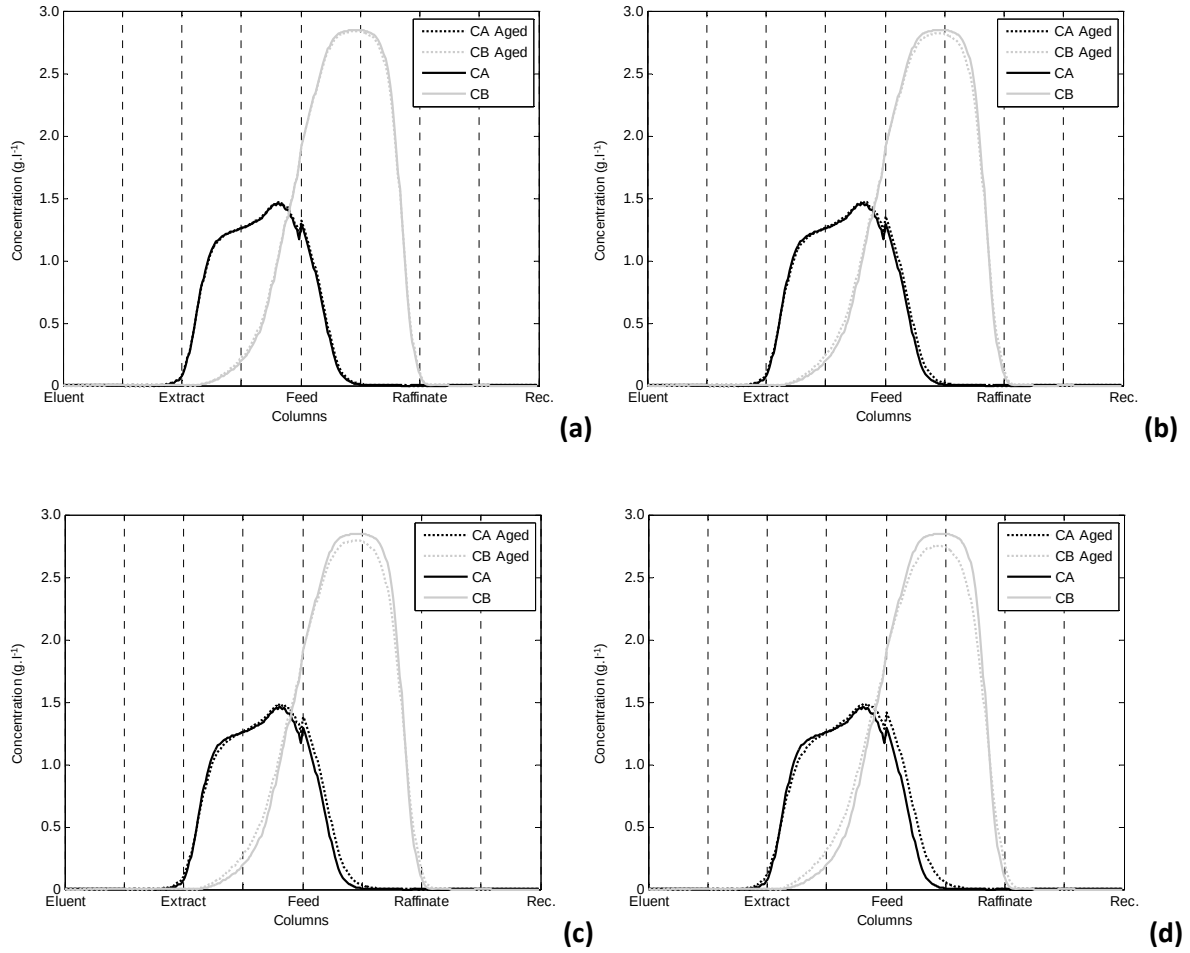

Figure 4.8 – SMB concentration profiles for enantiomers separation with increasing mass transfer resistance (a) k_{LDF}=0.30 s^{-1} (less 10%), (b) k_{LDF}=0.26 s^{-1} (less 20%), (c) k_{LDF}=0.23 s^{-1} (less 30%) and (d) k_{LDF}=0.20 s^{-1} (less 40%), at half swicthing time in the CSS.

Again, from Figure 4.8 and Table 4.8, it can be noted that, when the mass transfer resistances increases, lower purity and recovery are obtained; either for the more retained product in the extract or for the less retained one in the raffinate. In this case, as in the case of linear isotherm, the plateaus remain unchanged, but the concentration profiles become more dispersed and thus, the contaminating fronts have been stretched leading to SMB products contamination.

Table 4.8 – SMB performance parameters for different levels of adsorbent deactivation: 10, 20, 30 and 40 % (adsorbent mass transfer resistance increase: k_{LDF}=0.30 s^{-1}, k_{LDF}=0.26 s^{-1}, k_{LDF}=0.23 s^{-1} and k_{LDF}=0.20 s^{-1}, respectively).

Deactivation (%)	PU_X (%)	PU_R (%)	RE_X (%)	RE_R (%)
0	99.0	100.0	100.0	99.0
10	98.7	100.0	100.0	98.7
20	98.3	100.0	100.0	98.4
30	97.8	100.0	99.9	97.9
40	97.0	99.9	99.8	97.1

At this point, it is important to note that the adsorbent capacity decline or mass transfer resistance increase have different influence on the concentration profiles in certain sections. Both ageing consequences led to similar behaviours on concentration profiles for the more retained component in section III and the less retained species in section IV. The contaminating or collection fronts in sections III and IV have moved to the right (in the direction of the fluid movement). Therefore, if the two ageing factors are present at the same time it is difficult to know which one is the dominant. On the other hand, the changes in concentration profiles as a result of adsorbent capacity decline and mass transfer resistance increase are different in sections I and II. In fact, with adsorbent capacity decline, the mentioned fronts are moving to the right while, in the case of ageing mechanisms that lead to mass transfer resistances increase, the same fronts move to the left. As consequence, different consequences which allow the use the movement of fronts in section I and II for the diagnosis of the dominant ageing factor.

4.3 CORRECTIVE STRATEGIES

For each of the adsorbent ageing consequences analysed before: adsorbent capacity decline and increase of mass transfer resistances, one corrective strategy will be stated to compensate them.

4.3.1 ADSORBENT CAPACITY DECLINE DUE TO ADSORBENT DEACTIVATION

From Figure 4.2 and Figure 4.6, it can be concluded that to have similar SMB performance with aged adsorbent as those with fresh absorbent, the γ_j operating parameters should be decreased, keeping the same relative distance to the respective constraints (triangle borders).

Keeping the same inlet and outlet flow rates, two straightforward corrective strategies to decrease the γ_j values are possible: i) decrease the SMB switching time period (increase of the solid velocity); and ii) decrease the recycle flow rate (Q_{IV}). The paths of these corrective measurements, presented in the $(\gamma_{II} \times \gamma_{III})$ plane, are shown in Figure 4.9. The switching time corrective path (c), follows the adsorbent ageing pathway, (see the vertex line in Figure 4.9). However, the recycle flow rate corrective measurement lead to corrective path (p) parallel to the $\gamma_{II} = \gamma_{III}$ line in the $(\gamma_{II} \times \gamma_{III})$ plan.

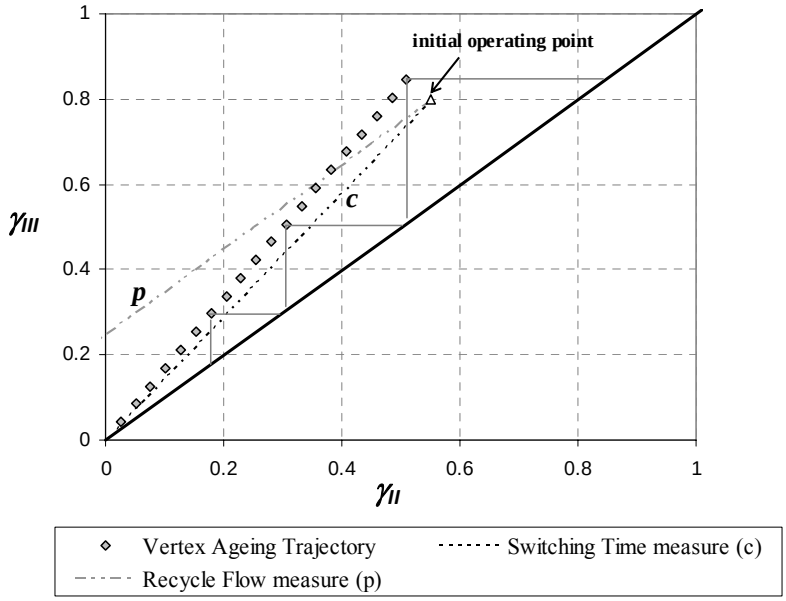

Figure 4.9 – Comparison between two possible corrective measures to adsorbent capacity decline, the switching time decrease (solid flow rate increase, path (c)) and internal flow rate decrease, path (p).

Also, it is simple to understand that the adsorbent deactivation can be compared to the decrease of the "active" solid flow rate and thus a simple way to compensate it is to increase the solid flow rate.

A better visualization of this assumption can be obtained by reformulation of Figure 4.2, presenting the Equilibrium Theory constraints in terms of fluid phase flow rates. In Figure 4.10 the separation zone is presented in the $(Q_{II} \times Q_{III})$ plan and the regeneration region is presented in the $(Q_I \times Q_{IV})$ plan. The separation region constraints are now $H_B Q_s < Q_{II} < Q_{III} < H_A Q_s$; and the regeneration region limited by $Q_{IV} < H_B Q_s$ and $H_A Q_s < Q_I$.

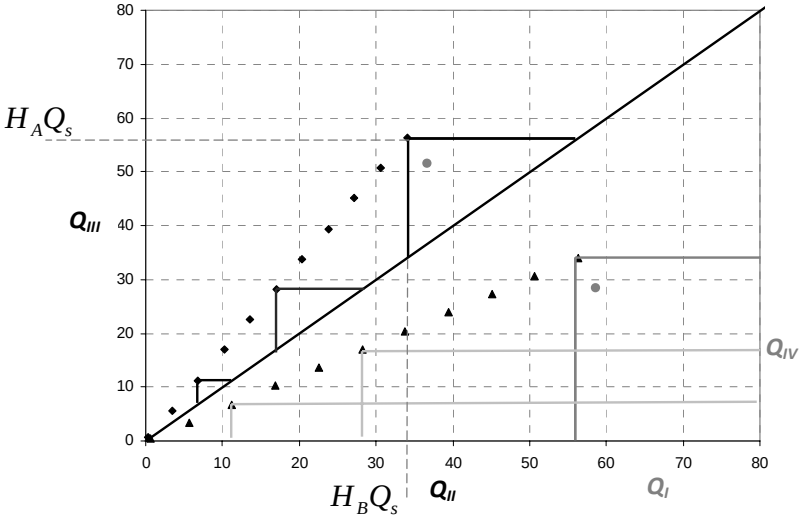

Figure 4.10 – Separation and regeneration zones represented in $(Q_{II} \times Q_{III})$ and $(Q_I \times Q_{IV})$ plans, respectively: black dots are vertexes for different solid flow rates, grey dots are possible operating point (Q_s=100 ml.min^{-1}).

At this stage, it becomes quite easy to understand that a simple and direct corrective measure of the adsorbent capacity decline in the SMB units operating under equilibrium conditions could be the decrease of the SMB switching time (increase of the solid flow rate). However, in the SMB separations where mass transfer limitations are considerable, the solution of the adsorbent aging problem related to adsorption capacity decline will not be so simple as stated before.

The separation regions for the fructose/glucose SMB separation for different product purities requirements was drawn from successive simulations of different ($\gamma_{II} \times \gamma_{III}$) pairs by means of the TMB model with LDF approach (as presented in Chapter 2) for a fresh adsorbent, Figure 4.11. By these means it is possible to infer about the influence of several parameters, such what have been done for the influence of γ_I and γ_{IV} under the Separation Volume Methodology (Azevedo and Rodrigues, 1999), in one more accurate representation of the separation region.

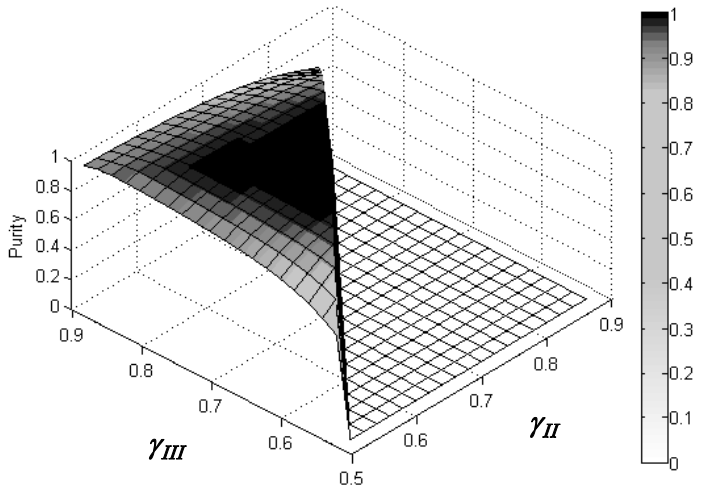

Figure 4.11 – Separation region for different product purities requirements for the case of glucose/fructose SMB separation, Q_s=20.93 ml.min^{-1}.

As mentioned before in Chapter 2, the separation region is not a rectangular triangle for a given purity value as stated by the Equilibrium Theory, but has a rounded shape. This rounded shape is also function of the solid flow rate. Namely, when higher values of the solid flow rates are used the mass transfer resistances become more important and the deviation from the separation regions defined by the Equilibrium Theory becomes more significant. In fact, the solid residence time becomes shorter and the ratio between the switching time (solid residence time) and the τ_p (intraparticle mass transfer time constant $\tau_p = \frac{1}{k_{LDF}}$) decreases. Therefore, the study of the corrective strategy stated before, should also take into account the mass transfer limitations described by the TMB model with LDF approach**.**

The SMB (TMB) inlet/outlet flow rates [Q_E Q_X Q_F Q_R] = [8.23 5.62 1.28 3.89] ml.min^{-1} as the section flow rates will be kept constant.

The analysis on the corrective measure is done by applying a one degree of freedom (DOF) analysis, decreasing the operating parameters γ_j, varying Q_s and observing the performance parameters evolution for different values of adsorbent deactivation.

By increasing the solid flow rate Q_s (decrease of switching time), it is possible as a first approach, to reach the new optimum operating conditions obtaining performance parameters near to those predicted when using fresh adsorbent. Consequently, it is interesting to observe the performance parameters dependence on the switching time at different levels of deactivation, presented in Figure 4.12. The influence on the productivity parameters is similar to the recovery, as stated in eqs (2.73) or (2.74).

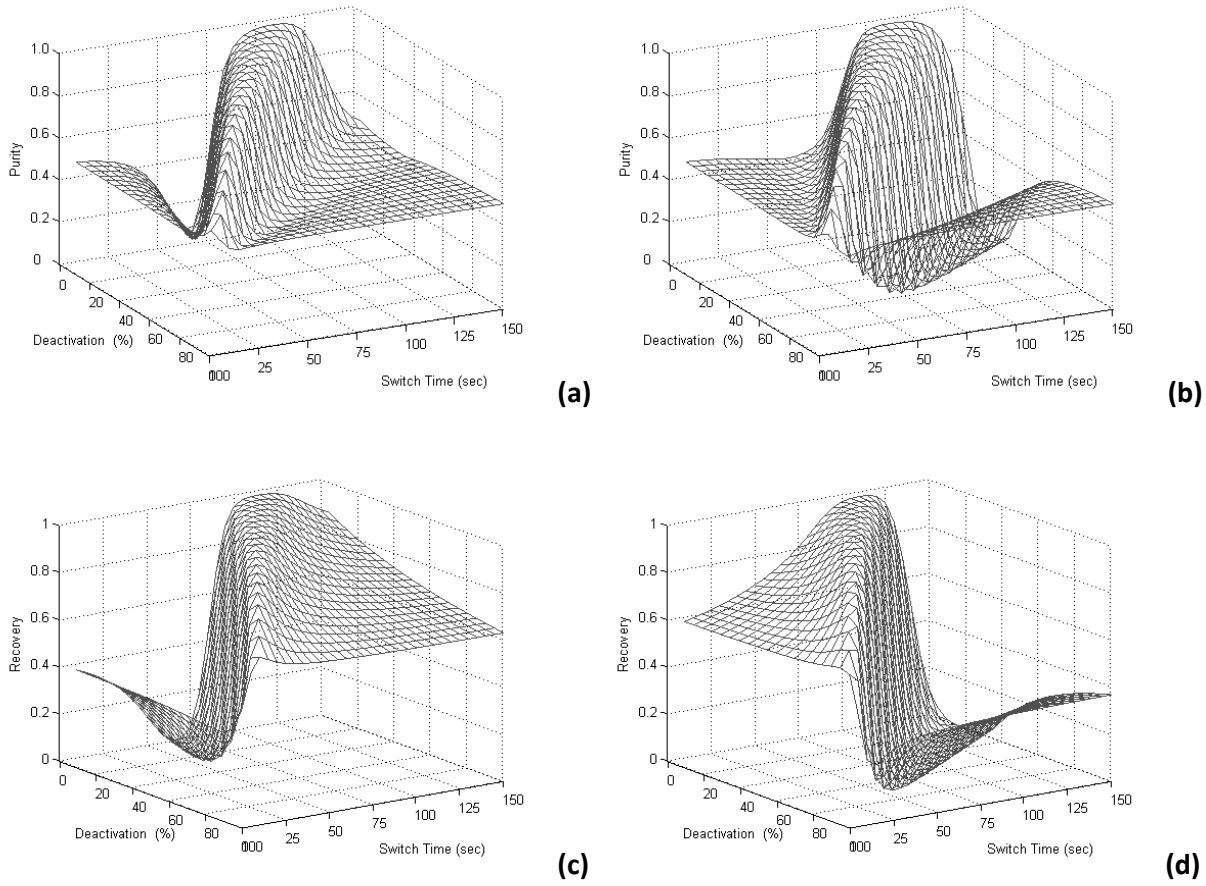

Figure 4.12 – Effect of switching time analysis for different values of adsorbent ageing deactivation values (percentage of adsorbent capacity decrease), in the SMB performance parameters, (a) A purity in the extract, (b) B purity in the raffinate, (c) A recovery in the extract and (d) B recovery in the raffinate, linear isotherms case.

As can be observed in Figure 4.12, the adsorbent capacity decline leads to a decrease of the SMB performance, even when the optimum switching time is used for the compensation at each degree of adsorbent ageing.

However, there is a narrow plateau (in the range between 0 % and +/-30 % of adsorbent capacity decline) where the variation of the time switch helps in the ageing problem compensation, as detailed in Figure 4.13.

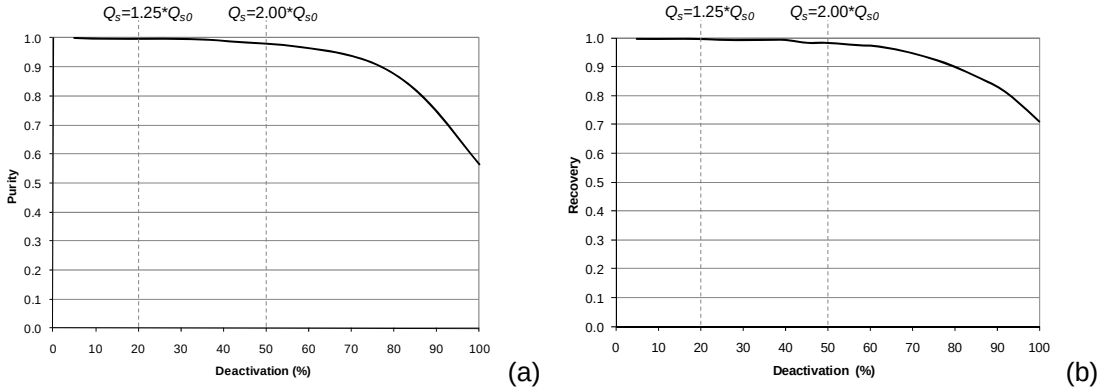

Figure 4.13 – Solid flow rates optimum values, leading to the highest possible purity for different adsorbent ageing deactivation values (percentage of adsorbent capacity decrease) (a), and recovery (b). The Q_s equivalent solid flow rate and Q_{s0} is the solid flow rate for fresh adsorbent.

4.3.2 MASS TRANSFER RESISTANCES INCREASE DUE TO ADSORBENT DEACTIVATION

In this analysis it is useful to rewrite the TMB and SMB model approaches (with LDF approximation) presented in Chapter 2, to account for all mass transfer resistances and axial dispersion effects in a pseudo-LDF equivalent number of intraparticle mass transfer units (Ruthven, 1984), and thus becoming,

$$\frac{1}{\widetilde{k_{LDF}}H_i} = \frac{D_{b_j}}{u_j^*}\frac{(1-\varepsilon_b)}{\varepsilon_b} + \frac{r_p}{3k_f} + \frac{{r_p}^2}{15D_{pe_i}H_i} \tag{4.12}$$

For the SMB model approach a global $\widetilde{k_{LDF}^*}$ based on u_j^* should be used.

Eq. (4.12) results from the equivalence of the model represented by eq. (2.31) and (2.32) (or 2.63 and 2.64), and a simpler one which considered plug flow for the fluid phase and lumped all kinetic effects in a pseudo-LDF parameter ($\widetilde{k_{LDF}}$ or $\widetilde{k_{LDF}^*}$). This is an extension of the Glueckauf approximation for linear systems in which more than one mass transfer resistance and axial dispersion are significant and based on the equality of moments of impulse responses for both models. The term $\frac{1}{Pe_j}\frac{\partial^2 C_{b_{i,j}}}{\partial x^2}$ in eq. (2.31) or $\frac{1}{Pe_k^*}\frac{\partial^2 C_{b_{i,k}}}{\partial x^{*2}}$ in eq. (2.63) is then neglected, since the axial dispersion contribution is already considered in eq. (4.12).

Thus, the TMB model approach with this pseudo-LDF approximation becomes, for the Steady State:

for the bulk fluid mass balance,

$$0 = -\frac{dC_{b_{i,j}}}{dx} - \frac{(1-\varepsilon_b)}{\varepsilon_b}\frac{\widetilde{k_{LDF}}}{u_j}L_c n_j\left(q_{i,j}^{eq} - \langle q_{i,j}\rangle\right) \tag{4.13}$$

and for the "solid phase" mass balance,

$$0 = \frac{d\langle q_{i,j}\rangle}{dx} + \frac{\widetilde{k_{LDF}}}{u_s}L_c n_j\left(q_{i,j}^{eq} - \langle q_{i,j}\rangle\right) \tag{4.14}$$

For the SMB mode approach the transient equations are now:

in the case of the bulk fluid mass balance,

$$\frac{\partial C_{b_{i,k}}}{\partial \theta} = -\frac{u_j^* t_s}{L_c}\frac{\partial C_{b_{i,k}}}{\partial x^*} - \frac{(1-\varepsilon_b)}{\varepsilon_b}\widetilde{k_{LDF}^*}\, t_s\left(q_{i,k}^{eq} - \langle q_{i,k}\rangle\right) \tag{4.15}$$

and for the "solid phase" mass balance,

$$\frac{\partial \langle q_{i,k}\rangle}{\partial \theta} = \widetilde{k_{LDF}^*}\, t_s\left(q_{i,k}^{eq} - \langle q_{i,k}\rangle\right) \tag{4.16}$$

It can be easily understood that a $\widetilde{k_{LDF}}$ (or $\widetilde{k_{LDF}^*}$) decrease can be compensated by a same amplitude decrease on u_j (or u_j^*) and u_s (or t_s increase) values, and therefore, maintaining the unit purity and recovery values. Nevertheless, this compensation measure leads to a productivity value reduction, with the same amplitude as for the mass transfer coefficient decrease. For example, if the mass transfer coefficient decreases 10 % the productivity will also decrease around 10 %. This strategy will maintain the same dimensionless operating parameters γ_j (or γ_j^*), since u_j (or u_j^*) and u_s values decrease is done by the same factor, equal to that of $\widetilde{k_{LDF}}$ (or $\widetilde{k_{LDF}^*}$). For the corrected values of u_j (or u_j^*) and u_s (or t_s), the separation region ($\gamma_{II} \times \gamma_{III}$) will be the same as the one obtained when new adsorbent is used.

With this short-cut strategy it is impossible to maintain the same productivity value as the one calculated for a fresh adsorbent unit, but it is easy to understand and it will allow operating the unit keeping the purity requirements. A more complete analysis would be necessary to compensate the mass transfer resistance increase and at same time guarantee maximum productivity; however, it would require a considerable effort considering all operating conditions, solid and all liquid flow rates, and therefore, a more complex compensating measure.

The calculation effort will be almost the same as to design a new unit. With the re-optimization new values of the solid and liquid flow rates will be establish in a manner of mass transfer resistances increase compensation without losing to much in unit productivity, but losing in other performance parameters, either the extract purity and raffinate recovery or *vice-versa*.

Once again the glucose/fructose SMB separation is used as a case study in this analysis. The concentration profiles and unit performances obtained for the case presented in Figure 4.7b, when adsorbent mass transfer resistances increases for 20 % and 20 % decrease correction is applied for both u_j^* as u_s (t_s increase), are presented in Figure 4.14 and Table 4.9, respectively.

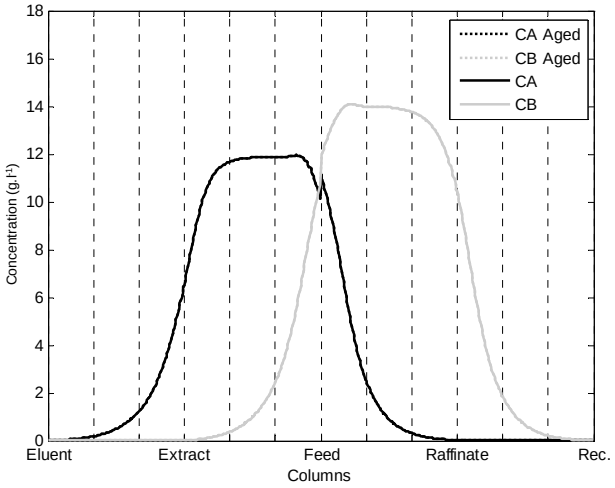

Figure 4.14 – Concentration profiles for fresh adsorbent and 20 % deactivation with mass transfer compensation (both profiles are coincident); linear adsorption isotherms.

Table 4.9 – Performance parameters for fresh adsorbent, 20 % deactivation by mass transfer resistance increase and compensated case: linear adsorption isotherms.

Deactivation (%)	PU_X (%)	PU_R (%)	RE_X (%)	RE_R (%)
0	99.5	99.6	99.6	99.5
20	98.9	99.0	99.0	98.9
20 (corrected)	99.5	99.6	99.6	99.5

As can be observed from Figure 4.14 and Table 4.9, with application of the proposed straightforward compensating measure is was possible to achieve the same concentration profiles as the ones obtained when the adsorbent was fresh, keeping the same product purity and recovery performances. As was expected the productivity drops for 20 %.

4.3.3 UNIT REARRANGEMENT

The strategies presented before are dynamic and can be applied continuously if the ageing law is well know. In the case of adsorbent capacity decline some sections have improved their function (see Figure 4.3), namely sections I and II, where the length needed for solid regeneration and extract purification is shorter than the one needed with fresh adsorbent. The opposite is observed for sections III and IV. A simple corrective measure to the adsorbent capacity decline due to ageing could be utilization of the "non-used" columns from sections I and II in sections III and IV, where they are needed most. Nevertheless, the practical application of the SMB columns distribution re-arrangement would be difficult to implement, since this corrective measurement would require more problematic unit stabilization (the achievement of a novel CSS).

It would be possible to implement the SMB columns relocation in the cases where the adsorbent capacity decline law is smooth, *i.e.*, when a long time is required to loose some of the adsorbent capacity and the unit has a large

number of columns. Otherwise, the only way for its implementation is to use asynchronous port switching as in the Varicol strategy. By applying variable time switches in the Varicol operational mode it is be possible to change the number of columns per section as corrective measure for the adsorbent ageing problem, for example passing from [2 2 1 1] configuration to [1.5 1.5 1.5 1.5] and [1 1 2 2], etc.

This corrective strategy will be analysed for the SMB enantiomer separation studied by Pais and Rodrigues (2003), in which the equilibrium adsorption isotherms used are the same as in eq. 2.40 and eq. 2.41, the nonlinear case study. The SMB unit characteristics parameters and operating conditions are presented in Table 4.10 and Table 4.11.

Table 4.10 – SMB characteristic parameters and operating conditions, (Pais and Rodrigues, 2003).

Model Parameters	SMB Columns
Pe_j=1600	$\sum_{j=I}^{IV} n_j$=5
ε_b=0.4	L_c=15.84 cm
r_p=2.25x10^{-5} m	d_c=2.6 cm
	SMB Operating Conditions
k_{LDF}=0.4 s^{-1}	C_i^F=5 g.l^{-1}
	t_s=317 s; Q_s =9.55 ml.min^{-1}
	Q_E =25.02 ml.min^{-1}; Q_X =17.34 ml.min^{-1};
	Q_F =0.66ml.min^{-1}; Q_R =8.34 ml.min^{-1};
	Q_{IV}^*=17.76ml.min^{-1}.

Table 4.11 – SMB and equivalent TMB section operating conditions

SMB model approach	TMB model approach
γ_j^*=[6.72 4.00 4.10 2.79]	γ_j =[5.72 3.00 3.10 1.79]
Q_j^*=[42.78 25.44 26.10 17.76] ml.min^{-1}	Q_j =[36.42 19.08 19.74 11.40] ml.min^{-1}

This case study is simulated by the SMB model approach for the corresponding [1 1.5 1.5 1] Varicol configuration and [1 1.75 1.25 1] Varicol configuration, in the case of fresh adsorbent.

When the [1 1.75 1.25 1] Varicol configuration is used all concentration fronts will move to left, as presented in Figure 4.15.

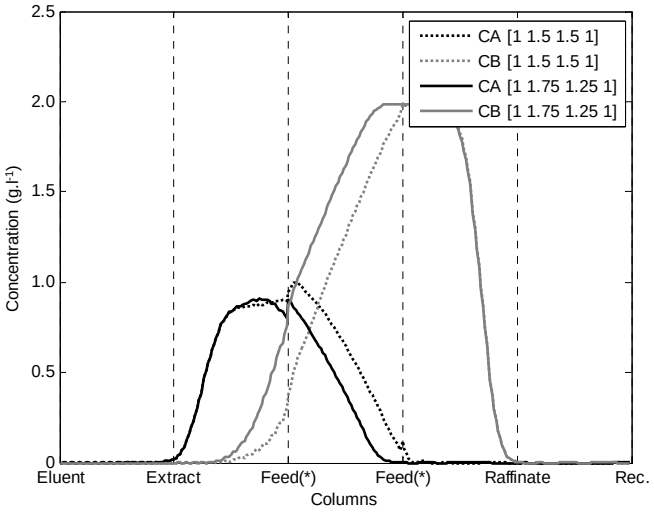

Figure 4.15 – Enantiomers concentration profiles for [1 1.5 1.5 1] and [1 1.75 1.25 1] Varicol configuration, at half switching time in CSS (fresh adsorbent).

This fact is important since the adsorbent ageing problem (capacity decline) will do the opposite. Figure 4.16 shows the [1 1.5 1.5 1] Varicol simulation values for the example described by the adsorption equilibrium isotherm for the aged adsorbent:

$$q_A^{eq} = 1.31C_{b_A} + \frac{7.00 \cdot 0.163 C_{b_A}}{1+0.163C_{b_A}+0.087C_{b_B}} \tag{4.17}$$

$$q_B^{eq} = 1.31C_{b_B} + \frac{7.00 \cdot 0.087 C_{b_B}}{1+0.163C_{b_A}+0.087C_{b_B}} \tag{4.18}$$

with C_{b_i} in g.l^{-1} and q_i^{eq} in g.l$^{-1}_{\text{adsorbent}}$.

Where the adsorbent capacity was decreased in the Langmuir part as in the linear part.

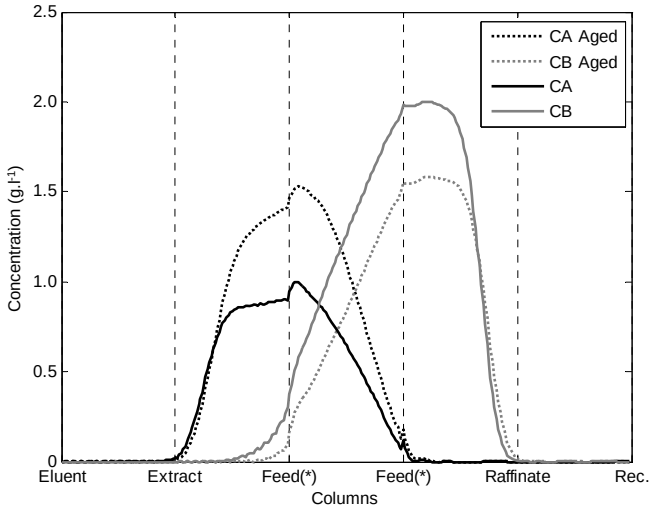

Figure 4.16 – Concentration profiles for [1 1.5 1.5 1] Varicol configuration: new adsorbent - solid line; aged adsorbent - dashed line, at half switching time in CSS, The initial adsorbent (eq. 4.11 and 4.12) and the aged ones (eq. 4.9 and 4.10).

Similarly to the analysis of the standard SMB configuration, the bulk concentration profiles with aged adsorbent, appear to the right from those obtained with fresh adsorbent. Also, the enantiomer concentration plateau has increased in section II and decreased in section III, as result of the adsorbent capacity decline.

In order to avoid the raffinate contamination, a new [1 1.75 1.25 1] Varicol configuration has been tested for the case of aged adsorbent**.** In Figure 4.17, the concentration profiles in the case of aged adsorbent for [1 1.5 1.5 1] and [1 1.75 1.25 1] Varicol configuration are presented.

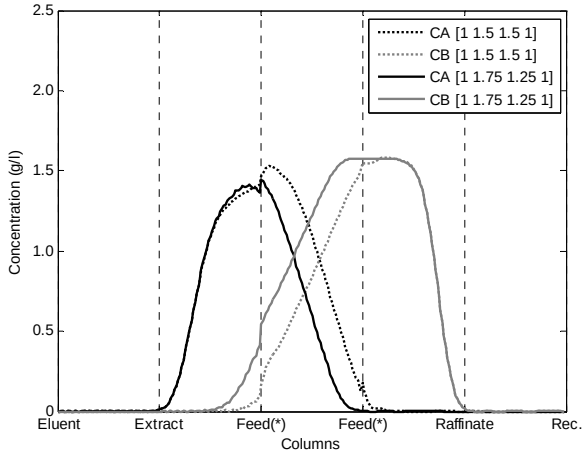

Figure 4.17 – Enantiomers concentration profiles for aged adsorbent: [1 1.5 1.5 1] Varicol configuration– dashed line and [1 1.75 1.25 1] Varicol configuration – solid line, at half time switch in CSS.

In this case, only by changing the feed strategy (during 0.75 of switch time feed is in column 3 inlet and remaining time in the column 4 inlet), the problem caused by the adsorbent ageing was almost compensated.

A more detailed study of this strategy, including dynamic optimization of the Varicol schemes in the next section.

4.4 AGEING ASPECTS DURING THE OPERATION OF AN INDUSTRIAL SMB UNIT FOR *P*-XYLENE SEPARATION

As stated before in Chapter 2, since its introduction, the SMB technology has been successfully applied, firstly to various large petrochemical separations, such as the *p*-xylene separation from its C_8 isomers, *n*-paraffins from branched and cyclic hydrocarbons, olefins separation from paraffins, sugar processing industry and later in the pharmaceutical and fine chemical industries.

Despite all of the efforts motivated by these applications, the *p*-xylene separation continues to be the subject of numerous studies and analyses (Minceva and Rodrigues, 2002; Minceva and Rodrigues, 2003; Silva *et al.*, 2004; Jin and Wankat, 2005a; Kurup *et al.*, 2006b, 2006c; Jin and Wankat, 2007a; Minceva and Rodrigues, 2007). This point is understandable given the implementation of new design and process techniques to the so-called "Old"

SMB applications, which increased, raising the performance obtained in these units. Secondly, the actual problematic of oil prices stress and its direct (as a raw material) and indirect influence (energetic source, market dependence, etc.), demanded from the old separation processes more eco-efficient, cleaner, safer and less energy spending technology. Additionally, there is a growing demand on polymeric materials such as polyester fibbers, molded plastics used in films and blown beverage bottles produced by polyethylene terephthalate (PET), obtained from *p*-xylene as a raw material. All this interest in the *p*-xylene production resulted in design and installation of considerable number of industrial SMB units for *p*-xylene separation form its C_8 isomers, mainly from UOP (Parex process) and IFP (Eluxyl process).

In this section a complete analysis of the adsorbent ageing effect on the performance parameters of an industrial SMB (conventional and Varicol) unit for *p*-xylene separation, as well as the development of strategies to overcome this problem is addressed.

4.4.1 CASE STUDY: AN INDUSTRIAL UNIT FOR *P*-XYLENE SEPARATION

The *p*-xylene system here-by analysed has been reported by Minceva and Rodrigues in several published works, represented by the non stoichiometric Langmuir Competitive isotherm model as follows:

$$q_i^{eq} = \frac{q_{m_i} K_i \langle C_{p_i} \rangle}{1+\sum_{l=1}^{NC} K_l \langle C_{p_l} \rangle} \tag{4.19}$$

with, q_i^{eq}, the adsorbed phase concentration of component i represented by the equilibrium with species i the average pore concentration $\langle C_{p_i} \rangle$. The adsorption equilibrium data of the single *p*-xylene, *o*-xylene and ethylbenzene on Ba exchanged faujasite zeolite in liquid phase at 180 ºC and 9 bar was determined experimentally in a batch mode by Minceva and Rodrigues (Silva *et al.*, 2004). The adsorption parameters for *m*-xylene are similar to those for o-xylene in this type of zeolites according to Santacesaria *et al.* (1982). The *p*-DEB isotherm was taken from (Neves, 1995; Silva *et al.*, 2004). All adsorption equilibrium parameters are presented in Table 4.12.

Table 4.12 – Parameters of Langmuir adsorption equilibrium isotherms for the *p*-xylene separation over Ba exchanged faujasite zeolite.

Component	K_i (l.g^{-1})	q_{m_i} (g.g$^{-1}_{adsorbent}$)
(A) *p*-xylene	1.9409	0.1024
(B) *m*-xylene	0.8884	0.0917
(C) *o*-xylene	0.8884	0.0917
(D) ethylbenzene	1.0263	0.0966
(E) *p*-diethylbenzene	1.2000	0.1010

The SMB unit geometry design and operating conditions are presented in Table 4.13, considering constant apparent solid density (ρ_p) and taking into account that the xylenes density (ρ_i) were calculated by means of the commercial flow sheeting package from Aspen (www.aspentech.com) at 180 ºC and 9 bar.

Table 4.13 – Parex unit characteristics and model parameters.

Model Parameters	SMB Columns
Pe_j=1000	n_j=[6 9 6 3]
ε_b=0.387; ε_p=0.37	L_c=1.135 m
r_p=0.031 cm	d_c=4.117 m
	SMB Operating Conditions (inlets)
ρ_p=1480 g.l^{-1}	
ρ_A=710 g.l^{-1} ρ_B=713 g.l^{-1}	C_A^F=23.6 wt%; C_B^F=49.7 wt%
ρ_c=733 g.l^{-1} ρ_D=716 g.l^{-1}	C_C^F=12.7 wt%; C_D^F=14.0 wt%
ρ_E=724 g.l^{-1}	C_E^{De}=100.0 wt%
$k_{LDF_{(A,B,C,D)}}$=8.1 min^{-1}; $k_{LDF_{(E)}}$=6.8 min^{-1}	

4.4.2 MATHEMATICAL MODEL

The model used in this section differs from the ones previously presented. The *p*-xylene and its isomers system should be considered as an high concentration system (bulk separation) and thus the model should account for velocity variations due to adsorption/desorption to provide more accurate results. Therefore, the modelling strategy used to analyse this system is here-by described.

As mentioned before, it is possible to model an SMB unit based on the TMB *modus operandi*. In fact this kind of approach provides acceptable results when a large number of columns per section is considered (Minceva and Rodrigues, 2002), as the *p*-xylene separation process, saving a considerable computation time, and providing the steady state solutions instead of the CSS obtained with the SMB models.

Therefore, the TMB modelling approach was used, avoiding a significant computation effort and calculation time. The equivalence between the SMB and the TMB model is established by means of the relation between the SMB average liquid phase interstitial velocity $\langle u_j^* \rangle$ with the TMB average liquid interstitial velocity $\langle u_j \rangle$ and the solid interstitial velocity (u_s) in each section j: $\langle u_j^* \rangle = \langle u_j \rangle + u_s$, with $u_s = {}^{L_c}/_{t_s}$. Again, the average internal flow-rates in both models are not the same, but related by $\langle Q_j^* \rangle = \langle Q_j \rangle + \frac{\varepsilon_b V_c}{t_s}$, where $\langle Q_j^* \rangle$ and $\langle Q_j \rangle$ are the average internal liquid flow rates in the SMB and TMB, respectively. Respecting the section nodes balances:

Desorbent (De) node: $$C_{b\,i,IV}\Big|_{z=L_{IV}} = \frac{u_I|_{z=0}}{u_{IV}|_{z=L_{IV}}} C^0_{b\,i,I} - \frac{u_{De}}{u_{IV}|_{z=L_{IV}}} C_i^{De} \quad (4.20)$$

Extract $(X, j=2)$ and Raffinate $(R, j=4)$ nodes: $$C_{b\,i,(j-1)}\Big|_{z=L_{(j-1)}} = C^0_{b\,i,j} \quad (4.21)$$

Feed (F) node: $$C_{b\,i,II}\Big|_{z=L_{II}} = \frac{u_{III}|_{z=0}}{u_{II}|_{z=L_{II}}} C^0_{b\,i,III} - \frac{u_F}{u_{II}|_{z=L_{II}}} C_i^F \quad (4.22)$$

and,

$$u_I|_{z=0} = u_{IV}|_{z=L_{IV}} + u_{De}, \quad \text{Desorbent(De) node;} \tag{4.23}$$

$$u_{II}|_{z=0} = u_I|_{z=L_I} - u_X, \quad \text{Extract(X) node;} \tag{4.24}$$

$$u_{III}|_{z=0} = u_{II}|_{z=L_{II}} + u_F, \quad \text{Feed(F) node;} \tag{4.25}$$

$$u_{IV}|_{z=0} = u_{III}|_{z=L_{III}} + u_R, \quad \text{Raffinate (R) node.} \tag{4.26}$$

The TMB model assumes: convective axial dispersed liquid flow, with variable velocity, flowing counter currently to the solid plug flow; homogeneous particles with constant radius r_p; constant axial dispersion and intraparticle mass transfer resistances approximated by an LDF type approach; and negligible pressure drops and thermal effects.

The mass balance for the component i in the bulk fluid phase in section j:

$$\frac{\partial C_{b\,i,j}}{\partial t} = D_{b,j}\frac{\partial^2 C_{b\,i,j}}{\partial z^2} - \frac{\partial\left(C_{b\,i,j}u_j\right)}{\partial z} - \frac{(1-\varepsilon_b)}{\varepsilon_b}k_{LDF\,i}\left(C_{b\,i,j} - \langle C_{p\,i,j}\rangle\right) \tag{4.27}$$

The particle mass balance for component i :

$$\rho_p\frac{\partial q_{i,j}^{eq}}{\partial t} + \varepsilon_p\frac{\partial\langle C_{p\,i,j}\rangle}{\partial t} = u_s\left\{\rho_p\frac{\partial q_{i,j}^{eq}}{\partial z} + \varepsilon_p\frac{\partial\langle C_{p\,i,j}\rangle}{\partial z}\right\} + k_{LDF\,i}\left(C_{b\,i,j} - \langle C_{p\,i,j}\rangle\right) \tag{4.28}$$

With the initial

$$\begin{cases} C_{b\,i,j}(z,0) = 0 \\ \langle C_{p\,i,j}(z,0)\rangle = 0 \\ q_{i,j}(z,0) = 0 \end{cases} \quad i = A,B,C,D \text{ and } \begin{cases} C_{b\,E,j}(z,0) = \rho_E \\ \langle C_{p\,E,j}(z,0)\rangle = \rho_E \\ q_{E,j}(z,0) \cong q_{m_E} \end{cases} \tag{4.29}$$

and boundary conditions:

$$z = 0: \quad C_{b\,i,j}^0 = C_{b\,i,j}\Big|_{z=0} - \frac{D_{b,j}}{u_{j_{z=0}}}\frac{\partial C_{b\,i,j}}{\partial z}\Big|_{z=0} \tag{4.30}$$

$$z = L_j: \quad \frac{\partial C_{b\,i,j}}{\partial z}\Big|_{z=L_j} = 0 \tag{4.31}$$

$$\begin{cases} \langle C_{p_{i,j}} \rangle \Big|_{z=L_j} = \langle C_{p_{i,(j+1)}} \rangle \Big|_{z=0}, & j = I, II, III \\ \langle C_{p_{i,IV}} \rangle \Big|_{z=L_j} = \langle C_{p_{i,I}} \rangle \Big|_{z=0} \end{cases} \tag{4.32}$$

$$\begin{cases} q_{i,j}^{eq} \Big|_{z=L_j} = q_{i,(j+1)}^{eq} \Big|_{z=0}, & j = I, II, III \\ q_{i,IV}^{eq} \Big|_{z=L_j} = q_{i,I}^{eq} \Big|_{z=0} \end{cases} \tag{4.33}$$

The adsorption equilibrium isotherm defined as:

$$q_{i,j}^{eq} = f_i \left(\langle C_{p_{i,j}} \rangle, \langle C_{p_{l,j}} \rangle \right) \tag{4.34}$$

with $l \neq i$ for all species i and in section j, see eq. (4.19)

Since the pressure drops were assumed to be negligible, it is considered that:

$$\sum_{i=1}^{NC} \frac{C_{b_{i,j}}}{\rho_i} = 1 \tag{4.35}$$

It is possible to calculate the interstitial fluid velocity by means of the total mass balance (see Annex II for more details):

$$\frac{du_j}{dz} = -\frac{(1-\varepsilon_b)}{\varepsilon_b} \sum_{i=1}^{NC} \frac{k_{LDF_i}}{\rho_i} \left(C_{b_{i,j}} - \langle C_{p_{i,j}} \rangle \right) \tag{4.36}$$

where C_i^F the species i concentration in the feed, $C_{b_{i,j}}$, $\langle C_{p_{i,j}} \rangle$, $q_{i,j}^{eq}$ the bulk, the average pore and the adsorbed concentration, respectively, t is the temporal coordinate, z is the axial coordinate, $L_j = n_j L_c$ is the section length and k_i is the particle mass transfer coefficient.

The Varicol mode of operation, characterised by an asynchronous ports shift, was also studied on this work and for the sake of simplicity, modelled by means of an equivalent TMB unit working with a non integer number of columns per section. In the limit we consider that a Varicol unit with infinite number of columns and infinite number of sub-switching-intervals within the principal switching time interval, is equivalent to the mentioned TMB unit (with non integer number of columns per section, or different columns length), see Annex III.

4.4.3 PERFORMANCE PARAMETERS

The commonly used SMB unit performance parameters are: purity, recovery, desorbent consumption and productivity. The SMB outlet streams must satisfy purity and recovery specifications. The definitions of extract purity (PU_A^X, %), recovery of *p*-xylene in the extract (RE_A^X, %) in free desorbent basis and the unit productivity in terms of *p*-xylene in the extract (PR_A^X), obtained by the TMB model approach at the steady-state are:

$$PU_A^X = \frac{C_{b\,A}^X}{C_{b\,A}^X + C_{b\,B}^X + C_{b\,C}^X + C_{b\,D}^X} \tag{4.37}$$

$$RE_A^X = \frac{Q_X C_{b\,A}^X}{Q_F C_A^F} \tag{4.38}$$

$$PR_A^X = \frac{Q_X C_{b\,A}^X}{V_{realsolid}} = \frac{RE_A^X Q_F C_A^F}{V_{realsolid}} \tag{4.39}$$

where Q_X and Q_F are the extract and feed flow rates, respectively and $V_{realsolid}$ is the adsorbent volume.

4.4.4 OPTIMIZATION OF A CONVENTIONAL SMB UNIT FOR *P*-XYLENE SEPARATION

The optimization problems are usually classified considering the number of objective functions: single or multiple-objective. The objective function could be based on different unit performance parameters (as for example, the productivity, the desorbent consumption (where is implicit the dilution factor, energetic duty for distillation or other process for desorbent recovery, etc.) or the adsorbent requirements) or could be homogenized/normalized into the total separation cost (in this case function of relative weights given to the different cost factor inherent to the separation cost).

Several optimization studies have been performed considering the *p*-xylene separation, principally multi-objective ones, accounting for the maximization of SMB unit productivity and minimization of desorbent consumption (Kurup *et al.*, 2005; Minceva and Rodrigues, 2005; Kurup *et al.*, 2006c).

Taking into account that the main objective of this study is related to the adsorbent ageing analysis, the optimization procedures were reduced to a single objective function problem: the maximization of unit productivity under a constant desorbent flow rate (Q_{De} = 129.00 $m^3.h^{-1}$), constant adsorbent amount (= 24 columns, column length and diameter given in Table 4.13) and constrained by the *p*-xylene purity (≥ 99.5 %) and recovery (≥ 97.5 %) in the extract stream.

Following this procedure the industrial SMB unit for the *p*-xylene separation with a fresh adsorbent was optimized. The maximum productivity of: $PR_A^X = 120.85 \left.\frac{kg_{p-xylene}}{h.m^3_{realsolid}}\right|_{TMB}$, with $RE_A^X = 97.5\,\%|_{TMB}$ and $PU_A^X = 99.5\,\%|_{TMB}$ was obtained by optimization of the control variables: the internal (recycle) flow rate, that leaves section IV to section I (Q_{IV}=248.80 $m^3.h^{-1}$); the extract flow rate (Q_X=94.39 $m^3.h^{-1}$); the feed flow rate (Q_F=103.57 $m^3.h^{-1}$) and the switching time (t_s=1.04 min), the remaining parameters were calculated from the mass balance taking into account the constant desorbent flow rate as mentioned before. By simulating this solution with the TMB model it was possible to obtain the unit bulk internal concentration profiles presented in Figure 4.18.

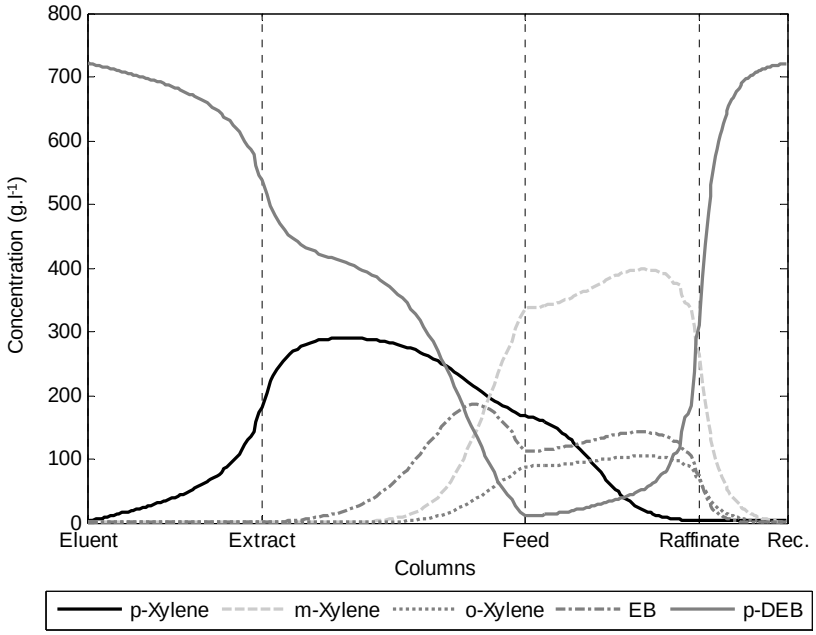

Figure 4.18 – Steady state concentration profiles for a [6 9 6 3] SMB unit simulated by the TMB model approach.*

4.4.5 OPTIMIZATION OF VARICOL SMB UNIT FOR *P*-XYLENE SEPARATION

The operation of a *p*-xylene separation unit by means of a Varicol *modus operandi* has been studied previously (Kurup *et al.*, 2005). The single objective function problem was considered again, assuming a unit with fresh adsorbent. Namely, maximization of unit productivity under a constant desorbent flow rate (Q_{De} = 129.00 $m^3.h^{-1}$), adsorbent amount (= 24 columns, column length and diameter as in Table 4.13) and constrained by the *p*-xylene recovery (≥ 97.5 %) and purity (≥ 99.5 %), but now taking also into account the control variables n_j (number of columns per sections) where $\sum_{j=I}^{IV} n_j = 24$. It was possible to extend the maximum productivity value to: $PR_A^X = 123.89 \left.\frac{kg_{p-xylene}}{h.m^3_{realsolid}}\right|_{TMB}$ (more 2.52 % than the classic unit, an expected result since the classic unit with 24 columns has optimal section lengths, and therefore, there are no considerable improvements with the use of Varicol mode of operation), with $RE_A^X = 97.6\ \%|_{TMB}$ and $PU_A^X = 99.5\ \%|_{TMB}$. The following optimal values of the control variables were obtained: the internal recycle flow rate, that leaves section IV to section I ($Q_{IV\,Rec}$=267.89 $m^3.h^{-1}$); extract flow rate (Q_X=99.96 $m^3.h^{-1}$); feed flow rate

* The TMB model, constituted by systems of PDE (Partial Differential Equations), ODE (Ordinary Differential Equations) and AE (Algebraic Equations), was numerically solved using the commercial package gPROMS v.3.0.3 (www.psenterprise.com), using the Orthogonal Collocation on Finite Elements (OCFEM) discretization methods for the axial domain (with 2 collocation points per element, 50 elements in each section). After the axial discretization step, the time integration is performed by the ordinary differential equation solver SRADAU, a fully-implicit Runge-Kutta method that implements a variable time step, the resulting system is then solved by the gPROMS BDNSOL (Block decomposition NonLinear SOLver). For all simulations was set a tolerance value equal to 10^{-5}.

For the optimization procedure it was used one of the optimization algorithms within the gPROMS (gOPT) package, namely: the CVP_SS, a control vector parameterisation (CVP) approach which assumes that the time-varying control variables are piecewise-constant (for the Varicol studies) functions of time over a specified number of control intervals, with a "single-shooting" dynamic optimisation algorithm (SS), using the TMB model approach until the Steady State (set on 200 complete cycles).

(Q_F=106.10 $m^3.h^{-1}$) and switching time (t_s=1.00 min), and column configuration [5.6 7.4 6 5]*, providing the following steady state bulk concentration profiles presented in Figure 4.19.

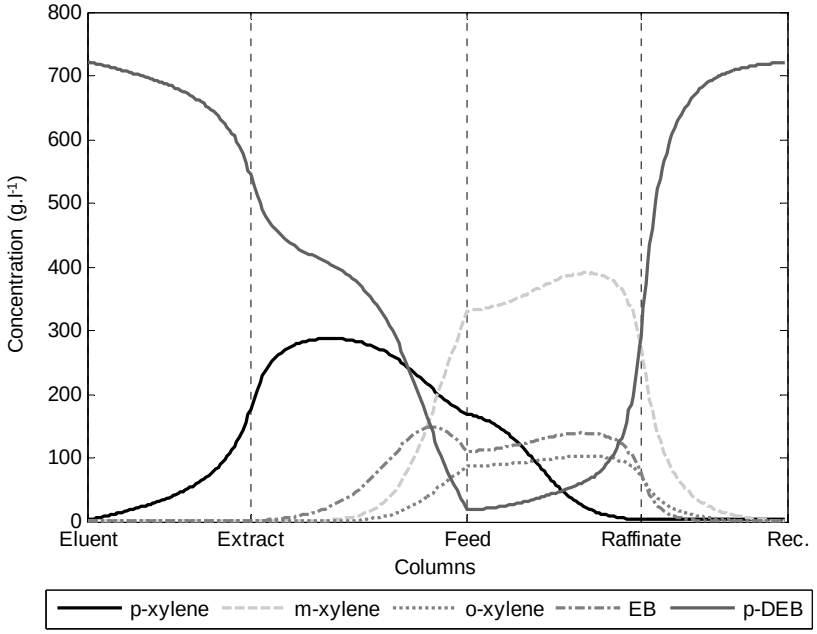

Figure 4.19 – Steady state concentration profiles for Varicol unit simulated by a TMB model approach with configuration of [5.6 7.4 6 5].

4.4.6 EFFECT OF THE ADSORBENT AGEING ON SMB UNIT PERFORMANCES AND COMPENSATING MEASURES

The operation of SMB units for the separation of *p*-xylene accounting for ageing effects, adsorbent deactivation or increase of mass transfer resistances, is not a usual issue on the scientific publications, nor mentioned in industrial brochures. Nevertheless, adsorbent deactivation, poisoning, particles crush, particle size redistribution etc. are indeed a present problem (2003; Yu, 2004). The use of guard beds, avoiding impurities to enter in the separation process, is one of the more successful as common countermeasures applied. However, some impurities appear/are formed just inside the separation columns in presence of the adsorbent (the presence of oxygenated contaminates in presence of Faujasite zeolites for instance, (Methivier, 1998)). One can deal with these aspects by means of online control. However, the efficiency of these control routines would be considerably improved by means of short cut routines to these specific problems. Additionally, the initial project of these units should also take into account this "natural" deactivation process inside the columns happening during the unit operation.

* columns configuration representing a Varicol system as non integer number of columns in an "equivalent" TMB approach.

As stated in the previous sections on this Chapter, the adsorbent ageing phenomena can be classified into two major classes, according to the consequences observed during unit operation: adsorbent capacity decline and mass transfer resistances increase.

One may argue that in the case of *p*-xylene separation units the dominant cause for SMB performances decline is due to the adsorbent capacity decline, as pointed out by Minceva and Rodrigues (2002) and Yu (2004). In particular Yu pointed out two types of adsorbent capacity decline: due to temporary poisoning and permanent one. Additionally, and as pointed out in the introduction, also particle size re-distribution (associated with the pressures variation within the columns during long periods operation), is one of the major concerns in the operation of these type of units. But one can also include its major consequences in a sort of "global adsorbent capacity decline", *i.e.*, the particle crush (as result of pressure variation etc.) will manly reduce particles size (the formation of fines), as consequence, one should expect that some parts of the packed column will experience channelling/dead volumes, which we considered as an adsorbent capacity decline (overall is like loosing a part of the available adsorbent).

Minceva and Rodrigues mentioned that usually an industrial *p*-xylene unit will suffer an adsorbent capacity decline around 20 % in 20 years, a permanent capacity decline. The major objective of this work is therefore the study of this permanent capacity decline.

4.4.7 ADSORBENT AGEING IN A *P*-XYLENE SEPARATION UNIT

Let us consider that an SMB unit for the *p*-xylene separation will lose 20 % of its adsorbent capacity during a period of 20 years (1 %.year^{-1}). The unit design should account for it and study what measures could be implemented to maintain the unit operating at acceptable performance parameters (purity, recovery), before complete adsorbent substitution.

In this study the adsorbent capacity decline rate (ξ) is also assumed to be constant at value of 1 %.year^{-1}, similar to all species,

$$q_{m_i} = q_{m_i}^0(1 - \xi t) \tag{4.40}$$

where $q_{m_i}^0$ represents the initial adsorption isotherm constant and t the time variable here in years.

A conventional unit operating with fresh adsorbent for 10 years, will recover 1.4825 Mton of *p*-xylene (over a 10 years period), at a purity rate of 99.5 % and recovery of 97.5 %. If one consider the absorbent capacity decline mentioned above, at the end of the 10th year the unit would recovered just 1.3264 Mton (for a 10 years period) of *p*-xylene in the extract stream (*i.e.* less 10.39 %) with *p*-xylene purity of 99.0 % and recovery of 75.9 %. The evolution of the internal bulk concentration profiles after 10 days, after 5 years and after 10 years, without any absorbent capacity decline compensating measure are presented in Figure 4.20.

In Figure 4.20, one can observe that *p*-xylene is being driven to the raffinate port over the time of adsorbent ageing, affecting the *p*-xylene recovery. Therefore, it should be studied how much this separation performances could be improved and which is the countermeasure that should be applied to minimise the adsorbent capacity decline effect.

Similar bulk concentration profiles where obtained for the Varicol operation mode. A Varicol unit operating with fresh adsorbent for 10 years, will recover 1.5198 Mton of *p*-xylene (over a 10 years period), with purity of 99.5 % and recovery of 97.6 %. If one consider the absorbent capacity decline mentioned above, at the end of the 10^{th} year the unit would recovered just 1.3630 Mton of *p*-xylene (over 10 years) in the extract stream (*i.e.*, less 10.53 %) with 99.0 % *p*-xylene purity and 76.0 % *p*-xylene recovery.

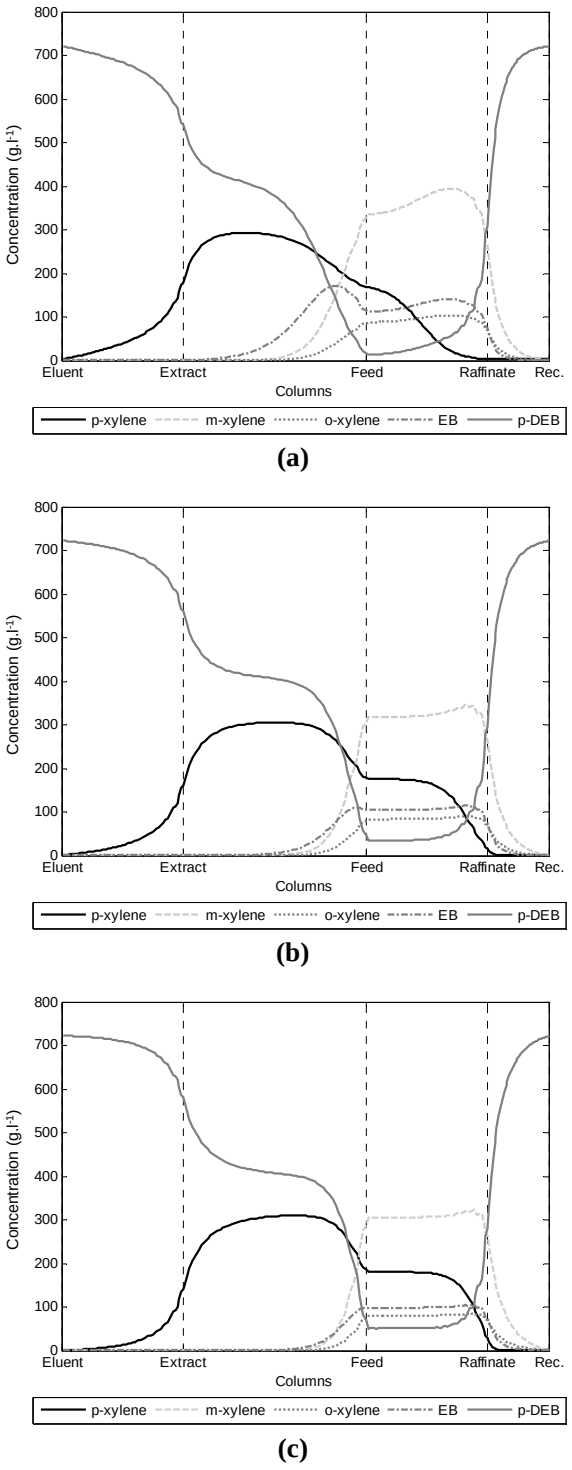

Figure 4.20 – Bulk concentration profiles evolution over a 10 years period without any compensating measure, (a) after 10 days, (b) after 5 years and (c) after 10 years.

4.4.8 COMPENSATING MEASURES

This study considers the use of compensating measures by which all inlet and outlet SMB streams flow rates are kept unchanged, keeping the auxiliary units (distillation columns, etc.) dimensioned as for the initial state. Therefore, three operating parameters can be manipulated as compensating measures: (i) the solid flow rate (switching time); (ii) the section length (by means of columns redistribution) and (iii) the fluid recycle flow rate. We stated before that both the decrease of recycle flow rate and increase of solid flow rate (decrease of switching time) have similar effect on the operating conditions. However, the solid flow rate compensation follows the adsorbent decline tendency and the recycle flow rate correction measure will only give results in the initial ageing stage. Consequently, just the first two measures are considered in this study (i) and (ii). Additionally both strategies were applied together in a Varicol *modus operandi*, *i.e.*, a simple extension of strategy (i) to the non-conventional operating mode (Varicol).

a) Switching time (solid flow rate) compensation

It was proposed that if the adsorbent capacity decline rate is similar for all species (linear or non linear isotherms case) then, one simple and straight forward countermeasure is the solid flow rate increase (switching time decrease). The same analysis can be applied to this particular case. In Figure 4.21, the influence of adsorbent capacity decline on the separation region (here defined in terms of $(Q_{II} \times Q_{III})$ for better understanding), shows the same tendency as in the cases studied in the previous sections.

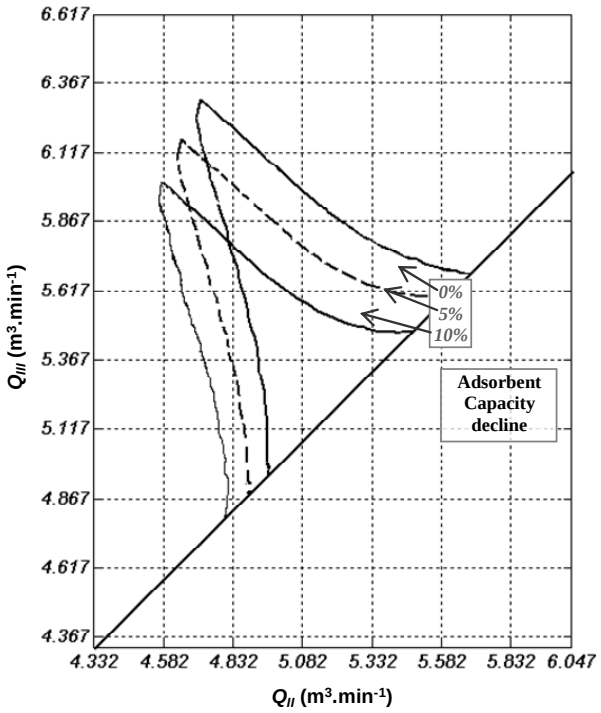

Figure 4.21 – Adsorbent capacity decline influence on the separation region (purity over 99.50 % of *p*-xylene in the extract and other C_8 isomers in the raffinate currents), where 0 % represents the initial state adsorbent, 5 % and 10 % after 5 % and 10 % of adsorbent capacity decline respectively; all operating parameters kept constant as presented in Table 4.13.

For a 10 % adsorbent capacity decline one should decrease the switching time by 10 %. With a better look on equation (4.28), and if one consider that the particle porosity is kept constant during the unit operation, it is

simple to understand that this countermeasure should be weighted with the porosity information, thus, porosity weight factor α_p was introduced. Let us assume that the switching time compensation measure for this system is:

$$t_s = t_s^0 \left(1 - \frac{1}{\alpha_p}\xi t\right) \tag{4.41}$$

where t_s^0 represents the initial time switch value, t the time variable again in years.

A first estimative to the α_p value can be obtained from a closer look on eq. 4.28 and substituting the isotherm information on $q_{i,j}^{eq}$.

Since the adsorption equilibrium term of species i $\frac{q_{m_i} K_i \langle C_{p_{i,j}} \rangle}{1+\sum_{l=1}^{NC} K_l \langle C_{p_{l,j}} \rangle}$ is dependent on average pore concentration, not equal along the SMB unit, let us simplify and assume that:

$$\sum_{l=1}^{NC} K_l \langle C_{p_{l,j}} \rangle \approx \bar{K_l} \overline{\langle C_p \rangle} \tag{4.42}$$

And

$$\begin{cases} \bar{K_l} = K_i \overline{\langle x_{p_l} \rangle} \\ \overline{q_{m_l}} = q_{m_i} \overline{\langle x_{p_l} \rangle} \end{cases} \tag{4.43}$$

where $\bar{K_l}$ and $\overline{q_{m_l}}$ represents a weighted average values for the adsorption constant and the adsorbed phase saturation concentration of component *i*, respectively, and $\overline{\langle x_{p_l} \rangle}$ and $\overline{\langle C_p \rangle}$ obtained from:

$Q_F C_i^F + Q_{De} C_i^{De} = \overline{\langle x_{p_l} \rangle}\,\overline{\langle C_p \rangle}(Q_F + Q_{De})$, where $\sum_{i=1}^{NC} \overline{\langle x_{p_l} \rangle} = 1$

obtaining,

$$\begin{cases} \overline{\langle x_{p_A} \rangle} = 0.105 \\ \overline{\langle x_{p_B} \rangle} = 0.222 \\ \overline{\langle x_{p_C} \rangle} = 0.058 \text{ and } \overline{\langle C_p \rangle} = 720.317 \text{ g.l}^{-1} \\ \overline{\langle x_{p_D} \rangle} = 0.063 \\ \overline{\langle x_{p_E} \rangle} = 0.552 \end{cases}$$

leading to $\alpha_p = 1.8$. By optimization of the case study during 10 years (maximization of amount of *p*-xylene recovered in the extract with a purity value equal of higher than 99.5 %), it was found that the value of α_p that better suits the switching time compensating measure is $\alpha_p = 3.2$.

Considering this α value, it is possible to achieve at the end of the 10th year 1.4462 Mton (over a 10 years period) of *p*-xylene production (less 2.30 % than with the fresh adsorbent unit) with *p*-xylene purity of 99.5 % and recovery of 92.3 %. Figure 4.22 presents the dynamic simulation of this particular scenario.

One can observe in Figure 4.22 that the effect noted in Figure 4.20 was almost "corrected" by implementation of this compensating measure.

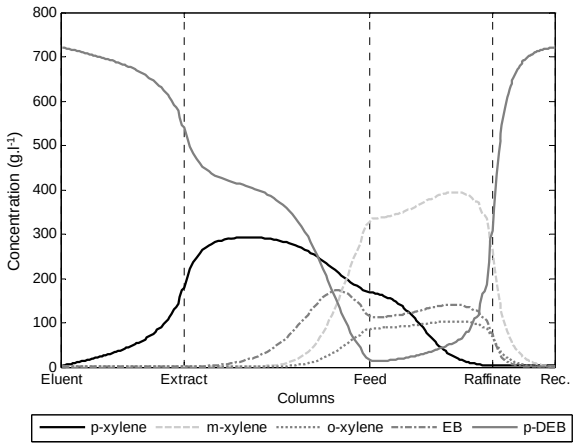

(a)

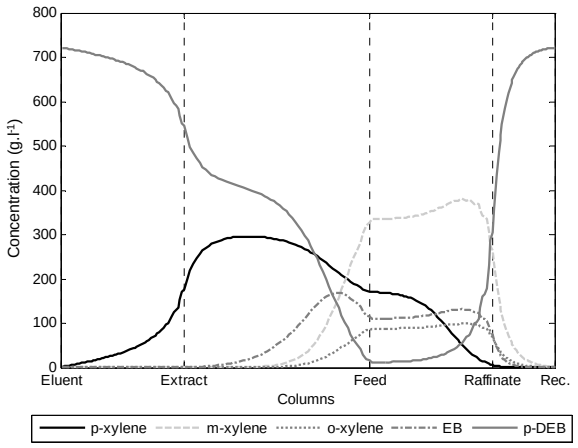

(b)

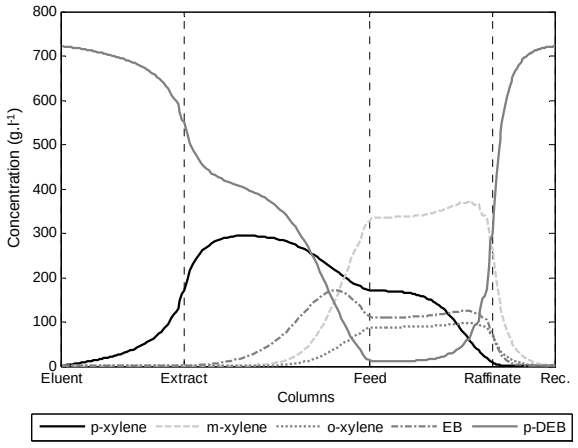

(c)

Figure 4.22 - Concentration profiles evolution over a 10 years period without with the switching time compensating measure, (a) after 10 days, (b) after 5 years and (c) after 10 years.

b) Variable section length compensation

Using the operating conditions found for the Varicol mode of operation, now affected by 1 % per year adsorbent capacity decline rate, it was implemented an optimization procedure to find the best column re-configuration during a period of 10 years. The optimization considers maximization of *p*-xylene recovery in the extract above 99.5 % purity rate by changing the column configuration in the last 5 years, *i.e.*, in the first 5 years the unit runs with the [5.6 7.4 6 5], the initial optimum, in the last 5 years with a different configuration (the variable section length countermeasure). With this approach it was possible to achieve at the end of the 10th year production of 1.3862 Mton of *p*-xylene (over a 10 years period) with an extended *p*-xylene purity of 99.5 % and *p*-xylene recovery of 76.1 %, the unit operates under [5.6 7.4 6 5] configuration in the first 5 years and [7.6 4.6 4.7 7.1] configuration in the 5 remaining ones. The obtained *p*-xylene productivity is lower for 8.80 % than the one obtained with fresh adsorbent and higher for 1.70 % in comparison with the Varicol unit running without any compensating measure. The dynamic simulation of this case is presented in Figure 4.23.

As can be observed in Figure 4.23, the columns in sections II and III moved to the regeneration ones (I and IV), this evidence is easily stated with a better look on Figure 4.20 (one should remind that the classic profiles are similar to the Varicol ones). With adsorbent capacity decline, the importance of the length of section II and III decreases and some plateaus are already seen (for instance, all species in section III), showing that there is already some unused "column space".

a) Variable section length compensation with switching time compensation

Let us now implement the switching time compensating measure on the Varicol *modus operandi* (constant section lengths [5.6 7.4 6 5] during first 5 years and [7.6 4.6 4.7 7.1] in the 5 remaining ones) and adsorbent capacity decline rate of 1 % per year (for the sake of simplicity the α value was kept at 3.2, as for the classic operation, the sub-section is just a simple extension). With this unit is possible to achieve in the end of the 10th year production of 1.487 Mton of *p*-xylene (over a 10 years period) for 2.2 % less than when fresh adsorbent is used, but operating at the end of the 10 years period, with a *p*-xylene purity value of 99.4 % and a recovery of 92.7 %.

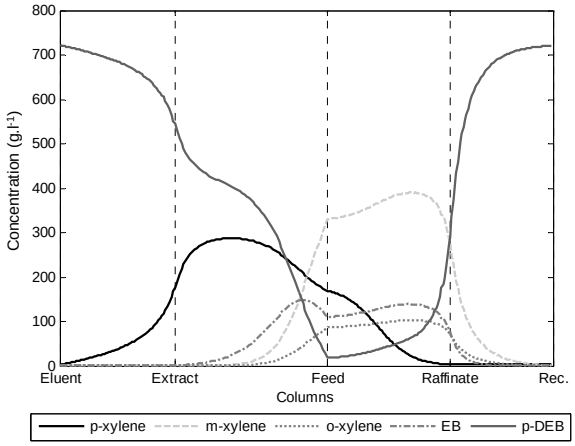

(a)

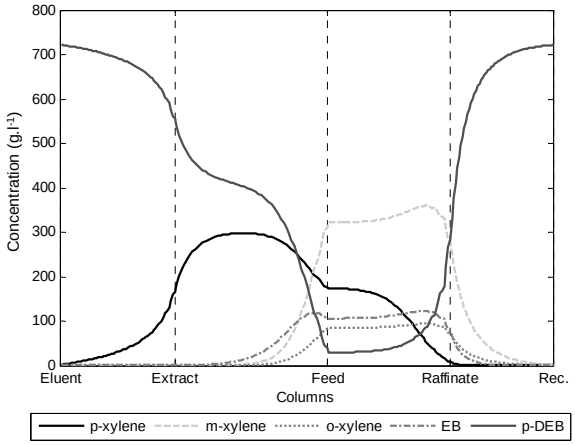

(b)

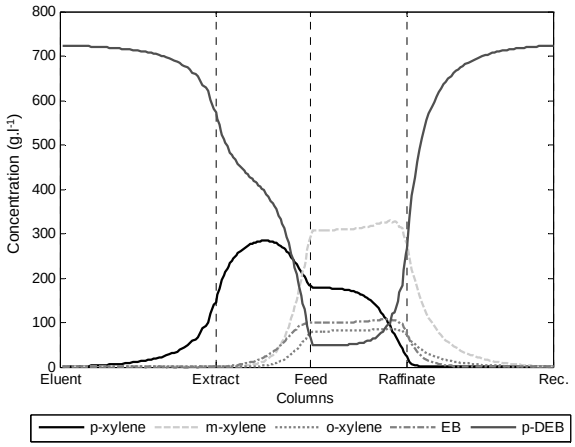

(c)

Figure 4.23 - Concentration profiles evolution over a 10 years period with the asynchrounous switching time compensating measure, (a) after 10 days, (b) after 2.5 years and (c) after 7.5 years.

4.5 CONCLUSIONS

The consequences of adsorbent deactivation described by adsorbent capacity decline or mass transfer resistances increase are presented. The operation of SMB units has been studied for three different systems: (i) sugar separation, (linear adsorption) isotherms case and ageing by adsorbent capacity decline and increased mass transfer resistance; (ii, iii) non-linear isotherms case for ageing with adsorbent capacity decline only. In both cases it has been observed that there is a decrease of purities/recoveries and therefore unit productivity as a result of adsorbent ageing. Three different corrective strategies to the ageing problem were developed:

(i) - To compensate the adsorbent capacity decline it has been found that decreasing switching time it is possible to maintain the initial SMB performance, until the limit when mass transfer limitations become important due to short solid residence time;

(ii) - To compensate the mass transfer resistances increase it has been shown that the decrease of solid and internal flow rates would lead to the same purity and recovery; however, the productivity will decrease;

(iii) - Also, it was shown how a variable switch times use in the non-conventional application of Varicol strategy could compensate the loss of adsorbent capacity.

The operation of an industrial scale SMB unit for *p*-xylene separation in presence of adsorbent ageing was studied. The standard SMB and the Varicol mode of operation were simulated accounting for the adsorbent capacity decline using the TMB approach. In the case of Varicol unit, the non integer number of columns per section was used in the simulations. Taking into account that *p*-xylene and its isomers are present in the system in high concentration, the model considered variable fluid velocity due to the adsorption/desorption rate. The effect of 1 % per year on the adsorbent capacity decline was simulated over a 10 years period in a classic as well as in the Varicol unit. It was found that by the implementation of short cut countermeasures (switching time compensation and section length variation) it is possible to extended the adsorbent life under the minimum purity requirements. Nevertheless, the switching time measure leads to better productivity results than the variable section length, either when applied to the classic or to the Varicol *modus operandi*.[*]

[*] A significant part of this Chapter 4 was published on: Sá Gomes, P., M. Minceva and A. E. Rodrigues, "Operation strategies for simulated moving bed in the presence of adsorbent ageing." Separation Science and Technology 42(16), 3555-3591, (2007c). and Sá Gomes, P., M. Minceva and A. E. Rodrigues, "Operation of an industrial SMB unit for *p*-xylene separation accounting for adsorbent ageing problems." Separation Science and Technology 43(8), 1974-2002, (2008b). And presented on: Sá Gomes, P., M. Minceva and A. E. Rodrigues Operation of SMBs in presence of adsorbent ageing. AIChE annual meeting. San Francisco-California, USA, (2006b).; Sá Gomes, P., M. Minceva and A. E. Rodrigues Operation of an industrial SMB unit for *p*-xylene separation accounting for adsorbent ageing problems. AIChE Annual Meeting. Salt Lake City, Utah-USA, (2007b). and Sá Gomes, P., M. Minceva and A. E. Rodrigues Adsorbent ageing compensation strategies for industrial scale SMB unit for *p*-xylene separation. DECHEMA Jahrestreffen der ProcessNet-Fachausschüsse Adsorption und Fluidverfahrenstechnik. Bingen-Germany, (2008a).

Chapter 5

DESIGN OF GAS-PHASE SMB FOR THE SEPARATION OF PROPANE/PROPYLENE

5.1 INTRODUCTION

Propylene is one of the world's more important commodities, related with the production of polypropylene, acrylonitrile, isopropanol, acrylic acid, cumene, oxo alcohols, etc. It is expected that the annual global propylene demand will continue to grow at an average value of 5 % through 2012. In fact, since 2002 the propylene demand expanded by 4-5 % per year even though in 2005 it slowed to about half of this value, but then reaching 72 million tons in 2007 (CMAI, 2007). Several ways are possible to obtain propylene based either on natural gas (Methanol to Olefins process - MTO; Propane Dehydrogenation, Steam Cracking of ethane, propane or butane), or on crude oil (Naphtha Steam Cracking; Gas Oil Fluid Catalytic Cracking - FCC). Currently, approximately two thirds of the total world propylene production comes from steam cracking of liquid feedstocks. However, the attractiveness of alternatives not based on crude oil derived feedstocks gains importance as the price of this raw material suffers from market, political or social stresses. Even though the natural gas approaches presents some costly disadvantages (transport, conditioning, etc), they are appearing as promising alternatives, providing more space to propylene supply risk management. Therefore, processes as the parafins steam cracking or dehydrogenation increases their importance, and by consequence the propane-propylene separation, as recovery of parafins for recycle purposes or propylene purification at high grades.

Propane-propylene separation, usually performed by means of distillation (operating near 243 K at 308 kPa in a column with more than 100 trays (Keller *et al.*, 1992), is one of the most difficult energy-consuming operation currently practiced. As a result, extensive studies on various alternatives have been developed to provide more

sustainable solutions (Bryan, 2004). In this line, the cyclic adsorption processes, such as pressure swing adsorption (PSA), shown a special potential (Rege and Yang, 2002), but presenting low recovery values as high-energy gaps, principally in the vacuum necessities.

The application of SMB technology to this separation has been studied by Rao *et al.* (2005) and Cheng and Wilson (2001); however, these processes also relies in pressure swing cycles to regenerate the solid adsorbent. In this study, a "classical" SMB mode of operation, making use of a desorbent species, as patented by Rodrigues and co-workers, (2006), is considered for the separation of a propane-propylene mixture over 13X zeolite with isobutane as desorbent.

Due to this process novelty a different design strategy is also presented, based on three major questions:

1) Is it possible? 2) Is it reasonable and 3) Is it worth it?

The objective of this Chapter is to obtain well stated answers to both questions 1 and 2 and to introduce some pertinent aspects necessaries to answer question 3, considering the separation of propane-propylene with an SMB unit over 13X zeolite and isobutane as desorbent.[*]

To state if the process is possible, equilibrium and kinetic data are used under adsorption equilibrium assumptions to determine a first estimation for the SMB operating parameters; maximum productivity values, from analogous separations techniques, are used to determine the total amount of adsorbent and pressure constraints to find an estimation for the columns geometry. These results are then used to find if the process is reasonable, by introducing continuous models accounting for mass transfer resistances, heat transfer and pressure drop effects; the simulation results are then analysed (separation region analysis) and an optimization procedure is then applied to improve the separation productivity for a given desorbent consumption, feed flow rate and constant columns number (as columns arrangement); the optimized solution is then detailed, simulating it with a discontinuous model.

5.2 IS IT POSSIBLE?

The detailed, or complete, design of new processes should follow a decision tree that accounts for several promising routes. For each of these promising alternatives, the design of base cases should be performed for consideration by a senior design team. The more complete these preliminary studies are, lower are the probabilities of missing any advantage, or to account for some disadvantage in the chosen solution. Nevertheless, one should not try to do an exhaustive study of all alternatives. Even if with the advent of low cost, but powerful, computers provided us more and more support in the mathematical simulation of processes, the total time to do such detailed analysis will not be feasible whatsoever and engineers still have to rely on heuristics, intuition, and experience when designing a process.

The process design procedure in this work is then divided in three major items, or questions: Is it possible?; Is it reasonable? and Is it worth it?

[*] Some of the contents of this chapter, namely the SMB operating mode, modelling and designs aspects, were mentioned before; nevertheless, are here-by repeated to present a complete design strategy.

Any process design starts at the conceptual level, is chosen as the more competitive option and ends in the form of fabrication and construction plans. First, one should state the main objective (the main project specification), and then conduct a complete literature survey attesting for the process novelty. If it is new, the next step is then to perform a primitive design (scheme) and at this point, the question to be made is simple: "Is it possible?". To answer this question one has to focus on a main item: the base concept of the process under evaluation. In this work, and taking into account the motivation paragraphs from the introduction section, it was chosen a simple, but quite innovative case: the separation of propane-propylene *via* SMB technology using isobutane as desorbent in 13X zeolite. Therefore, gas phase adsorption is identified as the main base concept. Consequently, one should proceed gathering the equilibrium and kinetic data necessary to perform the preliminary study. Additionally, a brief characterization of the main aspects for the process, *i.e.*, specification of the more representative operating parameters, should be done.

5.2.1 LITERATURE (PATENTS) SURVEY

From literature, it is possible to find relevant references to the SMB application in the separation of propane-propylene mixtures, *e.g.*, US Patent no. 6 293 999 by Cheng and Wilson, (2001) and as in Rao and co-workers, (Rao *et al.*, 2005; Sivakumar, 2007), all considering pressurization or depressurization steps for the adsorbent reutilization, similar to the PSA. The use of a "classical" SMB, considering the employment of desorbent species, has only been mentioned in the patent of Rodrigues and co-workers, (2006). Since this patent application has been recently accepted, it will attest for this process novelty.

5.2.2 EQUILIBRIUM AND KINETICS

To design a conventional SMB unit, that will provide a satisfying gas separation, one should take into account not only the choice of a good solid adsorbent but the selection of an efficient desorbent as well. Lamia *et al.*, (Lamia *et al.*, 2007) studied the separation of a propane-propylene mixture over a column packed with 13X zeolite using isobutane as desorbent. It was proved through multicomponent breakthrough experiments that isobutane is able to displace propane and propylene from 13X zeolite as it was itself easily displaced from the adsorbent, so that the zeolite could be reused in a cyclic gas separation processes such SMB. Thus, this system was taken as case study, and therefore, the 13X zeolite characteristic parameters, as well as equilibrium and kinetic data, were compiled and are presented in the following tables, Table 5.1 to Table 5.4.

As mentioned before, the choice of the packing material is important in this kind of separations, and several are the characteristics that one should account for when choosing an appropriated adsorbent, Figure 5.1.

From the mechanical point of view, if in one hand, one should not consider large particles, which have considerable mass transfer resistances, in the other hand, it should not be considered "fine dusty" particles as well, since the pressure drop will become an issue.

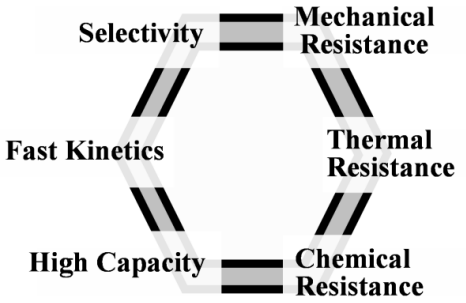

Figure 5.1 – Important adsorbent characteristics for SMB processes.

In this work, the pellets geometry is based on published results from Lamia *et al.,* (2007), a quite common geometry in separation processes such as the Pressure Swing Adsorption (PSA), (Da Silva and Rodrigues, 1999, 2001). The adsorbent properties are listed in Table 5.1.

Table 5.1 - Proprieties of 13X zeolite.

Particle radius	r_p	0.8 mm
Crystal radius	r_c	1.0 μm
Pore radius	r_{pore}	0.17 μm
Particle density	ρ_p	1357 kg.m^{-3}
Particle porosity	ε_p	0.395
Heat capacity	$\widehat{C_{ps}}$	920 J.kg^{-1}.K^{-1}

The adsorption equilibrium isotherm is described by a physically consistent extended Toth model (PCET), which can be effectively applied to describe the multicomponent equilibrium adsorption for the propane/propylene/isobutane system (Lamia *et al.*, 2007), eq. (5.1).

$$\bar{n}_i^{eq} = q_{m_i} \frac{K_i \bar{c}_i R T_s}{\left(1+\left(\sum_{l=1}^{NC} K_l \bar{c}_l R T_s\right)^{\vartheta}\right)^{1/\vartheta}} \tag{5.1}$$

where K_i the adsorption equilibrium constant for each species i, q_{m_i} the maximum adsorption capacity for each species i, ϑ a dimensionless parameter related to the solid heterogeneity, $\bar{c}_i$ the i species pore concentration, T_s the solid temperature and R the ideal gas constant. The equilibrium adsorption parameters are shown in Table 5.2.

Table 5.2 - Equilibrium adsorption parameters for the Toth isotherm of propane, propylene and isobutane over 13X zeolite, (Lamia *et al.*, 2007).

Gas	q_{m_i} (mol.kg^{-1})	K_i^0 (kPa^{-1})	$-\Delta H$ (kJ.mol^{-1})	ϑ
Propane	2.20	2.5 x 10^{-7}	36.88	0.892
Propylene	2.59	2.5 x 10^{-7}	42.45	0.658
Isobutane	1.78	2.5 x 10^{-7}	41.54	0.848

The Henry constants for different temperatures as well as a brief literature survey on enthalpies for the considered system is shown in Table 5.3.

Table 5.3 - Henry constants at different temperatures and review of different adsorption enthalpies for the gases related with the studied separation over 13X zeolite.

	$H_{333\ K}$ (mol.kg^{-1}.kPa^{-1})	$H_{353\ K}$ (mol.kg^{-1}.kPa^{-1})	$H_{373\ K}$ (mol.kg^{-1}.kPa^{-1})	$H_{393\ K}$ (mol.kg^{-1}.kPa^{-1})	$-\Delta H$ (kJ.mol^{-1})	$-\Delta H^{literature}$ (kJ.mol^{-1})
Propylene	2.899	1.218	0.561	0.279	42.45	42.5[a] ; 46.1-52.7[b]
Propane	0.337	0.158	0.081	0.044	36.88	35.8[a] ; 32.4-38.4[c]
Isobutane	1.492	0.637	0.298	0.151	41.54	39.3[d]

[a] (Da Silva and Rodrigues, 1999);
[b] (Costa *et al.*, 1991); (Jarvelin and Fair, 1993); (Huang *et al.*, 1994);
[c] (Loughlin *et al.*, 1990); (Tarek *et al.*, 1995); (Siperstein and Myers, 2001), (Van Miltenburg *et al.*, 2008);
[d] (Hyun and Danner, 1982);

The mass and heat transfer parameters are summarized in Table 5.4.

Table 5.4 – Calculated parameters for propane, propylene and isobutane over 13X zeolite at 373 K and 150 kPa, (Lamia *et al.*, 2007).

		C_3H_8	C_3H_6	i-C_4H_{10}	units
		Mass transfer			
D_c	Cristal Diffusion	1.55 x 10^{-11}	2.69 x 10^{-11}	1.58 x 10^{-11}	m^2.s^{-1}
D_{pore}	Pores	5.45 x 10^{-6}	5.74 x 10^{-6}	5.14 x 10^{-6}	m^2.s^{-1}
D_b	Axial Dispersion	9.98 x 10^{-4}	10.49 x 10^{-4}	9.73 x 10^{-4}	m^2.s^{-1}
K_m	External Mass coefficient	4.39 x 10^{-2}	4.56 x 10^{-2}	4.51 x 10^{-2}	m.s^{-1}
		Heat transfer			
k_g	Heat conductivity fluid phase	2.77 x 10^{-2}	3.34 x 10^{-2}	3.11 x 10^{-2}	W.m^{-1}.K^{-1}
$\widetilde{C_p}$	Fluid Heat capacity	76.40	89.33	118.0	J.mol^{-1}.K^{-1}
$\widetilde{C_v}$	Fluid Heat Capacity	68.08	81.02	109.7	J.mol^{-1}.K^{-1}
Bi_m	Biot Number	5.05	4.98	5.52	-

Additionally, some problem specifications and constraints can be included. In this case, the specifications can be summarized by a feed flow rate of 65.14 mol.s^{-1} of propane-propylene mixture at 25 %/75 % in volume fraction at 373 K (a traditional proportion from the conventional FCC processes), and purity requirements above 99.5 % (polymeric grade propylene), and recovery values higher than 95.0 %.

5.2.3 THE SMB CONCEPT AND TMB EQUIVALENCE

An SMB is no more than a practical implementation of its subjacent continuous chromatographic process, the TMB, and the analogy between the practical and the ideal concept can be, and is in fact, explored in the design as modelling field. The principle of a TMB is based on the continuous circulation of a fluid phase counter currently with a solid one, Figure 5.2c.

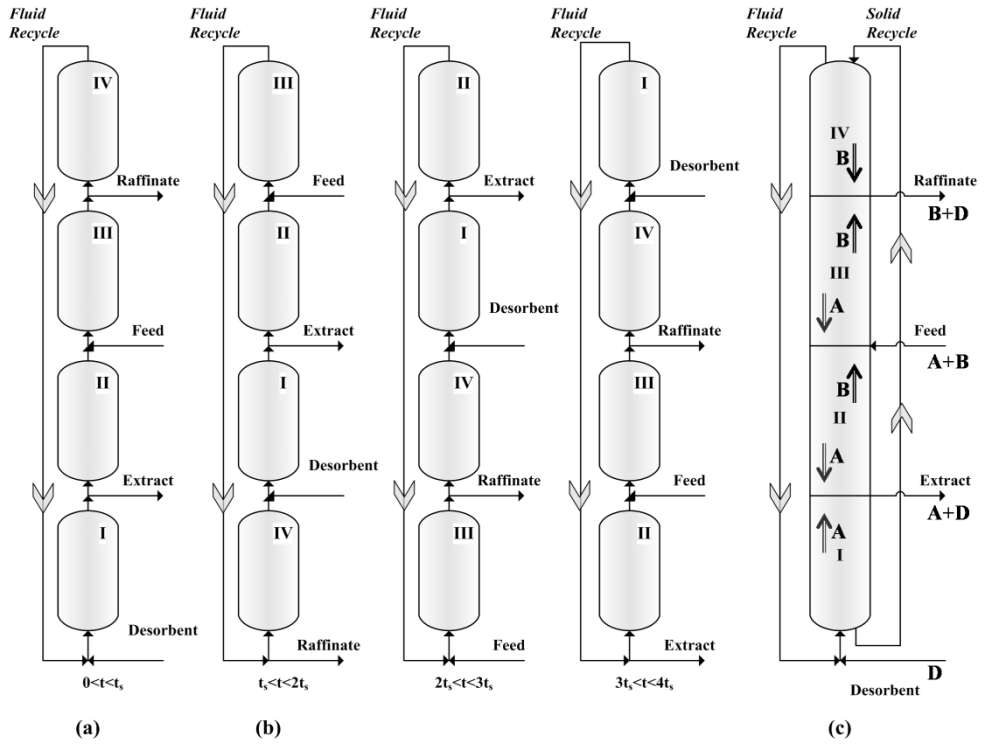

Figure 5.2 - Schematic representation of a 4 columns SMB unit operating over a complete cycle, from 0 to $4t_s$ (with t_s representing the ports switching time); (a) period of the first switch; (b) period of the second switch and an equivalent 4 "columns length" TMB unit (c) A and B the more and less retained products, D the desorbent.

To understand the SMB mode of operation let us consider that at a certain moment in the operation of the SMB the positions of all inlets and outlets ports are represented by Figure 5.2a. After a switching time (t_s) all ports suffer a synchronous advance of one column, *i.e.*, all injection and withdrawn points move one column in the direction of the fluid flow, Figure 5.2b; this way the solid phase movement is simulated with a $u_s = \frac{L_c}{t_s}$, where u_s represents the interstitial solid velocity, and L_c the column length. Therefore, the inner velocities, or inner flow rates, are not the same in TMB and SMB but related as indicated in Table 5.5, where u_j and u_j^* represents the interstitial fluid velocity in section j in the TMB and SMB modes, Q_s and Q_j the solid and fluid phase flow rate, respectively, and V_c the column volume.

Table 5.5 - Equivalence relations between SMB and TMB.

		TMB	SMB
Solid phase	Interstitial velocity	$u_s = \frac{L_c}{t_s}$	0
	Flow rate	$Q_s = V_c \frac{(1-\varepsilon_b)}{t_s}$	0
Fluid phase	Interstitial velocity	u_j	$u_j^* = u_j + u_s$
	Flow rate	Q_j	$Q_j^* = Q_j + \frac{\varepsilon_b V_c}{t_s}$

** indicates SMB*

From Figure 5.2 it is possible to identify four different sections, in both SMB as TMB modes of operation, delimited by one inlet (Feed or Desorbent) and one outlet (Extract or Raffinate) current, namely:

Section I - between Desorbent (D) and Extract (X) line, the solid regeneration zone;

Section II - between Extract (X) and Feed (F) line, a separation zone;

Section III - between Feed (F) and Raffinate (R) line, a separation zone;

Section IV - between Raffinate (R) and Desorbent (D) line, the desorbent regeneration zone.

Moreover, these four sections classified into regeneration and separation regions, according to their finality: the regeneration region, comprised by section I, and section IV; and the separation region with sections II and III.

When the initial location of all injection/collection streams is reencountered, one cycle is completed (in a four equally sections SMB, it takes $\sum_{j=I}^{IV} n_j t_s$ to complete one cycle, where n_j is the number of columns in each of the four sections). It is possible to observe in Figure 5.2a and Figure 5.2b that during one cycle the same column is in different sections, assuming therefore different roles in the separation process.

5.2.4 SMB OPERATING PARAMETERS, *THE POWER OF SCHEMES*

Let us make use of the TMB analogy with the SMB and consider the separation of two species (A and B) with different affinities with the solid phase, Figure 5.2c. To achieve a complete separation between the two species it is easier to start by defining appropriate operating conditions, *i.e.*, parameters that will represent the dominant aspects in the process under study. In this case, they are the internal flow rates for the fluid phase and the SMB switching time. A simple way to combine them, and usually employed in the field by several research groups, is to relate the interstitial fluid velocity with the solid one (represented by the switching time in the SMB), by the ratio between them, γ_j. Taking into account that the more retained product should be recovered in the extract stream and the less retained one in the raffinate port (Figure 5.2c), one should expect to fulfil the following conditions:

$$\frac{(1-\varepsilon_b)}{\varepsilon_b}\frac{\langle n_{A,I}\rangle}{C_{A,I}} < \gamma_I \tag{5.2}$$

$$\frac{(1-\varepsilon_b)}{\varepsilon_b}\frac{\langle n_{B,II}\rangle}{C_{B,II}} < \gamma_{II} < \frac{(1-\varepsilon_b)}{\varepsilon_b}\frac{\langle n_{A,II}\rangle}{C_{A,II}} \tag{5.3}$$

$$\frac{(1-\varepsilon_b)}{\varepsilon_b}\frac{\langle n_{B,III}\rangle}{C_{B,III}} < \gamma_{III} < \frac{(1-\varepsilon_b)}{\varepsilon_b}\frac{\langle n_{A,III}\rangle}{C_{A,III}} \tag{5.4}$$

$$\gamma_{IV} < \frac{(1-\varepsilon_b)}{\varepsilon_b}\frac{\langle n_{B,IV}\rangle}{C_{B,IV}} \tag{5.5}$$

where $C_{i,j}$is the bulk fluid phase concentration of species i in section j, $\langle n_{i,j}\rangle$ the total average solid concentration of species i in section j and ε_b the bed porosity.

There are several design methodologies to achieve a complete separation with an SMB unit based on different theories, from the plates theory and McCabe-Thiele diagrams (Ruthven and Ching, 1989), to the determination of waves velocities as in the standing waves methodology (Ma and Wang, 1997), where the flow rate in a given zone is chosen so that a given key concentration wave (boundary of a solute band) in a given zone migrates at the same speed as the ports, as result, all band boundaries, or waves, remain stopped (standing) with respect to the ports. Nevertheless, the question to be answered is simple, "Is it possible?", and therefore requires simple models. In this case one can simplify the relation $\frac{\langle n_{i,j}\rangle}{C_{i,j}}$ assuming that the adsorption equilibrium is established everywhere at every time, resulting in a feasible separation region formed by the above constraints (5.3) and (5.4), which in the case of linear isotherms takes the shape of a right triangle in the $(\gamma_{II} \times \gamma_{III})$ plane, and a rectangular shape in the $(\gamma_I \times \gamma_{IV})$ plane, actually, this is the most used methodology in the SMB design field.

Such strategy has been developed for multicomponent separations modelled by linear and non linear isotherms such as Langmuir type as in Storti *et al.*, (1989a; 1993; 1995); Mazzotti *et al.*, (1994; 1996c; 1997b; 2006a); Chiang (1998); Migliorini *et al.*, (2000), the so-called Triangle Theory, or equilibrium based shortcut design methods (Migliorini *et al.*, 2002). However, there are no extensions of this methodology for the case of Toth equilibrium isotherms in multicomponent systems.

Nevertheless, one can make use of the equilibrium theory methodology to obtain a reasonable approach for the Toth case, and therefore establishing the regeneration, as well as, the separation conditions.

a) Regeneration region γ_I, γ_{IV}

i.Section I : γ_I

Considering that equilibrium is established everywhere at every time and that the total amount of adsorbable species in the particle pores is irrelevant when compared with the adsorbed one, constraint (5.2) can be rewritten in the following way:

$$\frac{(1-\varepsilon_b)}{\varepsilon_b}\frac{Q_I}{Q_s} > \gamma_{I,min} \text{ with } \gamma_{I,min} = \frac{(1-\varepsilon_b)}{\varepsilon_b}\rho_p \frac{q_{m_A} K_A R T_{s,I}}{\left(1+\left(\sum_{l=1}^{NC} K_l P_{l,I}\right)^{\vartheta}\right)^{1/\vartheta}}$$

If one consider that there is only isobutane in section *I*, one can simplify and obtain the following equation:

$$\gamma_{I,min} = \frac{(1-\varepsilon_b)}{\varepsilon_b}\rho_p \frac{q_{m_A} K_A R T_{s,I}}{\left(1+(K_D P_I)^{\vartheta}\right)^{1/\vartheta}} \tag{5.6}$$

where P_I is the total pressure in section I.

ii.Section *IV* : γ_{IV}

The same assumption for section I can be now applied to section IV and then becoming:

$$\frac{(1-\varepsilon_b)}{\varepsilon_b}\frac{Q_{IV}}{Q_s} < \gamma_{IV,max} \quad \text{with} \quad \gamma_{IV,max} = \frac{(1-\varepsilon_b)}{\varepsilon_b}\rho_p \frac{q_{m_B} K_B R T_{s,IV}}{\left(1+(K_D P_{IV})^{\vartheta}\right)^{1/\vartheta}}$$

However, it is easy to understand that this last condition was obtained under a weak assumption, that there is only isobutane in the beginning of section IV, therefore, higher values for γ_{IV} can be found (in this case of intermediary adsorption constants for the desorbent species, Table 5.2 and Table 5.3), this aspect will be taken into account in the further steps.

b) Separation region γ_{II}, γ_{III}

The simplification used to obtain the regeneration region limits should not be used in the separation region. In these sections (II and III), and considering full separation as instantaneous equilibrium between the fluid and the solid phase, one should expect to find the more retained species in section II as the less retained one in section III, Figure 3. Nevertheless, there is an infinitesimal point were both species are present, the feed node. In this particular point, where the right boundary section II and left boundary of section III match, the adsorption equilibrium is based on the 3 components (A, B and D), and in fact, any slight variation in some species concentration can lead to the violation of constraint (5.3) or (5.4). Therefore, in the separation region analysis one should take into account the 3 species at least in the adsorption term. In this work, we will make use of species mass balance: balance to *A* and balance to *B*, as shown in Figure 5.3, where the boundary region for each balance is presented, both touching the feed node and thus representing the use of the feed node concentrations for both adsorption terms.

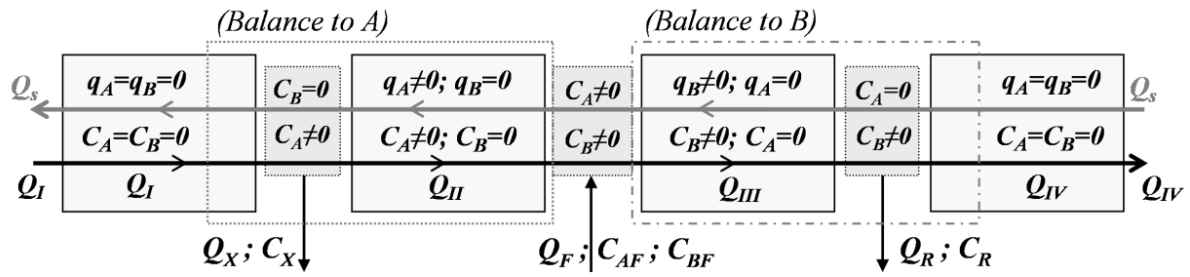

Figure 5.3 – Schematic representation of species balances for section II and III, under equilibrium assumptions.

Therefore, if one assumes that the more retained species fed to the SMB unit will entirely come out in the extract stream $C_A^F Q_F = C_A^X Q_X$ it can be written that:

$$Q_S \frac{q_{m_A} K_A C_{A,II}}{\left(1+\left(\alpha C_{A,II} K_B + C_{A,II} K_A + C_{D,II} K_D\right)^{\vartheta}\right)^{1/\vartheta}} - Q_{II} C_{A,II} = Q_F C_A^F \tag{5.7}$$

And by analogy for the less retained one in the raffinate:

$$Q_{III} C_{B,III} - Q_S \frac{q_{m_B} K_B C_{B,III}}{\left(1+\left(\beta C_{B,III} K_A + C_{B,III} K_B + C_{D,III} K_D\right)^{\vartheta}\right)^{1/\vartheta}} = Q_F C_B^F \tag{5.8}$$

where α and β represents $\left(\frac{C_{B,II}}{C_{A,II}}\Big|_{Feed*}\right)$ and $\left(\frac{C_{A,III}}{C_{B,III}}\Big|_{Feed*}\right)$, respectively (with *Feed** the infinitesimal point where both species are present). One can now remind constraints (5.3) and (5.4), and assume that the limiting line that will represent the γ_{II} constraint in the $(\gamma_{II} \times \gamma_{III})$ can be derived from $\frac{(1-\varepsilon_b)}{\varepsilon_b}\frac{\langle n_{B,II}\rangle}{C_{B,II}} < \gamma_{II}$, thus obtaining the following expression:

$$\gamma_{II} = \frac{(1-\varepsilon_b)}{\varepsilon_b} \frac{q_{m_B} K_B}{\left(1+\left(\alpha C_{A,II} K_B + C_{A,II} K_A + C_{D,II} K_D\right)^{\vartheta}\right)^{1/\vartheta}} \tag{5.9}$$

Making use of equation (5.9), and considering that $C_{D,II} = C_T - (1+\alpha) C_{A,II}$ (being C_T the total concentration), one can now derive the Q_{II} (or γ_{II}) in terms Q_F (or γ_F), α, the feed concentrations and the equilibrium constants. In the case of Toth Isotherm the result will lead to a implicit formula of Q_{II}, here, and for the sake of simplicity, one will only derive a Langmuir version (similar to Toth when $\vartheta = 1$) of the referred formula:

$$\gamma_{II} = \frac{(1-\varepsilon_b)}{\varepsilon_b} \frac{-\left(\alpha C_A^F \frac{\varepsilon_b}{(1-\varepsilon_b)} \gamma_F (K_B - K_D) + C_A^F \frac{\varepsilon_b}{(1-\varepsilon_b)} \gamma_F (K_A - K_D) - q_{m_A} K_A + q_{m_B} K_B\right)}{(C_T K_D + 1)(q_{m_A} K_A - q_{m_B} K_B)} q_{m_B} K_B \tag{5.10}$$

Following the same procedure for the $\gamma_{III} < \frac{(1-\varepsilon_b)}{\varepsilon_b}\frac{\langle n_{A,III}\rangle}{C_{A,III}}$ limit one should find that:

$$\gamma_{III} = \frac{(1-\varepsilon_b)}{\varepsilon_b} \frac{-\left(\beta C_B^F \frac{\varepsilon_b}{(1-\varepsilon_b)} \gamma_F (K_A - K_D) + C_B^F \frac{\varepsilon_b}{(1-\varepsilon_b)} \gamma_F (K_B - K_D) - q_{m_A} K_A + q_{m_B} K_B\right)}{(C_T K_D + 1)(q_{m_A} K_A - q_{m_B} K_B)} q_{m_A} K_A \tag{5.11}$$

Apart from other parameters, α and β play a main role on this approach, namely the pollution at the feed node of the less retained component in section II and the more retained in section III, respectively. One can now make use of a rough, but quite useful, approximation, relating the pollution with the less retained species to section II with the feed ratio (free of desorbent) and therefore having $\alpha = \frac{C_B^F}{C_A^F}$, and similarly for the pollution of the more retained product into section III becoming $\beta = \frac{C_A^F}{C_B^F}$. These approximations will be more accurate as higher is the feed flow rate, near to the optimal operating point (in terms of higher productivity values).

In the case of Toth isotherms from Lamia *et al.*, (2007), and a feed concentration of 75 % of propylene and 25 % of propane, at different total pressures (110, 150 and 250 kPa), one can already have some idea about the values of some "internal" (intrinsic to the SMB unit) operating parameters with $\vartheta = 0.80$, from $\vartheta = \sum_{i=1}^{NC} \overline{x_i}\, \vartheta_i$, where $\overline{x_i}$, represents the average fraction of species i in the SMB unit, calculated considering that the desorbent is 60 %

and feed 40 % of the total volumetric inlet to the SMB unit. The resulting separation regions, based on this equilibrium based assumptions, are shown in Figure 5.4.

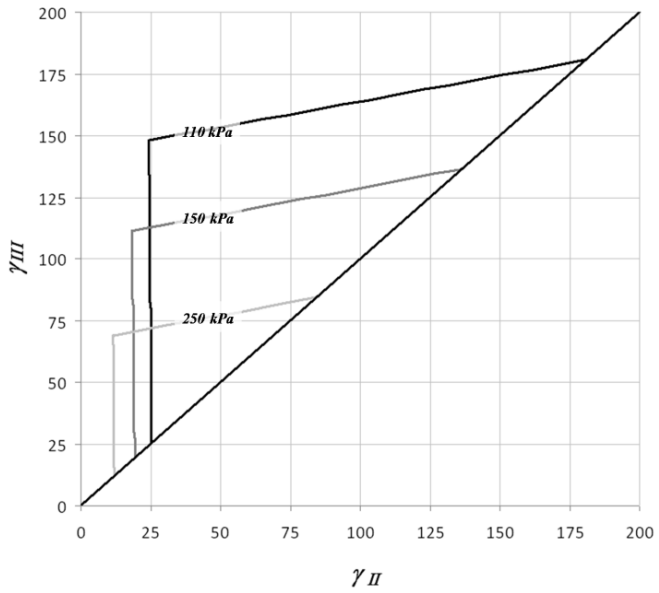

Figure 5.4 - Equilibrium based separation regions for the Toth isotherms at different pressures, 110, 150 and 250 kPa, in terms of (γ_j).

It is already possible to note some changes in the separation region caused by the different pressure operation; one can now continue detailing this study.

5.2.5 EQUILIBRIUM ANALYSIS ON THE OPERATING CONDITIONS

The approximations stated before can be useful in the determination of some operating parameters, as can also be quite helpful in the prediction and analysis on the influence of certain operating conditions, as it will be now demonstrated on a short analysis on the total pressure (concentration); columns geometry (as well as, total adsorbent amount) and solid flow rate.

a) Influence of total pressure (concentration) in separation and regeneration regions

Considering a feed stream of 1.35 $m^3.s^{-1}$ at 150 kPa (65.14 $mol.s^{-1}$ as stated in problem specifications), is already possible to obtain a first estimation for the Q_S value, based on a γ_F value of 63.0 (near to the middle height of the 150 kPa triangle in Figure 5.4), where γ_F stands for $\gamma_F = \gamma_{III} - \gamma_{II}$, in this case $Q_S \approx 0.032$ $m^3.s^{-1}$. Consequently, one can already calculate the same triangles in terms of flow rates, as presented in Figure 5.5 and Table 5.6.

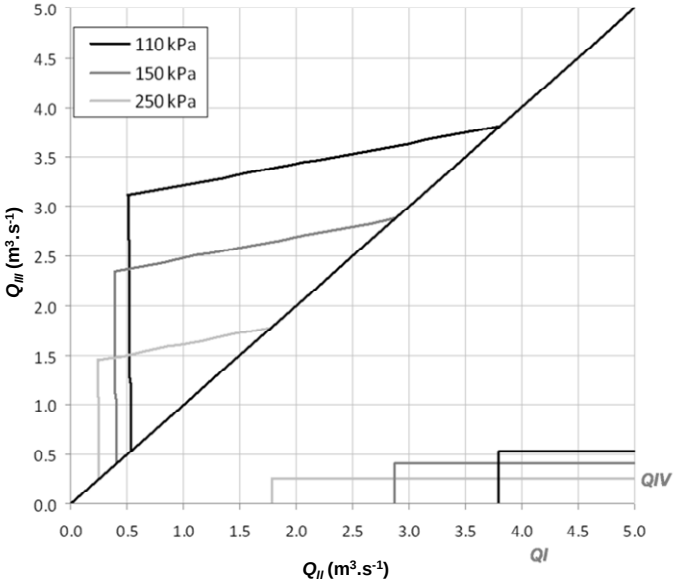

Figure 5.5 - Equilibrium based separation and regeneration regions for the Toth isotherms at different pressures, 110, 150 and 250 kPa, in terms of volumetric flow rate (Q_j), for Q_S= 0.032 $m^3.s^{-1}$.

From Figure 5.5, it is possible to obtain the minimum desorbent amount needed to run each separation at different total pressures (total concentrations), Table 5.6 with 10 % as tolerance factor, (more 10 % in section one flow rate and less 10 % in the section IV (recycle) flow rate).

Table 5.6 – Minimum and 10 % tolerance (10 % more in the Q_I min and 10 % less in the Q_{IV} max flow rates), desorbent requirements (under equilibrium theory assumptions, as stated before); Q_S = 0.032 $m^3.s^{-1}$.

Inlets pressure (kPa)	Q_I min ($m^3.s^{-1}$)	Q_{IV} max ($m^3.s^{-1}$)	Q_D min ($m^3.s^{-1}$)
110	3.803	0.537	3.266
150	2.874	0.406	2.468
250	1.785	0.252	1.533
Tolerance	*of 10%*		
Inlets pressure (kPa)	Q_I min ($m^3.s^{-1}$)	Q_{IV} max ($m^3.s^{-1}$)	Q_D min ($m^3.s^{-1}$)
110	4.183	0.483	3.700
150	3.161	0.365	2.796
250	1.964	0.227	1.737

Considering the feed molar flow rate of 65.14 $mol.s^{-1}$ it is now possible to have a reasonable estimation for the minimum, maximum extract flow rate, dilution factor (Feed/D), as well as the minimum and maximum fraction of propylene in the extract flow rate, for a Q_S flow rate of 0.032 $m^3.s^{-1}$, at 110, 150 and 250 kPa, Table 5.7 and Figure 5.6.

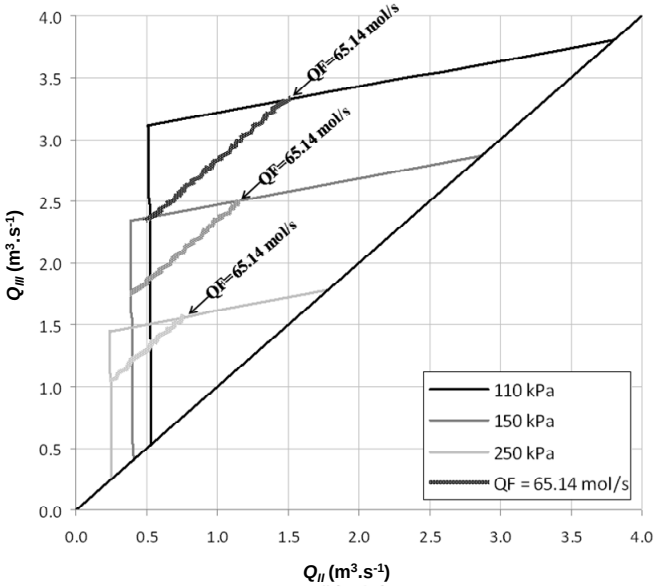

Figure 5.6 - Equilibrium based separation and regeneration regions for the Toth isotherms at different pressures, 110, 150 and 250 kPa, in terms of volumetric flow rate (Q_j), for Q_s = 0.032 m^3.s^{-1}, and Feed molar flow rate of 65.14 mol.s^{-1} at the given pressures.

Table 5.7 – Minimum, maximum and 10 % tolerance dilution factors, for a Feed molar flow rate of 65.14 mol.s^{-1} and Q_s = 0.032 m^3.s^{-1}.

Inlets pressure (kPa)	Dilution Factor(*)	Q_X min (m^3.s^{-1})	Q_X max (m^3.s^{-1})	Outlet Propylene Fraction max	min
110	0.562	2.303	3.303	0.598	0.417
150	0.546	1.724	2.474	0.586	0.408
250	0.527	1.035	1.535	0.585	0.393
Tolerance of 10%					
Inlets pressure (kPa)	Dilution Factor(*)	Q_X min (m^3.s^{-1})	Q_X max (m^3.s^{-1})	Outlet Propylene Fraction max	min
110	0.496	2.833	3.633	0.486	0.379
150	0.482	2.126	2.721	0.475	0.371
250	0.465	1.289	1.689	0.471	0.359

(*) dilution factor given by $\left({}^{Q_F}/_{Q_D}\right)$

From Table 5.6 and Table 5.7, it can be noted that even in the lower pressure condition (110 kPa), where the desorbent flow rate consumption is considerable higher, the same will happen to the feed flow rate (for the same molar rate), giving similar dilution factors for the different operating pressures.

From Figure 5.6, it can be perceived that the length of the intersection between the feed molar flow rate of 65.14 mol.s^{-1} line with the separation region for 250 kPa, is lower than in the other concentrations. It should be reminded that these separation regions are based on the equilibrium theory; therefore, one should expect them to be reduced by the inclusion of mass transfer effects. Factors such as adsorbent ageing will be much problematic in such cases (Sá Gomes *et al.*, 2007d, 2008b), leading to the separation requirements violation. Therefore,

operating an SMB at lower pressures (lower concentrations) can result in more robust units. However, with lower concentrations, it is needed to operate at higher flow rates, and pressure drop limitation can be an issue. Consequently, and since no more advantages have been noted in the lower pressure condition, we will not extend any longer the analysis to this pressure (110 kPa), and from now on, just consider the 150 kPa operating condition.

b) Total adsorbent amount and columns geometry

Some parameters are still missing. For each of these a first shot can be obtained by the use of suitable correlations based on theory or empirical data, as well as from the state-of-the-art of similar processes (by extrapolation or comparison), and then adjusted for the separation specifications or constraints.

Searching the literature for similar processes, namely cyclic adsorption processes, as the Pressure Swing Adsorption (PSA) technology with 13X zeolite, Table 5.8, one can find that the higher purity values are obtained for 0.82 mol.(kg.h)$^{-1}$ of productivity in Da Silva and Rodrigues, (2001), while the higher productivity values in Ramachandran and Dao (1994), with 2.74 mol.(kg.h)$^{-1}$ and a propylene purity rate of 89.9 %.

Table 5.8 – Literature on fixed-bed PSA for the separation of propane/propylene mixtures with 13X zeolite, (Sivakumar, 2007).

Reference	P_{High} (kPa)	P_{Low} (kPa)	Feed faction (molar %)	T (K)	Q_F (SLPM)	PU (%)	RE (%)	PR (mol.(kg.h)$^{-1}$)
Ramachandran and Dao (1994)	170	10	Propylene =88 Propane =12	363	10.28	89.9	87.6	2.74
Da Silva and Rodrigues (2001)	500	50/10	Propylene =25 Propane =25 N_2 =50	423	2.0	99.3	12.5	0.82

Using as reference the higher productivity value, and increasing it by 150 %, it is then possible to calculate a first estimation for the total volume needed to make the SMB process attractive. Therefore, and making use of the SMB and TMB equivalences from Table 5.5, one can derive the following equality:

$$Q_j^* = Q_j + \frac{Q_S \varepsilon_b}{(1-\varepsilon_b)} \tag{5.12}$$

and using the $Q_I\ min$, it is possible to obtain an estimated value for $\overline{Q_I^*}$, in this case 3.2 m^3.s^{-1}.

Introducing now the definition of productivity $\left(PR_{C_3H_6}^X\right)$, and relating it with the recovery of propylene in the extract $\left(RE_{C_3H_6}^X\right)$, $PR_{C_3H_6}^X = \frac{Q_X C_{C_3H_6}^X}{V_{ads}} = \frac{RE_{C_3H_6}^X Q_F C_{C_3H_6}^F}{V_{ads}}$, assuming a 100 % recovery, it is possible to calculate a total column volume of 32 m^3, approximately.

From the literature (Sá Gomes *et al.*, 2006c), the column diameter/height ratio in the industrial SMB units for liquid phase separation (petrochemical as fine chemical ones) is around 10, and several fluid distribution apparatus are used to avoid the problems related with the operation in large diameter columns (Frey *et al.*, 2006). While in the liquid phase separations it is normal to operate more than 20 columns of 10 m diameter (maximum)

and 1 m height (as in *p*-xylene separation from its isomers), in the gas separation field, the number of columns lower than 20 and columns aspect ratio (diameter/height) is quite lower than one (as in the PSA processes for the propane-propylene separation and other gases). In fact, in gas phase adsorption processes, the typical columns height is from 1 to 3 times the bed diameter and a reasonable superficial velocity around 1.5 $m.s^{-1}$, (Seider *et al.*, 2004).

At this point, one can make use of the pressure drop constraints to estimate the column geometry that will better suit the information related with the column diameter/height ratios from both technologies mentioned before. Is usually accepted that pressure drop is proportional to the plant productivity; therefore, we will make use of this information to project the unit by calculating, *a priori*, the maximum allowable pressure drop.

The maximum allowable pressure drop (ΔP) can be calculated by considering that the unit should work above 100 kPa, leading to the constraint $\Delta P \leq 50$ kPa for the 150 kPa operation, that with a 10 % tolerance becomes 45 kPa. The SMB pressure profiles should be stabilized by a constant pressure inlet, that can be applied to the unit itself, to each section or each column, *i.e.*, since we are in presence of a considerable pressure drop, in some point in the system the pressure must reach again an higher value (where the system can passes through a compressive stage, or is compensated by an high pressure inlet stream). This step can be performed by means of the desorbent or feed stream, as well as, by re-pressurization of the fluid stream just before each section or each column. Even if this repressurization strategy appears to be more costly and difficult to implement, it can represent an increased value for the SMB performance, allowing to operate the unit at different pressure ranges in each section, and therefore, different equilibrium requirements, as well as, a better control in system operational pressure. For instance, high pressure in section I, improving the solid regeneration step, and low pressure in section IV, helping in the desorbent regeneration step, or with more elaborated schemes (Lacava and McKeigue, 1995; Cheng and Wilson, 2001; Rao *et al.*, 2005; Kostroski and Wankat, 2008), or similar as section temperature control (Migliorini *et al.*, 2001; Jin and Wankat, 2007b).

In this study, these pressure modular operating schemes will not be analysed; nonetheless, the system will be simulated to account for it considering that the pressure at the inlet of each section is again the initial pressure, P_0.

The pressure drop constraint will then be evaluated with the Ergun eq. (5.13).

$$\frac{\Delta P}{L_c n_I} \geq \frac{150\mu(1-\varepsilon_b)^2}{{\varepsilon_b}^3 {d_p}^2}\overline{u_{I\,0}^*} + \frac{1.75(1-\varepsilon_b)\overline{\rho_f}}{{\varepsilon_b}^3 d_p}\overline{u_{I\,0}^*}^2 \qquad (5.13)$$

where $\overline{u_{I\,0}^*}$, represents the SMB average superficial velocity in section I (where the higher velocity values are observed); d_p the particle diameter; μ and $\overline{\rho_f}$ are the average fluid viscosity and density, respectively (for a 60 % mixture of isobutane with 40 % of Feed (75 % of propylene and 25 % of propane), as mentioned in the initial specifications) at 150 kPa and 373 K; and $L_c n_I$ the column height times the total number of columns in section I,

From the relation $\overline{u_{I\,0}^*} = \frac{\overline{Q_I^*}}{A_c}$, where A_c represents the column section area, it is possible to obtain, by an iterative procedure a first estimation for the column geometry. In this case one can consider a unit of 8 columns, 2 per each section leading to a 2.09 m diameter and 1.18 m height column, the aspect ratio is about 1.8. The number of

columns, as well as its distribution along the unit, is difficult to analyze at this point, nonetheless, it is commonly accepted that 8 columns systems can solve most of the SMB separations problems (Nicoud and Majors, 2000).

c) Solid flow rate influence

Let us now analyze the influence of the solid flow rate, or switching time, in the separation region. It is known that for a given couple Q_I/Q_{IV}, it is possible to define several separation regions in the plane $(Q_{II} \times Q_{III})$, which clearly shows the influence of the solid flow rate in these operating parameters, Figure 5.7.

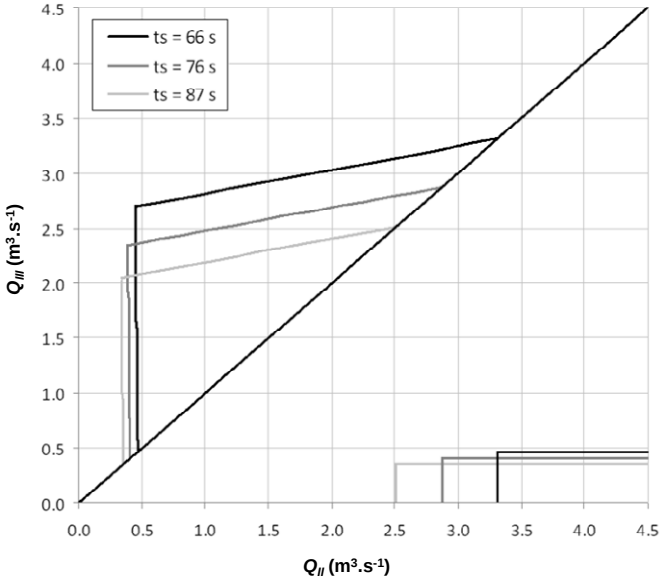

Figure 5.7 – Influence of switching time (solid flow rate) in the separation region, in the plane $(Q_{II} \times Q_{III})$ for total pressure of 150 kPa for t_s=[66 76 87] s.

If we look closely at Figure 5.7, we see that as the switching time increases (in other words, the solid flow rate decreases) the separation region is reduced. On the other hand, if the switching time is low (a high solid flow rate), we get a larger area for the separation region and thus a potential higher productivity, but with a significant increase in the desorbent consumption (that should be understood as desorbent recovery duty in the separation units after the SMB, see section 5.4-Is it worth it?), as shown in Figure 5.7, or better stated by equation (5.14)

$$\frac{Q_{D,min}}{Q_s} \cong \frac{Q_{I,min} - Q_{IV,max}}{Q_s} \cong \frac{\varepsilon_b}{(1-\varepsilon_b)}\left(\gamma_{I,min} - \gamma_{IV,min}\right) \tag{5.14}$$

Other pertinent aspects, such as the operational temperature (not analysed in this work, since one should expect similar results as the ones obtained for the operational pressure), can already be analysed by means of these simplifications. The conclusions and observations obtained from this analysis can be quite useful, and probably most of them will be taken into account after, with the introduction of more detailed studies.

To summarize, it is possible to condense in a scheme the procedure hereby adopted to answer the first question: Is it possible? Figure 5.8.

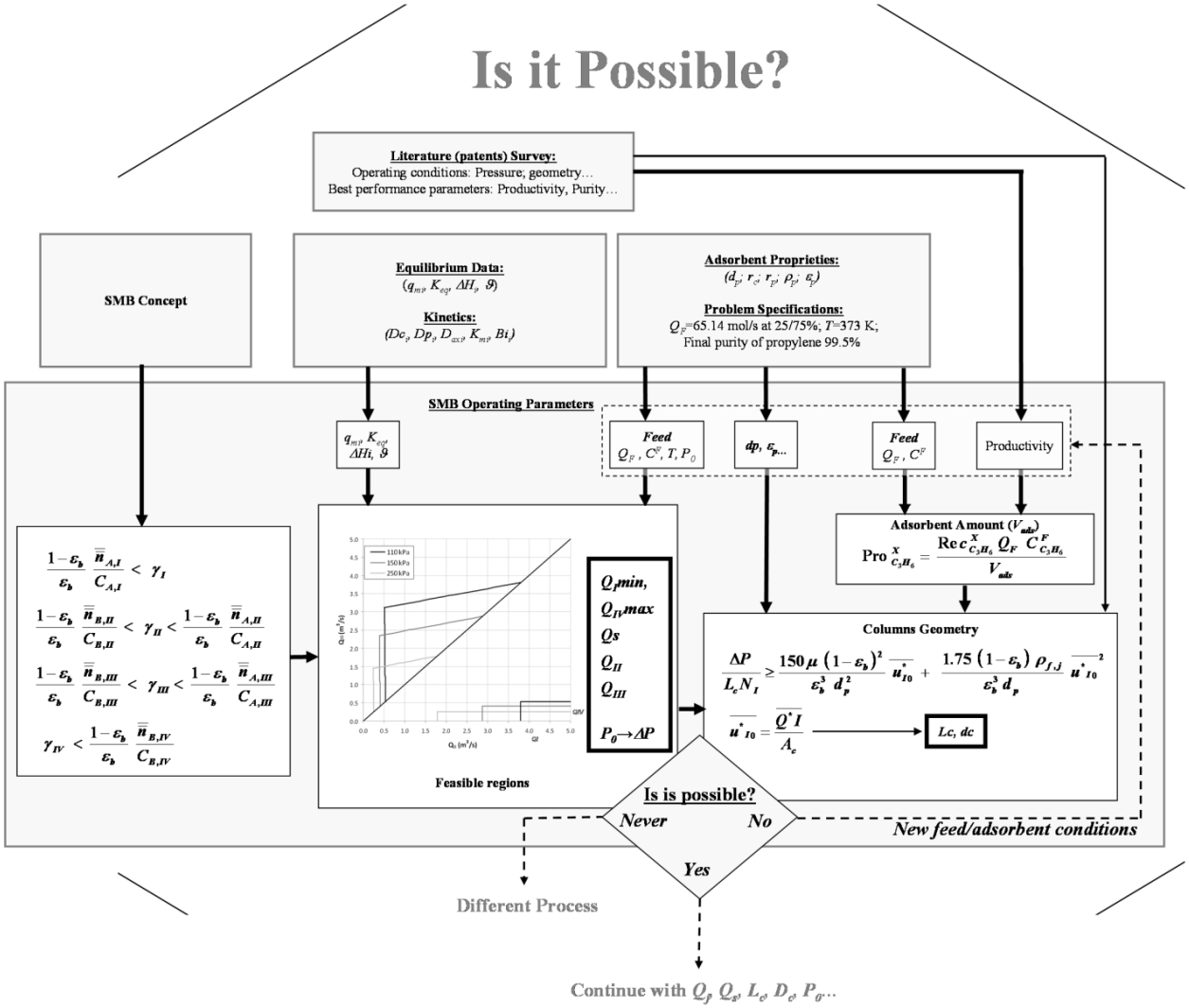

Figure 5.8 – Schematic procedure to answer the first design question: Is it Possible?.

From Figure 5.8, one can note that the question Is it possible? can have 3 different answers: Yes, in this case one should proceed to the next step using the calculated operating parameters in the black boxes; No, in this case one should re consider the initially taken assumptions and re calculate the problem with new operating conditions and Never (non convergent), obtained after successive iterations with different assumptions, which means that the process is not possible and one should try a different technology.

In this case, it was proved that the separation of propane-propylene via SMB technology over 13X zeolite with isobutane as desorbent is in fact possible, and therefore, worthy of a more detailed study, now provided with the next step in our decision design flowchart.

5.3 IS IT REASONABLE?

If the separation is possible under the selected technology, one can continue the analysis by including more complex restrictions, and therefore, detailing the study. Most of the chemical engineering studies deal with mass transfer, accounted in mass balances. In fact, one can argue that mass transfer is at the core of separations processes.

5.3.1 MATHEMATICAL STRATEGY, *THE POWER OF MODELS*

Once again, one can make use of the TMB analogy with the SMB and model the SMB unit by means of a continuous TMB model approach. This strategy will provide fast simulations in addition to steady state results that, at this stage, can be quite useful to predict some of the unit performance parameters, as well as, to implement some optimization routines.

Generally, one can model a chromatographic separation process by means of two approaches: making use of partial differential equations, derived from a mass (energy or momentum) balance to a differential volume element (Adz), a continuous flow model (plug flow or axial dispersed plug flow); or by a cascade of mixing cells (Ruthven and Ching, 1989). Each of these approaches can include mass transfer resistances, thermal, and/or pressure drop effects. In this work, and based on most of the literature concerning SMB as PSA processes, we will make use of the continuous approach.

It is possible to model both the real SMB as the equivalent TMB using more complete models, detailing the particle diffusion and/or film mass transfer (the detailed particle model), or by approximation of the intraparticle mass transfer rate with the Linear Driving Force (LDF) approach. This second methodology proved to be adequate to describe most of experimental results and, in fact, is used by the majority of researchers in the field. Therefore, the model here by described will take into account that:

- the fluid motion is modelled by a plug flow with axial dispersion;
- the solid phase motion is assumed to be a piston flow (later it will be introduced a more detailed model accounting for the ports discontinuities, and therefore, the solid movement simulation, see annex);
- fluid velocity is supposed to be variable along the column;
- it is considered that there are two particle levels of mass transfer, represented by a *bi*-Linear Driving Force approximation;
- the system is supposed to be non-isothermal and non-adiabatic;
- the thermal effects are considered by means of an heterogeneous energy balance distinguishing temperatures in the fluid, solid and at the wall of the column;
- the pressure drop effects are considered by means of a continuous formulation of the Ergun equation.

a) Mass Balances

- **Mass balance for species i in section j**

$$\frac{\partial(C_j Y_{i,j})}{\partial t} = \frac{\partial}{\partial z}\left(D_{b,j} C_j \frac{\partial Y_{i,j}}{\partial z}\right) - \frac{\partial(u_j C_j Y_{i,j})}{\partial z} - N_{i,j} \quad i = 1, \dots, NC \quad j = I, \dots, IV \tag{5.15}$$

where, $Y_{i,j}$ represents the molar fraction of i species in section j.

- **Mass transfer flux between the bulk and the "macro pore" phases**

$$N_{i,j} = \frac{(1-\varepsilon_b)}{\varepsilon_b}\frac{aK_{m_i}}{(Bi_{m_i}+1)}\left(C_j Y_{i,j} - \bar{c}_j \bar{y}_{i,j}\right) \quad (5.16)$$

with $\overline{c_j y_{i,j}}$ the average concentration of i species in the "macro pore" phase in section j, K_{m_i} the global mass transfer coefficient, a, the specific surface, and $Bi_{m_{i,j}}$ the Biot number $\left(\frac{r_p K_{m_i}}{5\varepsilon_p D_{p_i}}\right)$.

- **Total mass balance for a bulk volume element, in section *j***

$$\frac{\partial C_j}{\partial t} = -\frac{\partial(u_j C_j)}{\partial z} - \sum_{i=1}^{NC} N_{i,j} \quad (5.17)$$

with C_j the total bulk concentration in section j, $C_j = \frac{P_j}{RT_{g_j}}$.

- **Mass balance in the particle pellet, in section *j***

To reflect the counter current solid phase motion, a convective term was introduced in the expression of the "macro pore" phase balance, this aspect is in fact the base of TMB model approach. In addition, it should be noted that the transfer between bulk phases and macropores, makes use of the Linear Driving Force approximation.

$$\frac{\partial(\bar{c}_j \bar{y}_{i,j})}{\partial t} - u_s \frac{\partial(\bar{c}_j \bar{y}_{i,j})}{\partial z} + \frac{\rho_p}{\varepsilon_p}\left(\frac{\partial \bar{\bar{n}}_{i,j}}{\partial t} - u_s \frac{\partial \bar{\bar{n}}_{i,j}}{\partial z}\right) = \frac{15 D_{p_i}}{{r_p}^2}\frac{Bi_{m_{i,j}}}{Bi_{m_{i,j}}+1}\left(C_j Y_{i,j} - \bar{c}_j \bar{y}_{i,j}\right) \quad (5.18)$$

where D_{p_i} represents the effective diffusion coefficient in the macropores and ρ_p and ε_p the particle density and porosity, respectively.

- **Mass balance inside the "crystal", in section *j***

The mass transfer at the micropores level can also be represented by means of an LDF approach as:

$$\frac{\partial \bar{\bar{n}}_{i,j}}{\partial t} - u_s \frac{\partial \bar{\bar{n}}_{i,j}}{\partial z} = \frac{15 D_{c_i}}{{r_c}^2}\left({n_{i,j}}^{eq} - \bar{\bar{n}}_{i,j}\right) \quad (5.19)$$

The pellet averaged adsorbed concentration can be obtained from $\bar{\bar{n}}_{i,j} = \frac{3}{{r_p}^3}\int_{r=0}^{r=r_p} \bar{n}_{i,j}\, r^2 dr$, with ${n_{i,j}}^{eq}$ the crystal adsorbed concentration in equilibrium, D_{c_i}, the diffusion coefficient in the micropores and r_c the crystal radius.

b) Energy balances

The mathematical treatment of heat transfer in a moving bed is generally comparable to the one usually used for the fixed bed, safe for the adsorbent particles movement. To simplify some of the general considerations, the radial thermal gradient has been neglected and the heat transfer was supposed to be linear between the different phases, as well as the different heat capacities remain constant throughout the temperature range.

- **Energy Balance in the gas phase**

$$\frac{\partial T_{g_j}}{\partial t} = \frac{1}{\varepsilon_b C_j \tilde{C}_v}\frac{\partial}{\partial z}\left(\lambda_j \frac{\partial T_{g_j}}{\partial z}\right) - u_j \frac{\tilde{C}_p}{\tilde{C}_v}\frac{\partial T_{g_j}}{\partial z} + \frac{RT_{g_j}}{C_j \tilde{C}_v}\frac{\partial C_j}{\partial t} - \frac{(1-\varepsilon_b)}{\varepsilon_b}\frac{ah_f}{C_j \tilde{C}_v}\left(T_{g_j} - T_{s_j}\right) - \frac{2h_w}{\varepsilon_b C_j \tilde{C}_v R_w}\left(T_{g_j} - T_{w_j}\right) \quad (5.20)$$

with T_{g_j}, T_{s_j}, T_{w_j} the temperatures for gas, solid and wall in section j, respectively; and where h_f and h_w represents the heat transfer coefficient between the gas phase to the particles and to the wall, respectively. $h_f$obtained from the correlation: $h_f = \frac{k_g}{d_p}\left(2.0 + 1.1Re^{0.6}Pr^{1/3}\right)$ (Wakao and Kaguei, 1982) with Pr and Re the Prandtl and Reynolds numbers, respectively and for h_w it can be used the correlation from (Yagi and Kunii, 1960):

$h_w = \frac{k_g}{d_p}(0.18Re^{0.8} + 0.069PrRe)$, $\tilde{C}_v$ and $\tilde{C}_p$ are average the molar heat capacities for the fluid at constant volume and pressure, and λ_j, the thermal axial dispersion coefficient, obtained by Wakao and Funazkri (1978) correlation: $\lambda = k_g(\gamma_3 + \gamma_4 RePr)$, with $\gamma_3 = 7$ and $\gamma_4 = 0.5$.

- **Energy Balance in the solid phase**

Unlike the fixed-bed model, the energy balance of intraparticular phase involves a convective term to reflect the adsorbent strong movement, relative to the TMB approach. Nevertheless, we continued to neglect the heat dispersion of the solid and the heat transfer between the adsorbent bed and the wall of the column.

$$\frac{\partial T_{s_j}}{\partial t} - u_s \frac{\partial T_{s_j}}{\partial z} = \frac{(1-\varepsilon_b)\varepsilon_p R T_{s_j}}{B}\left(\frac{\partial \bar{c}_j}{\partial t} - u_s \frac{\partial \bar{c}_j}{\partial z}\right) + \frac{\rho_b}{B}\sum_{i=1}^{NC}(-\Delta H_i)\left(\frac{\partial \bar{\bar{n}}_{i,j}}{\partial t} - u_s \frac{\partial \bar{\bar{n}}_{i,j}}{\partial z}\right) + \frac{(1-\varepsilon_b)ah_f}{B}\left(T_{g_j} - T_{s_j}\right) \quad (5.21)$$

With $B = (1-\varepsilon_b)\left\{\varepsilon_p \sum_{i=1}^{NC} \bar{c}_{i,j}\tilde{C}_{v_i} + \rho_p \sum_{i=1}^{NC} \bar{\bar{n}}_{i,j}\tilde{C}_{v_i} + \rho_p \hat{C}_{ps}\right\}$

where $\hat{C}_{ps}$ represents the solid heat capacity.

- **Energy balance to the wall**

By neglecting the possible release of heat generated by friction of the solid phase with the inner surface of the column, the energy balance to the wall becomes:

$$\frac{\partial T_{w_j}}{\partial t} - u_s \frac{\partial T_{w_j}}{\partial z} = \frac{1}{\rho_w \hat{C}_{pw}}\left(\alpha_w h_w\left(T_{g_j} - T_{w_j}\right) - \alpha_{wl} U\left(T_{w_j} - T_\infty\right)\right) \quad (5.22)$$

with U the global heat transfer coefficient to the wall; ρ_w and $\hat{C}_{pw}$ the density and mass heat capacity at the wall and $\alpha_w = \frac{d_w}{e(d_w+e)}$ and $\alpha_{wl} = \left((d_w + e)ln\left(\frac{d_w+e}{d_w}\right)\right)^{-1}$, with e the wall thickness.

The solid velocity term in eq. (5.22) is due to the simulated wall velocity in the SMB unit, one should keep in mind that the TMB model approach is being used to simulate an SMB unit and in fact is not representing a "true"-TMB unit.

c) Adsorption equilibrium

It is considered an adsorption equilibrium as presented by the Toth model mentioned before with equation (5.1) and Table 5.2.

d) Momentum balance

The change in pressure can be accounted through the momentum balance, considering that the Ergun equation is valid locally, eq. (5.23), a steady-state simplification used for the sake of simplicity, (Sereno and Rodrigues, 1993).

$$-\frac{\partial P}{\partial z} \geq \frac{150\mu(1-\varepsilon_b)^2}{\varepsilon_b{}^3 {d_p}^2} u_j + \frac{1.75(1-\varepsilon_b)\rho_{f_j}}{\varepsilon_b{}^3 d_p} u_j^2 \tag{5.23}$$

With $\rho_{f_j} = C_j\left(\sum_{i=1}^{NC} Y_{i,j} M_i\right)$.

The pressure drop can easily influence the retention time of gas phase separation in a simple fixed bed apparatus, (Zwiebel, 1969; Chahbani and Tondeur, 2001). In the SMB, it is expected that this aspect becomes quite more significant, either due to the velocity variations, as the total concentration (total pressure) influence on the separation conditions, as previously analysed. Nevertheless, one expect to reduce this influence with the implementation of the repressurization steps just before each section, as mentioned before.

e) Initial and boundary conditions

Initial conditions:

$$t = 0$$

$$C_{i,j} = \bar{c}_{i,j} = y_{i,j}^0 {C_j}^0 \tag{5.24}$$

$$\bar{\bar{n}}_{i,j} = {n_{i,j}}^{eq}\left(y_{i,j}^0, T^0\right) \tag{5.25}$$

$$T_{s\,j} = T_{g_j} = T_{w\,j} = T^0 \tag{5.26}$$

Boundary conditions to section j (Danckwerts, 1953):

- $z = 0$

$$-D_{b_j} \frac{\partial Y_{i,j}}{\partial z}\Big|_{z=0} + u_j\big|_{z=0}\left(Y_{i,j}\big|_{z=0} - {Y_{i,j}}_0\right) = 0 \tag{5.27}$$

$$-\lambda_j \frac{\partial T_{g_j}}{\partial z}\Big|_{z=0} + u_j\big|_{z=0} C_j\big|_{z=0} \tilde{C}_p\left(T_{g_j}\Big|_{z=0} - {T_{g_j}}_0\right) = 0 \tag{5.28}$$

$$P_j\big|_{z=0} = P^0 \tag{5.29}$$

- $z = L_j$

$$D_{b\,j}\left.\frac{\partial Y_{i,j}}{\partial z}\right|_{z=L_j} = 0 \tag{5.30}$$

$$\lambda_j \left.\frac{\partial T_{g\,j}}{\partial z}\right|_{z=L_j} = 0 \tag{5.31}$$

For $j = I, II, III$

$$\bar{c}_{i,j}\big|_{z=L_j} = \bar{c}_{i,(j+1)_0} \quad \bar{\bar{n}}_{i,j}\big|_{z=L_j} = \bar{\bar{n}}_{i,(j+1)_0} \quad T_{s\,j}\big|_{z=L_j} = T_{s_{(j+1)_0}} \quad T_{w\,j}\big|_{z=L_j} = T_{w_{(j+1)_0}} \tag{5.32a-d}$$

For $j = IV$

$$\bar{c}_{i,IV}\big|_{z=L_{IV}} = \bar{c}_{i,I_0} \quad \bar{\bar{n}}_{i,IV}\big|_{z=L_{IV}} = \bar{\bar{n}}_{i,I_0} \quad T_{s_{IV}}\big|_{z=L_{IV}} = T_{s_{I_0}} \quad T_{w_{IV}}\big|_{z=L_{IV}} = T_{w_{I_0}} \tag{5.33a-d}$$

i.Nodes balances:

At the Desorbent (D) node:

$$u_I|_{z=0} = u_{IV}|_{z=L_{IV}} \left(\frac{P_{IV}|_{z=L_{IV}}}{P^0}\right) + u_D \tag{5.34}$$

$$Y_{i,IV}\big|_{z=L_{IV}} = \left(\frac{u_I|_{z=0}}{u_{IV}|_{z=L_{IV}}} Y_{i,I_0} - \frac{u_D}{u_{IV}|_{z=L_{IV}}} Y_i{}^D\right)\left(\frac{P_{IV}|_{z=L_{IV}}}{P^0}\right)^{-1} \tag{5.35}$$

$$T_{g_{IV}}\big|_{z=L_{IV}} = \left(\frac{u_I|_{z=0}}{u_{IV}|_{z=L_{IV}}} T_{g_{IV_0}} - \frac{u_D}{u_{IV}|_{z=L_{IV}}} T_g{}^D\right)\left(\frac{P_{IV}|_{z=L_{IV}}}{P^0}\right)^{-1} \tag{5.36}$$

At the Extract (X) node :

$$u_{II}|_{z=0} = u_I|_{z=L_I} \left(\frac{P_I|_{z=L_I}}{P^0}\right) - u_X \tag{5.37}$$

$$Y_{i,I}\big|_{z=L_I} = Y_{i,II}{}^0 \tag{5.38}$$

$$T_{g_I}\big|_{z=L_I} = T_{g_{II}}{}^0 \tag{5.39}$$

At the Feed (F) node :

$$u_{III}|_{z=0} = u_{II}|_{z=L_{II}} \left(\frac{P_{II}|_{z=L_{II}}}{P^0}\right) + u_F \tag{5.40}$$

$$Y_{i,II}\big|_{z=L_{II}} = \left(\frac{u_{III}|_{z=0}}{u_{II}|_{z=L_{II}}} Y_{i,III_0} - \frac{u_F}{u_{II}|_{z=L_{II}}} Y_i{}^F\right)\left(\frac{P_{II}|_{z=L_{II}}}{P^0}\right)^{-1} \tag{5.41}$$

$$T_{g_{II}}\Big|_{z=L_{II}} = \left(\frac{u_{III}|_{z=0}}{u_{II}|_{z=L_{II}}} T_{g_{III}}{}_0 - \frac{u_F}{u_{II}|_{z=L_{II}}} T_g{}^F\right)\left(\frac{P_{II}|_{z=L_{II}}}{P^0}\right)^{-1} \quad (5.42)$$

At the Raffinate (R) node :

$$u_{IV}|_{z=0} = u_{III}|_{z=L_{III}}\left(\frac{P_{III}|_{z=L_{III}}}{P^0}\right) - u_R \quad (5.43)$$

$$Y_{i,III}\Big|_{z=L_{III}} = Y_{i,IV}{}^0 \quad (5.44)$$

$$T_{g_{III}}\Big|_{z=L_{III}} = T_{g_{IV}}{}^0 \quad (5.45)$$

f) Performance parameters

The definitions of the purity of the extract (PU_X), and raffinate (PU_X), using the variables related to TMB in the following manner:

$$PU_X = \frac{C^X_{C_3H_6}}{C^X_{C_3H_6}+C^X_{C_3H_8}} \qquad PU_R = \frac{C^R_{C_3H_8}}{C^R_{C_3H_6}+C^R_{C_3H_8}}$$

Similarly, for the recovery of the more retained species in the Extract stream (RE_X) and the less one in the raffinate port (RE_R):

$$RE_X = \frac{Q_X C^X_{C_3H_6}}{Q_F C^F_{C_3H_6}} \qquad RE_R = \frac{Q_R C^R_{C_3H_8}}{Q_F C^F_{C_3H_8}}$$

The productivity is expressed in terms of propylene recovered in the Extract stream (PR_X), or propane in the Raffinate port (PR_R):

$$PR_X = \frac{Q_X C^X_{C_3H_6}}{V_{ads}} = \frac{RE_X Q_F C^F_{C_3H_6}}{V_{ads}} \qquad PR_R = \frac{Q_R C^R_{C_3H_8}}{V_{ads}} = \frac{RE_R Q_F C^F_{C_3H_68}}{V_{ads}}$$

5.3.2 SIMULATION, ANALYSIS AND OPTIMIZATION, *THE POWER OF COMPUTERS*

The model described before results in a system of PDE (Partial Differential Equations), ODE (Ordinary Differential Equations) and AE (Algebraic Equations), that can be solved by means of numerical solution giving some first simulations based on the estimated operating parameters.

a) Simulation

In Table 5.9, operating parameters and column geometry as stated before, for the first simulation, and in Figure 5.9, the correspondent bulk concentrations profiles, at the steady state.

As can be observed from Figure 5.9, the concentration profiles of the less retained species in section II and IV and of the more retained component in section I and III, do not occupy all section length, *i.e.*, there is not any propane polluting the end of section IV nor in the beginning of section II. In addition, there is not any propylene in the beginning of section I nor in the end of section III; therefore, it is possible to obtain the 100 % performance parameters values in Table 5.10.

Table 5.9 – Operating conditions and column geometry for the first simulation.

Columns Geometry	Operating Conditions
L_c = 1.18 m	$T_{T,D}$ = 373 K $P_{T,D}$ = 150 kPa
d_c = 2.09 m	t_s = 76.5 s
V_c = 4.05 m^3	Q_F = 1.35 m^3.s^{-1}
$n_j = [2\ \ 2\ \ 2\ \ 2]$	Q_X = 2.65 m^3.s^{-1}
	Q_R = 1.49 m^3.s^{-1}
	Q_D = 2.79 m^3.s^{-1}
	Q_{IV} = 0.36 m^3.s^{-1}

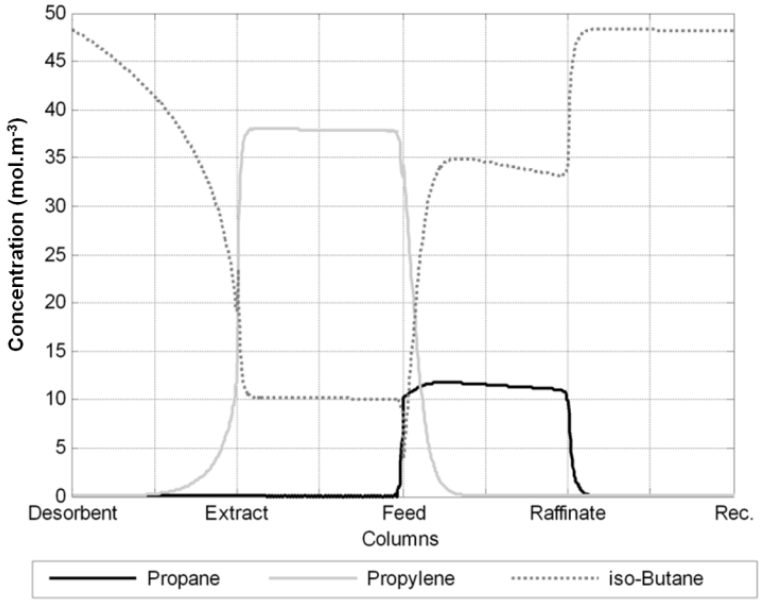

Figure 5.9 – Bulk concentration profiles for the operating conditions presented in Table 5.9, at steady state*.

Also, it is possible to realise that the weak condition for the first shot value for the operating condition in section IV (γ_{IV}), was overestimated, giving now more space to increase the recycle flow rate than the possible space to decrease the flow rate in section I. The gas phase temperature, interstitial velocity and total pressure profiles at the steady state are shown in Figure 5.10 and performance parameters in Table 5.10.

* For the simulation purpose, a numerical solution was obtained using the commercial package from Process Systems Enterprise: gPROMS v.3.1.3 applying one of the discretization methods available, namely, the Orthogonal Collocation on Finite Elements (OCFEM), with 2 collocation points per element, with 50 elements in each section for the axial coordinate. After the axial discretization step, the time integration is then performed by an ordinary differential equation solver DASOLV based on variable time step/variable order Backward Differentiation Formulae (BDF). For all simulations was fixed a tolerance value equal to 10^{-5}.

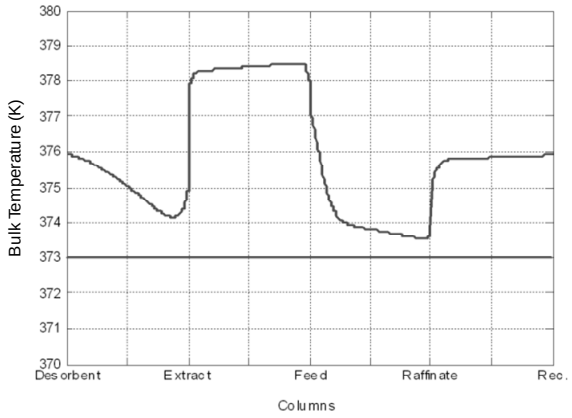

(a)

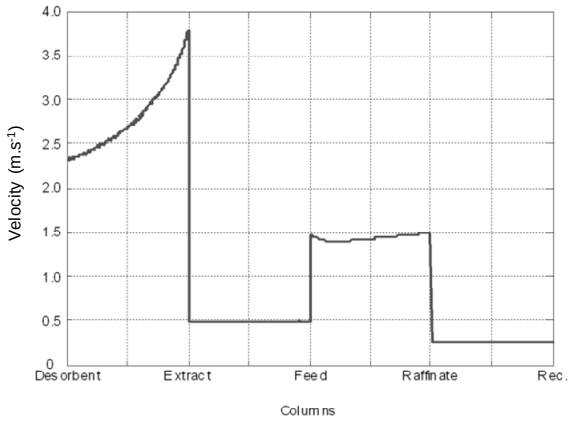

(b)

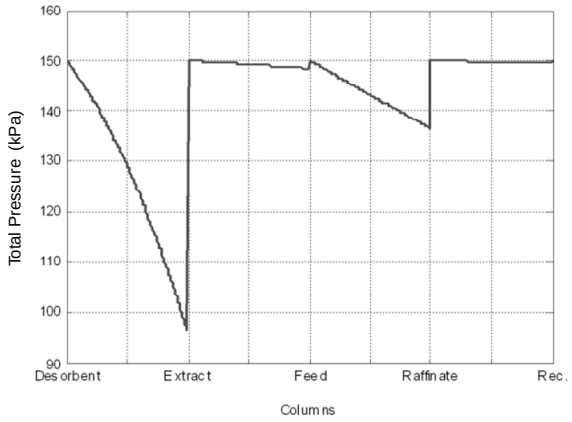

(c)

Figure 5.10 – Profiles of gas phase bulk temperature (a); interstitial velocity (b); and total pressure (c), for the operating conditions presented in Table 5.9, at the steady state.

By observing Figure 5.10a close to Figure 5.9, it can be noted that when a more retained species is displaced by a less adsorbed one, there is a temperature decrease and the *vice-versa*, this fact is due to the adsorption

phenomena itself (exothermic), accounted in the model by the adsorption enthalpies values (Figure 5.2) on the energy balance. However, and based on the solid and fluid specific heats, this temperature variation is observed next to the left of the adsorption or desorption zone, *i.e.*, the temperature waves are following the solid movement direction and not the fluid one. The total bulk concentration variation along the unit is similar to the total pressure variation, since the temperature influence is almost imperceptible (varying within a maximum range of 6 K, Figure 5.10a), when compared with the pressure variations.

The pressure drop presented in Figure 5.10c demonstrates that the previously stated ΔP limitation on section I was violated. One should keep in mind that this limitation was stated for constant velocity. The results presented in Figure 10c, even though being based on the same operating parameters, now account for several detailed phenomena, such as the variation of velocity. Observing Figure 5.10b and Figure 5.10c, it is then possible to understand why this violation took place in section I. Running the same simulation but now considering that the pressure drop is just function of a constant (initial) velocity value one obtains the following Figure 5.11.

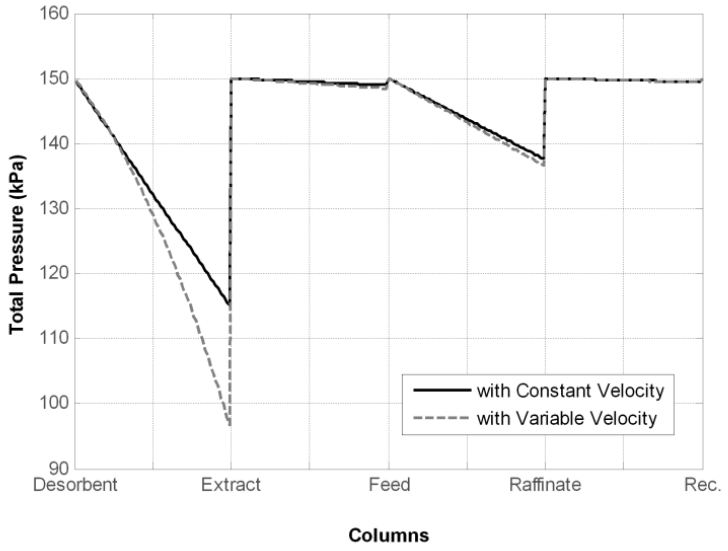

Figure 5.11 – Profiles total pressure for to different scenarios: Ergun equation based on constant velocity and variable velocity.

With the constant velocity approach the pressure constraint is already fulfilled. Due to the considerable difference between the two approaches on should keep the more detailed one.

The performance parameters from Table 5.10 show that even with the equilibrium based estimation, it was possible to obtain a quite good separation, with promising productivity values.

Table 5.10 – Performance parameters for the first simulation, operating conditions from Table 5.9.

PU_X = 100 %
RE_X = 100 %
PR_X = 6.63 mol.(kg_{ads}.h)$^{-1}$ = 377.9 kg.(m^3_{ads}.h)$^{-1}$
PU_R = 100 %
RE_R = 100 %
PR_R = 2.21 mol.(kg_{ads}.h)$^{-1}$ = 132.0 kg.(m^3_{ads}.h)$^{-1}$

b) Separation Analysis

As mentioned before, it is possible to understand that a significant part of the unit is running near the equilibrium. If we manipulate equations (5.15-5.19), by introducing the following dimensionless variables $\left\{\theta = \frac{t}{t_s} \quad x = \frac{z}{n_j L_c}\right\}$, neglecting the axial dispersion term, considering constant fluid velocity and rewriting for the steady state eqs. (5.15), (5.18) and (5.19) become:

$$0 = -\frac{\partial(C_j Y_{i,j})}{\partial x} - \frac{(1-\varepsilon_b)}{\varepsilon_b}\left[\frac{n_j L_c}{u_j}\frac{15 D_{p_j}}{r_p^2}\frac{Bi_{m_{i,j}}}{Bi_{m_{i,j}}+1}\right]\left(C_j Y_{i,j} - \overline{c_j y_{i,J}}\right) \tag{5.46}$$

$$0 = \frac{\partial(\overline{c_j y_{i,J}})}{\partial x} + \frac{\rho_p}{\varepsilon_p}\frac{\partial \bar{n}_{i,j}}{\partial x} + \left[\frac{n_j L_c}{u_s}\frac{15 D_{p_j}}{r_p^2}\frac{Bi_{m_{i,j}}}{Bi_{m_{i,j}}+1}\right]\left(C_j Y_{i,j} - \overline{c_j y_{i,J}}\right) \tag{5.47}$$

$$0 = \frac{\partial \bar{n}_{i,j}}{\partial x} + \left[\frac{n_j L_c}{u_s}\frac{15 D_{c_j}}{r_c^2}\right]\left(n_{i,j}^{\ eq} - \bar{n}_{i,j}\right) \tag{5.48}$$

which means that multiplicative factors next to the mass transfer terms are the fluid and solid contact time constants: $\left\{\frac{n_j L_c}{u_j} = t_j \quad \frac{n_j L_c}{u_s} = n_j t_s\right\}$, respectively. The increase of these "constants" is similar to augment the mass transfer coefficients, and therefore, the improvement of the mass transfer and *vice-versa*. By working with these parameters it is possible to shrink and stretch the pollution or collection fronts in Figure 5.9. Let us redraw the separation region triangle, but now accounting for all the mass transfer effects, as well as, the temperature variations as considered by the detailed model. Figure 5.12 shows the complete separation region for column geometry mentioned in Table 9, with $T_{F,D}$=373 K; P_0=150 kPa; t_s=76.5 s; Q_{IV}=0.27 $m^3.s^{-1}$ and Q_I=3.76 $m^3.s^{-1}$, obtained by consecutive simulations with different (Q_{II}, Q_{III}) pairs, (step of 0.075 $m^3.s^{-1}$).

The Q_{IV} and Q_I flow rates were set with an higher tolerance factor (25%) than the 10 % used for the equilibrium assumptions. This fact is related with the influence of these flow rates in the separation region shape, as studied before by Azevedo and Rodrigues (1999), and presented as the Separation Volume Theory. A similar separation region was obtained for isothermal conditions (at 373 K), which can be stated by the reduced temperature variations observed in Figure 5.9.

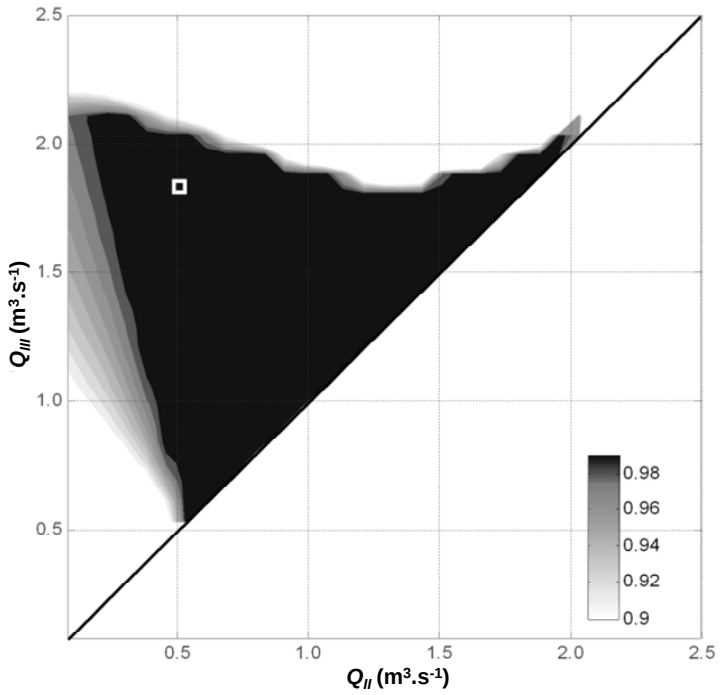

Figure 5.12 – Separation region for column geometry mentioned in Table 5.9, lower purity values in the raffinate or extract outlets over 90 % (0.9)-gray to over 99 % (0.99)-black; white square the operating point mentioned in Table 5.9.

If one observe Figure 5.12 close to Figure 5.5, it can be perceived that this complete separation region fits inside the predicted one (Figure 5.5 for 150 kPa); however, some small differences are noted, namely the vertex point (higher productivity value, maximum Q_{III} for minimum Q_{II}), related with the approximations used for the α and β parameters in the design procedure based on the adsorption equilibrium, as well as, for the consideration (in Figure 5.12) of mass transfer resistances. Nevertheless, the equilibrium based methodology provides a good estimation, placing the corresponding operating point near to the upper triangle limit.

If we run consecutive simulations for different (Q_{II}, Q_{III}) pairs, as well as different Q_s values, within the range of the possible separation for a given $n_j L_c$, it is then possible to obtain that complete separation regions that will take into account both these contact time constants influences. This procedure was implemented to obtain 3 different separation regions for 2 different adsorbent amounts: as in Table 5.9 – separation regions in Figure 5.13a; and half of this amount – separation regions in Figure 5.13b.

Each different switching time the Q_{IV} and Q_I values were corrected to maintain the same initial γ_j operating parameters corrected by the 25 % tolerance factor, as in Figure 5.12.

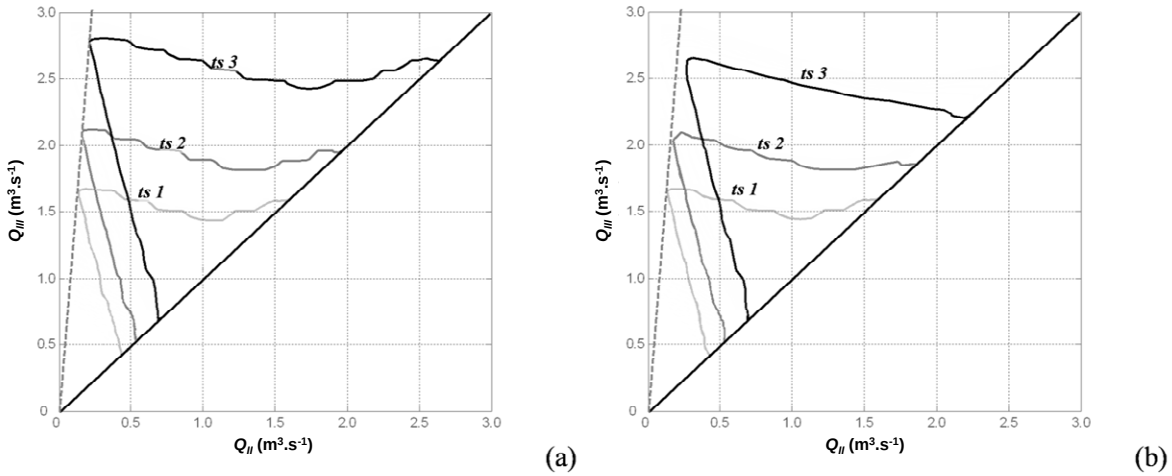

Figure 5.13 – Separation region for column geometry mentioned in Table 5.9 (a) and half column volume (b), lower purity values in the raffinate or extract outlets over 99 %, for t_s1=95.6 s, t_s2=76.5 s and t_s3=57.4 s.

From Figure 5.13a it can be perceived that by increasing the internal flow rates it is possible to process more feed, nevertheless, the mass transfer resistances become an issue, as the contact times decreases. This point can be shown by connecting most of the vertex points in a line that passes over the origin point. The operation line that states that the unit productivity is proportional to the solid flow rate for a given γ_F, $\gamma_F = \frac{(1-\varepsilon_b)}{\varepsilon_b}\frac{Q_F}{Q_s} = \frac{(1-\varepsilon_b)}{\varepsilon_b}\frac{(Q_{III}-Q_{II})}{Q_s}$, and by consequence to the unit pressure drop obtained from the Q_j flow rate for a given γ_I, $\gamma_I = \frac{(1-\varepsilon_b)}{\varepsilon_b}\frac{Q_I}{Q_s}$. This line will state the equilibrium considerations; nevertheless, when mass transfer resistances become an issue (particularly in the presence of reduced amount of adsorbent, Figure 5.13b), the contact times become a major problem and the area of the separation regions for higher solid flow rates can even start to decrease relatively to the ones draw for lower solid flow rates, consequently the vertex point appears below the mentioned line.

This aspect has to be taken into account, and therefore, will also be considered in the following optimization procedures, by including as problem decision variables also the switching time as internal flow rates, closely related with Q_{IV}.

c) Optimization

From experience, it is known that a reasonable unit should not present too much column length occupied by concentration *plateaux*, and therefore, the polluting as collection fronts should be placed near to the nodes. To place these fronts on that positions, either the operating parameters can be changed (increase of Q_X, Q_F and Q_{IV} and/or decrease of Q_D flow rates), and/or the adsorbent amount be reduced resulting in the improvement of the unit performance, namely productivity.

In this particular case, since the Q_F is already established, one can start to decrease the adsorbent amount, and then recalculate the columns geometry always considering the pressure drop limitations, by means of equation (5.23).

It can be practical to use an optimization procedure. A simple optimization procedure will now be applied to demonstrate how these optimization tools can add value in the design decision making, either for process performance improvement, either as diagnose method already demonstrated with more exhaustive approaches in the recent published works (see section 2.3.4 for further details in relatively to optimization).

An optimization problem can be based on single-objective or multiple-objective functions. The case of multiple-objective optimization a global optimum may not exist, and an entire set of optimal solutions found can be equally good, the so-called Pareto Optimal Solutions. In this work it will only be considered a single-objective optimization procedure. In a single optimization procedure all the different performance parameters mentioned before can be homogenized/normalized by the separation cost, where several separation costs indirectly related to the separation itself (labour, maintenance, etc.) and the directly dependent ones (adsorbent, plant, desorbent/eluent consumption, desorbent/eluent recycling, feed losses, etc.) are considered by means of different weight factors related to the specific cost mentioned before. However, each of these weight factors are difficult to characterize at this point, and probably are better understood after some cost simulations and judgments of worth in further evaluation steps. This point is not the purpose of this work, and therefore, we will make use of an optimization procedure considering only the maximization of the SMB unit productivity for a given desorbent flow rate. A two level optimization strategy could be used for optimize both productivity as desorbent consumption, as proposed by Minceva and Rodrigues (2005); nevertheless, as mentioned before and better stated in the following section (5.4-Is it worth it?), one should regard to desorbent consumption as a desorbent recovery duty in fact. Nevertheless, this aspect can only be evaluated if one simulates this recovery unit.

Therefore, and at this point, one will only base the optimization problem on the maximum unit productivity for a given Q_F; Q_D and n_j by changing Q_{IV}, Q_X (and by consequence Q_R), t_s and L_c, Ld_c using as initial shot the conditions from Table 5.9, bounded by more or less 30 % in each control variable,constrained by extract purity values over 99.5 % (it is assumed that the separation of isobutane from the extract mixture, in the desorbent recovery step, will provide a 99.5 % pure propylene as well), and raffinate purity over 99.25 % (what should result in a higher propylene recovery values, above 99.0 %); and maximum pressure drop in section I limited by 45 kPa, Table 5.11.

The initial conditions for the optimization problems are in fact a major issue; from different initial shots, different solutions can be found; nevertheless, and for the sake of simplicity one will only use the case mentioned in Table 5.9 as first shot.

The columns distribution will not be optimized, although it is an important variable and further optimization steps can be implemented to obtain it, in terms of section length or by relating it with an asynchronous port shift (also called Varicol mode of operation, presented by Adam *et al.*, (2000)), as in Sá Gomes *et al.*, (2008) and Kawajiri and Biegler, (2008).

Table 5.11 – Optimization problem: objective function, control variables and constraints.

$Fobj = \max(PR_X)$	Constraints	
	Q_F=1.35 m^3.s^{-1}	$PU_X \geq$99.50 %
Control Variables	Q_D=2.79 m^3.s^{-1}	$PU_R \geq$99.25 %
Q_{Rec}; Q_X; t_s; L_c; d_c	n_j= [2 2 2 2]	$P_1|_{z=n_1L_c} \leq$45 kPa

The solution is presented in Table 5.12.

Table 5.12 – Operating conditions, and column geometry results (underlined) from the optimization procedure*.

Columns Geometry	Operating Conditions
$\underline{L_c = 0.52}$ m	$T_{T,D}$ = 373 K; $P_{T,D}$ = 150 kPa
$\underline{d_c = 1.76}$ m	$\underline{t_s = 29.1}$ s
V_c = 1.26 m^3	Q_F = 1.35 m^3.s^{-1}
n_j = [2 2 2 2]	$\underline{Q_X = 2.94}$ m^3.s^{-1}
	Q_R = 1.20 m^3.s^{-1}
	Q_D = 2.79 m^3.s^{-1}
	$\underline{Q_{IV} = 0.36}$ m^3.s^{-1}

This operating point will appear in the edge of the separation triangle, and thus the concentration profiles as in Figure 5.14 and the performance parameters in Table 5.13.

A quite higher productivity, despite the lower purity and recovery values obtained for the first estimative simulation. As can be observed in Figure 5.12, there is some space in section II that is still "unused", an optimization procedure accounting for the variable section length would solve this problem an get even higher productivity values, nevertheless, and as stated before, one will not continue to improve the unit performance, and making use of big optimization efforts, while there is still some important information needed. Nonetheless, this aspect will be taken into account in further studies, were more information, mainly related with the

*To solve this problem it was used one of the optimization algorithms within the gPROMS (gOPT) package, namely: the CVP_SS, a control vector parameterisation (CVP) approach that assumes time-varying control variables are piecewise-constant functions of time over a specified number of control intervals, with a "single-shooting" dynamic optimisation algorithm.

desorbent consumption etc. will be introduced, and therefore detailing the study, and thus making it profitable to a more complete optimization procedure.

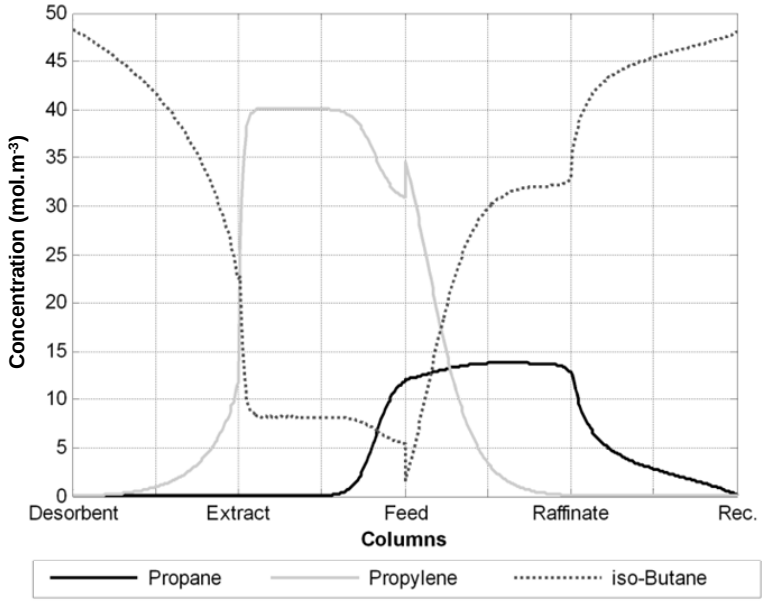

Figure 5.14 – Bulk concentration profiles for the conditions presented in Table 5.12, at steady state.

With a total pressure value in the end of section I of 106.24 kPa, 1.24 kPa higher than the respective constraint, and a column diameter/height of 3.4, higher than the previously obtained.

Table 5.13 – Performance parameters for the first simulation, operating conditions from Table 5.9.

PU_X = 99.9%
RE_X = 99.4%
PR_X = 21.18 mol.($kg_{adsorbent}h$)$^{-1}$= 1207.2 kg.($m^3_{adsorbent}h$)$^{-1}$
PU_R = 99.3%
RE_R = 99.7%
PR_R = 7.09 mol.($kg_{adsorbent}h$)$^{-1}$= 423.0 kg.($m^3_{adsorbent}h$)$^{-1}$

d) Detailing the model

The TMB model approach was useful until now, providing rapid solutions and making possible to use some optimization procedures based on a continuous model. Nevertheless, one can now detail the model and introduce some of the SMB discontinuities, by means of a more realistic approach, here by called real SMB model. If we set the solid velocity to zero, in the TMB model approach, and apply the same model equations, but now for a volume element in each column *k*, as presented in the annex, it is then possible to obtain more accurate solutions

as shown in Figure 5.15 for the operating conditions in Table 5.12, calculated for a "real SMB" model (making use of the equivalence relations from Table 5.5).

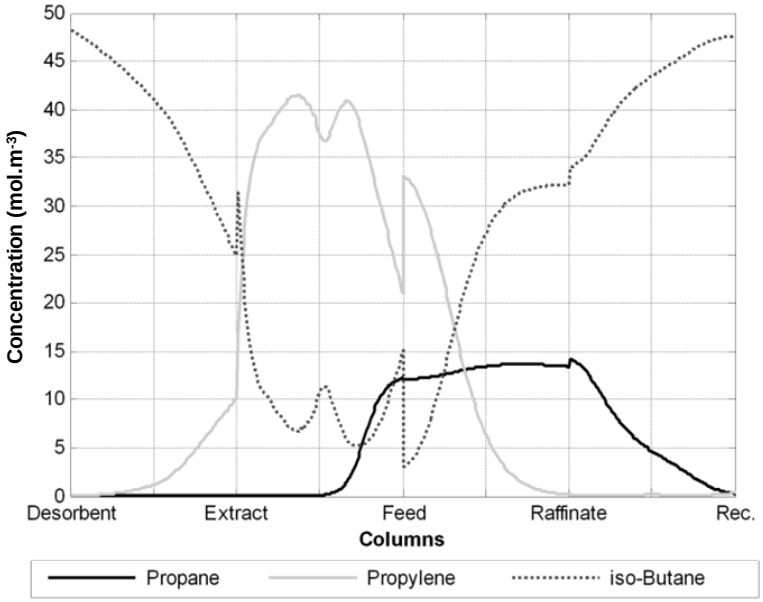

Figure 5.15 – Bulk concentration profiles at half switching time, for the TMB optimized solution simulated by means of a "real SMB" model approach at the cyclic steady state, operating conditions from Table 5.12.

The extract as raffinate concentration history over a switching time period, Figure 5.16,

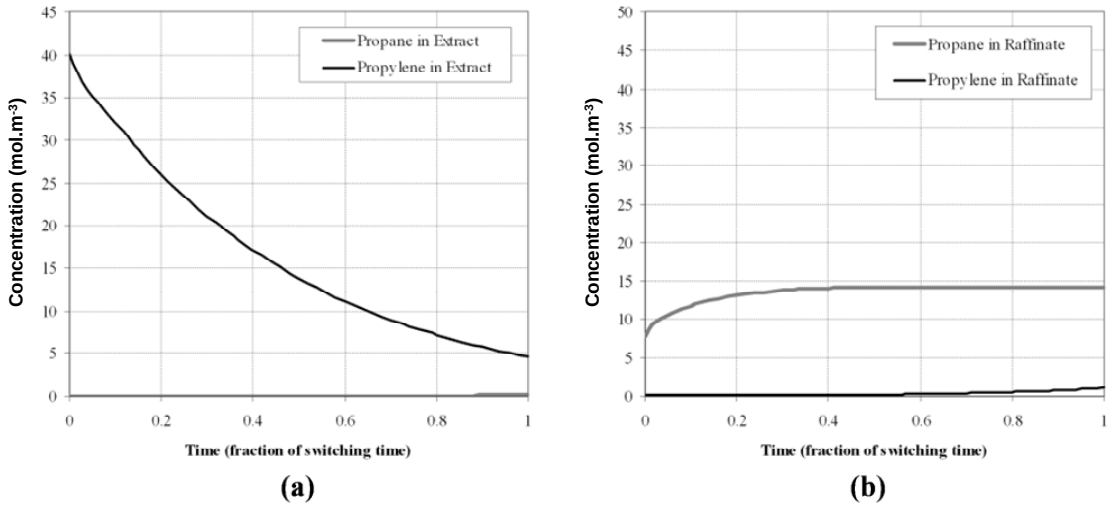

Figure 5.16 – Extract (a) and Raffinate (b) concentration histories over a switching time period, for the optimized solution by means of a "real SMB" model approach at the cyclic steady state.

The corresponding performance parameters are listed in Table 5.14.

Table 5.14 – Performance parameters for the TMB optimized solution simulated by means of a "real SMB" model approach, operating conditions from Table 5.12, calculated for a "real SMB" model.

PU_X* 99.7= %
RE_X* = 99.3 %
PR_X* = 21.16 mol.($kg_{adsorbent}h$)$^{-1}$=1206.0 kg.($m^3_{adsorbent}h$)$^{-1}$
PU_R* 97.6= %
RE_R* = 99.6 %
PR_X* = 7.08 mol.($kg_{adsorbent}h$)$^{-1}$=422.6 kg.($m^3_{adsorbent}h$)$^{-1}$

The solutions obtained with the SMB model approach show lower performance parameters. This can be explained by the discontinuities introduced by the port shift in a system of only 2 columns per section, running with the optimum solution from a TMB model approach, as well as the influence of the repressurization procedure, before each section (which propagates within the unit by oscillations, mostly noted in section II). Therefore, and if we plan to use only 8 columns, one should apply the optimization procedure to the discontinuous model, since the difference between each model starts to be considerable. Even if the TMB model approach can produce a reasonable estimation, at this level one should truly make use of the more detailed model. Nevertheless, this procedure will not be studied in this work, in a further study one can make use of these assumptions.

To answer to the question: It is Reasonable? One should detail the case study and introduce relevant aspects as mass transfer resistances, thermal and pressure drops effects, Figure 5.17.

By means of mathematical models, and making use of the operating parameters, as operating conditions stated from the previous section (Is it possible?), it is possible to simulated the base case, and consequently analyse the results. Again, three answer are possible: Yes, it is reasonable, one should then continue; No, meaning that one should try different operating parameters and if it does result after successive iterations go to the Is it possible stage with new operating conditions and Never (non convergent), once again obtained after successive iterations with different assumptions meaning that the process is not reasonable and one should try a different technology.

It was found that the process is indeed reasonable, and in fact this first optimized solution can be used to pursue in our process design flowchart adding now a cost function and relating the several performance parameters by means of cost weight factors.

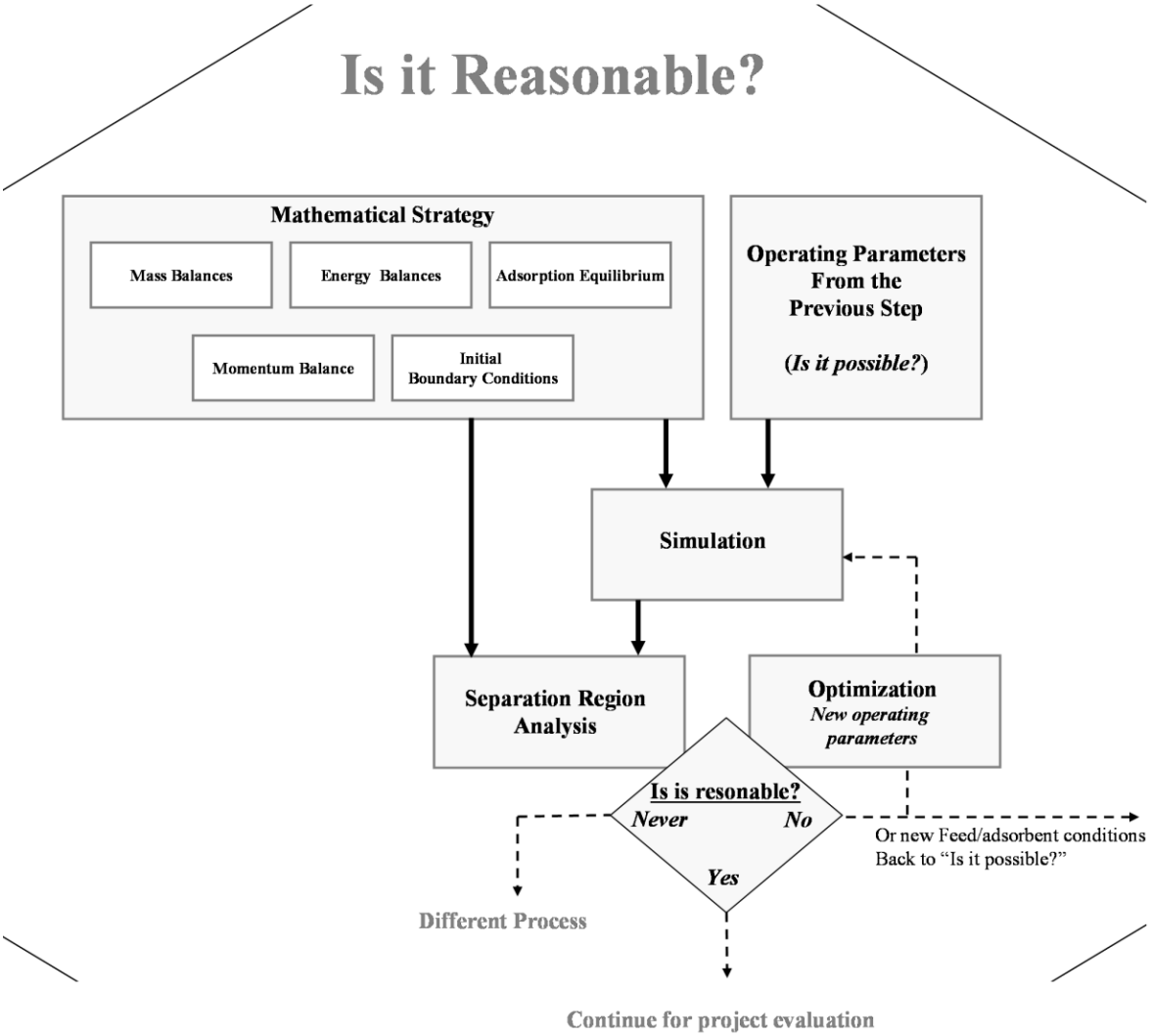

Figure 5.17 – Schematic procedure to answer the second design question: Is it Reasonable?

5.4 IS IT WORTH IT?

The main objective of any chemical process is to create value in the more sustainable way. Therefore, a complete understanding of economic, environmental, as well as social aspects is then critical in process design. This point becomes an issue in the project evaluation step, a systemic procedure that will provide to project information and that enables it about making judgements of 'worth'. One can consider the project evaluation step as a simple investment analysis, and thus make use of the several publications on investment analysis, or simply using chemical project evaluation procedures such as Seider *et al.* (2004). Nevertheless, in this section we will just focus in some of the particular details related with SMB technology process design and usually not mentioned in the published works in the field, as some general considerations on the actual project evaluation, mentioned under the topics of environmental and social values.

5.4.1 ECONOMICAL VALUE

Process economics are always an important factor, and generally each of the considered competing alternatives may offer an attractive solution under specific conditions. In fact, it is quite difficult to find a process that represents the most suitable solution for a particular objective. Therefore, it becomes important to identify and understand what are the key factors that will determine which alternatives better suits a particular project. Among others, the feedstock availability (its cost and flexible usage); yield and co-products; capacity; capital costs and installed equipment are some of the key factors that can make the difference from the economical point of view.

The objective of any chemical process is to create value. The "economical value" (V_{Ec}), can be well represented by the sum of present value of all process' cash-flows (the Net Present Value),

$$V_{Ec} = \sum_{i_{inv}=0}^{N_{inv}} \frac{CF_{i_{inv}}}{(1+r_{inv})^{i_{inv}}} \tag{5.49}$$

where N_{inv} represents the total number of years for the investment (total operating time), $CF_{i_{inv}}$ the i_{inv} Cash Flow, and r_{inv} the discount rate for the given project (for instance, if the project will be financed by debt and equity capital one should make use of the Weighted Average Cost of Capital (WACC), if the project and the promoting firm have the same systematic risk (otherwise one can make use of finance tolls, such as the Capital Asset Pricing Model (CAPM)); and the project and the firm have the same debt capacity). To estimate the CF values, one has to consider the whole separation site, and not just the SMB, *i.e.*, the SMB unit and the desorbent recovery unit as well. In fact, the SMB technology is only comparable to others, such as PSA or distillation, if one considers the desorbent recovery units, which can be constituted for instance by a distillation apparatus Figure 5.18.

By simulating them, it is then possible to estimate the total equipment needs, and consequently the fixed assets and its costs, as the operating costs over the time. This factor is indeed an issue in the design of SMB units, and sometimes forgotten.

The separation costs associated with the desorbent recovery can decrease the operational range of the separation solution. It is possible that performing an easy, but high purity, separation by means of an SMB, would become a quite expensive separation in the following, let say, distillation steps, see Annex IV for further details.

Probably it would be easier to separate at lower purity values, by using less desorbent (and therefore lower flow rates in the outlet streams, as well as less diluted), or at lower productivity values, by increasing the adsorbent amount, if not to change the selected desorbent/adsorbent pair.

By putting the economical value equation in the form of an optimization problem, is then possible to find an equilibrium between these design factors. It is not the easier way, but the more reasonable one, that will homogenize all the separation performance in terms of a cost function given by certain weight factors for each of the performance parameters previously mentioned.

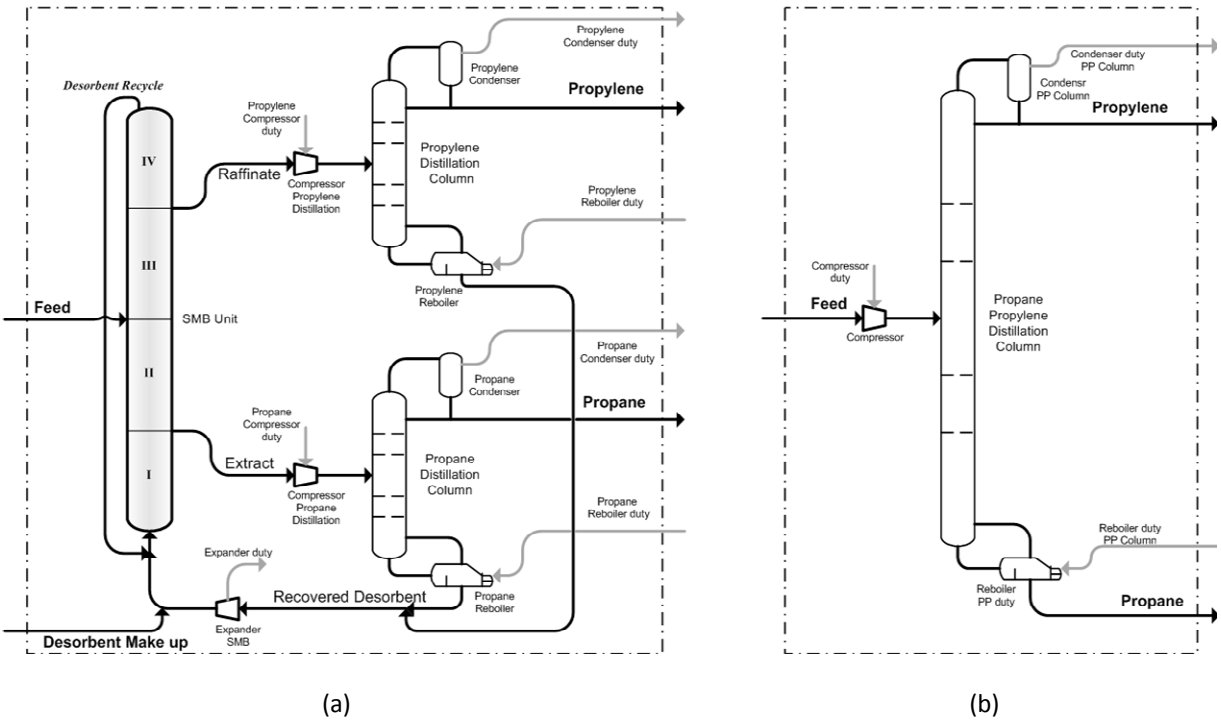

Figure 5.18 - The propane/propylene separation: (a) SMB based process as its subsequent desorbent recovery unit and (b) a classic distillation apparatus.

5.4.2 ENVIRONMENTAL AND SOCIAL VALUES

Even though environmental changes are difficult to value, having any price or market associated with it, it is commonly accepted that environment is a quite valuable asset for each one of us. Additionally, one can consider pollution as an inefficiency factor, and by opposition, regard the operation of a so-called "green process" as the implementation of a more competitive strategy, (Green is Competitive) as pointed in the seminal work of M. Porter and C. van der Linde (1995). Therefore, it is easy to understand why nowadays any project evaluation is only completed if it contains an environmental impact assessment study. This kind of studies will provide additional information, foreseeing some potential problems at an early stage in the process planning and design. However, these studies differ from ordinary scientific/technical approach, dealing with events which may not occur, and that are conditioned by several other factors difficult to predict per itself. Therefore, interdisciplinary methods, such as Real Options based models (Kemna, 1993) can be quite useful at this stage. A process designer cannot forget to include all the technical/scientific information related with this issue, as well as, to try to find ways and means to reduce adverse impacts. Moreover, it is now commonly accepted that not only the environmental issues can make difference in the process viability but the social aspects as well. In fact, Porter himself updates the concept of competitive advantage, relating competitive advantage with social responsibility (Porter and Kramer, 2006). The social aspect should also takes part in a process development stage. Any process designer should also try to shape the project to suit the local social environment. By this way it will be possible to reduce the process fingerprint (social or environmental) at an early stage of its own design, and by

consequence, make use of all the potential that the new technique can provide in the more sustainable way, without making any wrong judgment of worth. This type of approach will then be reflected in the two different variables back in equation (5.49): either in the CF evaluation (costs for pollution treatment, contention measures etc.); as in the discount rate value (for instance, a more sustainable project can obtain lower interest rates, as being associated with lower risk investment).

If the process is reasonable, but does not worth, one should re-optimize the all separation to account for better cost weight factors and a cost based optimization procedure, going back to the design strategy to the optimization step. If changing these factors results always in a not worthy process, one should find a different process and restart.

5.5 CONCLUSIONS

It was proposed a design strategy driven to process evaluation and applied to a novel propane-propylene separation process based on a Simulated Moving Bed unit, using isobutane as desorbent over 13X zeolite. This methodology makes use of a decision tree supported by three simple questions: Is it possible?; It is reasonable? and Is it worth it? For each of these questions different tools were used, namely: equilibrium assumptions to obtain a first shot for the operating conditions; continuous, as discontinuous mathematical models based on mass balances to a unit of volume to evaluate the concentration, pressure, velocity and temperature profiles, as it was enunciated some particular aspects in the process evaluation step concerned with SMB separations, Figure 5.19.

Two answers were found, it is possible and reasonable; and therefore, is it attractive to continue the process evaluation of a gas phase SMB unit for propane-propylene separation, detailing now the process value function to obtain solid judgments of worth. These cost related aspects will be considered in further studies.

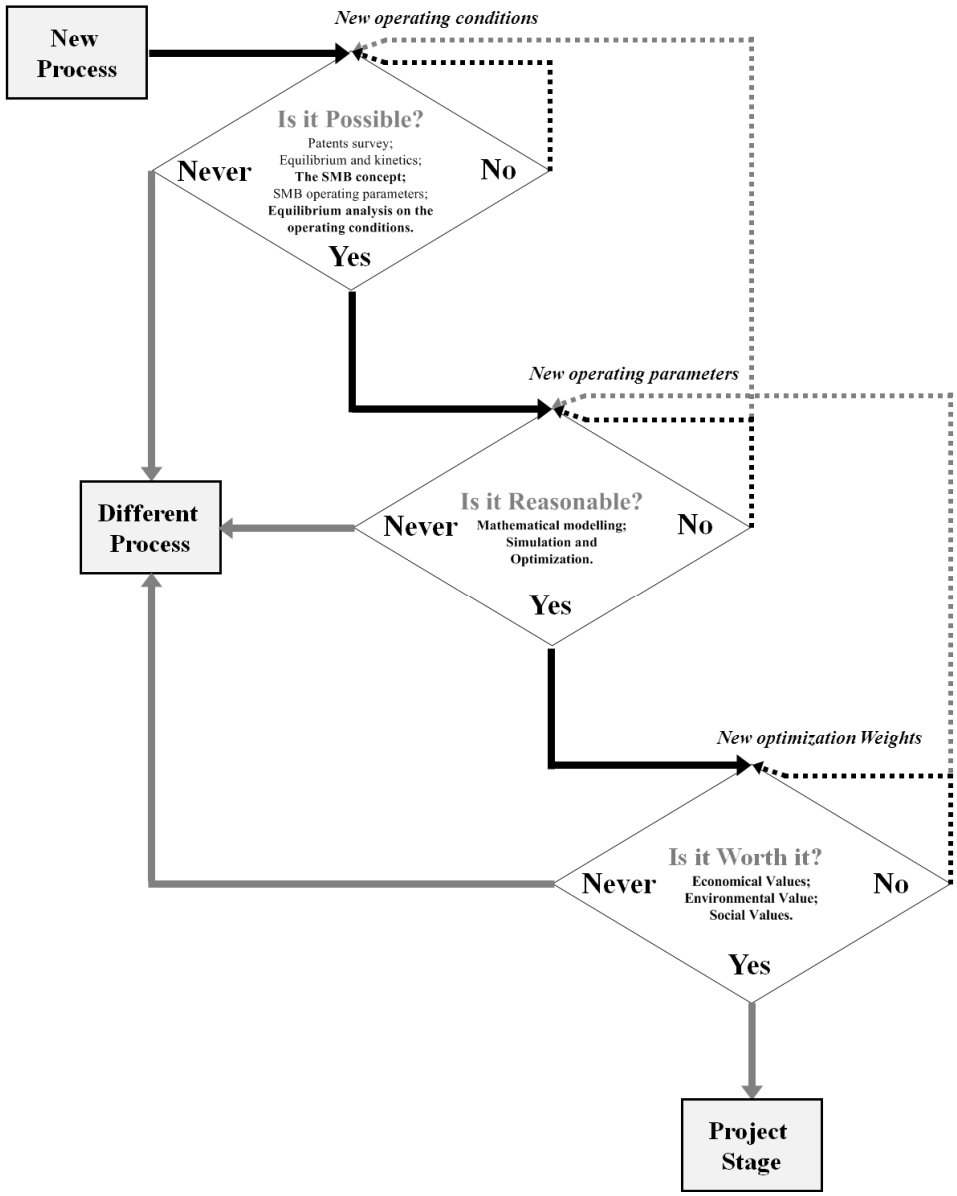

Figure 5.19 – Process design flowchart used in this work: the propane-propylene separation by means of SMB technology, (see Figure 5.8 and Figure 5.17 for detail).*

* A significant part of Chapter 5 was published in: Sá Gomes, P., N. Lamia and A. E. Rodrigues, "Design of a gas phase simulated moving bed for propane/propylene separation." Chemical Engineering Science 64(6), 1336-1357, (2009a). And presented on: Rodrigues, A. E., M. A. Granato, P. Sá Gomes and N. Lamia Propane/propylene Separation: From Molecular Scale to Process. AIChE Annual Meeting. Philadelphia – Pennsylvania USA, (2008).

Chapter 6

DESIGN, CONSTRUCTION AND OPERATION OF A FLEXIBLE SMB UNIT: THE FLEXSMB-LSRE®

6.1 INTRODUCTION

It has been mentioned before that until the 90s the major implementation of the Simulated Moving Bed (SMB) technology was mainly related with petrochemical or sugars applications. Nevertheless, the use of SMB technology experienced a considerable growth in the past 10-15 years, mainly related with its scale down and fine chemical applications.

This late demand on the SMB technique has been the cause and consequence of an also emergent interest in the study and research on SMB technology, leading to the formulation of quite singular/different operation modes since the original patent. Non conventional strategies, such as the introduction of asynchronous inlet/outlet shifts (Varicol) or the variable flux with/or variable composition in the inlet/outlet streams, as well as the utilization of multiple feed or distributed feed and the Outlet Streams Swing (OSS), have increased the potential of this technique for a vast range on binary the separation field, as reviewed before.

However, the practical application of these so-called "non conventional modes of operation" in Simulated Moving Bed (SMB) units is per itself a challenge. Generally an SMB unit, industrial, pilot of laboratory-scale, is limited to one or two modes of operation and to implement a new operating mode is necessary to contact the supplier, do adjustments, even to reformulate the entire unit if not to acquire a new one. Therefore, flexibility is seen as one of the more relevant qualities for this kind of equipment, principally for laboratory-scale applications in technology demonstration stage, as for the separation reduced product quantities in the fine chemical area.

For more than 15 years, the SMB/R technology demonstration stage at the Laboratory of Separation and Reaction Engineering (LSRE) was mainly performed by means of the Licosep 12-26 pilot scale SMB unit (Separex, now Novasep, France), installed at LSRE under the BRITE-EURAM project on Chiral Separations. Nevertheless, and despite of this unit's scale, its limited operational flexibility started to be an issue, mainly for the demonstration stage of the more recent SMB operating modes. In addition, the construction of a new SMB unit at LSRE, making use of its own resources, was seen as a major advantage, complementing what can be called as "R&D flow sheet", Figure 6.1.

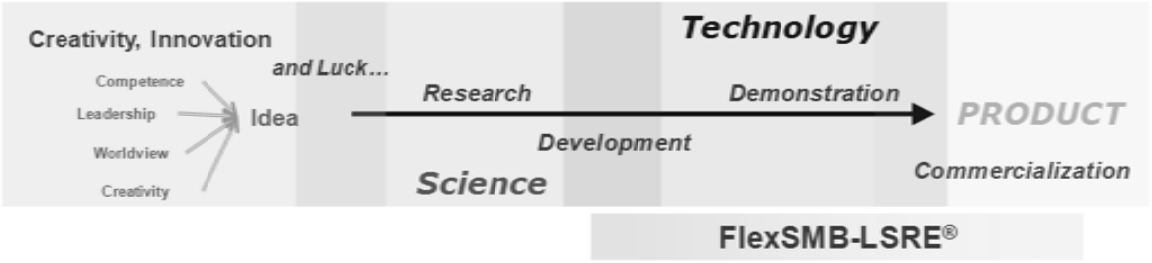

Figure 6.1 – Positioning of the FlexSMB-LSRE® unit as pilot/lab scale unit in the "R&D flow sheet".

These aspects, among others, led to the design and construction of a flexible unit at LSRE, the FlexSMB-LSRE®*.

6.2 THE FLEXSMB-LSRE® UNIT DESIGN AND CONSTRUCTION

As mentioned before, (Chapter 2), there are several ways to operate an SMB unit; therefore, when designing a new SMB unit, one should take into account its flexibility as a key objective (Chin and Wang, 2004). This aspect is particularly relevant in the design of SMB units for study and research purposes, which will mostly operate several different systems with different specifications.

6.2.1 VALVES AND PUMPS DESIGN

If one considers an SMB unit as a certain number of packed columns interconnected and feed-controlled by a specific valves and pumps arrangement, it will be easy to understand that the key factor related with an SMB unit expandability and flexibility is in fact its valves system (Chin and Wang, 2004). This aspect led us to carry out a review on the different SMB units valves schemes patented over the years, presented in Annex V.

Making use of this information, the two SD (Select-Dead-end flow path) valves per stream in the extract and raffinate currents, one SD per stream in the feed and eluent/desorbent currents and one two-way valve per column, similar to the Negawa and Shoji in US Patent 5 456 825 from 1995, was chosen for the FlexSMB-LSRE® configuration, Figure 6.2. In this way, it is possible to operate most of the non-conventional SMB operating modes and perform columns re-configuration simply by changing some parameters in the automation

* The FlexSMB-LSRE® is a registered trade mark propriety of Faculdade de Engenharia da Universidade do Porto-Laboratory of Separation and Reaction Engineering (LSRE); INPI no.:424497.

routines on the computer interface. Additionally, with this scheme, just one pump is within the main system line and always in the same position (extract/raffinate, in the beginning of section II or section IV, respectively).

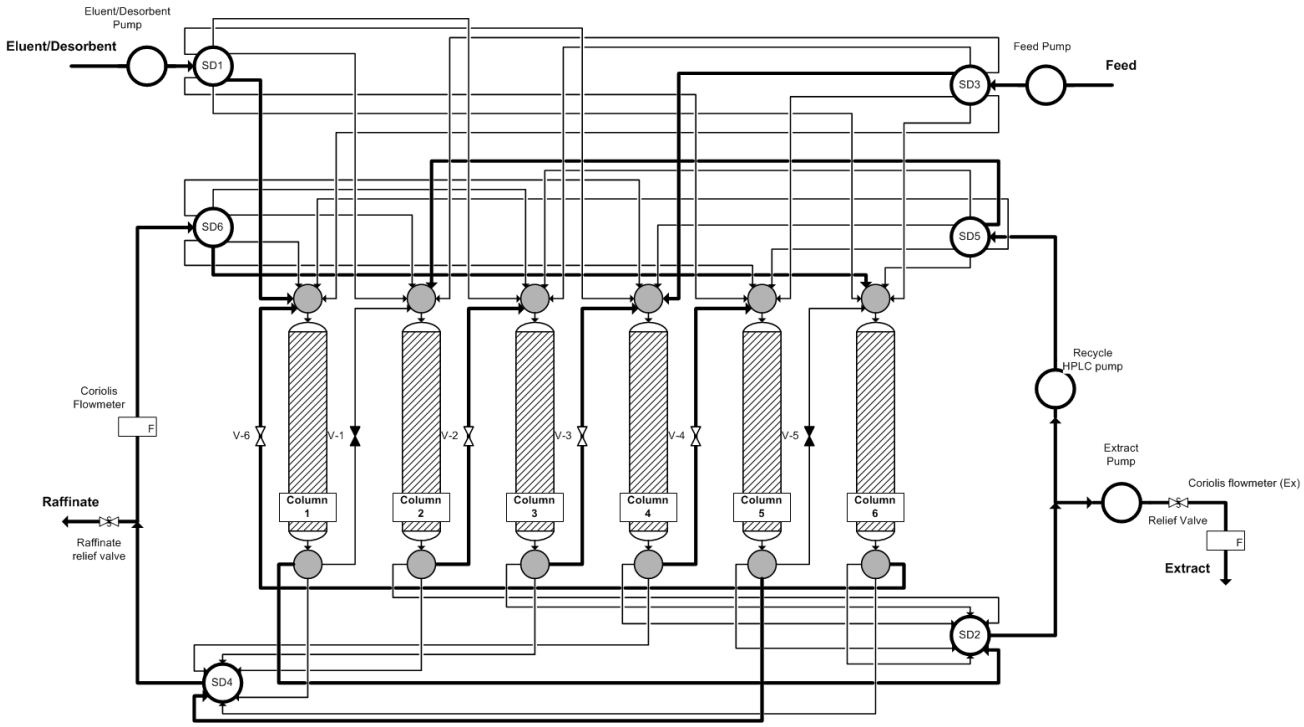

Figure 6.2 – FlexSMB-LSRE® pumps and valves scheme under a 6 columns configuration, operating a during the first step of a [1 2 2 1] classic SMB. Bold lines are the active connections; thick lines are stagnant volumes.

It can be observed that the stream leaving section I, in this case, from column 1, is fully withdrawn by valve SD2. Part of this stream leaves as the extract and the remaining is pumped to valve SD5 which returns the stream to the inlet of column 2. Similarly, valve SD4 withdraws the complete stream from column 5, splits part of it into the raffinate outlet and the remaining follows to valve SD6 which returns the stream to the inlet of column 6. The Feed inlet flows to column 4 by means of SD3 valve and the eluent/desorbent current with valve SD1 to column 1. Between each column is placed a two-way valve (acting as on-off valve) that is closed to direct all fluid to either extract of raffinate lines. Just four pumps are used: one pump, positioned next to the extract node (in the beginning of section II), allows the fluid recycle within the system; another pump, placed in the extract line, withdraws the extract current; and two pumps are used to feed the system (one for the feed itself and other for the eluent/desorbent current.

6.2.2 CONSTRUCTION

The equipment necessary to follow the scheme in Figure 6.2 is described in Table 6.1. Once the equipment was delivered the manuals were studied and convenient tests were performed to detect equipment limitations and try-out the data acquisition and control routines.

Table 6.1 – Equipment installed in the FlexSMB-LSRE® unit.

Description	Manufacture	Suplier	Contact	Un	Price (€)	Total (€)
SD valves (EMT6CSD12UW)	Vici-valco, Switzerland	Elnor, S.A., Portugal	21 842 9500	6	2 320.5	13 923.0
Two way valves	Vici-valco, Switzerland	Paralab, S.A., Portugal	22 466 4320	6	1 904.0	11 424.0
Relief Valve AJ A 1/4	Swagelok, USA	STECInstruments, Lda., Portugal	22 550 4077	5	140.6	702.8
HPLC VWR P130 + 50ml Head	VWR international, USA	VWR International, Lda., Portugal	21 361 3500	4	4 926.6	19 706.4
Coriolis flow meter (M53-ABD-22-0-B)	Bronkhorst B.V., Netherlands	STV Lda., Portugal	21 956 3007	2	4 789.3	9 578.7
Stainless Steel Set up	Neves & Neves, Lda., Portugal	Neves & Neves, Lda., Portugal	22 981 1727	1	1 247.7	1 247.7
Degasser (Flom 722 2)	Flow Co., Japan	r. fischer, Germany	+49 672 149 8462	1	2 850.0	2 850.0
Column HPLC in stainless steel	Grom (now Grace-USA)	ILC, Lda., Portugal	21 782 6039	6	283.4	1 700.2
Notebook (F3SC-AP186C)	Asus, Korea	Poweron, Lda., Portugal	22 550 0373	1	849.9	849.9
Acquisition Boards NI USB-6008	National Instruments, USA	National Instruments, Portugal	21 031 1210	2	173.6	347.2
Acquisition Boards NI USB-6501	National Instruments, USA	National Instruments, Portugal	21 031 1210	3	106.4	319.2
Power supply and cables	Benjamim Vaz, Lda., Portugal	Benjamim Vaz, Lda., Portugal	22 764 6005	1	1 250.0	1 250.0
Electric Cables	Benjamim Vaz, Lda., Portugal	Benjamim Vaz, Lda., Portugal	22 764 6005	18	5.0	90.0
Data Acquisition Cables	J.P. Silva, Lda., Portugal	J.P. Silva, Lda., Portugal	25 683 4976	3	15.6	46.9
Fittings, tubing and accessories	----------	----------	---------	---	---------	3 319.8
					total	67 355.7

The main structure was built in stainless steel type 316. A CAD scheme was then performed based in two main bodies (one for columns and two-way valves and the other for the remaining equipment) and sent to our usual contractor (Neves & Neves-Metalomecânica Lda, Portugal), Figure 6.3.

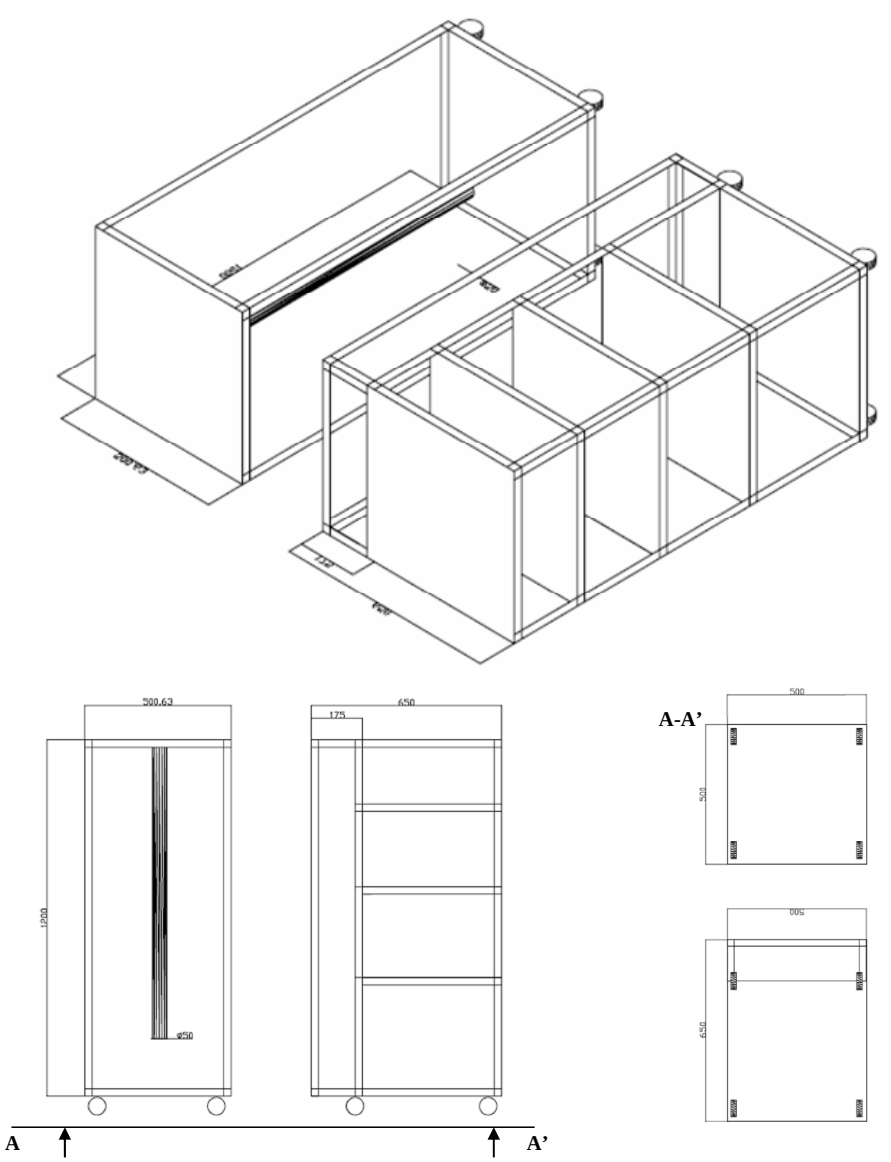

Figure 6.3 – FlexSMB-LSRE® structure in CAD scheme; dimensions in mm.

With this structure, it is possible to easily detach the columns apparatus and change it for another one (an isothermal conditional part, for instance) without considerable changes at the level of the main equipment part.

The tubing and equipment dead volumes were reduced by using of 1 mm *i.d.* tubes and short dead end valves (SD, Valco Instruments Co., Inc.). To reduce the dead volumes asymmetries, tubes with the same length were used for the same function and all columns assembled in a carousel scheme, Figure 6.4.

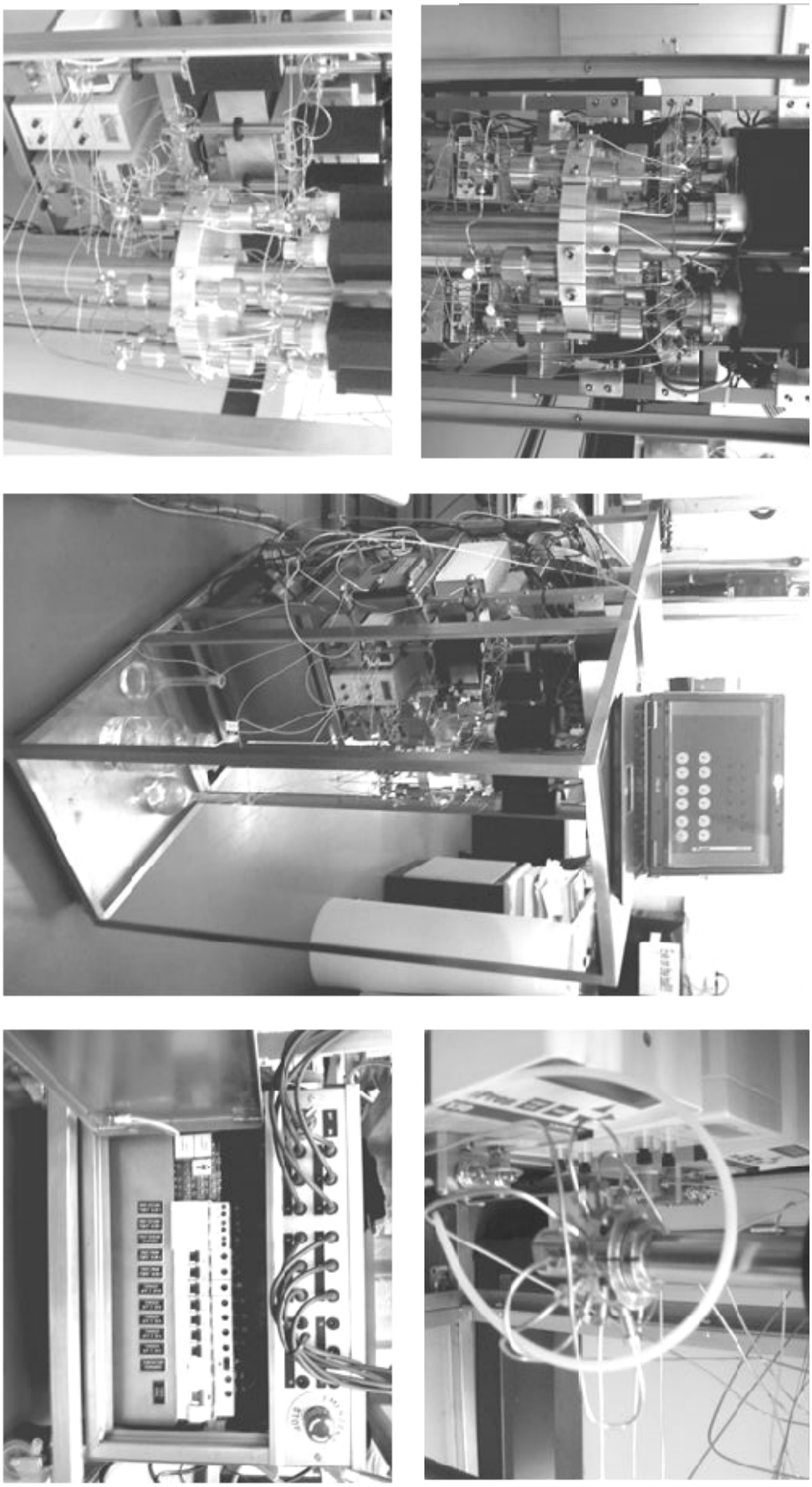

Figure 6.4 - The FlexSMB-LSRE® unit assembled with 6 columns.

To reduce the pumps flow rates fluctuations (fluid inlets, outlets and internal flow rates), four HPLC pumps (VWR International, USA) were used, assisted by two Coriolis flow meters (Bronkhorst High-Tech B.V., Netherlands). The ceramic heads installed in the HPLC pumps allow a maximum flow rate of 50.0+/-0.1 ml.min^{-1}; however, the range of operability of these pumps is limited to 37.5+/-0.1 ml.min^{-1}, due to the current limitation of the data acquisition boards. Four purge valves (Swagelok, USA) were installed after each pump to avoid extreme pressures at pumps head* during the valves switching step. One additional purge valve was installed in the outlet of raffinate stream that together with the purge valve installed next to the extract pump serves to manually regulate the total system pressure, as well as security valves.

To avoid variations related to the ports switching velocity asymmetries a distributed connection scheme for the SD valves was used. The FlexSMB-LSRE® can operate with a maximum number of columns of 12. For a 6 columns apparatus, all columns were connected to the 12 ways SD valves using just the odd valve connecting positions (*i.e.*, 1,3,…,9, 11) in order to reduce the switching time discrepancies (see Figure 6.4).

All equipment is connected to an integrated power supply that assures protection from electrical fluctuations as a possible current discharge.

6.2.3 AUTOMATION

The automation of any laboratorial/industrial unit is a critical task, and as it concerns to an SMB unit, it is probably even more crucial. In fact, a relevant part of these units' flexibility relies in its automation and control routines. Recalling the Licosep 12-26 unit at LSRE, it can be easily understood that what limits its operation is in fact its old automation routines, which just considers the classic mode of operation. Thus, the automation stage of the FlexSMB-LSRE® unit was always seen as the most relevant task during this design and construction procedure. The LabView platform (National Instruments, USA), which provides a robust, as well as user friendly interface, was chosen and thus 5 USB data acquisition (DAQ) boards were acquired from NI to connect the computer to all controllable equipment: (valves, pumps and flow meters).

a) SD valves

As stated before, the FlexSMB-LSRE® unit was assembled with 6 SD†-valves of 12 positions (one inlet and 12 outlets or vice versa). Since the present unit is only operating with 6 columns, only 6 of the 12 inlets/outlets are used being the others remain 6 closed. The operation of each SD-valve is performed by a control module and a stepper motor/gearbox assembly connected to on plug of 24 VDC in the power supply. The control is performed by a 26-pin using TTL digital input/output signals, Table 6.2.

For the sake of simplicity the control scheme only uses the "home", "step" and "manual direction" commands (pins 1, 3 and 5; Table 6.2). This way it is possible to fully operate the valve without an extensive usage of a DAQ boards channels. To recognise the real position of each valve, and thus control it, the pins 10, 12, 14, 16,

* the ceramic head of the HPLC pumps currently installed in the FlexSMB-LSRE® allows a maximum pressure of 150 bar; however one should remind that the maximum pressure limitation of an SMB unit is usually established by its packing;

† SD stands for Select-Dead-end.

17 and 18 were connected to the DAQ boards as well. By means of the digital signal from these 5 pins it is possible to automatically compute the real position of each valve in real time. The complete connection scheme can be consulted in Annex VI.

Table 6.2 – Signal and command on the SD valves; in bold, the used pins.

Pin	Signal Description	Direction	Pin	Signal Description	Direction
1	**Home**	**Input**	**14**	**4 BCD**	**Output**
2	Motor run	Output	15	20 BCD	Output
3	**Step**	**Input**	**16**	**2 BCD**	**Output**
4	Error	Output	**17**	**10 BCD**	**Output**
5	**Manual Dir.**	**Input**	**18**	**1 BCD**	**Output**
6	Direction	Output	19	80 BCD	Input
7	Auto Dir.	Input	20	8 BCD	Input
8	Data latch	Input	21	40 BCD	Input
9	+5 VDC 100 ma	Output	22	4 BCD	Input
10	**Ground**	**Output**	23	20 BCD	Input
11	80 BCD	Output	24	2 BCD	Input
12	**8 BCD**	**Output**	25	10 BCD	Input
13	40 BCD	Output	26	1 BCD	Input

b) Two-way-valves

The 6 two-way-valves currently installed in the FlexSMB-LSRE® unit, (one per each column), are also operated by a control module and a stepper motor/gearbox assembly connected to a plug of 24 VDC in the power supply. The control is performed by a 10-pin connector by means of TTL digital input/output signals, Table 6.3.

Table 6.3 - Signal and command on the two-way valves; in bold, the used pins.

Pin	Signal Description	Direction	Pin	Signal Description	Direction
1	**Ground**	**Input**	**6**	**Position B**	**Input**
2	+5 VDC	Output	7	Position A relay contact	Output
3	**Position A**	**Output**	8	Position B relay contact	Output
4	**Position B**	**Output**	9	Position A relay contact	Input
5	**Position A**	**Input**	10	Position B relay contact	Input

By asserting input pin 5 causes the actuator to go to Position A and asserting input pin 6 sends it to Position B (LED on the control box, referent to close or open positions). The operation in this mode requires four relays, 2 input and 2 output for control procedures. More information on the connection scheme of these valves can be found in Annex VI.

c) HPLC pumps

The automation of the VWR HPLC pumps model P130 can be done either via TTL or RS-232 interface. The TTL interface was chosen to use similar DAQ boards as the ones used for the others devices. With the pump control via TTL it is possible to operate the volumetric flow rates and to acquire the pressure pump outlet values (analog signals), as well as error message and start and stop control (digital signals), Table 6.4, and Figure 6.5.

Table 6.4 - Signal and command on HPLC pump.

Signal Description	Direction	Signal Description	Direction
Stop	Digital Input	Error	Digital Output
Ground	---	Ground	---
Flow	Analog Input	Pressure	Analog Output
Ground	---	Ground	---

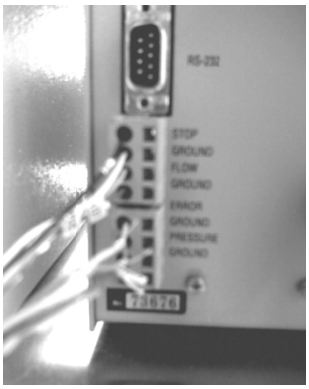

Figure 6.5 – HPLC pump remote control connection.

All channels were connected to the DAQ boards and more details on the pumps connection can be found in Annex VI.

d) Flow meters

Also the data acquisition from the two Coriolis flow meters (controllers) can be done either via analogic or RS-232 interface. For the same reason mentioned for the of the HPLC pumps, the analogic interface was chosen. Thus, two new cables were ordered to make use of the standard RS-232 communication port from the coriolis flow meters (controllers) and acquire the necessary analogic lines, connected to the DAQ boards, Table 6.5.

Just the signal acquisition is being monitored and thus just pins 2 and 8 are connected to the DAQ boards, for more details see Annex VI.

Table 6.5 - Signal and command on oriolis flow meters; in bold, the used pins.

Pin	Signal Description	Direction	Pin	Signal Description	Direction
1	---		5	Valve out	Analog Output
2	**Flow**	**Analog Output**	6	---	
3	Set point	Analog Input	7	+24 V dc	
4	0 V		**8**	**0V sense**	

e) Interface

A LabView based application was then built to provide a user friendly interface between the operator and the equipment. In the screen four major partitions are shown:

(i) Operating Parameters (Figure 6.6); where all conditions to run the FlexSMB-LSRE® unit, both classical as non conventional operating modes, are set (Switching time; columns arrangement n_j, and flow rates). Also it is possible to input some of the columns (L_c, d_c), as particle (d_p) parameters that can be used to compute the solid flow rate (equivalent TMB). In the bottom, one can find two major subsections concerning the non conventional operation of the FlexSMB-LSRE® unit, namely: *Asynchronous Shift* (where the asynchronous port shift can be performed to each port, independently controlled by switching any of the *As Feed*, *As Raffinate*… button, in multiples of $1/5t_s$; if the *Asynchronous Shift* button is switched *off*, the unit will work in classical mode); and Variable Flow (where it is possible to set different flow rates within subintervals of $1/5t_s$, necessary for running Partial Feed, PowerFeed or OSS operating modes; if any the *Variable Flow* button is not switched *on*, the unit will not consider the flow rates in this subsection and will account for the flow rates set in the top subsection, in the SMB scheme).

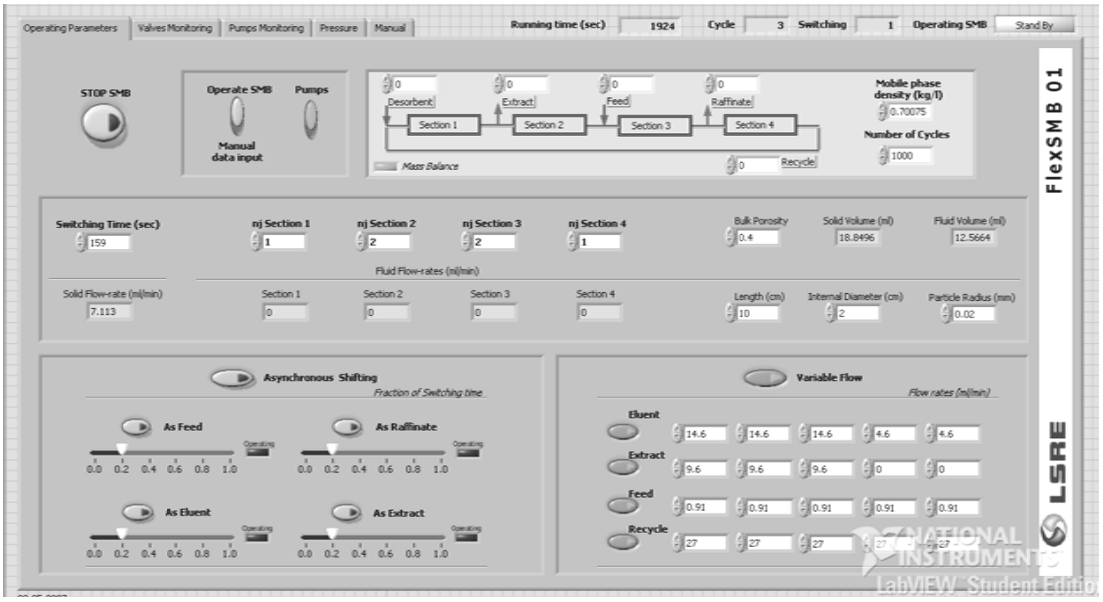

Figure 6.6 - Operating parameters partition in the FlexSMB-LSRE® automation interface.

Pumps can also be stopped independently of the valves shifting procedure by switching to *on* or *off* the button *Pumps* in the top. The general *Stop* button will end all the experiment.

(ii) Valves Monitoring (Figure 6.7); where both the SD, as the two-way (on/off), valves position can be checked. The *Theoretical Position* refers to the one computed from the n_j, or asynchronous shifting, parameters set on the first (Operating Parameters) partition, the *Real Position* is acquired from the valves, the *Error* signal will switch off if something is going wrong, (if the theoretical and real positions do not match). It does not mean that the operator always must be checking this partition for a proper operation, an automatic procedure within the application will continuously check it and an error message will be shown and operation stopped if at least one of these conditions are not positives (the theoretical = real position).

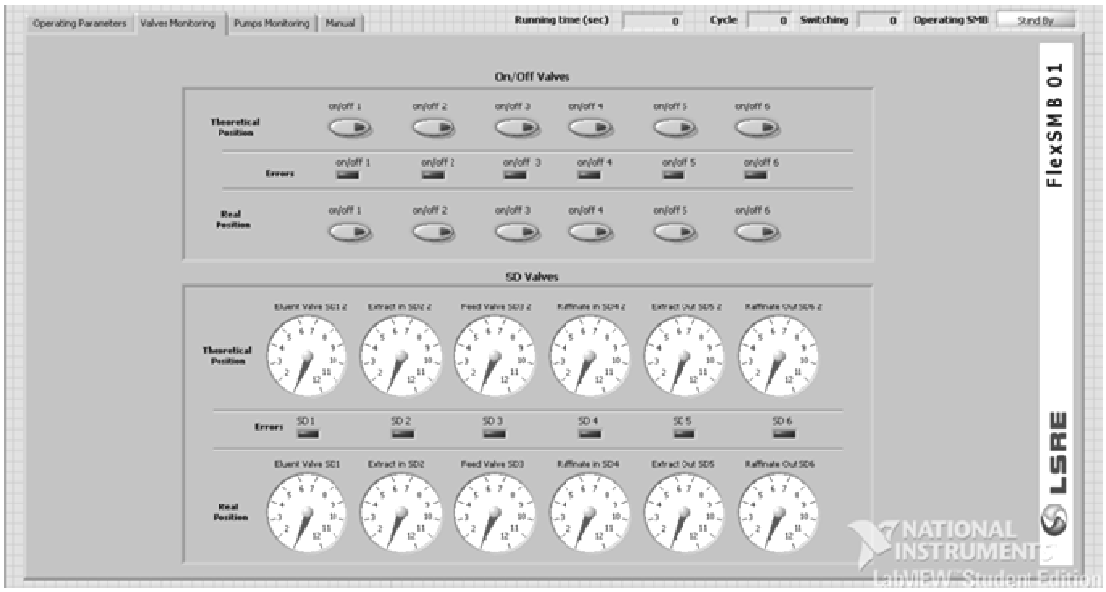

Figure 6.7 – Valves Monitoring partition in the FlexSMB-LSRE® automation interface.

(iii) Pumps Monitoring (Figure 6.8); This partition will show the information acquired from the two Coriolis flow meters, which is also being saved to two text files. The *Flow rates* subsection in the left shows the signal send to the pumps. If the signal from the Coriolis flow meters is not the correct the operator should go to the first partition and adjust the signal sent to the pumps.

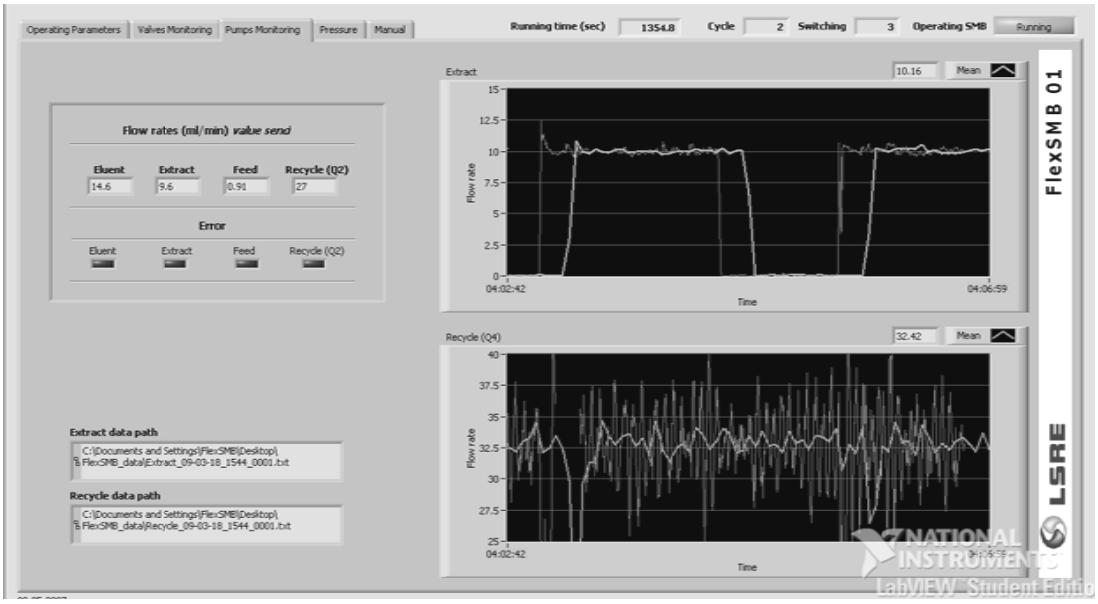

Figure 6.8 – Pumps Monitoring partition in the FlexSMB-LSRE® automation interface.

(iv) Manual (Figure 6.9); by setting to *Manual Position* the switch button in the Operating Parameters partition this Manual partition will be active and thus, it will be possible to operate all the FlexSMB-LSRE® valves as pumps *per se*, which, among other possibilities, allow a simple and quick flush to all unit.

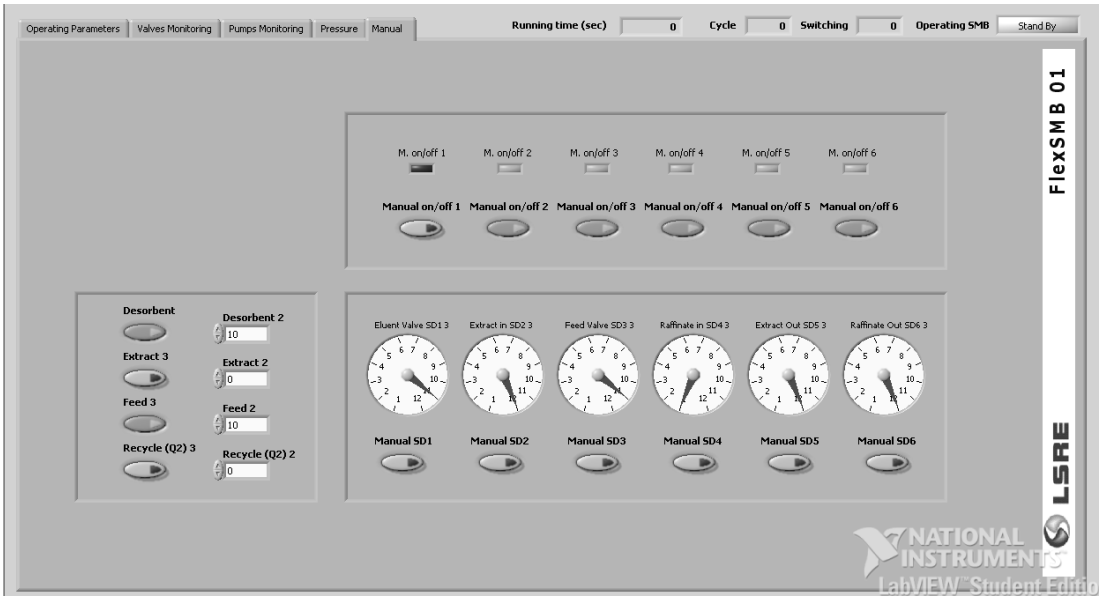

Figure 6.9 - Manual partition in the FlexSMB-LSRE® automation interface, operating a flush.

6.2.4 COLUMNS PACKING AND CHARACTERIZATION

An SMB unit is usually assembled with similar columns, and packing material, as the ones used in the batch systems. In this unit 6 columns with 10.0 cm of length and diameter of 2.0 cm (Grom, Germany, now Grace-USA), in stainless steel are used.

The common modelling strategies assume that all these SMB columns have identical characteristics. However, it is quite difficult to find several columns manufactured with the same specifications (column tubes may have slightly different geometric dimensions, thus, different retention times for a given flow rate…), as well as it is almost impossible to pack them with the same characteristics (packing procedure is quite irreproducible, and therefore, it results on local fluctuations of the packing density) (Mihlbachler *et al.*, 2001; Mihlbachler *et al.*, 2002). Consequently, once the operator introduces the theoretical optimized operating parameters, the differences between columns arise and different values from the ones expected can appear.

As a matter of fact, from the 7 original columns (6 for the SMB unit and one for fixed bed experiments), 3 empty columns were weighted and the following mass values registered:

$$m_{Column\,0} = (374.0 \pm 0.1)\ \text{g}; \quad m_{Column\,2} = (373.5 \pm 0.1)\ \text{g}; \quad m_{Column\,5} = (373.1 \pm 0.1)\ \text{g}$$

As can be observed there are already slightly differences between each column (a difference to the average value lower than 0.2 %). Therefore the packing procedure, as its characterization is now described.

a) Columns Packing Procedure

There are two satisfactory ways to pack adsorption chromatographic columns: the slurry method and the dry pack method. In this case, the slurry method as chosen and each column packed by means of Analytical Slurry Packer from Alltech Associates Inc. (USA), Figure 6.10.

For each column a slurry of approx. 18.5 g of Chiral AD 20 μm, amylose tris-(3,5 dimethylphenylcarbamate coated onto 20 μm silica-gel), provided by Chiral Technologies Europe (France) in approx. 36 ml of 2-propanol (GC-grade from Sigma-Aldrich Chemie, Germany) was prepared (pure 2-propanol was chosen as slurry solvent taking into account its physical proprieties, namely its viscosity). The column was filled with solvent (2-propanol) and the slurry poured to the upper reservoir (see Figure 6.10). Then, the analytical slurry packer pump was connected to the upper reservoir and operated for 10 min, at a max solvent pressure of 20 bar (approx. 300 $ml.min^{-1}$), the solvent used was a mixture of -hexane/2-propanol, 90/10%, volumetric fraction, (GC-grade from Sigma-Aldrich Chemie, Germany)

Figure 6.10 – Column packing apparatus.

After 10 min, the reservoir was opened and the excess solvent was drained with a pipette until reaching the top level the solid phase and the remain slurry was poured into the reservoir. The reservoir was connect again to the analytical slurry packer pump and operated for more 30 min at the same conditions mentioned above. Then, the reservoir was opened and the excess solvent drained again; the column disconnected from the reservoir and the excess of solid in the top of the column cut with a blade.

b) Columns Characterization

In the case of SMB operation, the main consequences associated with columns packing fluctuations remains in the heterogeneity of the retention factors and asymmetrical pressure drops. The columns should present similar retention factors for a given specie. Therefore, Column 0 was tested for HETP (Height Equivalent to the Theoretical Plate) numbers, for comparison, tracer experiences were performed to the remaining columns as well pressure drop curves for each column.

i. HETP Characterization

Therefore, a solution was prepared with 0.00667+/-0.00001 g of TSO (Trans – Stilbene Oxide, racemic mixture standard for this type of operations) and 0.00700+/-0.00001 g of TTBB (1,3,5 – TriTert ButyBenzol, considered non adsorbed) in 25.00+/-0.05 ml of heptane-2-propanol (95 %-5 %, volume fraction). A pulse of 100 μl injected to column 0 in a Gilson HPLC system for (5.0; 10.0; 20.0; 30.0; 40.0; 50.0)+/-0.1 $ml.min^{-1}$ and the following HETP numbers obtained, Figure 6.11.

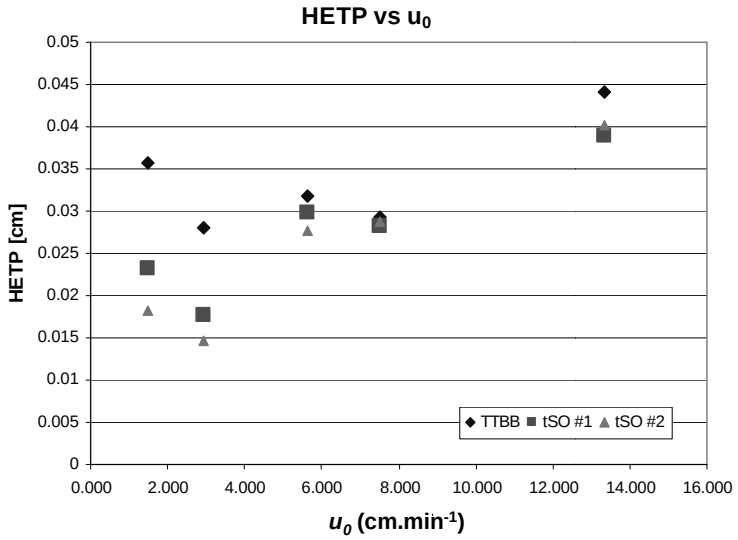

Figure 6.11 – HETP experiences for Column 0, measured in the outlet of the UV detector, of 7.80+/-0.05ml.min^{-1}, the total porosity found to be 0.62.

ii. Tracer Experiments

The remaining columns were compared with column 0 by means of tracer experiences with the same species mentioned before, Figure 6.12.

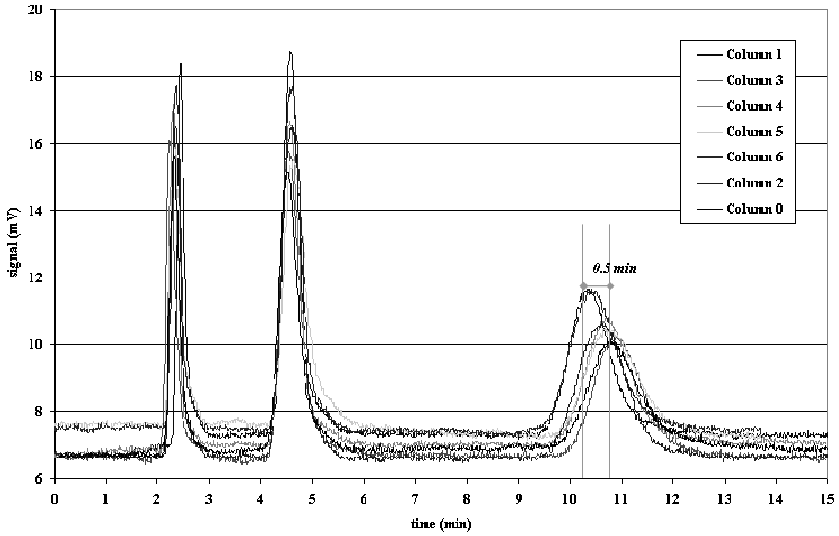

Figure 6.12 – Tracer experiences for the 7 columns, first peak TTBB, second and third the racemic mixture of TSO.

All peaks were found within a 5 % deviation of its main retention time, therefore, and accounting with the packing supplier, the columns were considered suitable for the SMB operation.

iii. Pressure Drop Curve

In this procedure one of the HPLC pumps of the SMB unit was used to determine the pressure drop curve for Column 0. Pure 2-propanol was fed at 6 different flow rates (limited by the available pressure manometer), namely: (1.0; 2.5; 5.0; 7.5; 10.0; 15.0)+/-0.1 ml.min^{-1}, and the following results obtained, Table 6.6.

Table 6.6 – Measured pressure drops for the different flowrates on column 0; Q_0 on the pump screen, Real flow rate - measured at the end by means of a lab. balance (+/-0.1 g).

Q_0 (Pump) (ml.min^{-1})	Real flow rate (ml.min^{-1})	ΔP (bar)
1.0	0.99	0.270
1.0	1.02	0.281
2.5	2.56	0.675
2.5	2.56	0.676
5.0	4.96	1.315
5.0	5.03	1.319
7.5	7.54	1.996
7.5	7.56	1.993
10.0	9.92	2.677
10.0	10.10	2.686
15.0	14.96	4.107
15.0	15.11	4.157

By relating the pressure drop with superficial velocity it was possible to calculate de permeability value (k^{per}) for each column, $\Delta P = u_0 L_c \frac{\mu}{k^{per}}$.

The same procedure was then extended for all other columns and is presented in Table 6.7.

Table 6.7 - Permeability values deviation and relative deviation to column 0.

	permeability (m^2)	dev	(%)
Column 0	3.962 x10^{-13}	0.000	0.000
Column 1	4.148 x10^{-13}	0.047	4.692
Column 2	3.979 x10^{-13}	0.004	0.422
Column 3	3.892 x10^{-13}	-0.018	-1.764
Column 4	4.106 x10^{-13}	0.036	3.638
Column 5	4.206 x10^{-13}	0.061	6.144
Column 6	4.173 x10^{-13}	0.053	5.301

The highest deviation between columns observed is lower than 8 %, between column 5 and column 3. It was found a value of 0.40 for the average bulk porosity.

6.3 OPERATION AND DEMONSTRATION

The technology demonstration stage is a quite important step in the "R&D flow sheet", Figure 6.1, and in fact, when it accounts to equipment development it is probably the most important one. To operate and demonstrate some of the potential of the FlexSMB-LSRE® unit, a set of different experiments was planned regarding both linear as non linear adsorption isotherms, under different modes of operation (classic and non-conventional).

However, the operation of SMB units is not as straightforward as other batch techniques, and a particular attention must also be directed for some aspects not accounted (or simplified) in the modelling stage.

6.3.1 REAL SMB UNITS MODELLING AND DESIGN

Most of the design assumptions mentioned so far rely in Equilibrium assumptions (see for instance in Chapter 3 the guafeinesin separation analysis) and thus, do not account neither for the mass transfer resistances, nor for real SMB unit's particularities (*i.e.*, tubing and equipment dead volumes, switching time asymmetries and delays, pumps flow rates variations and equipment limitations).

It is well known that a robust unit design should also consider the mass transfer resistances (Azevedo and Rodrigues, 1999). Based on the model stated before for guafeinesin separation (Chapter 3), it is possible to construct a more accurate separation region, which will account for the several aspects described in the model. This can be done by successive simulation of different $(\gamma_{II} \times \gamma_{III})$ pairs, considering significantly higher values for γ_I and lower values for γ_{IV} than the ones predicted by the Triangle Theory. In this way, the regeneration region does not influence the shape and size of the separation region, as stated by the Separation Volume concept (Azevedo and Rodrigues, 1999).

In addition, it should be taken into account that the performance of a real SMB unit differs from the ones described by the commonly used modelling and design strategies. There are several factors that can influence the precision of the SMB model predictions, such as: uncertainty in adsorption equilibrium kinetics and hydrodynamics data (diffusivity, axial dispersion coefficients etc.) and bed voidage (packing asymmetries), as well as, extra column dead volumes (tubing, equipment, asymmetries), variation in the port switching velocity (asymmetries and delays), fluctuations in pump flow rates (fluid inlets, outlets and internal), which are not accounted for it in the most commonly used SMB models (Mun *et al.*, 2006). Consequently, if one runs an experimental SMB unit based on the operating parameters obtained by a simple mathematical model, such as the one described in Chapter 3, the experimental results may not match the ones that were predicted by the model.

Concerning the uncertainty in the equilibrium isotherm data, kinetics data, and even the asymmetries of columns packing, the more precise, and/or accurate, these factors are, better will be the SMB model predictions. Therefore, detailed and precise measurements of all these parameters have to be done *a priori*, so that they introduce a minimal discrepancy between the SMB model results and the experiments itself.

The remaining deviation factors, such as the tubing and equipment dead volumes, pumps and valves asymmetries, related to each SMB unit design and equipment particularities should be taken into account before starting to construct a new SMB unit, as detailed before.

However, even after all the work done concerning the system dead volumes and operation asymmetries:

- the unit still has 11.5 % of dead volumes, Table 6.8.

Table 6.8 – Dead volumes per function and total dead volumes percentage in the FlexSMB-LSRE® unit.

	V_{each} (ml)	Total
Fritz and manifold	0.50	3.01
Ext in	0.36	2.17
Raf in	0.36	2.17
Ext out	0.32	1.93
Raf out	0.32	1.93
Interc	0.31	1.89
Sampler	0.47	0.47
Ext 1	0.12	0.12
Ext 2 (Rec pump)	3.93	3.93
Raf 1	0.12	0.12
Raf 2 (flow meter)	6.67	6.67
$V_c^{(*)}$ (ml)		188.5
(%) dead volumes		11.5 %

(*) considering 6 columns of 10 cm height and 2 cm of i.d.;

The values given in Table 6.8 include also the value of the stagnant volumes. Considering only the actives lines (see Figure 6.2), the dead volumes for each section are: $V_I^D = 1.09$ ml; $V_{II}^D = 5.48$ ml; $V_{III}^D = 1.71$ ml; $V_{IV}^D = 7.61$ ml.

- The port switching velocity variation (delay) can represent around 0.5 % of the switching time (0.8 seconds); with a 6 columns apparatus: 1 complete switch = switch + 0.4 seconds hold (zero flow rates) + switch;

- The fluctuation of the pumps flow rates are still considerable, Figure 6.13.

If the average internal flow rates in each section are kept constant during the SMB operation (as assumed by some SMB design procedure) the SMB performances would not be affected, despite their considerable local variations shown in Figure 6.13. This is due to the cyclic mode of operation of these units, leading to compensation of these variations with time.

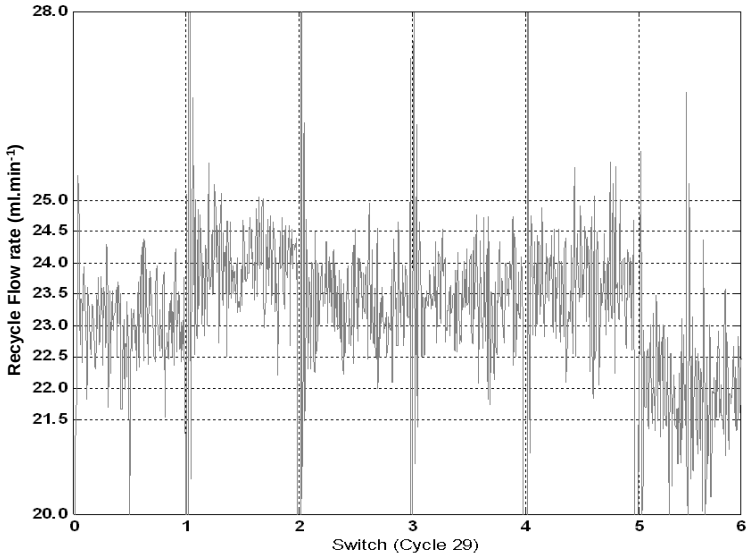

Figure 6.13 – Variation of the recycle flow rate during a complete cycle for a 6 columns SMB, test done with pure eluent mixture of n-heptane/2-propanol (95/5 % v/v).

However, there are still two major issues concerning the prediction of the SMB performances: the unit SMB design features related with the dead volumes and the switching time asymmetries or delay. To deal with discrepancies between the real SMB operation and that predicted with commonly used models that account only for the presence of SMB columns (and do not consider the surrounding equipment features) one can apply two different compensation strategies, *a priori* or *a posteriori*:

- *a priori* compensation strategy. Predict the operating parameters by means of the regular SMB models and then apply a compensation measure during the unit operation (to account with the units' discrepancies from the used model);
- *a posteriori* compensation strategy. Use a detailed SMB model by including as more units' particularities as possible.

The first strategy is represented, for instance, by the asynchronous port shift in the Licosep units (Hotier and Nicoud, 1995; Hotier and Nicoud, 1996; Blehaut and Nicoud, 1998), and hereby simplified by switching time compensating strategy, see details in Annex VII. The second strategy was discussed by several authors, within the Triangle Theory spectrum (Migliorini *et al.*, 1999b; Katsuo *et al.*, 2009), or in the case of the Standing Wave Theory (Mun *et al.*, 2003a; Mun *et al.*, 2006).

One can now analyse both situations. For that purpose, a detailed model was applied to the FlexSMB-LSRE® unit accounting for its tubes and equipment dead volumes, filters and manifold as well as the switching asymmetries (or switching time delay), as presented in Figure 6.14.

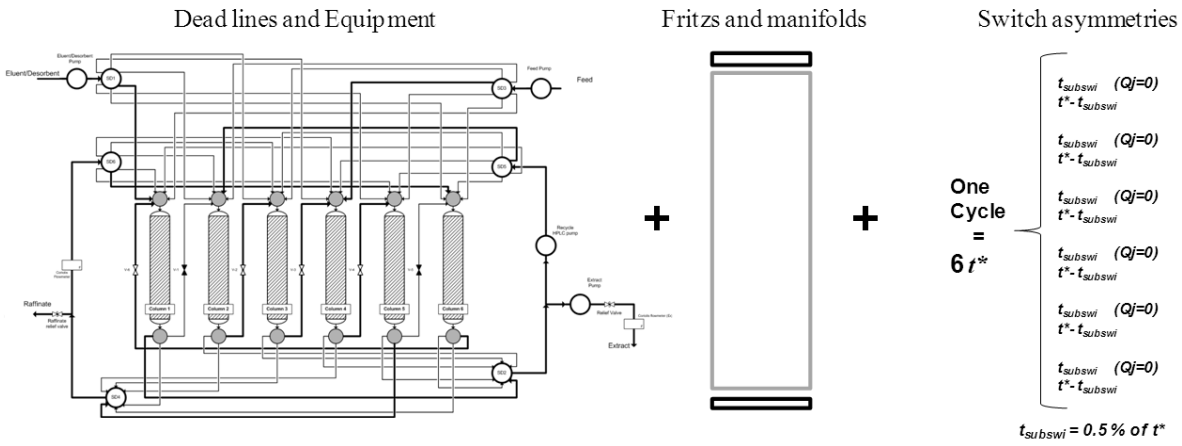

Figure 6.14 – Schematic illustration for the unit particularities included in the detailed FlexSMB-LSRE® model.

Similarly to what is mentioned in Annex VII for the Licosep SMB unit, all dead volumes are modelled by an axial dispersive plug and flow approach and the switching time discontinuities detailed.

By running successive simulations for different $(\gamma_{II}^{*} \times \gamma_{III}^{*})$ pairs, it is possible to draw the "true" separation region for the case of gaufenesin separation, introduced before in Chapter 3. In Figure 6.15 are shown the Equilibrium Theory, *SMB-zero dead volumes* and the FlexSMB-LSRE® (the extended model as stated in Figure 6.14 and Annex VII).

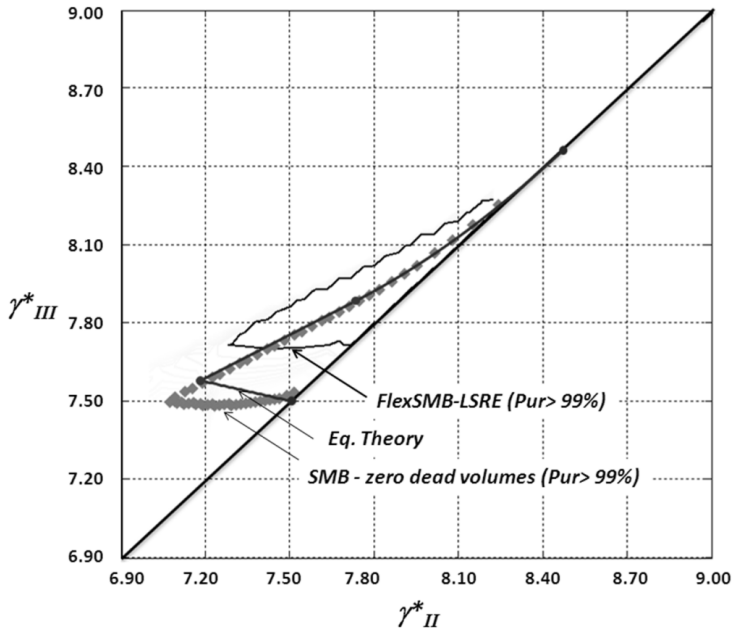

Figure 6.15 - Separation regions according to the Equilibrium Theory, SMB zero dead volumes and the FlexSMB-LSRE®, the last two obtained for a minimum purity requirement of 99 % in both extract and raffinate.

As can be observed from Figure 6.15, the separation region obtained with the dead volumes and switching time asymmetries respecting the FlexSMB-LSRE® unit, appears to be shifted from those obtained with the

Equilibrium Theory and *SMB-zero dead volumes* model. The *SMB-zero dead volume* separation region is slightly larger than that calculated by the Equilibrium Theory. This difference is due to the different product purities in both cases, minimum 99 % in the SMB-zero dead volume model and 100 % from the Equilibrium Theory.

Let us now make use of the *SMB-zero dead volumes* separation region and correct it to account with the unit dead volumes by shifting it using the following equation:

$$\gamma_j^*\big|_{FlexSMB} = \gamma_j^*\big|_{SMB} + \frac{(1-\varepsilon_b)}{\varepsilon_b}\frac{\langle V_j^D\rangle_{II,III}}{V_c(1-\varepsilon_b)} \tag{6.1}$$

This procedure is similar to the one proposed by Migliorini *et al.* (1999a) (recently detailed to account for each section connection lines and respective volumetric flow rate (Katsuo *et al.*, 2009)), but simplified for section II and III by using the average dead volumes of these sections $\langle V_j^D\rangle_{II,III} = \frac{1}{2}(V_{II}^D + V_{III}^D)$. We call this *a priori* compensation procedure: "SMB with Design" (the design accounts for dead volumes compensation).

The second *a priori* compensation strategy proposed in our work is the switching time compensating measure described in Annex VII, hereby called Switching time compensation.

$$t_s|_{FlexSMB} = t_s|_{SMB} + \frac{\sum_{j=I}^{IV} V_j^D}{\overline{Q_j^*}}\frac{1}{\sum_{j=I}^{IV} n_j} \tag{6.2}$$

Both *a priori* compensation strategies were used to correct the *SMB-zero dead volumes* separation region and compare it with the one obtained using the detailed FlexSMB-LSRE® model, Figure 6.16.

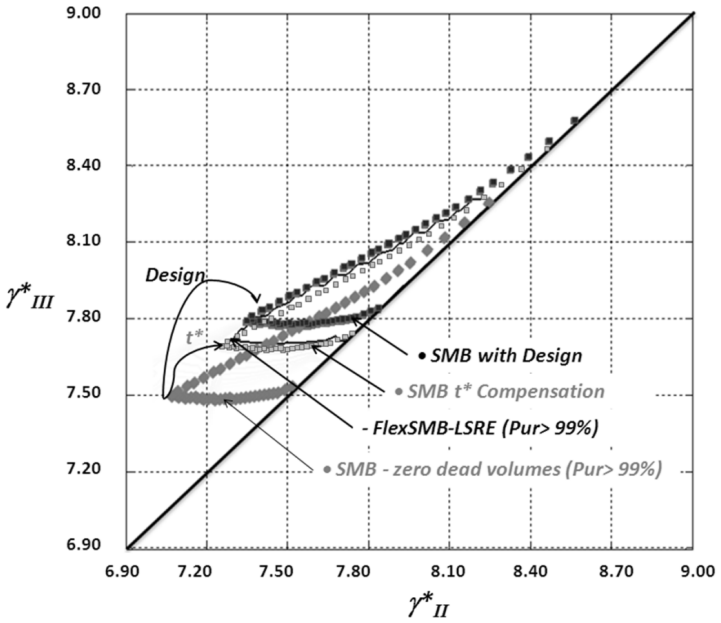

Figure 6.16 - Comparison between the separation regions obtained with the *a priori* (Switching time and "SMB with design") compensating measures and *a posteriori* compensation (detailed FlexSMB-LSRE® model) measure.

As can be observed from Figure 6.16, both the "SMB with Design" and the Switching time compensation strategies shifted up the *SMB-zero dead volumes* separation region near to the FlexSMB-LSRE® separation region. However, the separation region obtained after applying the Switching time compensating measure is closer to the FlexSMB-LSRE® separation region than that obtained with the "SMB with Design" strategy. The last one could be improved, by detailing the compensation to each section and using more elaborated procedures (Katsuo *et al.*, 2009). However, due to its simplicity, the Switching time compensating measure would be preferred.

The switching time compensating measure accounts only for equipment dead volumes, the switching time delay or asymmetry is still not compensated when this measure is used. They can be included in the switching time compensation measure as true delay in the switching time, as follows:

$$t_s|_{FlexSMB} = t_s|_{SMB} + \frac{\sum_{j=I}^{IV} V_j^D}{\overline{Q_j^*}} \frac{1}{\sum_{j=I}^{IV} n_j} + t_{subswitch} \tag{6.3}$$

For the FlexSMB-LSRE®:

$$t_s|_{FlexSMB} = t_s|_{SMB}(1 + 2.6\% + 0.5\%) \tag{6.4}$$

Where $t_s|_{SMB}$ represents the switching time for a ideal SMB unit with zero dead volumes, V_j^D the total dead volumes in section j, $\overline{Q_j^*} = 38.5$ ml.min^{-1}, the unit's average flow rate and $t_{subswitch}$ the sub switching time delay (see Figure 6.14).

The corrected separation region using the extension to the switching time compensating measure is shown in Figure 6.17.

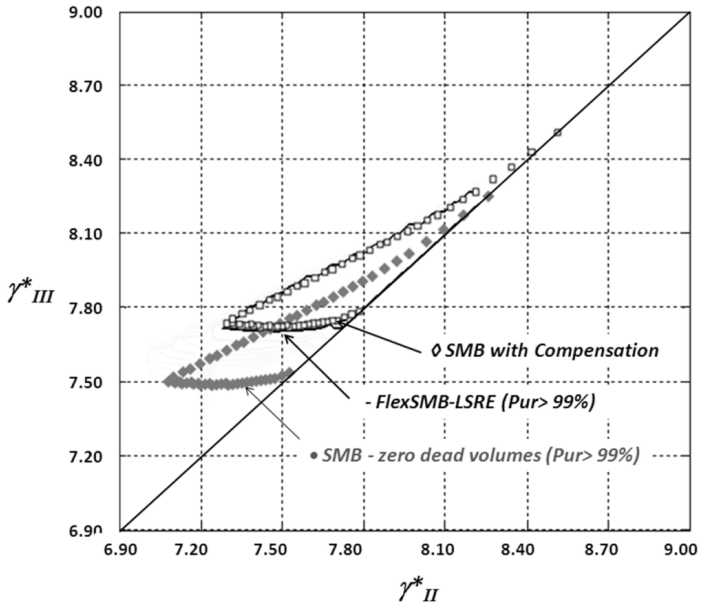

Figure 6.17 - Separation region obtained by the extended switching time compensation measure (corrected by the subswitch interval)

As can be observed in Figure 6.17, the *SMB-zero dead volumes* separation region corrected by the dead volumes and switching time delay (asymmetries) almost matches the one obtained with the detailed model. By this means it is possible to easily obtain a precise and realistic separation region without running tedious simulations related with the more detailed SMB models.

One can now improve the estimation based on the Equilibrium Theory assumptions to obtain corrected operating conditions that will account for the mass transfer resistances and the particular unit dead volumes and switching time delay.

6.3.2 SEPARATION OF RACEMIC MIXTURE OF (S,R)-α-TETRALOL ENANTIOMERS (LINEAR ISOTHERMS)

The first separation operated on the FlexSMB-LSRE® unit involved the resolution of a racemic mixture of (S,R)-α-Tetralol* at the concentration of 1.0 g.l^{-1} in a n-heptane/2-propanol (95 %/5 % volumetric fraction) solvent basis, using the 6 stainless steel columns packed with CSP Chiralpak AD (diameter particle size of 20 μm). The objective at this stage was to test the unit and not to demonstrate any optimized conditions for the separation of a given mixture. The enantiomeric pair of (S,R)-α-Tetralol was chosen as case study based in the extensive work performed by Dr. M. Zabka at LSRE concerning this separation (Zabka *et al.*, 2006; Zabka and Rodrigues, 2007; Zabka *et al.*, 2008b).

a) Determination of adsorption and kinetic parameters

Since the racemic mixture to be separated would be prepared at 1.0 g.l^{-1}, near diluted conditions, the adsorption equilibrium was represented by means of a linear formula characterized by an Henry constant for each enantiomer i, H_i. Consequently, the sorption parameters were determined by means of pulse experiments in a stainless steel column (L_c=25 cm and I.D.=0.46 cm) packed with Chiralpak AD (diameter particle size of 20 μm) also using the Analytical Slurry Packer as described before. A racemic solution of 0.5 g.l^{-1} (S,R)-α-Tetralol (minimum 99% purity, Fluka Chemie, Switzerland) was prepared in a n-heptane/2-propanol (95 %/5 % volumetric fraction, also from Sigma Aldrich, previously degassed and filtrated trough a 0.2 μm and 50 mm I.D. NL 16-membrane filter (Schleicher & Schuell, Germany), and loaded into a 10 μl loop that was then injected by means of a Knauer injection valve installed on a Gilson HPLC unit. The consequent peaks were measured by means of a UV detector set at 270 nm. The procedure was repeated for four different flow rates (4.4 ml.min^{-1}; 8.5 ml.min^{-1}; 12.5 ml.min^{-1}; and 16.6 ml.min^{-1}). The peaks retention times (t_{r_i}) were then deducted from the equipment dead volumes (0.50 ml for the injector and 0.01 ml for the detector) and plotted in function of the measured flow rate, Figure 6.18.

The slopes obtained from both regression lines (Figure 6.18) were then used to determine the Henry adsorption constants of both enantiomers from $t_{r_i} Q = \varepsilon_b V_c \left(1 + \frac{(1-\varepsilon_b)}{\varepsilon_b}\left(\varepsilon_p + H_i\right)\right)$ and thus obtaining (R=A and S=B): $H_A = 3.07$ and $H_B = 2.75$.

* (S,R)-(±)-1,2,3,4 Tetrahydro-1-naphthol.

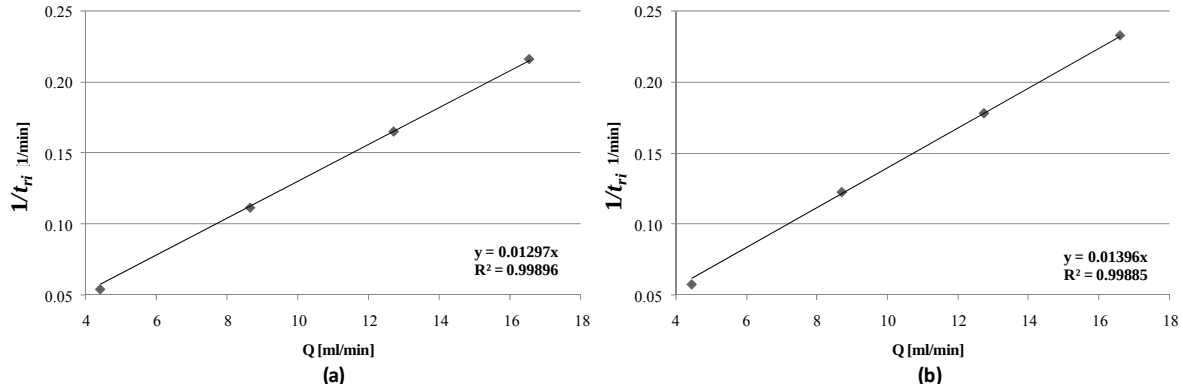

Figure 6.18 – (a) (R)-α-Tetralol and (b) (S) -α-Tetralol inverse of pulses retention time ($^1/_{t_{r_i}}$) in Chiralpak AD 20 μm as function of measured flow rates.

The same overall mass transfer coefficient ($k_{ov} = 0.25\ \text{cm.min}^{-1}$) as defined in Zabka and Rodrigues (2007), was used to lump both the intraparticle (k_{int}) as film (k_{ext}) mass transfer resistances and defined by $\frac{1}{k_{ov}} = \frac{1}{k_{int}} + \frac{1}{k_{ext}}$. Where k_{int} was calculated from the Linear Driving Force (LDF) approximation suggested by Glueckauf (1955) $k_{int} = \frac{5D_{pe}}{r_p}$ (with D_{pe} the effective pore diffusivity define by $D_{pe} = \frac{\varepsilon_p D_m}{\tau}$, ε_p the pore porosity, τ, the particle porosity obtained from $\tau = \frac{(2-\varepsilon_p)^2}{\varepsilon_p}$, D_m the molecular diffusivity calculated by the Wilke–Chang equation (1955) and extended to mixed solvents by Perkins and Geankoplis (1969) $D_m = 7.4 \times 10^{-8} T \frac{\sqrt{\phi M}}{\mu V_m^{0.6}}$ with $T(K)$ the absolute temperature, μ the solution viscosity, calculated according to Teja and Rice method for liquid mixtures (1981), V_m the solute molar volume and ϕM obtained form $\phi M = x_A \phi_A M_A + x_B \phi_B M_B$ where x_i are the molar fractions, M_i the molar masses and ϕ_i are the association factors constants which account for solute-solvent interactions); and k_{ext} obtained from $Sh = \frac{k_{ext} d_p}{D_m} = \frac{1.09}{\varepsilon_b}(ScRe)^{\frac{1}{3}}$, with Sh the Sherwood number, Sc the Schmidt number defined by $Sc = \frac{\mu D_m}{\rho_f}$ and Re the Reynolds number: $Re = \frac{\rho_f u \varepsilon_b d_p}{\mu}$.

The contribution of molecular diffusion to axial dispersion is assumed to be negligible and therefore the axial dispersion coefficient (D_b) obtained from $D_{b_j} = 0.5 d_p u_j$, (Zabka and Rodrigues, 2007).

b) Determination operating parameters and operation

After the determination of the equilibrium adsorption parameters it was possible to draw both the theoretical separation as the regeneration regions for the separation under study and choose suitable operating conditions, Figure 6.19.

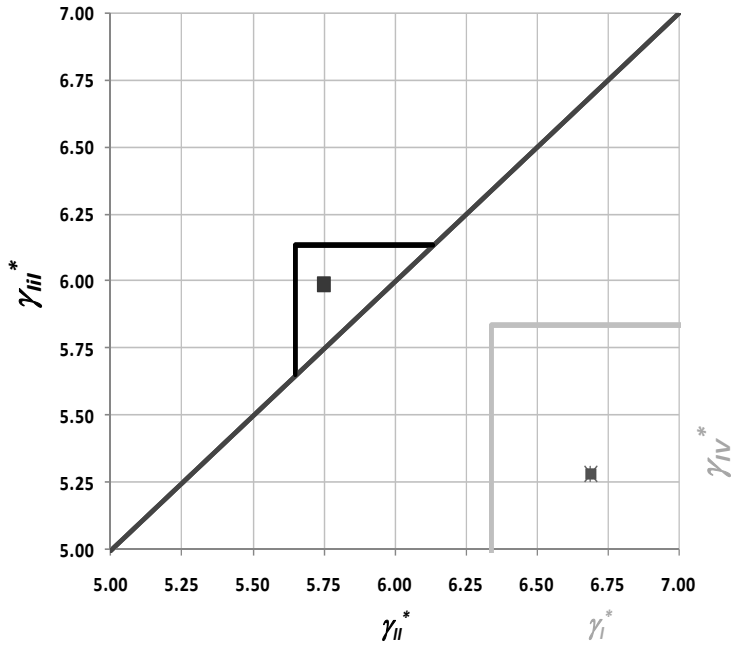

Figure 6.19 - Separation (black) and regeneration (grey) regions for the (S,R)-α-Tetralol, dots the operating point.

Taking into account the equipment limitations as maximum pressure drop allowable (20 bar), it was possible to calculate the following operating parameters: $Q_{IV}^* = 23.0$ ml.min^{-1}, Q_E=6.0 ml.min^{-1}, Q_F=1.0 ml.min^{-1}, Q_X=4.5 ml.min^{-1}, Q_R=2.5 ml.min^{-1}, t_s= 2.95 min.

Applying the dead volumes and switching time delay correction (from eq. 6.3) it was found that the switching time compensating measure should be about 4 % (based on an average flow rate of 25.0 ml.min^{-1}), and thus correcting the switching time for 3.05 min.

About 5 l of *n*-heptane/2-propanol (95 %/5 % volumetric fraction) solution was prepared and filtrated as mentioned before. This mixture served as Eluent as well as solvent for the preparation of 1 l of the racemic mixture of (S,R)-α-Tetralol at 1.0 g.l^{-1} used as Feed.

The extract and raffinate flow rates were monitored by means of the total recovered mass in each outlet over complete cycles and weighted on a laboratorial balance with 0.01 g of precision. The extract flow rate was also measured by means a Coriolis flow meter installed for control purposes at the extract stream outlet. The recycle flow rate was monitored by the other Coriolis flow meter. The experimental average flow rates, as well as geometric features, number of columns and SMB configuration are reported in Table 6.9.

Table 6.9 - Experimental operating conditions for the (S,R)-α-Tetralol racemic mixture separation .

Columns and packing parameters			
$n_j = [1\ 2\ 2\ 1]$		ε_b = 0.4	
L_c = 10 cm		C_i^F = 0.5 g.l^{-1}	
d_c = 2.0 cm		d_p = 20 µm	
SMB operating conditions (measured)			
$Q_I^* =$	28.7 ml.min^{-1}	Eluent	5.8 ml.min^{-1}
$Q_{II}^* =$	24.3 ml.min^{-1}	Extract	4.4 ml.min^{-1}
$Q_{III}^* =$	25.3 ml.min^{-1}	Feed	1.0 ml.min^{-1}
$Q_{IV}^* =$	22.9 ml.min^{-1}	Raffinate	2.4 ml.min^{-1}
t_s =3.05 min			
$\gamma_I^*\|_{FlexSMB} = 6.97$	$\gamma_{II}^*\|_{FlexSMB} = 5.90$	$\gamma_{III}^*\|_{FlexSMB} = 6.14$	$\gamma_{IV}^*\|_{FlexSMB} = 5.56$

The separation was undertaken through out 28 cycles. During the operation, samples of extract and raffinate average concentrations were withdrawn (referent to a complete cycle, namely: cycle 2; 4; 6; 8; 10; 13; 15; 17; 19; 27), Figure 6.20.

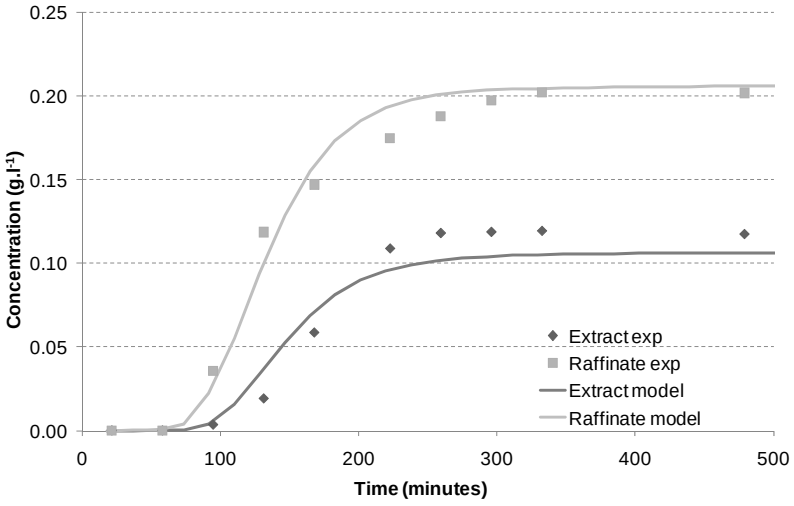

Figure 6.20 – History of the average concentration on more retained product on the extract and the less retained species in the raffinate current over a cycle, namely, cycle: 2; 4; 6; 8; 10; 13; 15; 17; 19; 27, diamonds R-Tetralol and squares the S-Tetralol; lines the theoretical profiles obtained from the dead volumes model approach*.

* The tetralol experiments are compared with an SMB model using and LDF approach (similar to the one presented in Chapter 2 with $k_{LDF} = \frac{3}{r_p} k_{ov}$) but extended for the FlexSMB-LSRE® dead volumes and switching time asymmetries, as mentioned in section 6.3.1. The resulting system of PDEs was then solved by means of the gPROMS commercial package from Process System Enterprise, with and absolute and relative tolerance set to 10^{-5}.

To plot the FlexSMB-LSRE® concentration profile, from cycle 20 to cycle 25, a single sample in each cycle was withdrawn for 10 seconds, at the middle of the switching time period $\left[\frac{t_s}{2} - 5s; \frac{t_s}{2} + 5s\right]$, by means of a 6 ports sampling valve installed on the outlet of column 6 for internal profile sample I, III, IV and V; and at the extract and raffinate ports for profiles samples VI and II, respectively, see Annex VIII. The same procedure was then repeated in cycle 27, but now with all sampling apparatus occurring within the same cycle. Both sampling procedures resulted in almost the same concentration profile, proving that collecting six samples per cycle will not influence too much the SMB internal profiles.

In Figure 6.21 the internal concentration profile obtained from cycle 20 to 27.

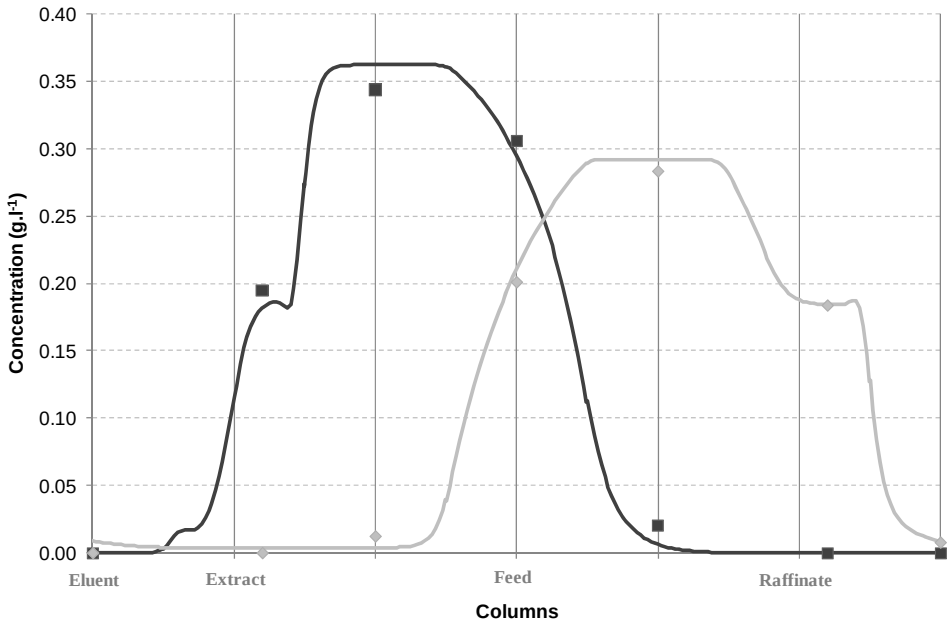

Figure 6.21 – Concentration profiles obtained from cycle 20 to 27, diamonds R-tetralol and squares the S-tetralol, lines the theoretical profiles obtained from the dead volumes model approach; with black squares representing experimental C_{b_A}, grey diamonds the experimental C_{b_B}; the black line the simulated C_{b_A} and the grey line the simulated C_{b_B}.

The simulated results fit well the experimental ones, even the "secondary plateau" noted next to the left of major plateau of the more retained species in section II and the right of the major plateau of the less retained species in section III (related with dead volumes of both extract and raffinate lines), are well predicted by the extended dead volumes model used.

All samples (extract and raffinate average concentrations, as well as internal profiles) were loaded into a 10 µl loop and then injected by means of a Knauer injection valve installed on a Gilson HPLC unit into an analytical column CHIRALCEL OBH (L_c =25 cm and d_c =0.46 cm I.D., supplied by Chiral Technologies, France) using as mobile phase the same solution used for eluent purposes.

The consequent peaks were measured by means of a UV detector set at 270 nm and concentrations determined according with calibration curve obtained from linear regression of Area vs. Concentration ($A = m[i]$) of 5 standards ($[i] = \{0.10016;\ 0.20032;\ 0.30048;\ 0.40064;\ 0.50080\}$ g.l^{-1}, of each enantiomer) with a with a $R_{correlation}{}^2 > 0.99$.

All experiments (separation with the SMB unit and analytical procedures) were run at laboratorial conditions (approximately 25 ºC).

6.3.3 SEPARATION OF RACEMIC MIXTURE OF GUAFEINESIN (NON LINEAR ISOTHERMS)

As introduced before, the resolution of a racemic mixture of guafeinesin enantiomers by means of Chiralpak AD (20 μm particles), with a *n*-neptane/ethanol mixture at 85/15 in volumetric percentage as mobile phase (Sá Gomes *et al.*, 2009b), was used to test the FlexSMB-LSRE® unit for non linear isotherms conditions under classic, Varicol and OSS *modus operandi*.

a) Classical SMB

The volumetric flow rates in section I and IV (41 ml.min^{-1} and 34 ml.min^{-1}, respectively) from Chapter 3 were re-calculated to account with a safety factor that will avoid contamination due to mass transfer effects. In this case the flow rate in section I was increased for 5 % and in section IV was decreased for 5 %: $Q_I^* =$ 43.0 ml.min^{-1} and $Q_{IV}^* = 32.5$ ml.min^{-1}.

From the separation region presented in Figure 3.10, the operation point ($\gamma_{II} = 6.38;\ \gamma_{III} = 6.58$) was selected, away from the triangle limits to avoid products pollution as consequence of the mass transfer effects. The switching time was corrected according to eq. (6.3) resulting in a new values of 2.65 min. Acording to the operation point chosen, the in section II and III were the calculated: $Q_{II}^* = 36.3$ ml.min^{-1} and $Q_{III}^* =$ 37.3 ml.min^{-1}, and consequently, the feed flow rate equal to 1.0 ml.min^{-1}.

The operating conditions chosen before were set on the FlexSMB-LSRE® control and automation routine. The extract and raffinate flow rates were monitored again by means of the total recovered mass in each outlet over complete cycles and weighted on a balance with 0.01 g of precision and extract stream outlet also by means of a Coriolis flow meter. The recycle flow rate was monitored by the other Coriolis flow meter. The experimental average flow rates, as well as geometric features, number of columns and SMB configuration are reported in Table 6.10.

The internal concentration profiles at the Cyclic Steady State (CSS) were again collected using a 6-port valve, as extract and raffinate ports. Samples were taken at half of the switching time, as well as at one quarter and three quarters of the switching time. In addition, a sample from the average concentration of every extract and raffinate as also collected.

Table 6.10 - Experimental operating conditions for the guafeinesin racemic mixture separation.

Columns and packing parameters			
$n_j = [1\ 2\ 2\ 1]$		ε_b = 0.4; ε_p = 0.33	
L_c = 10 cm		C_i^F = 2.0 g.l^{-1}	
d_c = 2.0 cm		d_p = 20 µm	
SMB operating conditions (measured)			
$Q_I^* =$	43.0 ml.min^{-1}	Eluent	10.5 ml.min^{-1}
$Q_{II}^* =$	36.3 ml.min^{-1}	Extract	6.7 ml.min^{-1}
$Q_{III}^* =$	37.2 ml.min^{-1}	Feed	0.9 ml.min^{-1}
$Q_{IV}^* =$	32.5 ml.min^{-1}	Raffinate	4.7 ml.min^{-1}
t_s =2.65 min			
$\gamma_I^*\vert_{FlexSMB} = 9.06$	$\gamma_{II}^*\vert_{FlexSMB} = 7.65$	$\gamma_{III}^*\vert_{FlexSMB} = 7.84$	$\gamma_{IV}^*\vert_{FlexSMB} = 6.85$

All collected samples were quantitatively analyzed by Dr. M. Zabkova using an analytical column packed with Chiralpak IB (particle size 5 µm)[*], with *n*-heptane/ethanol (60/40 %, volumetric fraction) as mobile phase on a HPLC system which includes a Smartline 1000 LC pump, UV detector model Smartline 2500, LPG block and degasser (Knauer, Germany). The detector was set at of 270 nm and a Rheodyne injection valve with a 10 µl sample loop was loaded manually using a syringe. Clarity (DataApex, Ltd., 2004) software was used for data acquisition and HPLC control. All experiments were carried at ambient temperature (approximately 25 °C), (Sá Gomes *et al.*, 2009b).

The experimental, as well as simulated, raffinate and extract histories obtained after 27 cycles are shown in Figure 6.22 (a) and Figure 6.22 (b) respectively.

[*] cellulose tris (3,5 dimethylphenylcarbamate immobilized onto 5 µm silica-gel), supplied by Chiral Technologies Europe (France).

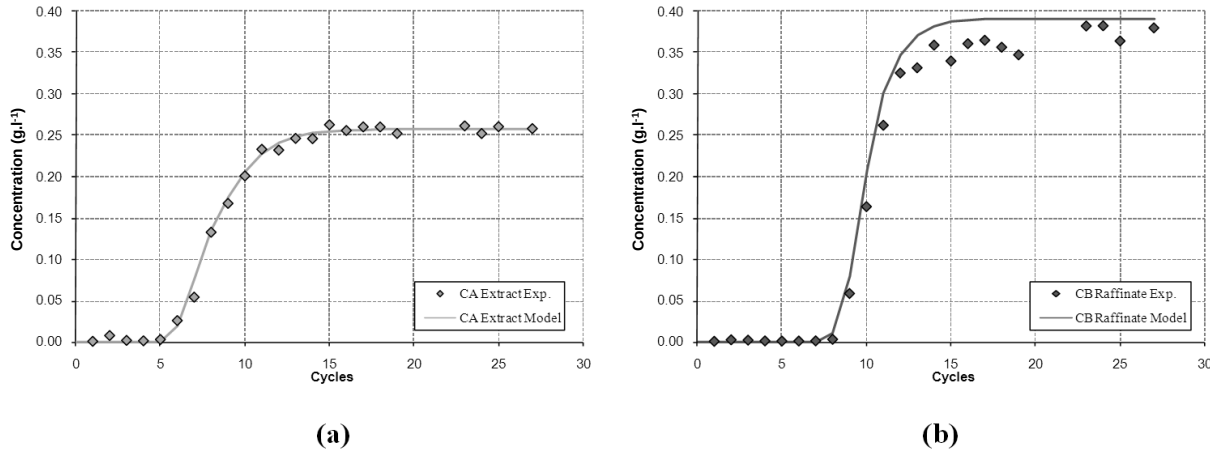

Figure 6.22 – Experimental and simulated average concentration of (a) A in the extract and (b) B in the raffinate streams*.

The detail of experimental, as well as simulated, extract and raffinate streams concentration profiles during cycle 27 are shown in Figure 6.23 (a) and Figure 6.23 (b), respectively.

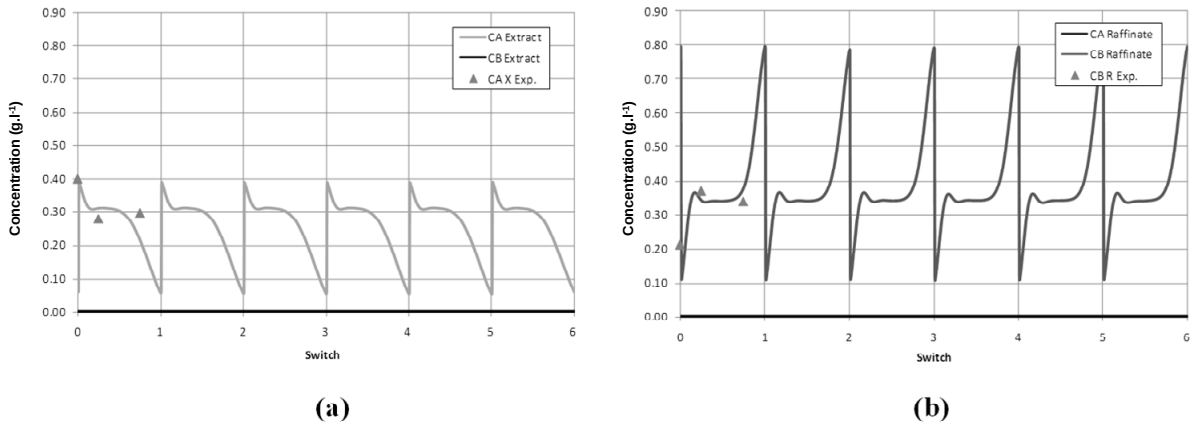

Figure 6.23 – (a) Extract and (b) Raffinate concentration profiles over a complete cycle, during the 27th cycle.

The experimental internal concentration profile, as well as the simulation results (obtained with the detailed model) at the 27th cycle (CSS) are shown in Figure 6.24.

* The model presented in section 6.3.1, that accounts for dead volumes and switching time asymmetries, was used to simulated all the following gaufenesin separations. Again, the commercial package from Process System Enterprise, gPROMS (ver. 3.1.5), was used to solve such model; the absolute as relative tolerance was set at 10^{-5}.

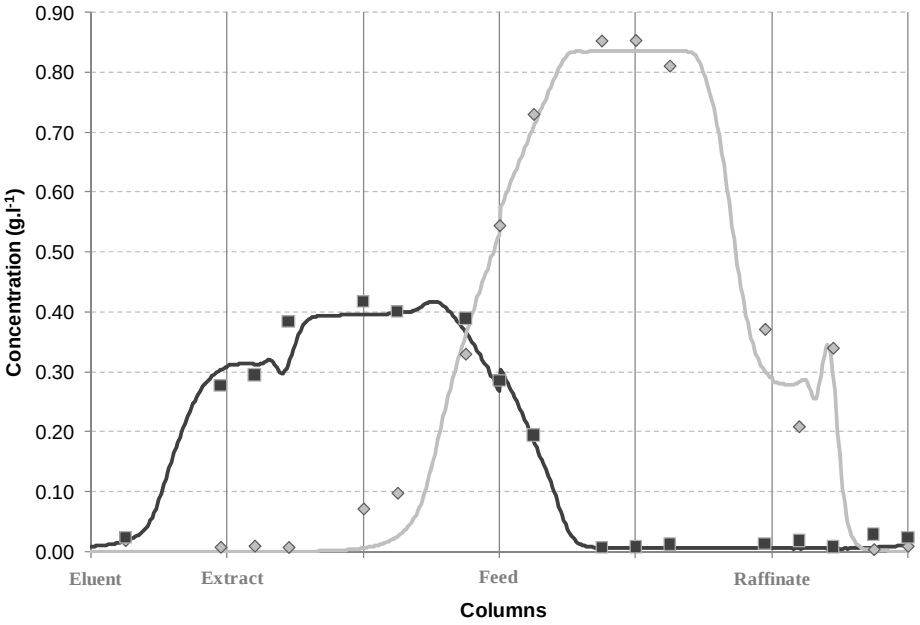

Figure 6.24 - Experimental internal concentration profile at half cyclic steady state (CSS) for feed concentration of 4.0 g.l^{-1} (racemate); with black squares representing experimental C_{b_A}, grey diamonds the experimental C_{b_B}; the black line the simulated C_{b_A} and the grey line the simulated C_{b_B}.

The purity and recovery of the extract and raffinate streams were calculated based on the sample collected during the whole one cycle $(6t_s)$. The experimental, as well as simulated (obtained by means of the detailed model) average values of purities and recoveries obtained from cycle 25 to cycle 29 are reported in Table 6.11.

The experimental and simulated results are in reasonable agreement proving that the dead volumes switching time compensating work either for the dead volumes compensating as the switching time asymmetries, providing a good separation (> 97.5 %) purity with a productivity value of 23 $g_{enantiomer}.(l_{CSP}.day)^{-1}$.

Table 6.11 – Simulated and experimental purities and recoveries from cycle 25 to 29.

	Simulated		Experimental	
	extract	raffinate	extract	raffinate
purity	99.98 %	99.46 %	97.92 %	97.94 %
recovery	99.47 %	99.98 %	96.12 %	98.69 %

Nevertheless, it can be noted some difference between the simulated and experimental purity results in both extract and raffinate streams, Table 6.11. Also some experimental points in the internal concentration profile shown in Figure 6.24, are not coincident with those predict by the detailed model. A possible reason on these discrepancies can be related with an overestimation of the mass transfer coefficient, $k_{int} = 0.20\ \text{cm.min}^{-1}$,

calculated by correlation (see Chapter 3). A particular attention was driven to this aspect and a new estimative was found that would better fit the experimental data: $k_{int} = 0.07\ \text{cm.min}^{-1}$. By simulating with this value one find now the following internal concentration profiles, Figure 6.25.

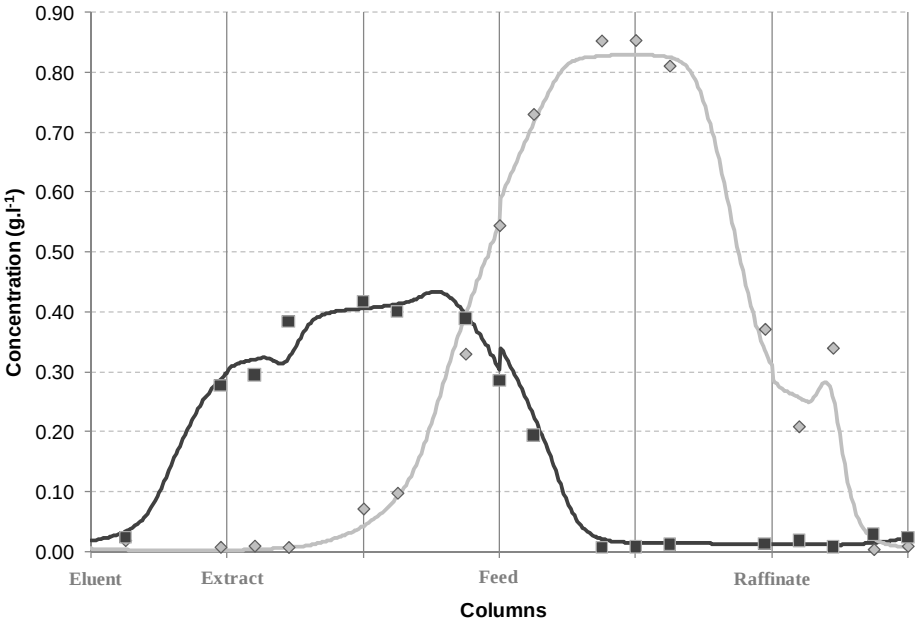

Figure 6.25 - Experimental internal concentration profile at half cyclic steady state (CSS) for $k_{int} = 0.07\ \text{cm.min}^{-1}$; with black squares representing experimental C_{b_A}, grey diamonds the experimental C_{b_B}; the black line the simulated C_{b_A} and the grey line the simulated C_{b_B}.

The respective purities and recovery values are shown in Table 6.12. Both the internal profiles as purity and recovery values fit better with this new mass transfer coefficient estimative.

Table 6.12 - Simulated and experimental purities and recoveries from cycle 25 to 29, for $k_{int} = 0.07\ \text{cm.min}^{-1}$.

	Simulated		Experimental	
	extract	raffinate	extract	raffinate
purity	99.20 %	97.20 %	97.92 %	97.94 %
recovery	97.20 %	99.21 %	96.12 %	98.69 %

b) Asynchronous SMB

To test the asynchronous shift automation routine, and thus the capabilities of the FlexSMB-LSRE® when running this sort of non-conventional modes of operation (also know as Varicol, (Adam *et al.*, 2000)), after the previously mentioned 29 cycles in classical mode of operation, the new operating conditions, as mentioned in Table 6.13, were set in the FlexSMB-LSRE® unit.

Table 6.13 - Experimental operating conditions for the guafeinesin racemic mixture separation operated under the asynchronous SMB.

Columns and packing parameters			
$n_j = [1\ \ 1.5\ \ 2.5\ \ 1]$		$\varepsilon_b = 0.4;\ \varepsilon_p = 0.33$	
L_c = 10 cm		C_i^F = 2.0 g.l^{-1}	
d_c = 2.0 cm		d_p = 20 µm	
SMB operating conditions (measured)			
$Q_I^* =$	42.6 ml.min^{-1}	Eluent	10.1 ml.min^{-1}
$Q_{II}^* =$	35.9 ml.min^{-1}	Extract	6.7 ml.min^{-1}
$Q_{III}^* =$	37.5 ml.min^{-1}	Feed	1.6 ml.min^{-1}
$Q_{IV}^* =$	32.5 ml.min^{-1}	Raffinate	5.0 ml.min^{-1}
t_s =2.65 min			
$\gamma_I^*\vert_{FlexSMB} = 8.98$	$\gamma_{II}^*\vert_{FlexSMB} = 7.57$	$\gamma_{III}^*\vert_{FlexSMB} = 7.91$	$\gamma_{IV}^*\vert_{FlexSMB} = 6.85$

After 10 cycles, 12 samples from the internal concentration profiles were withdrawn once again using the 6-port valve as well as the extract and raffinate ports and analyzed following the same analytical procedure used for the classic SMB experiment, and thus obtaining the following internal concentration profile as shown in Figure 6.26.

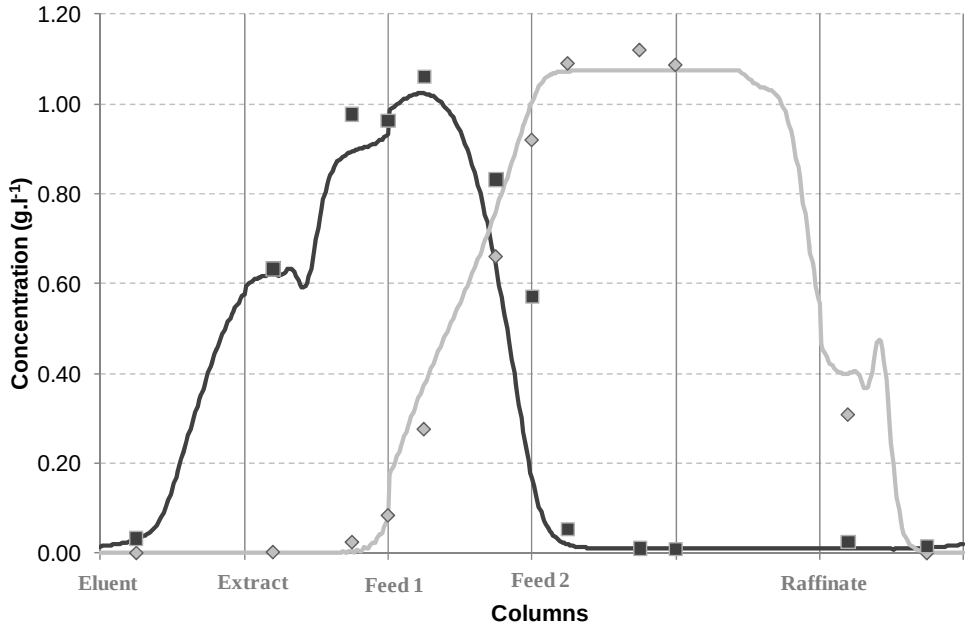

Figure 6.26 - Experimental internal concentration profile at half switching time period after 10 cycles operating as asynchronous SMB; black squares representing experimental C_{b_A}, grey diamonds the experimental C_{b_B}; the black line the simulated C_{b_A} and the grey line the simulated C_{b_B}.

And using the $k_{int} = 0.07$ cm. min^{-1}, one find the following fitting, Figure 6.27.

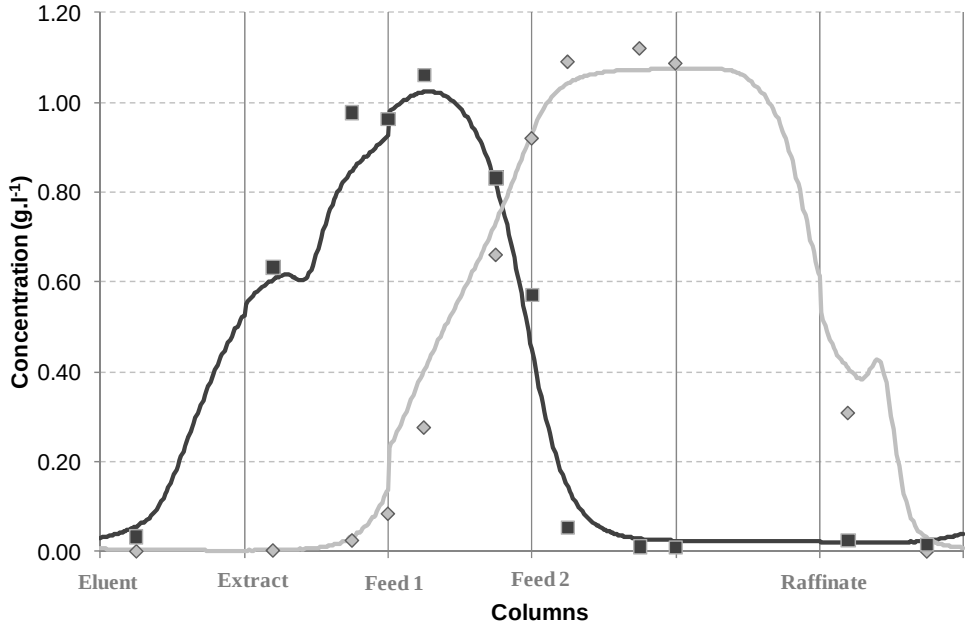

Figure 6.27 - Experimental internal concentration profile at half switching time period after 10 cycles operating as asynchronous SMB, for $k_{int} = 0.07$ cm. min^{-1}; black squares representing experimental C_{b_A}, grey diamonds the experimental C_{b_B}; the black line the simulated C_{b_A} and the grey line the simulated C_{b_B}.

The experimental purities (average purities over the 9th and 10th cycle) were in the extract 98.70 % and in the raffinate 96.81 %. However, these results are inconclusive since the mass balance was not closed (it was near 70% for each species). Nevertheless, and by means of the reasonable experimental points fitting with the theoretical simulation observed in Figure 6.26 (or Figure 6.27), the objective was completely fulfilled proving that the asynchronous port shift was being correctly operated.

c) Outlet Streams Swing - SMB

With FlexSMB-LSRE® unit it is also possible to run the OSS-*X0* mode of operation (or OSS-*0R*, by placing the extract pump in the raffinate outlet, see Figure 6.2). However, the problems associated with recycle flow rate variations, noted in either in the classical as asynchronous SMB modes of operation (Figure 6.13), were even more critical when operating under the OSS *modus operandi*. Instead of a different recycle flow rate for each switching time within a cycle (Figure 6.13), the recycle flow meter was in fact measuring two different flow rates within each switching time. As consequence, some attention was redirected for the extract node where, which according to Figure 6.2, two HPLC pumps (extract and recycle) were placed in its neighbourhoods. This arrangement seemed to be quite instable promoting a considerable asymmetry in the recycle flow rate and by consequence all internal flow rates. Thus, the recycle pump placed next to the extract node (in the beginning of section II) was changed to the recycle line next to the raffinate node (beginning of section IV) to avoid instabilities in the flow rate measurement by the Coriolis flow meter (usually noted when the coriolis flow meters are installed closer up to a pump) placed in this same position. The flow meter was changed to the previous position of this pump, *i.e.*, next to the extract node (in the beginning of section II). At the same time,

some dead volumes associated with the connections of both the flow meter and the recycle pump were reduced, by using 1 mm *i.d.* stainless steel capillary tubes where were before Teflon tubes.

This alteration led to a new pumps arrangement of the FlexSMB-LSRE® unit, Figure 6.28, as dead volumes distribution, Table 6.14.

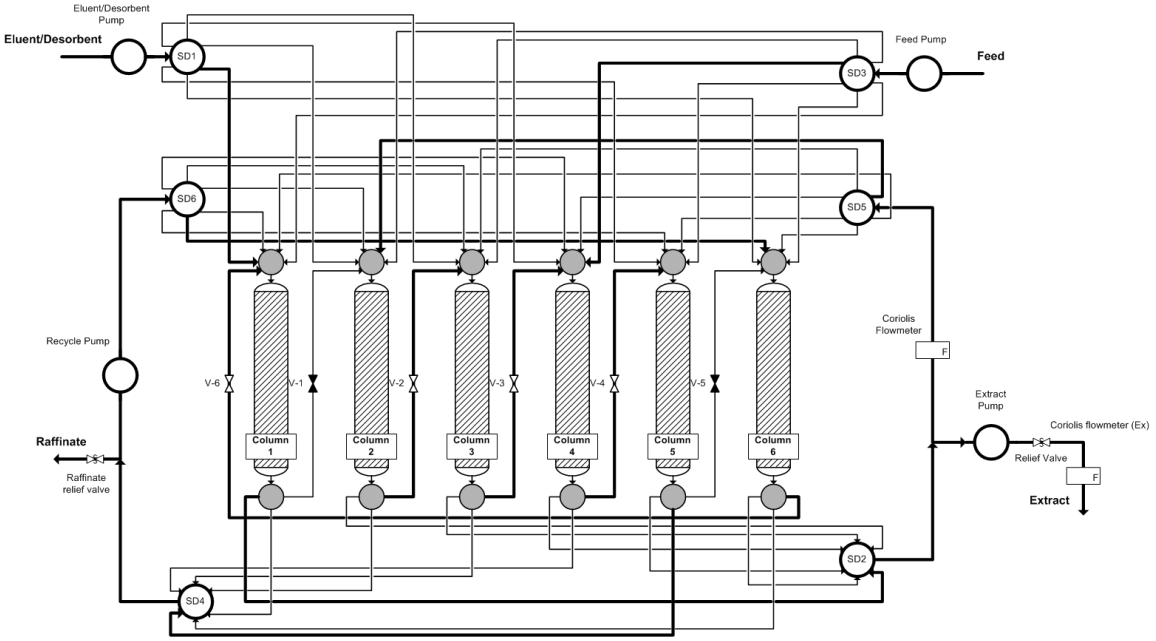

Figure 6.28 - FlexSMB-LSRE® pumps and valves scheme developed to avoid recycle flow rate asymmetries.

Table 6.14 – Dead volumes per function and total dead volumes percentage in the FlexSMB-LSRE® unit, after unit re-arrangement and dead volumes reduction.

	V_{each} (ml)	Total
Fritz and manifold	0.50	3.01
Ext in	0.36	2.17
Raf in	0.36	2.17
Ext out	0.32	1.93
Raf out	0.32	1.93
Interc	0.31	1.89
Sampler	0.47	0.47
Ext 1	0.12	0.12
Ext 2 (flow meter)	2.29	2.29
Raf 1	0.12	0.12
Raf 2 (Rec pump)	3.79	3.79
$V_c^{(*)}$ (ml)		188.5
(%) dead volumes		11.0 %

(*) considering 6 columns of 10 cm height and 2 cm of i.d.;

The values given in Table 6.4 include also the value of the stagnant volumes. Considering only the actives lines (see Figure 6.2), the dead volumes for each section are: $V_I^D = 1.09$ ml; $V_{II}^D = 3.84$ ml; $V_{III}^D = 1.71$ ml; $V_{IV}^D = 4.73$ ml, which led to a new dead volumes and swtihcing time compensation measure of 2.60 % in equation (6.3).

However, it was possible to achieve more stability in the unit operation, as well as a constant average value in the internal flow rates along a complete cycle, Figure 6.29.

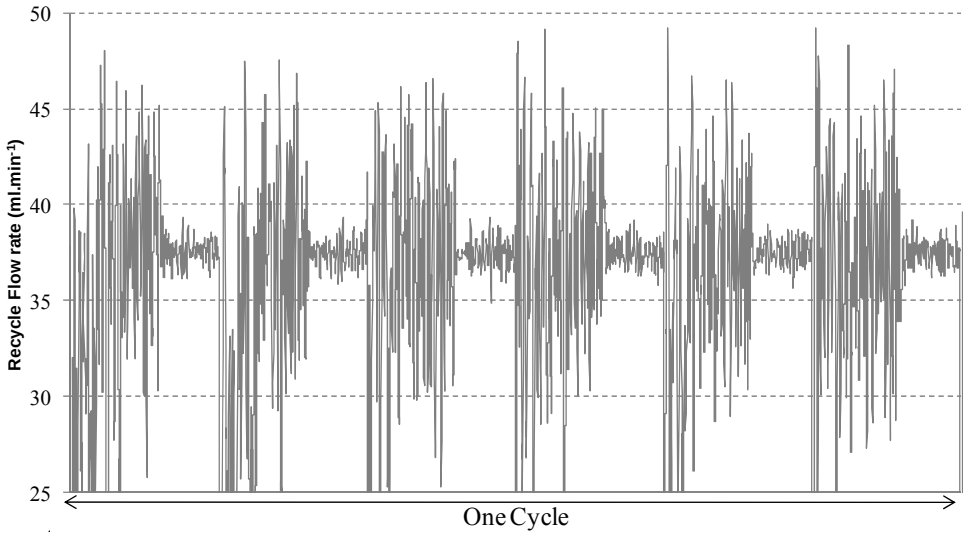

Figure 6.29 - Flow rate in the beginning of section II, after the unit alteration; FlexSMB-LSRE® operating in 60% OSS *X0* mode.

From Figure 6.29 it is possible to observe that the new position of the recycle pump (next to raffinate node or beginning of section IV, Figure 6.28), allowed a considerable stability in the internal flow rates (now measured by the coriolis flow meter installed next to the extract node). The two different oscillations within each switching time period noted in Figure 6.29 are directly related with the particularities of the 60% OSS *X0* mode of operation. The first oscillation has bigger amplitude than the second, probably related with the fact of the Coriolis flow meter has been just zeroed for the second part of the OSS operating mode.

For the OSS experiment, the variant 60% OSS *X0* was chosen to introduce the minimal flow rate oscillations and to fit the $^1/_5\, t_s$ discretization of the switching time period, allowed by the FlexSMB-LSRE® operating routines (see Figure 6.6).

The average operating points were the same as the ones stated for classic experiment. However, it was difficult to stabilize the unit at exactly the same conditions as for the last classical experiment. The operating conditions observed during the OSS experiment are presented in Table 6.15.

Table 6.15 - Experimental operating conditions for the guafeinesin racemic mixture separation operated under the 60% OSS *X0* -SMB.

Columns and packing parameters			
$n_j = [1\ 2\ 2\ 1]$		ε_b = 0.4; ε_p = 0.33	
L_c = 10 cm		C_i^F = 2.0 g.l^{-1}	
d_c = 2.0 cm		d_p = 20 µm	
Step 1 from *0 to 0.6*t_s - SMB operating conditions (measured)			
$Q_I^* =$	47.7 ml.min^{-1}	Eluent	14.9 ml.min^{-1}
$Q_{II}^* =$	36.4 ml.min^{-1}	Extract	11.3 ml.min^{-1}
$Q_{III}^* =$	37.3 ml.min^{-1}	Feed	0.9 ml.min^{-1}
$Q_{IV}^* =$	32.6 ml.min^{-1}	Raffinate	4.5 ml.min^{-1}
t_s =2.64 min			
$\gamma_I^*\vert_{FlexSMB} = 10.02$	$\gamma_{II}^*\vert_{FlexSMB} = 7.65$	$\gamma_{III}^*\vert_{FlexSMB} = 7.84$	$\gamma_{IV}^*\vert_{FlexSMB} = 6.85$
Step 2 from *0.6*t_s *to* t_s - SMB operating conditions (measured)			
$Q_I^* =$	36.7 ml.min^{-1}	Eluent	3.9 ml.min^{-1}
$Q_{II}^* =$	36.7 ml.min^{-1}	Extract	0 ml.min^{-1}
$Q_{III}^* =$	37.6 ml.min^{-1}	Feed	0.9 ml.min^{-1}
$Q_{IV}^* =$	32.9 ml.min^{-1}	Raffinate	4.8 ml.min^{-1}
t_s =2.64 min			
$\gamma_I^*\vert_{FlexSMB} = 7.71$	$\gamma_{II}^*\vert_{FlexSMB} = 7.71$	$\gamma_{III}^*\vert_{FlexSMB} = 7.90$	$\gamma_{IV}^*\vert_{FlexSMB} = 6.91$

The average operating conditions are presented in Table 6.16.

Table 6.16 - Average experimental operating conditions for the guafeinesin racemic mixture separation operated under the 60% OSS *X0* -SMB.

SMB operating conditions (Average)			
$Q_I^* =$	43.3 ml.min^{-1}	Eluent	10.5 ml.min^{-1}
$Q_{II}^* =$	36.5 ml.min^{-1}	Extract	6.8 ml.min^{-1}
$Q_{III}^* =$	37.4 ml.min^{-1}	Feed	0.9 ml.min^{-1}
$Q_{IV}^* =$	32.7 ml.min^{-1}	Raffinate	4.6 ml.min^{-1}
t_s =2.64 min			
$\gamma_I^*\vert_{FlexSMB} = 8.87$	$\gamma_{II}^*\vert_{FlexSMB} = 7.68$	$\gamma_{III}^*\vert_{FlexSMB} = 7.86$	$\gamma_{IV}^*\vert_{FlexSMB} = 6.88$

The internal concentration profiles at the CSS were once again withdrawn by means of the 6-port valve and extract and raffinate ports (see Annex VIII), and samples of extract and raffinate average concentrations were collected at each cycle.

The same analytical procedure as described before was followed, with exception of the mobile phase that was now the same as used for eluent purposes *n*-heptane/ethanol (85/15 %, volumetric fraction). The calibration curve used for this procedure is presented in Annex IX.

As mentioned before, during the first run of the OSS experiment some problems were noted (instability in the flow rates measurement), which led to the reformulation of the unit. After the reformulation of the unit, the parameters were again set on the computer interface and the unit operated for more 50 cycles (continuing the profiles from the first experiment). The average concentration history, as well as purities, in the extract and raffinate ports for the last 10 cycles (40 to 50) are shown in Figure 6.30.

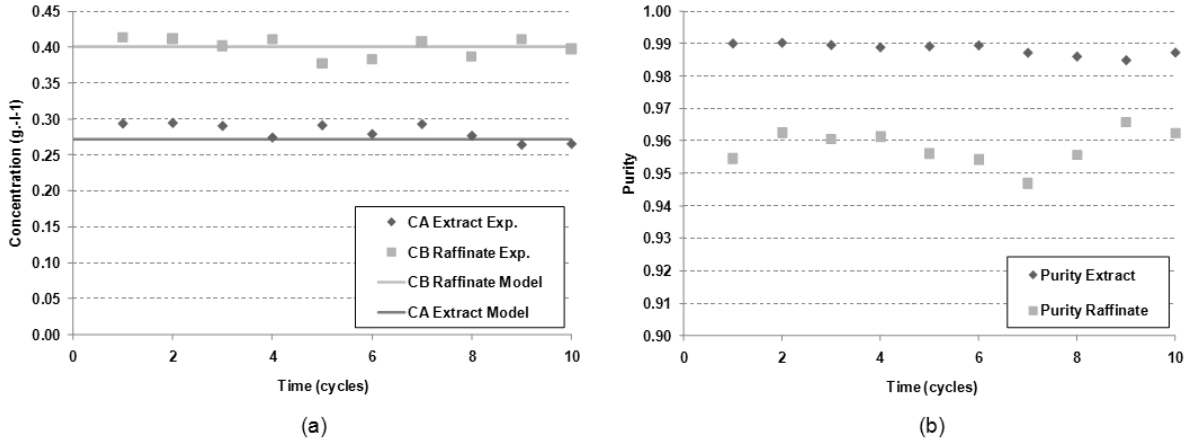

Figure 6.30 – (a) Average concentration history, (b) purities in the extract and raffinate ports from cycle 40 to 50; lines the simulated values.

As can be observed in Figure 6.30, at this stage (from cycle 40 to 50) the unit was already in/near the CSS (mass balance closed (+/- 3%) for each species).

The internal concentration profiles obtained for 25% 50% and 75% of the switching time are presented in Figure 6.31.

The average purity values for both the more retained product in the extract and less retained species in the raffinate ports are reported in Table 6.17.

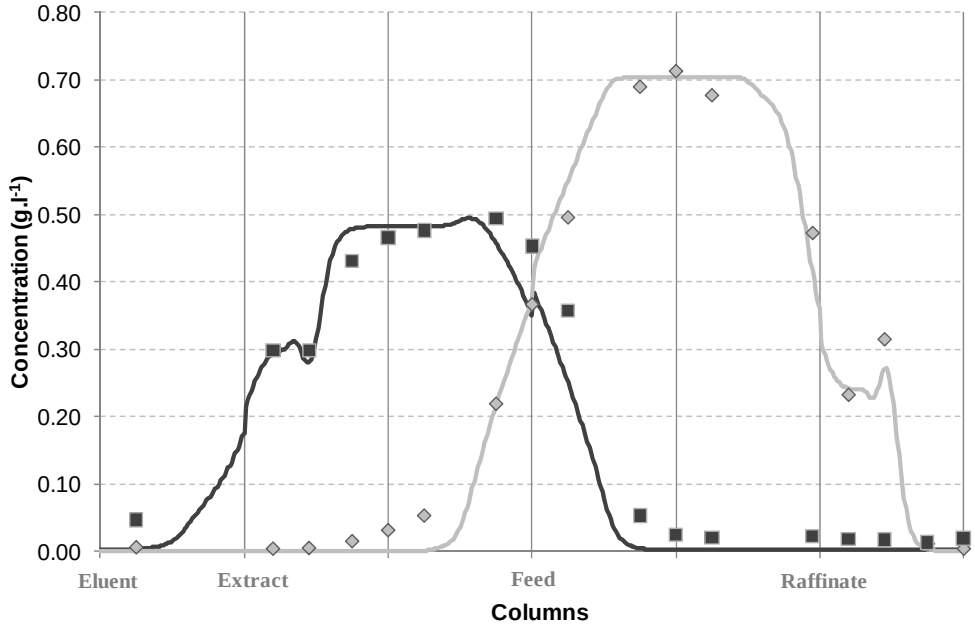

Figure 6.31 - Experimental internal concentration profile at half switching time period operating OSS-*X0* SMB; black squares representing experimental C_{b_A}, grey diamonds the experimental C_{b_B}; the black line the simulated C_{b_A} and the grey line the simulated C_{b_B}.

Table 6.17 – Experimental and simulated purity values for the more retained product in the extract and less retained one in the raffinate.

	Simulated		Experimental	
	extract	raffinate	extract	raffinate
purity	99.99 %	99.59 %	98.83 %	95.81 %
recovery	99.59 %	99.99 %	96.10 %	98.24 %

Once again the simulations for $k_{int} = 0.07\ \text{cm.min}^{-1}$ were performed and are presented in Table 6.18 and Figure 6.32.

Table 6.18 – Experimental and simulated (considering $k_{int} = 0.07\ \text{cm.min}^{-1}$) purity values for the more retained product in the extract and less retained one in the raffinate.

	Simulated		Experimental	
	extract	raffinate	extract	raffinate
purity	99.80 %	98.63 %	98.83 %	95.81 %
recovery	98.62 %	99.80 %	96.10 %	98.24 %

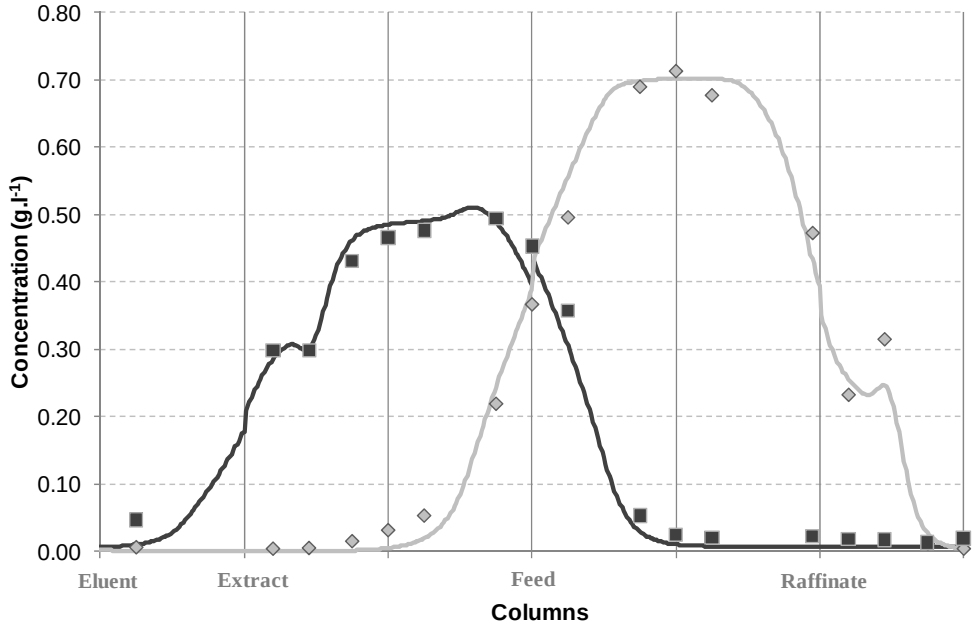

Figure 6.32 - Experimental internal concentration profile at half switching time period after 10 cycles operating as OSS *X0* SMB; black squares representing experimental C_{b_A}, grey diamonds the experimental C_{b_B}; the black line the simulated C_{b_A} and the grey line the simulated C_{b_B}, both considering $k_{int} = 0.07\ \text{cm.min}^{-1}$.

Again the simulated values obtained by considering $k_{int} = 0.07\ \text{cm.min}^{-1}$ are closer to the experimental ones. Even thought the results can not be directly compared with the classical experiment presented before (different operating conditions). It is possible to compare the simulated result obtained for the OSS *X0* simulation (considering $k_{int} = 0.07\ \text{cm.min}^{-1}$) with the ones that would be obtained by running the correspondent classical mode of operation (also considering $k_{int} = 0.07\ \text{cm.min}^{-1}$), Figure 6.33 and Table 6.19.

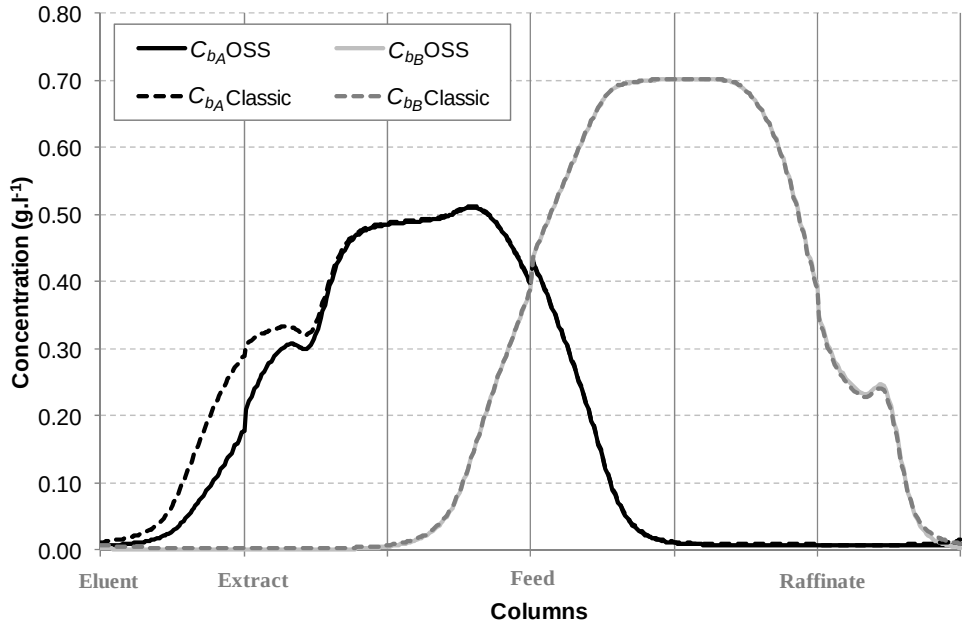

Figure 6.33 – Bulk concentration profile at half switching both OSS *X0* and Classic SMB modes of operation, both considering $k_{int} = 0.07\ \text{cm.min}^{-1}$.

Table 6.19 – Purity values for the more retained product in the extract and less retained one in the raffinate for the OSS *X0* and Classic SMB modes of operation, both considering $k_{int} = 0.07\ \mathrm{cm.min^{-1}}$.

	OSS-X0		Classic	
	extract	raffinate	extract	raffinate
purity	99.80 %	98.63 %	98.85 %	98.30 %
recovery	98.62 %	99.80 %	98.30 %	98.85 %

As can be observed from Figure 6.33, just the concentration profile around the extract port will change considerably. From Table 6.19, it can be note that if one operates under the classic SMB both the raffinate as extract purities will be more reduced, when compared with the OSS *X0* operating strategy. Both observations converge to the same conclusion: as expected (see Chapter 3) the contraction of the front of the more retained component in section I and II (near the extract port), consequence of the OSS *X0* operating mode, will allow a better separation (better purity values) than the ones that were observed if one runs under the classic mode of operation.

6.4 CONCLUSIONS

In this chapter, the design, construction and operation of a new flexible SMB unit, the FlexSMB-LSRE®, was presented. A major emphasis was given to the common deviations that "real" SMB units present when compared with the theoretical apparatus (due to tubing and equipment dead volumes, switching time asymmetries and delays, pumps flow rates variations). It was shown that these deviations should be analyzed before and after the design and construction of the FlexSMB-LSRE® unit.

A detailed model, that takes into account tubing and equipment dead volumes, as well as switching time asymmetries and delay, was employed to study and compare different dead volumes design and compensating strategies. This approach served to predict the experimental operating conditions and successfully run: two classical SMB experiments for the separation of a racemic mixture of $\alpha-$tetralol, and guafeinesin; a nonconventional separation of a racemic mixture of guafeinesin by means of the asynchronous mode of operating and considering variable flow rates (with the OSS technique)[*].

[*] A significant part of Chapter 6 was published on: Sá Gomes, P., M. Zabkova, M. Zabka, M. Minceva and A. Rodrigues, "Separation of Chiral Mixtures in Real SMB Units: the FlexSMB-LSRE®." accepted in AIChE Journal, (2009b). And presented in: Sá Gomes, P., M. Zabka, M. Minceva and A. E. Rodrigues Design and Construction of a Lab-Scale Simulated Moving Bed Unit: The FlexSMB-LSRE – from Theory to Practice. Chempor. Braga-Portugal, (2008c), Sá Gomes, P., M. Zabka, M. Zabkova, M. Minceva and A. E. Rodrigues Modelling and Design Strategies for Lab-Scale SMB Units Accounting for Dead Volumes and Tubing Connections – the FlexSMB-LSRE Unit. AIChE Annual Meeting. Philadelphia – Pennsylvania USA, (2008e).

Chapter 7

CONCLUSIONS AND SUGGESTIONS FOR FUTURE WORK

Although the Simulated Moving Bed (SMB) technology had long been established as a viable, practical, and cost-effective separation technique, the space to innovate is still considerable. Among several topics worth of attention, four major issues were addressed in the scope of this thesis:

(i) study and development of new non-conventional operating SMB modes;

A new non-conventional SMB mode of operation was introduced, the Outlet Streams Swing (OSS). This new technique, characterized by a periodical product withdrawal (performed by closing extract or raffinate ports for a given part of the switching time period, keeping sections II and III with constant flow rates by compensating it with the eluent/desorbent flow rate), improves the SMB outlet purities or allow productivity/desorbent increase/reduction, when compared with the classic operating mode. Throughout a methodical analysis, it was confirmed that, by means of the OSS technique, it is possible to compress or expand either the more retained product front in section I or the less retained product front in section IV, as the two fronts at same time. Compressing either one or other, or even both fronts, will allow purity improvement for a given eluent/desorbent consumption or a considerable eluent/desorbent reduction for a given purity requirement. Expanding either one or other, or even both fronts, will allow a purity improvement for a given feed flow rate or productivity increase for a given purity requirement. This new OSS technique was compared with the classical SMB approach for two different separations and tested in the FlexSMB-LSRE® unit for the separation of a racemic mixture of guafeinesin.

(ii) development of design procedures that accounts for SMB units' adsorbent ageing problems;

The effect of adsorbent ageing in the operation of SMB units was studied for systems characterized by linear and non-linear isotherms. Two different consequences of adsorbent deactivation were considered, one involving the loss of adsorption equilibrium capacity and the other related to the increase of mass transfer resistances. For each of these cases one direct and straightforward compensation measure was presented: the increase of the solid velocity (decrease of switching time) to compensate the adsorbent capacity decline and the decrease of solid and internal flow rates to compensate the mass transfer resistances increase. It was found that it is possible to compensate the adsorbent capacity decline, maintaining all SMB performance parameters, limited to the reduced contact time mainly related with operation at high solid velocities. When mass transfer resistance increases, it has been shown that the direct compensation strategy would lead to a decrease of productivity, keeping the same purity and recovery as with fresh adsorbent. The use of the non conventional asynchronous SMB as compensating measure was also studied. These methodologies were then applied for the industrial separation of *p*-xylene, where dynamic simulations were used to study the influence of the adsorbent capacity decline on the SMB unit performance for a 10 years period. The switching time decrease (solid flow rate increase) and the non conventional asynchronous SMB strategies were then tested as compensating measures. Both strategies kept the initial purity requirements and reached higher productivity values than the respective unit working without any compensation measure. The switching time compensating strategy proved to be more efficient than the second one, achieving, for the same purity requirements, higher productivity values.

(iii) development of a design procedure for an industrial gas phase SMB unit (Chapter 5);

An alternative separation of propane-propylene mixtures using SMB technology over 13X zeolite and isobutane as desorbent was presented. Driven by this process novelty, a design strategy for this separation was proposed, based on three major questions: Is it possible?; Is it reasonable? and Is it worth it? For each question, different approaches were used, starting form equilibrium assumptions through more detailed models, accounting for mass transfer resistances and temperature or pressure drops effects, and presenting, in the end, an introductive note to some relevant aspects for the project evaluation stage. The results shown that this separation is possible with the SMB technology, providing high purity propylene (>99.5 %), at high recovery (>99.0 %) and quite promising productivity values, above 1000 kg of propylene.$(m^3_{adsorbent}h)^{-1}$.

(iv) design, construction and operation of a flexible SMB unit (FlexSMB-LSRE®).

From the original sketch to the separation of different racemic mixtures of chiral drugs, the process of construction of the FlexSMB-LSRE® unit was detailed. It was shown that during the operating of real SMB units several deviations are noted, when compared with the theoretical SMB apparatus. These factors were analyzed, and minimized before the design and construction of the FlexSMB-LSRE® unit. An extended model, which considers different unit design particularities, can play a relevant role in the study and analysis of these operative deviations. By applying this type of models to two different units, a lab-scale (FlexSMB-LSRE®) and a pilot-scale (Licosep 12-26), it was possible to compare two different dead volumes compensating strategies and converged into only one that will easily compensate either dead volumes switching time asymmetries or delay. By applying this proposed compensation measure it was possible to separate a racemic mixture of tetralol as well as a racemic mixture of guafeinesin, this last performed in three different operating modes: classic SMB,

asynchronous SMB and OSS, proving the flexibility of the FlexSMB-LSRE® unit. The design, construction and operation of this unit, complemented the considerable know how related with design, simulation and optimization of SMB units for petrochemical, and specially, fine chemical separation and reaction fields, developed in the past years at LSRE, passing now from services to product development as well.

As a concluding remark, it can be considered that all major objectives of this thesis were accomplished, resulting in a new operating mode (the OSS); new design methodologies (SMB operation accounting for ageing effects and design of a gas-phase SMB unit for the separation of propane/propylene under bulk conditions) and the development of a new product (the FlexSMB-LSRE® unit).

In addition, the results of this thesis provided space to the horizontal (between academia-academia...) and vertical (intersectorial: academia-industry…) integration, allowing institutions synergies and cross fertilization within a knowledge-based framework (contacts were made between other research departments as well as technology holders and users).

A strong policy of stakeholders engagement was always present[*], based not only in reporting actions between the academia and the funding agency (FCT-Fundação para a Ciência e Tecnologia from the Ministry of Science, Technology and Higher Education of Portugal), but also to the peers (scientific publication and conferences), to institutional as private technology holders and users, and to population in general by means of voluntary participations in public driven actions (Mostra da Ciência da UP, Jornadas da ADI, Encontro Ciência em Portugal, Dia Aberto da Investigação - FEUP, among others).

The outcome of this thesis can now be directed towards more competitive, safer and cleaner production processes, promoting new fundamental as problem-oriented research. From each of the four major issues raised on the beginning of this thesis, new questions appeared:

(i) What would be the potential of OSS technique coupled with other non conventional SMB operating techniques?

There is much more potential when coupling most of the non-conventional SMB operating modes than its use *per se*. In this way, it is possible to augment the number of degrees of freedom and thus, extend further the performance of a given SMB unit. In fact, a considerable research effort has been driven in this direction; however, a substantial part of these latest developments rely in optimization procedures and empirical rules. One should not forget what somebody once remarked:

[*] See Sá Gomes, P.; H. Gonçalves and A. E. Rodrigues, "Developing a Sustainable Path for Research Institutions", submitted on the International Journal of Technology Management & Sustainable Development, 2009.

> "An essential condition for all fruitful research is to have at one's disposal a satisfactory technique. "*Tout progrès scientifique est un progrès de méthode*[*]." as somebody once remarked. Unfortunately the methodology is frequently the weakest aspect of scientific investigations".
>
> M.S. Tswett

Following this legacy, one should direct efforts in the development of methodical procedures that will allow not only the development of more efficient or sustainable solutions, but also to learn more and more about phenomena, dynamics and behaviors observed when studying different operational strategies. The methodology developed for the analysis of OSS technique, based in the separation and regeneration regions analysis, can play a particular role on this effort, allowing a deeper understanding of Partial Feed, Modicon and even PowerFeed operating modes.

(ii) It is possible to use the same analysis on the operation of SMB ageing problems to SMBR units?

Most of the reported SMBR units can be regarded as an SMB unit where a reaction takes place usually in the end of section II and beginning of section III. In this way, it is simple to notice a possible parallelism on the compensating strategies for adsorbent ageing decline stated on this thesis and the ones that one would expect to apply in the operation of SMBR units. There are mechanisms of catalyst deactivation that resembles the adsorbent capacity decline or the increase of mass transfer resistances, and thus similar solutions could be applied. However, when it accounts to catalyst deactivation suffered at different time scales than the ones observed for the adsorbent ageing effects, the problem starts to complicate, and different compensating strategies should be considered (the use of regeneration sections, operation at different temperatures rates, etc.). The role of deactivation dynamics will then play a particular function along side with more detailed models (non-isothermal, for instance), to find different solutions to different problems.

(iii) Is it worth it (the propane propylene separation by means of a gas phase SMB)?

It was stated that the gas-phase SMB separation of propane propylene is possible and reasonable, the next step is predictable, to find out if it is worth it. To answer to this question, one should now extend the separation analysis to the desorbent recovery units, pass from the process unit to the process itself, and then to evaluate its cost, in terms of economical, environmental and social value. Only in this way it will be possible a fair comparing between this new technology and the state-of-the-art technology, or other promising separation routes. Nevertheless, and from the point of view of a continuous innovation policy, one should not take the answer to this question as the process development concluding remark. It is also possible to make use of different advantages form different techniques, coupling them and try to find out even better solutions: hybrid solutions. To do so, the development of short cuts design methodologies will potentiate the progress of such procedures and the use of interdisciplinary approaches (from the physical fundamentals to the economics) will allow the development of more and more efficient processes.

[*] "All scientific progress is progress in a method." Statement attributed to the French philosopher René Descartes (1596-1650).

(iv) Would a strong control routine for the FlexSMB-LSRE® unit potentiate its introduction in the market?

The FlexSMB-LSRE® it is fully operational and several separations were already performed; however, it is easy to operate it if one possesses some background on SMB design technology. In fact, most of the units in the market suffer from the same problem, and thus SMB technology is still considered as complex. As consequence, a considerable effort has been driven towards the control of these units; nevertheless, each unit has its own particularities and control routines that will work well in one unit will probably not be suited for another. In addition, these control routines are usually protected by intellectual property agreements and thus, its accessibility reduced and conditioned. Even thought not necessary to fully operate it, a strong control routine for the FlexSMB-LSRE® would in fact potentiate its introduction in the market as a product *per se*.

NOMENCLATURE

A_c – Cross section area	(m^2)
Bi_m – Biot number	(-)
$C_i^{E/D}$ – Species i concentration Eluent/Desorbent streams	($kg.m^{-3}$) or ($mol.m^{-3}$)
C_i^F – Species i concentration Feed stream	($kg.m^{-3}$) or ($mol.m^{-3}$)
$C_{b\,i,j}^{\,0}$ / $C_{b\,i,k}^{\,0}$ – Species i concentration in the beginning of section j or column k	($kg.m^{-3}$) or ($mol.m^{-3}$)
$C_{b\,i,j}$ / $C_{b\,i,k}$ – Bulk fluid concentration of species i in section j or column k	($kg.m^{-3}$) or ($mol.m^{-3}$)
$CF_{i\,inv}$ – Investment Cash Flow in year i	(€)
$C_{p\,i,j}$ / $C_{p\,i,k}$ – Pore fluid concentration of species i in section j or column k	($kg.m^{-3}$) or ($mol.m^{-3}$)
$\widetilde{C_p}$ –Fluid phase heat capacity, molar at constant pressure	($J.mol^{-1}.K^{-1}$)
$\widehat{C_p}$ – Fluid phase heat capacity, mass at constant pressure	($J.kg^{-1}.K^{-1}$)
$\widehat{C_{p_s}}$ – Solid phase heat capacity	($J.kg^{-1}.K^{-1}$)
$\widehat{C_{p_w}}$ – Wall phase heat capacity	($J.kg^{-1}.K^{-1}$)
$C_{s\,i,j}$ / $C_{s\,i,j}$ – Adsorbed phase concentration of species i in section j or column k	($kg.m^{-3}$) or ($mol.m^{-3}$)
C_T – Total concentration	($kg.m^{-3}$) or ($mol.m^{-3}$)
$\widetilde{C_v}$ – Fluid phase heat capacity, molar at constant volume	($J.mol^{-1}.K^{-1}$)
$\widehat{C_v}$ – Fluid phase heat capacity, mass at constant volume	($J.kg^{-1}.K^{-1}$)
$D_{b\,j}$ – Axial dispersion coefficient in section j	($m^2.s^{-1}$)
d_c – Column diameter	(m^3)
D_{m_i} – Species i molecular diffusion coefficient	($m^2.s^{-1}$)
D_{pe_i} – Species i effective particle diffusion coefficient	($m^2.s^{-1}$)
D_{c_i} – Species i diffusion coefficient, cristal	($m^2.s^{-1}$)
d_p – Particle diameter	(m^3)
e – Wall thickness	(m)
EC – Eluent consumption	($m^3.kg$)
h_f – Fluid phase-solid heat transfer coefficient	($J.m^{-2}.K^{-1}.s^{-1}$)
H_i – Henry adsorption constant	($m^3.kg^{-1}$) or ($m^3.mol^{-1}$)

h_w – Fluid phase-wall heat transfer coefficient ($J.m^{-2}.K^{-1}.s^{-1}$)

k_c – Reaction kinetic constant ($mol.kg^{-1}.s^{-1}$)

K_{eq} – Reaction equilibrium constant (-)

k_{ext} – External mass transfer coefficient ($m.s^{-1}$)

k_f – Film mass transfer coefficient ($m.s^{-1}$)

k_g – Fluid phase heat conductivity ($J.m^{-1}.K^{-1}.s^{-1}$)

k_{LDF} – LDF mass transfer coefficient (s^{-1})

K_i – Langmuir (or Toth) adsorption constant ($m^3.kg^{-1}$) or (Pa^{-1})

k_{int} – Internal mass transfer coefficient ($m.s^{-1}$)

K_{m_i} – Global external mass transfer coefficient ($m.s^{-1}$)

k_{ov} – Overall mass transfer coefficient ($m.s^{-1}$)

L_C – Column length (m)

L_j / L_k – Section j or column k length (m)

M_i – Molecular mass of species i ($kg.mol^{-1}$)

N_c – Total number of columns (-)

NC – Total number of components (-)

N_f – Number of film mass transfer units (-)

N_{Feed} – Feed stage in the distillation (-)

N_{inv} – Total number of years for investment (year)

$n_{i,j}$ – Solid concentration of species i in section j ($kg.m^{-3}_{adsorbent}$) or ($mol.\ m^{-3}_{adsorbent}$)

$\langle n_{i,j} \rangle$ – Average solid concentration of species i in section j ($kg.m^{-3}_{adsorbent}$) or ($mol.\ m^{-3}_{adsorbent}$)

$n_{i,j}^{eq}$ – Equilibrium solid concentration of species i in section j ($kg.m^{-3}_{adsorbent}$) or ($mol.\ m^{-3}_{adsorbent}$)

n_j – Number of columns in section j (-)

N_{min} – Minimum number of stages, distillation (-)

N_p – Number of intraparticle mass transfer units (-)

P – Pressure (Pa)

Pe – Peclet number (-)

Pr – Prandtl number (-)

PR – Productivity ($kg.m^{-3}_{adsorbent}.s^{-1}$) or ($mol.kg^{-1}_{adsorbent}.s^{-1}$)

PU – Purity (%)

$q_{i,j}^{eq}$ – Equilibrium solid phase concentration ($kg.m^{-3}_{adsorbent}$) or ($mol.\ m^{-3}_{adsorbent}$)

$\langle q_{i,j} \rangle$ – Average solid phase concentration ($kg.m^{-3}_{adsorbent}$) or ($mol.\ m^{-3}_{adsorbent}$)

Q_j – Fluid flow rate in section j ($m^3.s^{-1}$)

q_{m_i} – Langmuir (or Toth) Maximum adsorption capacity	($kg.m^{-3}_{adsorbent}$) or ($mol.kg^{-1}_{adsorbent}$)
Q_S – Solid flow rate	($m^3.s^{-1}$)
R – Ideal gas constant	($J.K^{-1}.mol^{-1}$)
r – Radial coordinate	(m)
r_c – Cristal radius	(m)
Re – Reynolds number	(-)
RE – Recovery	(%)
R_{min} – Minimum reflux ratio, distillation	(-)
r_{inv} – Discount rate	(%)
r_p – Particle radius	(m)
Sc – Schmidt number	(-)
Sh – Sherwood number	(-)
t – Time coordinate	(s)
T / T_g / T_s / T_w – Temperature, gas, solid or wall	(K)
T_∞ – External temperature	(K)
t_s – Switching time	(s)
t_j / t_k– Section j or column k fluid phase space time	(-)
t_{r_i} – Species i retention time	(s)
u_j – Fluid interstitial velocity in section j	($m.s^{-1}$)
u_s – Solid interstitial velocity	($m.s^{-1}$)
U – Global heat transfer coefficient	($J.m^{-2}.K^{-1}.s^{-1}$)
V_C – Column volume	(m^3)
V_{Ec} – Economical value	(€)
V_j^D – Dead volume in section j	(m^3)
Vm_i – Molar volume	($m^3.mol^{-1}$)
x – Dimensionless axial coordinate	(-)
$Y_{i,j}$ – Gas phase molar fraction	(-)
z – Axial coordinate	(m)

Greek symbols

α – Ratio between the less and more retained species in feed	(-)
α_p – Ageing porosity weighting factor	(-)

β – Ratio between the more and less retained species in feed (-)

γ_j – Section j Ratio between the fluid and solid interstitial velocities (-)

ΔH – Adsorption enthalpy ($kJ.mol^{-1}$)

ΔP – Pressure drop (Pa)

ε_b – Bulk porosity (-)

ε_p – Particle porosity (-)

η – Effectiveness factor (-)

θ – Dimensionless time coordinate (-)

λ_j – Section j Heat axial dispersion coefficient ($J.m^{-2}.K^{-1}.s^{-1}$)

μ_f – Fluid phase viscosity (Pa.s)

υ_i – Species i stoichiometric coefficient (-)

ξ – Adsorbent capacity decline ($\%.year^{-1}$)

ρ – Dimensionless radial coordinate (-)

ρ_f – Fluid phase density ($kg.m^{-3}$)

ρ_s – Solid phase density ($kg.m^{-3}$)

ρ_w – Wall density ($kg.m^{-3}$)

τ – Particle tortuosity (-)

ϑ – Toth isotherm parameter (related with solid heterogeneity) (-)

ϕ – Association factor (-)

φ – LDF coefficient (-)

Subscripts and superscripts

i – Component index

j – Section index

k – Column index

tb – Tube index

$*$ – Referent to SMB

c – Column

p – Particle

s – Solid

b – Bulk

F – Feed

De – Desorbent

E – Eluent

X – Extract

R – Raffinate

It – Intermediary (JO process)

Abbreviations and acronyms

SMB – Simulated Moving Bed

TMB – True Moving Bed

SMBR – Simulated Moving Bed Reactor

LDF – Linear Driving Force

SS – Steady State

CSS – Cyclic Steady State

ISMB – Improved Simulated Moving Bed

OSS – Outlet Streams Swing

PSA – Pressure Swing Adsorption

OCFEM – Orthogonal Collocation on Finite Elements Method

ODE – Ordinary Differential Equations

PDE – Partial Differential Equations

HPLC – High Pressure (performance) Liquid Chromatography

HETP – Height of Equivalent Theoretical Plate

LSRE – Laboratory of Separation and Reaction Engineering

REFERENCES

"Successful regeneration of poisoned adsorbent for aromatics plant in Luoyang Petrochemical Company." China Petroleum Processing and Petrochemical Technology(1), 42, (2003).

Abdelmoumen, S., L. Muhr, M. Bailly and O. Ludemann-Hombourger, "The M3C process: A new multicolumn chromatographic process integrating a concentration step. I - The equilibrium model." Separation Science and Technology 41(12), 2639-2663, (2006).

Abel, S. and M. Juza, "Less Common Applications of Enantioselective HPLC Using the SMB Technology in the Pharmaceutical Industry." Chiral Separation Techniques (Third Edition). S. Dr. Ganapathy: 203-273, (2007).

Abel, S., M. Mazzotti and M. Morbidelli, "Solvent gradient operation of simulated moving beds - 1. Linear isotherms." Journal of Chromatography A 944(1-2), 23-39, (2002).

Abel, S., M. Mazzotti and M. Morbidelli, "Solvent gradient operation of simulated moving beds - 2. Langmuir isotherms." Journal of Chromatography A 1026(1-2), 47-55, (2004).

Abunasser, N. and P. C. Wankat, "One-column chromatograph with recycle analogous to stimulated moving bed adsorbers: Analysis and applications." Industrial and Engineering Chemistry Research 43(17), 5291-5299, (2004).

Abunasser, N., P. C. Wankat, Y. S. Kim and Y. M. Koo, "One-column chromatograph with recycle analogous to a four-zone simulated moving bed." Industrial and Engineering Chemistry Research 42(21), 5268-5279, (2003).

Adam, P., R. N. Nicoud, M. Bailly and O. Ludemann-Hombourger, "Process and device for separation with variable-length." US Patent 6 136 198, (2000).

Aida, T. and P. L. Silveston "Cyclic Separating Reactors." Oxford, Blackwell Publishing, (2005).

Amanullah, M., S. Abel and M. Mazzotti, "Separation of Troger's base enantiomers through a combination of simulated moving bed chromatography and crystallization." Adsorption 11(1), 893-897, (2005).

Amanullah, M., C. Grossmann, M. Mazzotti, M. Morari and M. Morbidelli, "Experimental implementation of automatic 'cycle to cycle' control of a chiral simulated moving bed separation." Journal of Chromatography A 1165(1-2), 100-108, (2007).

Amanullah, M. and M. Mazzotti, "Optimization of a hybrid chromatography-crystallization process for the separation of Troger's base enantiomers." Journal of Chromatography A 1107(1-2), 36-45, (2006).

Antos, D. and A. Seidel-Morgenstern, "Application of gradients in the simulated moving bed process." Chemical Engineering Science 56(23), 6667-6682, (2001).

Antos, D. and A. Seidel-Morgenstern, "Two-step solvent gradients in simulated moving bed chromatography: Numerical study for linear equilibria." Journal of Chromatography A 944(1-2), 77-91, (2002).

Araüjo, J. M. M., R. C. R. Rodrigues and J. P. B. Mota "Single-column simulated-moving-bed process with recycle lag." AIChE Annual Meeting, Conference Proceedings, (2005a).

Araüjo, J. M. M., R. C. R. Rodrigues and J. P. B. Mota, "Optimal design and operation of a certain class of asynchronous simulated moving bed processes." Journal of Chromatography A 1132(1-2), 76-89, (2006a).

Araüjo, J. M. M., R. C. R. Rodrigues and J. P. B. Mota, "Use of single-column models for efficient computation of the periodic state of a simulated moving-bed process." Industrial and Engineering Chemistry Research 45(15), 5314-5325, (2006b).

Araüjo, J. M. M., R. C. R. Rodrigues, R. J. S. Silva and J. P. B. Mota, "Single-column simulated moving-bed process with recycle lag: Analysis and applications." Adsorption Science and Technology 25(9), 647-659, (2007).

Araüjo, J. M. M., R. R. C. Rodrigues and J. P. B. Mota "Assessment of Smb performance using a single-column setup." AIChE Annual Meeting, Conference Proceedings, (2005b).

Ash, G., K. Barth, G. Hotier, L. Mank and P. Renard, "Eluxyl: A New Paraxylene Separation Process." Revue de I´Institut Français du Pétrole 49(5), 541-549, (1994).

Aumann, L. and M. Morbidelli, "Method and device for chromatographic purification." EP1716900 (A1), (2006).

Aumann, L. and M. Morbidelli, "A continuous multicolumn countercurrent solvent gradient purification (MCSGP) process." Biotechnology and bioengineering 98(5), 1043-1055, (2007).

Aumann, L. and M. Morbidelli, "A semicontinuous 3-column countercurrent solvent gradient purification (MCSGP) process." Biotechnology and bioengineering 99(3), 728-733, (2008).

Aumann, L., G. Stroehlein and M. Morbidelli, "Parametric study of a 6-column countercurrent solvent gradient purification (MCSGP) unit." Biotechnology and bioengineering 98(5), 1029-1042, (2007).

Azevedo, D. C. S., S. B. Neves, S. P. Ravagnani, Cavalcante C.V, Jr. and A. E. Rodrigues, "The influence of dead zones of simulated moving bed units." Fundamentals of Adsorption 6, 521-526, (1998).

Azevedo, D. C. S. and A. E. Rodrigues, "Design of a simulated moving bed in the presence of mass-transfer resistances." AIChE Journal 45(5), 956-966, (1999).

Azevedo, D. C. S. and A. E. Rodrigues, "Design methodology and operation of a simulated moving bed reactor for the inversion of sucrose and glucose-fructose separation." Chemical Engineering Journal 82(1-3), X95-107, (2001).

Bae, Y. S. and C. H. Lee, "Partial-discard strategy for obtaining high purity products using simulated moving bed chromatography." Journal of Chromatography A 1122(1-2), 161-173, (2006).

Bailly, M., P. Adam, O. Ludemann-Hombourger and R. M. Nicoud, "Separation Method and Device with Chromatographic Zones With Variable Length" WO2000025885, (2000).

Bailly, M., R.-M. Nicoud, P. Adam and O. Ludemann-Hombourger, "Method and Device for Chromatography Comprising a Concentration Step." EP20030767859, (2005).

Ballanec, B. and G. Hotier, "From Batch Elution to Simulated Countercurrent Chromatography." Preparative and Production Scale Chromatography. G. Ganetsos and P. E. Barker. New York, Marcel Dekker: 301-357, (1992).

Bartholomew, C. H., "Mechanisms of catalyst deactivation." Applied Catalysis A: General 212(1-2), 17-60, (2001).

Beste, Y. A. and W. Arlt, "Side-stream simulated moving-bed chromatography for multicomponent separation." Chemical Engineering and Technology 25(10), 956-962, (2002).

Bird, R. B., W. E. Stewart and E. N. Lightfoot "Transport Phenomena." Wiley, (2002).

Biressi, G., F. Quattrini, M. Juza, M. Mazzotti, V. Schurig and M. Morbidelli, "Gas chromatographic simulated moving bed separation of the enantiomers of the inhalation anesthetic enflurane." Chemical Engineering Science 55(20), 4537-4547, (2000).

Biressi, G., A. Rajendran, M. Mazzotti and M. Morbidelli, "The GC-SMB separation of the enantiomers of isoflurane." Separation Science and Technology 37(11), 2529-2543, (2002).

Blehaut, J. and R. M. Nicoud, "Recent aspects in simulated moving bed." Analusis 26(7), M60-M70, (1998).

Borges da Silva, E. A. and A. E. Rodrigues, "Design of Chromatographic multicomponent separation by a pseudo-simulated moving bed." AIChE Journal 52(11), 3794-3812, (2006).

Borges da Silva, E. A. and A. E. Rodrigues, "Design methodology and performance analysis of a pseudo-simulated moving bed for ternary separation." Separation Science and Technology 43(3), 533-566, (2008).

Borges da Silva, E. A., A. A. Ulson de Souza, S. G. U. de Souza and A. E. Rodrigues, "Analysis of the high-fructose syrup production using reactive SMB technology." Chemical Engineering Journal 118(3), 167-181, (2006).

Broughton, D. B., "Production of pure M-xylene and pure ethyl benzene from a mixture of C8 aromatic isomers." US 4,306,107, (1981).

Broughton, D. B., "Sucrose extraction from aqueous solutions featuring simulated moving bed." U.S. Patent No. 4,404,037 (1983).

Broughton, D. B. and C. G. Gerhold, "Continuous Sorption Process Employing Fixed Bed of Sorbent and Moving Inlets and Outlets." U.S. Patent No. 2,985,589, (1961).

Broughton, D. B., R. W. Neuzil, J. M. Pharis and C. S. Brearley, "The Parex Process for Recovering Paraxylene." Chemical Engineering Progress 66(9), 70-75, (1970).

Bryan, P. F., "Removal of propylene from fuel-grade propane." Separation and Purification Reviews 33(2), 157-182, (2004).

Cavoy, E., M. F. Deltent, S. Lehoucq and D. Miggiano, "Laboratory-developed simulated moving bed for chiral drug separations." Journal of Chromatography A 769(1), 49-57, (1997).

Chahbani, M. H. and D. Tondeur, "Pressure drop in fixed-bed adsorbers." Chemical engineering journal 81(1-3), 23-34, (2001).

Chan, S., N. Titchener-Hooker and E. Sørensen, "Optimal economic design and operation of single- and multi-column chromatographic processes." Biotechnology Progress 24(2), 389-401, (2008).

Cheng, L. S. and S. T. Wilson, "Process for separating propylene from propane." US Patent 6,293,999, (2001).

Chiang, A. S. T., "Equilibrium theory for simulated moving bed adsorption processes." AIChE Journal 44(11), 2431-2441, (1998).

Chin, C. Y. and N. H. L. Wang, "Simulated moving bed equipment designs." Separation and Purification Reviews 33(2), 77-155, (2004).

Clavier, J. Y. and R. M. Nicoud, "A new efficient fractionation process: The simulated moving bed with supercritical eluent." Third Italian conference on supercritical fluid and their applications, (1995).

Clavier, J. Y., R. M. Nicoud and M. Perrut, "A new efficient fractionation process: The simulated moving bed with supercritical eluent." High Pressure Chemical Engineering, 429-434, (1996).

Costa, E., G. Calleja, A. Jimenez and J. Pau, "Adsorption equilibrium of ethylene, propane, propylene, carbon dioxide, and their mixtures on 13X zeolite." Journal of Chemical and Engineering Data 36(2), 218-224, (1991).

Da Silva, F. A. and A. E. Rodrigues, "Adsorption equilibria and kinetics for propylene and propane over 13X and 4A zeolite pellets." Industrial and Engineering Chemistry Research 38(5), 2051-2057, (1999).

Da Silva, F. A. and A. E. Rodrigues, "Propylene/propane separation by vacuum swing adsorption using 13X zeolite." AIChE Journal 47(2), 341-357, (2001).

Danckwerts, P. V., "Continuous flow systems : Distribution of residence times." Chemical Engineering Science 2(1), 1-13, (1953).

Dapremont, O., F. Geiser, T. Zhang, S. S. Guhan, R. M. Guinn and G. J. Quallich, "Process for the Production of Enantiomerically Pure or Optically Enriched Sertaline-Tetralone Using Continous Chromatography." WO9957089 (A1), (1999).

Deb, K. "Multi-Objective Optimization Using Evolutionary Algorithms." Chichester, UK, Wiley, (2001).

Denet, F., W. Hauck, R. M. Nicoud, O. Di Giovanni, M. Mazzotti, J. N. Jaubert and M. Morbidelli, "Enantioseparation through supercritical fluid simulated moving bed (SF-SMB) chromatography." Industrial and Engineering Chemistry Research 40(21), 4603-4609, (2001).

Denet, F. and R. M. Nicoud, "Utilisation de la chromatographie HPLC, du lit mobile simule, et de la chromatographie avec eluant supercritique pour la purification industrielle des corps gras." OCL - Oleagineux Corps gras Lipides 6(3), 211-217, (1999).

Depta, A., T. Giese, M. Johannsen and G. Brunner, "Separation of stereoisomers in a simulated moving bed-supercritical fluid chromatography plant." Journal of Chromatography A 865(1-2), 175-186, (1999).

Dietz, A. and J. P. Corriou Comparison of model predictive control strategies for the simulated moving bed. Computer Aided Chemical Engineering. 25: 331-336, (2008).

Engelhardt, H., "One century of liquid chromatography: From Tswett's columns to modern high speed and high performance separations." Journal of Chromatography B 800(1-2), 3-6, (2004).

Engell, S., "Feedback control for optimal process operation." Journal of Process Control 17(3), 203-219, (2007).

Erdem, G., S. Abel, M. Morari, M. Mazzotti and M. Morbidelli, "Automatic control of simulated moving beds II: Nonlinear isotherm." Industrial and Engineering Chemistry Research 43(14), 3895-3907, (2004a).

Erdem, G., S. Abel, M. Morari, M. Mazzotti, M. Morbidelli and J. H. Lee, "Automatic Control of Simulated Moving Beds." Industrial and Engineering Chemistry Research 43(2), 405-421, (2004b).

Ettre, L. S., "Nomenclature for Chromatography (IUPAC Recommendations 1993)." Pure and Applied Chemistry 65(4), 819-872, (1993).

Ettre, L. S., "Two early, influential symposia in the development of gas chromatography." LC-GC North America 21(2), 144-149+167, (2003).

Ettre, L. S., "Early Petroleum Chromatographers." LC·GC North America 23(12), 1274-1280 (2005).

Ettre, L. S., "The centenary of "chromatography"." LC-GC North America 24(7), 680-692, (2006a).

Ettre, L. S., "Was Moses the first chromatographer?: Chromatography in the ancient world." LC-GC North America 24(12), 1280-1283, (2006b).

Francotte, E., P. Richert, M. Mazzotti and M. Morbidelli, "Simulated moving bed chromatographic resolution of a chiral antitussive." Journal of Chromatography A 796(2), 239-248, (1998).

Francotte, E. R. and P. Richert, "Applications of simulated moving-bed chromatography to the separation of the enantiomers of chiral drugs." Journal of Chromatography A 769(1), 101-107, (1997).

Frey, S. J., P. A. Sechrist and D. A. Kauff, "Fluid Distribution Apparatus." WO2006055222 (A1) (2006).

Gedicke, K., M. Kaspereit, W. Beckmann, U. Budde, H. Lorenz and A. Seidel-Morgenstern, "Conceptual design and feasibility study of combining continuous chromatography and crystallization for stereoisomer separations." Chemical Engineering Research and Design 85(7 A), 928-936, (2007).

Geier, D. and J. G. Soper, "Simultaneous Synthesis and Purification of a Fatty Acid Monoester Biodiesel Fuel." WO2007133299 (A2), (2007).

Gembicki, S. A., J. Rekoske, A. R. Oroskar and J. A. Johnson, "Adsorption, Liquid Separation." Kirk-Othmer's Encyclopedia of Separation Technology. D. M. Ruthven. New York, Wiley. 1: 664-691, (2002).

Glueckauf, E., "Theory of chromatography: Part 10. - Formula for diffusion into spheres and their application to chromatography." Transactions of the Faraday Society 51, 1540-1551, (1955).

Grill, C. M. and L. Miller, "Separation of a racemic pharmaceutical intermediate using closed-loop steady state recycling." Journal of Chromatography A 827(2), 359-371, (1998).

Grill, M. C., "Single column closed-loop recycling with periodic intra-profile injection ", WO9851391, (1998).

Grossmann, C., M. Amanullah, M. Morari, M. Mazzotti and M. Morbidelli, "Optimizing control of simulated moving bed separations of mixtures subject to the generalized Langmuir isotherm." Adsorption 14(2-3), 423-432, (2008a).

Grossmann, C., G. Erdem, M. Morari, M. Amanullah, M. Mazzotti and M. Morbidelli, "'Cycle to cycle' optimizing control of simulated moving beds." AIChE Journal 54(1), 194-208, (2008b).

Guest, D. W., "Evaluation of simulated moving bed chromatography for pharmaceutical process development." Journal of Chromatography A 760(1), 159-162, (1997).

Guiochon, G., "Preparative liquid chromatography." Journal of Chromatography A 965(1-2), 129-161, (2002).

Hashimoto, K., S. Adachi, H. Noujima and Y. Ueda, "A New Process Combining Adsortion and Enzyme Reaction for Producing Higher-Fructose Syrup." Biotechnol. & Bioeng. 25, 2371-2393, (1983).

Hashimoto, K., Y. Shirai and S. Adachi, "A simulated moving-bed adsorber for the separation of tricomponents." Journal of Chemical Engineering of Japan 26(1), 52-56, (1993).

Heikkilä, H., G. Hyöky and J. Kuisma, "Method for the recovery of betaine from molasses." EP0345511 (A2) (1989).

Helfferich, F. G., "Multicomponent ion exchange in fixed beds: Generalized equilibrium theorv for systems with constant separation factors." Industrial and Engineering Chemistry Fundamentals 6(3), 362-364, (1967).

Helfferich, F. G. and G. Klein "Multicomponent Chromatography: Theory of Interference." Marcel Dekker, New York., (1970).

Hotier, G. and R.-M. Nicoud, "Separation process by simulated moving bed chromatography with correction for dead volume by desynchronisation of periods." EP0688589, (1995).

Hotier, G. e. and R.-M. Nicoud, "Chromatographic simulated mobile bed separation process with dead volume correction using period desynchronization." US Patent 5578215 (1996).

Huang, Y. H., J. W. Johnson, A. I. Liapis and O. K. Crosser, "Experimental determination of the binary equilibrium adsorption and desorption of propane-propylene mixtures on 13X molecular sieves by a differential sorption bed system and investigation of their equilibrium expressions." Separations Technology 4(3), 156-166, (1994).

Hur, J. S. and P. C. Wankat "One-column analog to SMB for center-cut separation from quaternary mixtures." AIChE Annual Meeting Conference Proceedings, (2005a).

Hur, J. S. and P. C. Wankat "Simulated moving bed systems for center-cut separation from quaternary mixtures." AIChE Annual Meeting, Conference Proceedings, (2005b).

Hur, J. S. and P. C. Wankat, "Hybrid simulated moving bed and chromatography systems for center-cut separation from quaternary mixtures: Linear isotherm systems." Industrial and Engineering Chemistry Research 45(25), 8713-8722, (2006a).

Hur, J. S. and P. C. Wankat, "Two-zone SMB/chromatography for center-cut separation from ternary mixtures: Linear isotherm systems." Industrial and Engineering Chemistry Research 45(4), 1426-1433, (2006b).

Hur, J. S., P. C. Wankat, J. I. Kim, J. K. Kim and Y. M. Koo, "Purification of L-phenylalanine from a ternary amino acid mixture using a two-zone SMB/chromatography hybrid system." Separation Science and Technology 42(5), 911-930, (2007).

Hyun, S. H. and R. P. Danner, "Equilibrium adsorption of ethane, ethylene, isobutane, carbon dioxide, and their binary mixtures on 13X molecular sieves." Journal of Chemical and Engineering Data 27(2), 196-200, (1982).

Jarvelin, H. and J. R. Fair, "Adsorptive separation of propylene-propane mixtures." Industrial and Engineering Chemistry Research 32(10), 2201-2207, (1993).

Jensen, T. B., T. G. P. Reijns, H. A. H. Billiet and L. A. M. Van Der Wielen, "Novel simulated moving-bed method for reduced solvent consumption." Journal of Chromatography A 873(2), 149-162, (2000).

Jin, W. and P. C. Wankat "Parallel two-zone and four-zone hybrid Smb system for the separation of *P*-xylene." AIChE Annual Meeting Conference Proceedings, (2005a).

Jin, W. and P. C. Wankat, "Two-zone SMB process for binary separation." Industrial and Engineering Chemistry Research 44(5), 1565-1575, (2005b).

Jin, W. and P. C. Wankat, "Hybrid simulated moving bed processes for the purification of *p*-xylene." Separation Science and Technology 42(4), 669-700, (2007a).

Jin, W. and P. C. Wankat, "Thermal operation of four-zone simulated moving beds." Industrial and Engineering Chemistry Research 46(22), 7208-7220, (2007b).

Johannsen, M., S. Peper and A. Depta, "Simulated moving bed chromatography with supercritical fluids for the resolution of bi-naphthol enantiomers and phytol isomers." Journal of Biochemical and Biophysical Methods 54(1-3), 85-102, (2002).

Jupke, A., A. Epping and H. Schmidt-Traub, "Optimal design of batch and simulated moving bed chromatographic separation processes." Journal of Chromatography A 944(1-2), 93-117, (2002).

Juza, M., O. Di Giovanni, G. Biressi, V. Schurig, M. Mazzotti and M. Morbidelli, "Continuous enantiomer separation of the volatile inhalation anesthetic enflurane with a gas chromatographic simulated moving bed unit." Journal of Chromatography A 813(2), 333-347, (1998).

Juza, M., M. Mazzotti and M. Morbidelli, "Simulated moving-bed chromatography and its application to chirotechnology." Trends in Biotechnology 18(3), 108-118, (2000).

Kaspereit, M., K. Gedicke, V. Zahn, A. W. Mahoney and A. Seidel-Morgenstern, "Shortcut method for evaluation and design of a hybrid process for enantioseparations." Journal of Chromatography A 1092(1), 43-54, (2005).

Kaspereit, M., A. Seidel-Morgenstern and A. Kienle, "Design of simulated moving bed processes under reduced purity requirements." Journal of Chromatography A 1162(1), 2-13, (2007).

Katsuo, S., C. Langel, P. Schanen and M. Mazzotti, "Extra-column dead volume in simulated moving bed separations: theory and experiments." Journal of Chromatography A 1216(7), 1084-1093, (2009).

Kawajiri, Y. and L. T. Biegler, "Nonlinear programming superstructure for optimal dynamic operations of simulated moving bed processes." Industrial and Engineering Chemistry Research 45(25), 8503-8513, (2006a).

Kawajiri, Y. and L. T. Biegler, "Optimization strategies for simulated moving bed and powerfeed processes." AIChE Journal 52(4), 1343-1350, (2006b).

Kawajiri, Y. and L. T. Biegler, "Comparison of configurations of a four-column simulated moving bed process by multi-objective optimization." Adsorption 14(2-3), 433-442, (2008a).

Kawajiri, Y. and L. T. Biegler, "Large scale optimization strategies for zone configuration of simulated moving beds." Computers and Chemical Engineering 32(1-2), 135-144, (2008b).

Kawase, M., A. Pilgrim, T. Araki and K. Hashimoto, "Lactosucrose production using a simulated moving bed reactor." Chemical Engineering Science 56(2), 453-458, (2001).

Kawase, M., T. B. Suzuki, K. Inoue, K. Yoshimoto and K. Hashimoto, "Increased esterification conversion by application of the simulated moving-bed reactor." Chemical Engineering Science 51(11), 2971-2976, (1996).

Kearney, M. M. and K. L. Hieb, "Time variable simulated moving bed process." US patent 5102553, (1992).

Kearney, M. M. and M. W. Mumm, "Improvement of Chromatographic Separator Sorbent Bed Preparation." WO9006796, (1990).

Keller, G. E., A. E. Marcinkowsky, S. K. Verma and K. D. Williamson, "Olefin recovery and purification via silver complexation." Separation and Purification Technology, 59-83, (1992).

Kemna, A. G. Z., "Case Studies on Real Options." The Journal of the Financial Management Association 22(3), 259-270, (1993).

Kessler, L. C. and A. Seidel-Morgenstern, "Method and Apparatus for Chromatographic Component Separation with Partial Recirculation of Mixture." WO2008125679 (A1), (2008).

Kim, J. K., N. Abunasser and P. C. Wankat, "Use of two feeds in simulated moving beds for binary separations." Korean Journal of Chemical Engineering 22(4), 619-627, (2005).

Kim, J. K. and P. C. Wankat, "Designs of Simulated-Moving-Bed Cascades for Quaternary Separations." Industrial and Engineering Chemistry Research 43(4), 1071-1080, (2004).

Kim, J. K., Y. Zang and P. C. Wankat, "Single-cascade simulated moving bed systems for the separation of ternary mixtures." Industrial and Engineering Chemistry Research 42(20), 4849-4860, (2003).

Klatt, K.-U., F. Hanisch, G. Dünnebier and S. Engell, "Model-Based Optimization and Control of Chromatographic Processes." Comp. & Chem. Eng. 24, 1119-1126, (2000).

Klatt, K. U., F. Hanisch and G. Dünnebier, "Model-based control of a simulated moving bed chromatographic process for the separation of fructose and glucose." Journal of Process Control 12(2), 203-219, (2002).

Klein, G., D. Tondeur and T. Vermeulen, "Multicomponent ion exchange in fixed beds: General properties of equilibrium systems." Industrial and Engineering Chemistry Fundamentals 6(3), 339-351, (1967).

Kleinert, T. and J. Lunze, "Decentralised control of chromatographic simulated moving bed processes based on wave front reconstruction." Journal of Process Control 18(7-8), 780-796, (2008).

Kloppenburg, E. and E. D. Gilles, "Automatic control of the simulated moving bed process for C8 aromatics separation using asymptotically exact input/output-linearization." Journal of Process Control 9(1), 41-50, (1999a).

Kloppenburg, E. and E. D. Gilles, "A new concept for operating simulated moving-bed processes." Chemical Engineering & Technology 22(10), 813-+, (1999b).

Kniep, H., G. Mann, C. Vogel and A. Seidel-Morgenstern, "Separation of enantiomers through simulated moving-bed chromatography." Chemical Engineering and Technology 23(10), 853-857, (2000).

Kostroski, K. P. and P. C. Wankat, "Separation of dilute binary gases by simulated-moving bed with pressure-swing assist: SMB/PSA processes." Industrial and Engineering Chemistry Research 47(9), 3138-3149, (2008).

Kruglov, A., "Methanol Synthesis in a Simulated Countercurrent Moving-Bed Adsorptive Catalytic Reactor." Chem.Eng. Sci. 49(24A), 4699-4716, (1994).

Kurup, A. S., K. Hidajat and A. K. Ray, "Optimal operation of an industrial-scale parex process for the recovery of *p*-xylene from a mixture of C8 aromatics." Industrial and Engineering Chemistry Research 44(15), 5703-5714, (2005).

Kurup, A. S., K. Hidajat and A. K. Ray, "Comparative study of modified simulated moving bed systems at optimal conditions for the separation of ternary mixtures of xylene isomers." Industrial and Engineering Chemistry Research 45(18), 6251-6265, (2006a).

Kurup, A. S., K. Hidajat and A. K. Ray, "Comparative study of modified simulated moving bed systems at optimal conditions for the separation of ternary mixtures under nonideal conditions." Industrial & Engineering Chemistry Research 45(11), 3902-3915, (2006b).

Kurup, A. S., K. Hidajat and A. K. Ray, "Optimal operation of a Pseudo-SMB process for ternary separation under non-ideal conditions." Separation and Purification Technology 51(3), 387-403, (2006c).

Kusters, E., G. Gerber and F. D. Antia, "Enantioseparation of a chiral epoxide by simulated moving bed chromatography using Chiralcel-OD." Chromatographia 40(7-8), 387-393, (1995).

Lacava, A. and K. McKeigue, "Continuous pressure difference driven adsorption process." EP0681860 (A2), (1995).

Lamia, N., L. Wolff, P. Leflaive, P. Sá Gomes, C. A. Grande and A. E. Rodrigues, "Propane/propylene separation by simulated moving bed I. Adsorption of propane, propylene and isobutane in pellets of 13X zeolite." Separation Science and Technology 42(12), 2539-2566, (2007).

Leão, C. P. and A. E. Rodrigues, "Transient and steady-state models for simulated moving bed processes: Numerical solutions." Computers and Chemical Engineering 28(9), 1725-1741, (2004).

Lee, K. B., C. Y. Chin, Y. Xie, G. B. Cox and N. H. L. Wang, "Standing-wave design of a simulated moving bed under a pressure limit for enantioseparation of phenylpropanolamine." Industrial and Engineering Chemistry Research 44(9), 3249-3267, (2005).

Lee, K. B., R. B. Kasat, G. B. Cox and N. H. L. Wang, "Simulated moving bed multiobjective optimization using standing wave design and genetic algorithm." AIChE Journal 54(11), 2852-2871, (2008).

Lehoucq, S., A. Vande Wouwer and E. Cavoy, "Chiral Separations using a SMB System: Determination of Competitive Adsorption Equilibrium Isotherms." Fundamentals of Adsorption 6. F. Meunier. Amsterdam, Elsevier: 467-472, (1998).

Li, P., G. Xiu and A. E. Rodrigues, "Proteins separation and purification by salt gradient ion-exchange SMB." AIChE Journal 53(9), 2419-2431, (2007).

Li, P., J. Yu, G. Xiu and A. E. Rodrigues, "Separation region and strategies for proteins separation by salt gradient ion-exchange SMB." Separation Science and Technology 43(1), 11-28, (2008).

Lode, F., G. Francesconi and M. Morbidelli, "Synthesis of methyl acetate in a simulated moving bed reactor (SMBR): Experimental investigation." Chemie-Ingenieur-Technik 73(6), 672, (2001).

Lorenz, H., P. Sheehan and A. Seidel-Morgenstern, "Coupling of simulated moving bed chromatography and fractional crystallisation for efficient enantioseparation." Journal of Chromatography A 908(1-2), 201-214, (2001).

Loughlin, K. F., M. A. Hasanain and H. B. Abdul-Rehman, "Quaternary, ternary, binary, and pure component sorption on zeolites. 2. Light alkanes on linde 5A and 13X zeolites at moderate to high pressures." Industrial and Engineering Chemistry Research 29(7), 1535-1546, (1990).

Ludemann-Hombourger, O., R. M. Nicoud and M. Bailly, "The "VARICOL" process: A new multicolumn continuous chromatographic process." Separation Science and Technology 35(12), 1829-1862, (2000).

Ludemann-Hombourger, O., G. Pigorini, R. M. Nicoud, D. S. Ross and G. Terfloth, "Application of the "VARICOL" process to the separation of the isomers of the SB-553261 racemate." Journal of Chromatography A 947(1), 59-68, (2002).

Ma, Z. and N.-H. L. Wang, "Standing wave analysis of SMB chromatography: linear systems." AIChE Journal 43(10), 2488-2508, (1997).

Malek, A., S. Farooq, M. N. Rathor and K. Hidajat, "Effect of velocity variation due to adsorption-desorption on equilibrium data from breakthrough experiments." Chemical Engineering Science 50(4), 737-740, (1995).

Mallmann, T., B. D. Burris, Z. Ma and N. H. L. Wang, "Standing wave design of nonlinear SMB systems for fructose purification." AIChE Journal 44(12), 2628-2646, (1998).

Mata, V. G. and A. E. Rodrigues, "Separation of ternary mixtures by pseudo-simulated moving bed chromatography." Journal of Chromatography A 939(1-2), 23-40, (2001).

Mazzotti, M., "Design of simulated moving bed separations; generalized langmuir isotherm." Industrial and Engineering Chemistry Research 45(18), 6311-6324, (2006a).

Mazzotti, M., "Equilibrium theory based design of simulated moving bed processes for a generalized Langmuir isotherm." Journal of Chromatography A 1126(1-2), 311-322, (2006b).

Mazzotti, M., R. Baciocchi, G. Storti and M. Morbidelli, "Vapor-phase SMB adsorptive separation of linear/nonlinear paraffins." Industrial & Engineering Chemistry Research 35(7), 2313-2321, (1996a).

Mazzotti, M., A. Kruglov, B. Neri, D. Gelosa and M. Morbidelli, "A continuous chromatographic reactor: SMBR." Chemical Engineering Science 51(10), 1827-1836, (1996b).

Mazzotti, M., B. Neri, D. Gelosa and M. Morbidelli, "Dynamics of a Chromatographic Reactor: Esterification Catalyzed by Acidic Resins." Industrial and Engineering Chemistry Research 36(8), 3163-3172, (1997a).

Mazzotti, M., G. Storti and M. Morbidelli, "Robust design of countercurrent adsorption separation processes: 2. Multicomponent systems." AIChE Journal 40(11), 1825-1842, (1994).

Mazzotti, M., G. Storti and M. Morbidelli, "Robust Design of Countercurrent Adsorption Separation: 3. Nonstoichiometric Systems." AIChE J. 42(10), 2784-2796, (1996c).

Mazzotti, M., G. Storti and M. Morbidelli, "Robust design of countercurrent adsorption separation processes: 4. Desorbent in the feed." AIChE Journal 43(1), 64-72, (1997b).

Methivier, A., "Influence of Oxygenated Contaminants on the Separation of C8 Aromatics by Adsorption on Faujasite Zeolites." Industrial and Engineering Chemistry Research 37(2), 604-608, (1998).

Migliorini, C., A. Gentilini, M. Mazzotti and M. Morbidelli, "Design of simulated moving bed units under nonideal conditions." Industrial and Engineering Chemistry Research 38(6), 2400-2410, (1999a).

Migliorini, C., M. Mazzotti and M. Morbidelli, "Simulated moving-bed units with extra-column dead volume." AIChE Journal 45(7), 1411-1420, (1999b).

Migliorini, C., M. Mazzotti and M. Morbidelli, "Robust design of countercurrent adsorption separation processes: 5. Nonconstant selectivity." AIChE Journal 46(7), 1384-1397, (2000).

Migliorini, C., M. Mazzotti, G. Zenoni and M. Morbidelli, "Shortcut experimental method for designing chiral SMB separations." AIChE Journal 48(1), 69-77, (2002).

Migliorini, C., M. Wendlinger, M. Mazzotti and M. Morbidelli, "Temperature gradient operation of a simulated moving bed unit." Industrial and Engineering Chemistry Research 40(12), 2606-2617, (2001).

Mihlbachler, K., J. Fricke, T. Yun, A. Seidel-Morgenstern, H. Schmidt-Traub and G. Guiochon, "Effect of the homogeneity of the column set on the performance of a simulated moving bed unit - I. Theory." Journal of Chromatography A 908(1-2), 49-70, (2001).

Mihlbachler, K., A. Jupke, A. Seidel-Morgenstern, H. Schmidt-Traub and G. Guiochon, "Effect of the homogeneity of the column set on the performance of a simulated moving bed unit - II. Experimental study." Journal of Chromatography A 944(1-2), 3-22, (2002).

Miller, L., C. Orihuela, R. Fronek, D. Honda and O. Dapremont, "Chromatographic resolution of the enantiomers of a pharmaceutical intermediate from the milligram to the kilogram scale." Journal of Chromatography A 849(2), 309-317, (1999).

Minceva, M. and A. E. Rodrigues, "Modeling and simulation of a simulated moving bed for the separation of *p*-xylene." Industrial and Engineering Chemistry Research 41(14), 3454-3461, (2002).

Minceva, M. and A. E. Rodrigues, "Influence of the transfer line dead volume on the performance of an industrial scale simulated moving bed for *p*-xylene separation." Separation Science and Technology 38(7), 1463-1497, (2003).

Minceva, M. and A. E. Rodrigues, "Two-level optimization of an existing SMB for *p*-xylene separation." Computers and Chemical Engineering 29(10), 2215-2228, (2005).

Minceva, M. and A. E. Rodrigues, "Understanding and revamping of industrial scale SMB units for *p*-xylene separation." AIChE Journal 53(1), 138-149, (2007).

Minceva, M., P. Sá Gomes, V. Meshko and A. E. Rodrigues, "Simulated moving bed reactor for isomerization and separation of *p*-xylene." Chemical Engineering Journal 140(1-3), 305-323, (2008).

Morbidelli, M., A. Servida, G. Storti and S. Carrà, "Simulation of multicomponent adsorption beds. Model analysis and numerical solution." Industrial and Engineering Chemistry Fundamentals 21(2), 123-131, (1982).

Morbidelli, M., G. Storti, S. Carrà , G. Niederjaufner and A. Pontoglio, "Study of a separation process through adsorption of molecular sieves. Application to a chlorotoluene isomers mixture." Chemical Engineering Science 39(3), 383-393, (1984).

Mota, J. P. B. and J. M. M. Araüjo, "Single-column simulated-moving-bed process with recycle lag." AIChE Journal 51(6), 1641-1653, (2005).

Mota, J. P. B., J. M. M. Araüjo and R. C. R. Rodrigues, "Optimal design of simulated moving-bed processes under flow rate uncertainty." AIChE Journal 53(10), 2630-2642, (2007a).

Mota, J. P. B. and I. A. A. C. Esteves, "Optimal design and experimental assessment of time-variable simulated moving bed for gas separation." Industrial and Engineering Chemistry Research 46(21), 6978-6988, (2007).

Mota, J. P. B., I. A. A. C. Esteves and M. F. J. Eusébio, "Synchronous and asynchronous SMB processes for gas separation." AIChE Journal 53(5), 1192-1203, (2007b).

Müller-Späth, T., L. Aumann, L. Melter, G. Ströhlein and M. Morbidelli, "Chromatographic separation of three monoclonal antibody variants using multicolumn countercurrent solvent gradient purification (MCSGP)." Biotechnology and bioengineering 100(6), 1166-1177, (2008).

Mun, S., "Enhanced separation performance of the simulated moving bed process with two raffinate and two extract products." Journal of Chemical Engineering of Japan 39(10), 1054-1056, (2006).

Mun, S. and N.-H. L. Wang, "Optimization of productivity in solvent gradient simulated moving bed for paclitaxel purification." Process Biochemistry 43(12), 1407-1418, (2008a).

Mun, S. and N. H. L. Wang, "Optimization of productivity in solvent gradient simulated moving bed for paclitaxel purification." Process Biochemistry 43(12), 1407-1418, (2008b).

Mun, S., N. H. L. Wang, Y. M. Koo and S. C. Yi, "Pinched wave design of a four-zone simulated moving bed for linear adsorption systems with significant mass-transfer effects." Industrial and Engineering Chemistry Research 45(21), 7241-7250, (2006).

Mun, S., Y. Xie, J. H. Kim and N. H. L. Wang, "Optimal design of a size-exclusion tandem simulated moving bed for insulin purification." Industrial and Engineering Chemistry Research 42(9), 1977-1993, (2003a).

Mun, S., Y. Xie and N. H. L. Wang, "Robust pinched-wave design of a size-exclusion simulated moving-bed process for insulin purification." Industrial and Engineering Chemistry Research 42(13), 3129-3143, (2003b).

Nagamatsu, S., K. Murazumi and S. Makino, "Chiral separation of a pharmaceutical intermediate by a simulated moving bed process." Journal of Chromatography A 832(1-2), 55-65, (1999).

Natarajan, S. and J. H. Lee, "Repetitive model predictive control applied to a simulated moving bed chromatography system." Computers and Chemical Engineering 24(2-7), 1127-1133, (2000).

Negawa, M. and F. Shoji, "Optical resolution by simulated moving-bed adsorption technology." Journal of Chromatography 590(1), 113-117, (1992).

Neves, S. B., "Modeling of Adsorption Fixed-bed in Liquid-solid Systems." M.Sc. Thesis, Universidade Federal da Bahia, Brazil, (1995).

Nicolaos, A., L. Muhr, P. Gotteland, R. M. Nicoud and M. Bailly, "Application of equilibrium theory to ternary moving bed configurations (four+four, five+four, eight and nine zones) - I. Linear case." Journal of Chromatography A 908(1-2), 71-86, (2001a).

Nicolaos, A., L. Muhr, P. Gotteland, R. M. Nicoud and M. Bailly, "Application of the equilibrium theory to ternary moving bed configurations (4+4, 5+4, 8 and 9 zones) - II. Langmuir case." Journal of Chromatography A 908(1-2), 87-109, (2001b).

Nicoud, R. M., "The separation of optical isomers by simulated moving bed chromatography (Part I)." Pharmaceutical Technology Europe 11(3), 36-44, (1999a).

Nicoud, R. M., "The separation of optical isomers by simulated moving bed chromatography (Part II)." Pharmaceutical Technology Europe 11(4), 28-34, (1999b).

Nicoud, R. M., G. Fuchs, P. Adam, M. Bailly, E. Kusters, F. D. Antia, R. Reuille and E. Schmid, "Preparative scale enantioseparation of a chiral epoxide: Comparison of liquid chromatography and simulated moving bed adsorption technology." Chirality 5(4), 267-271, (1993).

Nicoud, R. M. and R. E. Majors, "Simulated Moving Bed Chromatography for Preparative Separations." LC-GC Europe 13(12), 887-891, (2000).

Otani, S., S. Akita, T. Iwamura, M. Kanaoka, K. Matsumura, Y. Noguchi, K. Sando, T. Mori, I. Takeuchi, T. Tsuchiya and T. Yamamoto, "Separation Process of Components of Feed Mixture Utilizing Solid Sorbent." U.S. Patent No. 3,761,533, (1973).

Pais, L. M. S., "Chiral Separation by Simulated Moving Bed Chromatography." PhD thesis, University of Porto, (1999).

Pais, L. S., J. M. Loureiro and A. E. Rodrigues, "Modeling, simulation and operation of a simulated moving bed for continuous chromatographic separation of 1,1'-bi-2-naphthol enantiomers." Journal of Chromatography A 769(1), 25-35, (1997a).

Pais, L. S., J. M. Loureiro and A. E. Rodrigues, "Separation of 1,1 prime -bi-2-naphthol enantiomers by continuous chromatography in simulated moving bed." Chemical Engineering Science 52(2), 245-257, (1997b).

Pais, L. S., J. M. Loureiro and A. E. Rodrigues, "Modeling strategies for enantiomers separation by SMB chromatography." AIChE Journal 44(3), 561-569, (1998).

Pais, L. S. and A. E. Rodrigues, "Design of simulated moving bed and Varicol processes for preparative separations with a low number of columns." Journal of Chromatography A 1006(1-2), 33-44, (2003).

Paredes, G. and M. Mazzotti, "Optimization of simulated moving bed and column chromatography for a plasmid DNA purification step and for a chiral separation." Journal of Chromatography A 1142(1 SPEC. ISS.), 56-68, (2007).

Paredes, G., H. K. Rhee and M. Mazzotti, "Design of simulated-moving-bed chromatography with Enriched Extract operation (EE-SMB): Langmuir isotherms." Industrial and Engineering Chemistry Research 45(18), 6289-6301, (2006).

Pedeferri, M., G. Zenoni, M. Mazzotti and M. Morbidelli, "Experimental analysis of a chiral separation through simulated moving bed chromatography." Chemical Engineering Science 54(17), 3735-3748, (1999).

Peper, S., M. Johannsen and G. Brunner, "Preparative chromatography with supercritical fluids. Comparison of simulated moving bed and batch processes." Journal of Chromatography A 1176(1-2), 246-253, (2007).

Peper, S., M. Lubbert, M. Johannsen and G. Brunner, "Separation of ibuprofen enantiomers by supercritical fluid simulated moving bed chromatography." Separation Science and Technology 37(11), 2545-2566, (2002).

Pereira, C. S. M., P. Sá Gomes, G. K. Gandi, V. M. T. M. Silva and A. E. Rodrigues, "Multifunctional reactor for the synthesis of dimethylacetal." Industrial and Engineering Chemistry Research 47(10), 3515-3524, (2008).

Pereira, C. S. M., V. M. T. M. Silva and A. E. Rodrigues, "Fixed Bed Adsorptive Reactor for Ethyl Lactate Synthesis: Experiments, Modelling and Simulation." Separation Science and Technology Accepted, (2009a).

Pereira, C. S. M., M. Zabka, V. M. T. M. Silva and A. E. Rodrigues, "A novel process for the ethyl lactate synthesis in a simulated moving bed reactor (SMBR)." Chemical Engineering Science In Press, (2009b).

Perkins, L. R. and C. J. Geankoplis, "Molecular diffusion in a ternary liquid system with the diffusing component dilute." Chemical Engineering Science 24(7), 1035-1042, (1969).

Pilliod, D. L., K. C. Randall and E. M. Harding, "An adsorption process with on-line adsorbent removal." WO118740, (2006a).

Pilliod, D. L., K. C. Randall and E. M. Harding, "A process for hydrocarbon conversion with on-line solid particulate material removal." WO118739, (2006b).

Porter, M. E. and M. R. Kramer, "Strategy and Society: The Link between Competitive Advantage and Corporate Social Responsibility." Harvard Business Review 84(12), 78-92, (2006).

Porter, M. E. and C. Van der Linde, "Green and Competitive: Ending the Stalemate." Harvard Business Review 73(5), 120-134 (1995).

Rajendran, A., "Equilibrium theory-based design of simulated moving bed processes under reduced purity requirements. Linear isotherms." Journal of Chromatography A 1185(2), 216-222, (2008).

Rajendran, A., G. Paredes and M. Mazzotti, "Simulated moving bed chromatography for the separation of enantiomers." Journal of Chromatography A 1216(4), 709-738, (2009).

Ramachandran, R. and L. H. Dao, "Method of producing unsaturated hydrocarbons and separating the same from saturated hydrocarbons." US Patent 5,365,011, (1994).

Rao, D. P., S. V. Sivakumar, S. Mandal, S. Kota and B. S. G. Ramaprasad, "Novel simulated moving-bed adsorber for the fractionation of gas mixtures." Journal of Chromatography A 1069(1), 141-151, (2005).

Rege, S. U. and R. T. Yang, "Propane/propylene separation by pressure swing adsorption: Sorbent comparison and multiplicity of cyclic steady states." Chemical Engineering Science 57(7), 1139-1149, (2002).

Rodrigues, A. E. Modelling and Simulation in Chemical Engineering: Tools for Process Innovation. ESCAPE-14. Lisbon, Portugal, (2004).

Rodrigues, A. E. and E. C. Beira, "Staged Approach of Percolation Processes - 1." AIChE J 25(3), 416-423, (1979).

Rodrigues, A. E., M. A. Granato, P. Sá Gomes and N. Lamia Propane/propylene Separation: From Molecular Scale to Process. AIChE Annual Meeting. Philadelphia – Pennsylvania USA, (2008a).

Rodrigues, A. E., N. Lamia, C. Grande, L. Wolff, P. Leflaive and D. Leinekugel-Le-Cocq, "Procédé de Séparation du Propylène en Mélange avec du Propane par Adsorption en Lit Mobile Simulé en Phase Gaz ou Liquide utilisant une Zéolithe de type Faujasite 13X comme Solide Adsorbant. ." FR. Patent no. 2 903 981 A1. and INT. Patent WO2008012410 A1., (2006).

Rodrigues, A. E., Z. P. Lu, J. M. Loureiro and L. S. Pais, "Separation of enantiomers of 1a,2,7,7a-tetrahydro-3-methoxynaphtha- (2,3b)-oxirane by liquid chromatography. Laboratory-scale elution chromatography and modelling of simulated moving bed." Journal of Chromatography A 702(1-2), 223-231, (1995).

Rodrigues, A. E. and M. Minceva, "Modelling and simulation in chemical engineering: Tools for process innovation." Computers and Chemical Engineering 29(6), 1167-1183, (2005).

Rodrigues, A. E. and L. S. Pais, "Design of SMB Chiral Separations Units using Concept of Separation Volume." Separation Science and Technology 39(2), 245-270, (2004a).

Rodrigues, A. E. and L. S. Pais, "Design of SMB Chiral Separations Using the Concept of Separation Volume." Separation Science and Technology 39(2), 245-270, (2004b).

Rodrigues, A. E. and V. M. T. M. Silva, "Industrial Process fro Acetals Production in a Simulated Moving Bed Reactor." WO05113476 (2005).

Rodrigues, R. C. R., J. M. M. Araüjo, M. F. J. Eusébio and J. P. B. Mota, "Experimental assessment of simulated moving bed and varicol processes using a single-column setup." Journal of Chromatography A 1142(1), 69-80, (2007a).

Rodrigues, R. C. R., J. M. M. Araüjo and J. P. B. Mota, "Optimal design and experimental validation of synchronous, asynchronous and flow-modulated, simulated moving-bed processes using a single-column setup." Journal of Chromatography A 1162(1), 14-23, (2007b).

Rodrigues, R. C. R., T. J. S. B. Canhoto, J. M. M. Araüjo and J. P. B. Mota, "Two-column simulated moving-bed process for binary separation." Journal of Chromatography A 1180(1-2), 42-52, (2008b).

Ruthven, D. M. "Principles of Adsorption and Adsorption Processes." New York, Wiley, (1984).

Ruthven, D. M. and C. B. Ching, "Counter-current and simulated counter-current adsorption separation processes." Chemical Engineering Science 44(5), 1011-1038, (1989).

Sá Gomes, P., N. Lamia and A. E. Rodrigues, "Design of a gas phase simulated moving bed for propane/propylene separation." Chemical Engineering Science 64(6), 1336-1357, (2009a).

Sá Gomes, P., C. P. Leão and A. E. Rodrigues, "Simulation of true moving bed adsorptive reactor: Detailed particle model and linear driving force approximations." Chemical Engineering Science 62(4), 1026-1041, (2007a).

Sá Gomes, P., M. Minceva, L. S. Pais and A. E. Rodrigues, "Advances in Simulated Moving Bed Chromatographic Separations." Chiral Separation Techniques (Third Edition). S. Dr. Ganapathy: 181-202, (2007b).

Sá Gomes, P., M. Minceva and A. E. Rodrigues Modelling, Simulation and Optimisation of Cyclic Separation Processes. PSE annual meeting 2006. London, U.K., (2006a).

Sá Gomes, P., M. Minceva and A. E. Rodrigues Operation of Simulated Moving Bed in Presence of Adsorbent Ageing. AIChE Annual Meeting. San Francisco, California-USA: 2006, (2006b).

Sá Gomes, P., M. Minceva and A. E. Rodrigues, "Simulated moving bed technology: Old and new." Adsorption 12(5-6), 375-392, (2006c).

Sá Gomes, P., M. Minceva and A. E. Rodrigues Operation of an industrial SMB unit for *p*-xylene separation accounting for adsorbent ageing problems. AIChE Annual Meeting. Salt Lake City, Utah-USA, (2007c).

Sá Gomes, P., M. Minceva and A. E. Rodrigues, "Operation strategies for simulated moving bed in the presence of adsorbent ageing." Separation Science and Technology 42(16), 3555-3591, (2007d).

Sá Gomes, P., M. Minceva and A. E. Rodrigues Adsorbent ageing compensation strategies for industrial scale SMB unit for *p*-xylene separation. DECHEMA Jahrestreffen der ProcessNet-Fachausschüsse Adsorption und Fluidverfahrenstechnik. Bingen-Germany, (2008a).

Sá Gomes, P., M. Minceva and A. E. Rodrigues, "Operation of an industrial SMB unit for *p*-xylene separation accounting for adsorbent ageing problems." Separation Science and Technology 43(8), 1974-2002, (2008b).

Sá Gomes, P. and A. E. Rodrigues, "Outlet Streams Swing (OSS) and MultiFeed operation of simulated moving beds." Separation Science and Technology 42(2), 223-252, (2007).

Sá Gomes, P., M. Zabka, M. Minceva and A. E. Rodrigues Design and Construction of a Lab-Scale Simulated Moving Bed Unit: The FlexSMB-LSRE – from Theory to Practice. Chempor. Braga-Portugal, (2008c).

Sá Gomes, P., M. Zabka, V. M. T. Silva and A. E. Rodrigues Separation of Fine Chemical Species by Means of Continuous Chromatography: The Simulated Moving Bed Technology. AIChE Annual Meeting. Philadelphia – Pennsylvania USA, (2008d).

Sá Gomes, P., M. Zabka, M. Zabkova, M. Minceva and A. E. Rodrigues Modelling and Design Strategies for Lab-Scale SMB Units Accounting for Dead Volumes and Tubing Connections – the FlexSMB-LSRE Unit. AIChE Annual Meeting. Philadelphia – Pennsylvania USA, (2008e).

Sá Gomes, P., M. Zabkova, M. Zabka, M. Minceva and A. Rodrigues, "Separation of Chiral Mixtures in Real SMB Units: the FlexSMB-LSRE®." accepted in AICHE Journal, (2009b).

Santacesaria, E., M. Morbidelli, P. Danise, M. Mercenari and S. Carra, "Separation of xylenes on Y zeolites. 1. Determination of the adsorption equilibrium parameters, selectivities, and mass transfer coefficients through finite bath experiments." Industrial and Engineering Chemistry Process Design and Development 21(3), 440-445, (1982).

Schramm, H., S. Gruner and A. Kienle, "Optimal operation of simulated moving bed chromatographic processes by means of simple feedback control." Journal of Chromatography A 1006(1-2), 3-13, (2003a).

Schramm, H., M. Kaspereit, A. Kienle and A. Seidel-Morgenstern, "Improving simulated moving bed processes by cyclic modulation of the feed concentration." Chemical Engineering and Technology 25(12), 1151-1155, (2002).

Schramm, H., M. Kaspereit, A. Kienle and A. Seidel-Morgenstern, "Simulated moving bed process with cyclic modulation of the feed concentration." Journal of Chromatography A 1006(1-2), 77-86, (2003b).

Seidel-Morgenstern, A., L. C. Keßler and M. Kaspereit, "New developments in simulated moving bed chromatography." Chemical Engineering and Technology 31(6), 826-837, (2008).

Seider, W. D., J. D. Seader and D. R. Lewin "Product and Process Design Principles: Synthesis, Analysis, and Evaluation." Wiley, (2004).

Sereno, C. and A. Rodrigues, "Can steady-state momentum equations be used in modelling pressurization of adsorption beds?" Gas Separation and Purification 7(3), 167-174, (1993).

Silva, V. and A. E. Rodrigues, "Novel process for diethylacetal synthesis." AIChE Journal 51(10), 2752-2768, (2005a).

Silva, V. M. T., M. Minceva and A. E. Rodrigues, "Novel analytical solution for a simulated moving bed in the presence of mass-transfer resistance." Industrial and Engineering Chemistry Research 43(16), 4494-4502, (2004).

Silva, V. M. T. M., "Diethylacetal Synthesis in Simulated Moving Bed Reactor." Ph.D. thesis, University of Porto, (2003).

Silva, V. M. T. M. and A. E. Rodrigues, "Novel process for diethylacetal synthesis." AIChE Journal 51(10), 2752-2768, (2005b).

Siperstein, F. R. and A. L. Myers, "Mixed-gas adsorption." AIChE Journal 47(5), 1141-1159, (2001).

Sivakumar, S. V., "Sharp Separation and Process Intensification in Adsorptive Separation Processes." PhD Thesis, Indian Institute of Technology (2007).

Storti, G., R. Baciocchi, M. Mazzotti and M. Morbidelli, "Design of optimal operating conditions of simulated moving bed adsorptive separation units." Industrial and Engineering Chemistry Research 34(1), 288-301, (1995).

Storti, G., M. Masi, S. Carra and M. Morbidelli, "Optimal design of multicomponent countercurrent adsorption separation processes involving nonlinear equilibria." Chemical Engineering Science 44(6), 1329-1345, (1989a).

Storti, G., M. Masi and M. Morbidelli, "Optimal Design of Simulated Moving Bed Adsorption Separation Units through Detailed Modeling and Equilibrium Theory." Adsorption Science and Technology. A. E. Rodrigues, M. D. LeVan and D. Tondeur. London, Kluwer. 158: 357-381, (1989b).

Storti, G., M. Mazzotti, M. Morbidelli and S. Carra, "Robust design of binary countercurrent adsorption separation processes." AIChE Journal 39(3), 471-492, (1993).

Storti, G., M. Mazzotti, L. Tadeu Furlan, M. Morbidelli and S. Carra, "Performance of a six-port simulated moving-bed pilot plant for vapor-phase adsorption separations." Separation Science and Technology 27(14), 1889-1916, (1992).

Strohlein, G., L. Aumann, M. Mazzotti and M. Morbidelli, "A continuous, counter-current multi-column chromatographic process incorporating modifier gradients for ternary separations." Journal of Chromatography A 1126(1-2), 338-346, (2006).

Strube, J., A. Jupke, A. Epping, H. Schmidt-Traub, M. Schulte and R. Devant, "Design, optimization, and operation of SMB chromatography in the production of enantiomerically pure pharmaceuticals." Chirality 11(5-6), 440-450, (1999).

Subramani, H. J., K. Hidajat and A. K. Ray, "Optimization of reactive SMB and Varicol systems." Computers and Chemical Engineering 27(12), 1883-1901, (2003a).

Subramani, H. J., K. Hidajat and A. K. Ray, "Optimization of simulated moving bed and varicol processes for glucose-fructose separation." Chemical Engineering Research and Design 81(5), 549-567, (2003b).

Tarek, M., R. Kahn and E. C. de Lara, "Modelization of experimental isotherms of n-alkanes in NaX zeolite." Zeolites 15(1), 67-72, (1995).

Teja, A. S. and P. Rice, "Generalized corresponding states method for the viscosities of liquid mixtures." Industrial and Engineering Chemistry Fundamentals 20(1), 77-81, (1981).

Tondeur, D., "Paradigms and paradoxes in modeling adsorption and chromatographic separations." Industrial and Engineering Chemistry Research 34(8), 2782-2788, (1995).

Tondeur, D. and G. Klein, "Multicomponent ion exchange in fixed beds: Constant-separation-factor equilibrium." Industrial and Engineering Chemistry Fundamentals 6(3), 351-361, (1967).

Toumi, A., S. Engell, O. Ludemann-Hombourger, R. M. Nicoud and M. Bailly, "Optimization of simulated moving bed and Varicol processes." Journal of Chromatography A 1006(1-2), 15-31, (2003).

Toumi, A., F. Hanisch and S. Engell, "Optimal operation of continuous chromatographic processes: Mathematical optimization of the VARICOL process." Industrial and Engineering Chemistry Research 41(17), 4328-4337, (2002).

Valery, E. and O. Ludemann-Hombourger, "Method and Device for Separating Fractions of a Mixture." WO2007012750 (A2) (2007).

Valery, E. and C. Morey, "Method and Device for Separating Franctions of a Mixture." EP2024049, (2009).

Van Miltenburg, A., J. Gascon, W. Zhu, F. Kapteijn and J. A. Moulijn, "Propylene/propane mixture adsorption on faujasite sorbents." Adsorption 14(2-3), 309-321, (2008).

Wachter, A. and L. T. Biegler, "On the implementation of an interior-point filter line-search algorithm for large-scale nonlinear programming." Mathematical Programming 106(1), 25-57, (2006).

Wakao, N. and T. Funazkri, "Effect of Fluid Dispersion Coefficients on Particle-to-Fluid Mass Transfer Coefficients in Packed Beds." Chemical Engineering Science 33(10), 1375-1384, (1978).

Wakao, N. and S. Kaguei "Heat and Mass Transfer in Packed Beds." New York, Gordon and Breach, Science Publishers, (1982).

Wang, C., K. U. Klatt, G. Dünnebier, S. Engell and F. Hanisch, "Neural network-based identification of SMB chromatographic processes." Control Engineering Practice 11(8), 949-959, (2003).

Wang, N.-H. L., Y. Xie, S. Mun, J.-H. Kim and B. J. Hritzko, "Insulin Purification Using Simulated Moving Bed Technology." WO0187924 (A2) (2001).

Wankatt, P. C., "Simulated moving bed cascades for ternary separations." Industrial and Engineering Chemistry Research 40(26), 6185-6193, (2001).

Wei, F. and Y. Zhao, "Modeling comparison between novel and traditional feed modes of simulated moving bed." Industrial and Engineering Chemistry Research 47(9), 3200-3206, (2008).

Wilke, C. R. and P. Chang, "Correlation of diffusion coefficients in dilute solutions." AIChE Journal 1(2), 264-270, (1955).

Wongso, F., K. Hidaja and A. K. Ray, "Optimal operating mode for enantioseparation of SB-553261 racemate based on simulated moving bed technology." Biotechnology and Bioengineering 87(6), 704-722, (2004).

Wongso, F., K. Hidajat and A. K. Ray, "Improved performance for continuous separation of 1,1?-bi-2-naphthol racemate based on simulated moving bed technology." Separation and Purification Technology 46(3), 168-191, (2005).

Xie, Y., S. Mun, J. Kim and N. H. L. Wang, "Standing wave design and experimental validation of a tandem simulated moving bed process for insulin purification." Biotechnology Progress 18(6), 1332-1344, (2002).

Xie, Y., D. Wu, Z. Ma and N.-H. L. Wang, "Extended Standing Wave Design Method for Simulated Moving Bed Chromatography: Linear Systems." Ind. Eng. Chem. Res. 39(6), 1993-2005, (2000).

Yagi, S. and D. Kunii, "Studies on Heat Transfer near Wall Surface in Packed Bed " AIChE Journal 6(1), 97-104, (1960).

Yoritomi, T., T. Kezuka and M. moriya, "Method for the Chromatographis Separation of Soluble Components in Feed Solution". U.S. Patent 4,267,054 (1981).

Yoritomi, T., T. Kezuka and M. moriya, "Method for the Chromatographis Separation of Soluble Components in Feed Solution". U.S. Patent 4,379,751 (1983).

Yu, F., "Analysis of *p*-xylene adsorbent deactivation and the countermeasures." Petroleum Refinery Engineering 34(1), 46-48, (2004).

Yu, W. F., K. Hidajat and A. K. Ray, "Modeling, simulation, and experimental study of a simulated moving bed reactor for the synthesis of methyl acetate ester." Industrial & Engineering Chemistry Research 42(26), 6743-6754, (2003a).

Yu, W. F., K. Hidajat and A. K. Ray, "Optimal operation of reactive simulated moving bed and Varicol systems." Journal of Chemical Technology and Biotechnology 78(2-3), 287-293, (2003b).

Zabka, M., P. Sá Gomes and A. E. Rodrigues, "Performance of simulated moving bed with conventional and monolith columns." Separation and Purification Technology 63(2), 324-333, (2008a).

Zabka, M., M. Minceva and A. E. Rodrigues, "Experimental and modeling study of adsorption in preparative monolithic silica column." Chemical Engineering and Processing: Process Intensification 45(2), 150-160, (2006).

Zabka, M., M. Minceva, P. Sá Gomes and A. E. Rodrigues, "Chiral separation of R,S-alpha- tetralol by simulated moving bed." Separation Science and Technology 43(4), 727-765, (2008b).

Zabka, M. and A. E. Rodrigues, "Thermodynamic and kinetic study of adsorption of R,S-alpha-Tetralol enantiomers on the chiral adsorbent CHIRALPAK AD." Separation Science and Technology 42(4), 739-768, (2007).

Zang, Y. and P. C. Wankat, "SMB operation strategy - Partial feed." Industrial and Engineering Chemistry Research 41(10), 2504-2511, (2002a).

Zang, Y. and P. C. Wankat, "Three-zone simulated moving bed with partial feed and selective withdrawal." Industrial and Engineering Chemistry Research 41(21), 5283-5289, (2002b).

Zhang, Y., K. Hidajat and A. K. Ray, "Multi-objective optimization of simulated moving bed and Varicol processes for enantio-separation of racemic pindolol." Separation and Purification Technology In Press, Corrected Proof.

Zhang, Y., K. Hidajat and A. K. Ray, "Enantio-separation of racemic pindolol on 1-acid glycoprotein chiral stationary phase by SMB and Varicol." Chemical Engineering Science 62(5), 1364-1375, (2007).

Zhang, Z., K. Hidajat and A. K. Ray, "Application of simulated countercurrent moving-bed chromatographic reactor for MTBE synthesis." Industrial and Engineering Chemistry Research 40(23), 5305-5316, (2001).

Zhang, Z., K. Hidajat, A. K. Ray and M. Morbidelli, "Multiobjective optimization of SMB and varicol process for chiral separation." AIChE Journal 48(12), 2800-2816, (2002a).

Zhang, Z., M. Mazzotti and M. Morbidelli, "Multiobjective optimization of simulated moving bed and Varicol processes using a genetic algorithm." Journal of Chromatography A 989(1), 95-108, (2003a).

Zhang, Z., M. Mazzotti and M. Morbidelli, "Continuous chromatographie processes with a small number of columns: Comparison of Simulated Moving Bed with Varicol, PowerFeed, and ModiCon." Korean Journal of Chemical Engineering 21(2), 454-464, (2004a).

Zhang, Z. Y., K. Hidajat, A. K. Ray and M. Morbidelli, "Multiobjective optimization of SMB and Varicol process for chiral separation." AIChE Journal 48(12), 2800-2816, (2002b).

Zhang, Z. Y., M. Mazzotti and M. Morbidelli, "PowerFeed operation of simulated moving bed units: changing flow-rates during the switching interval." Journal of Chromatography A 1006(1-2), 87-99, (2003b).

Zhang, Z. Y., M. Morbidelli and M. Mazzotti, "Experimental assessment of PowerFeed chromatography." Aiche Journal 50(3), 625-632, (2004b).

Ziomek, G. and D. Antos, "Stochastic optimization of simulated moving bed process: Sensitivity analysis for isocratic and gradient operation." Computers and Chemical Engineering 29(7), 1577-1589, (2005).

Zwiebel, I., "Fixed bed adsorption with variable gas velocity due to pressure drop." Industrial and Engineering Chemistry Fundamentals 8(4), 803-807, (1969).

ANNEXES

ANNEX I – PSEUDO-SMB: USE OF SMB AND TMB MODEL APPROACHES

In this Annex, the simulation of the Step 2 of a Pseudo-SMB, preformed by means of two modelling approaches: the TMB and SMB modelling strategies, is compared (see Chapter 2).

THE PSEUDO-SMB *MODUS OPERANDI*

The Pseudo-SMB *modus operandi* is based in two major stages: Step 1 and Step 2. During the first step a multicomponent mixture, in this case ternary, is fed to the unit while the intermediary species is being collected in the end of section II as consequence of the introduction of new eluent 1 in section I (Figure A. 1a). The second step operates as a classical SMB, safe the feed is now closed and the only inlet is the eluent 2 stream, also in the beginning of section I (Figure A. 1b), (Mata and Rodrigues, 2001).

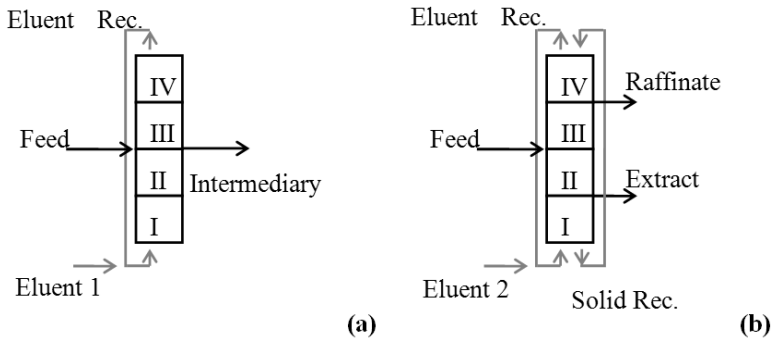

Figure A. 1 - Pseudo-SMB operation scheme (a) during Step 1 and (b) during Step 2.

While Step 1 can be considered as a simple fixed bed, where there is not any solid motion, the second step operates as an SMB unit, and thus can be modelled by means of the two strategies introduced before: the SMB and the TMB model approach (Chapter 2), and hereby compared.

MODELLING STRATEGIES

Step 1 (from 0 to t_{Step1})

During Step 1 the alimentation is performed and the intermediary product is purged as mentioned before leading to the node balances:

Eluent (E) node: $u_I^1 = u_{IV}^1 + u_{E_1}$ (A. 1)

Extract (X) node: $u_{II}^1 = u_I^1$ (A. 2)

Intermediary (It): $u_{It} = u_{II}^1$ (A. 3)

Feed (F) node: $u_{III}^{1} = u_F$ (A. 4)

Raffinate (R) node: $u_{IV}^{1} = u_{III}^{1}$ (A. 5)

And for each species i:

$$j = I: \quad C_{b\,i,IV}\Big|_{x=1} = \frac{u_I^1}{u_{IV}^1} C_{b\,i,I}^{0} - \frac{u_{E_1}}{u_{IV}^1} C_i^E \quad \text{(A. 6)}$$

$$j = III: \quad C_{b\,i,III}^{0} = C_i^F \quad \text{(A. 7)}$$

$$j = II, IV: \quad C_{b\,i,(j-1)}\Big|_{x=1} = C_{b\,i,j}^{0} \quad \text{(A. 8)}$$

with u_j^1 representing the section j Step 1 interstitial velocity.

Within each column, the concentration profiles are simulated by means of the well known fixed bed equations, initial and boundary conditions, similar to those expressed for the LDF approach for each column in the SMB modelling strategy (Chapter 2, eq. 2.63 to eq. 2.68).

Step 2 (from t_{Step1} to t_{Step2})

In the second operation stage (Step 2), the two methodologies mentioned before, the real SMB or the equivalent TMB, can be applied to solve this moving bed procedure, but always respecting the following nodes balances:

Eluent (E) node: $u_I^2 = u_{IV}^2 + u_{E_2}$ (A. 9)

Extract (X) node: $u_{II}^2 = u_I^2 - u_X$ (A. 10)

Feed/Intermediary (F/It) node: $u_{III}^2 = u_{II}^2$ (A. 11)

Raffinate (R) node: $u_{IV}^2 = u_{III}^2 - u_R$ (A. 12)

And for each species i:

$$j = I: \quad C_{b\,i,IV}\Big|_{x=1} = \frac{u_I^2}{u_{IV}^2} C_{b\,i,I}^{0} - \frac{u_{E_2}}{u_{IV}^2} C_i^E \quad \text{(A. 13)}$$

$$j = II, III, IV: \quad C_{b\,i,(j-1)}\Big|_{x=1} = C_{b\,i,j}^{0} \quad \text{(A. 14)}$$

and the LDF based TMB or SMB model approach as mentioned before, Chapter 2: (eq. 2.31 to eq. 2.37) or (eq. 2.63 to eq. 2.68), respectively.

SIMULATION RESULTS

The different model equations were numerically solved using the gPROMS v2.3.6 a commercial package from Process Systems Enterprise. The mathematical models are composed by systems of PDE (Partial Differential Equations), ODE (Ordinary Differential Equations) and AE (Algebraic Equations), that were solved by applying one of the discretization methods available with gPROMS, namely OCFEM (Orthogonal Collocation on Finite Elements) with 2 collocation points per element, 100 elements per column for the axial coordinate. After the axial discretization step, the time integration is performed by the ordinary differential equation solver SRADAU a fully-implicit Runge-Kutta method that implements a variable time step, the resulting system is then solved by the gPROMS BDNSOL (Block decomposition NonLinear SOLver) www.psenterprise.com.

The definitions of extract, intermediary and raffinate purities (PU_X, PU_{It}, PU_R, %), and recovery extract, intermediary and raffinate ports (Rec_X, Rec_{It}, Rec_R, %), of the more, intermediary and less retained components, respectively are stated as follows:

$$PU_X = \frac{\langle C_{b\,A}^{X} \rangle}{\langle C_{b\,A}^{X} \rangle + \langle C_{b\,B}^{X} \rangle + \langle C_{b\,C}^{X} \rangle}, \text{ with } \langle C_{b\,i}^{X} \rangle = \int_{t_{Step1}}^{t_{Step2}} C_{b\,i}^{X} dt \quad \text{(A. 15)}$$

$$PU_{It} = \frac{\langle C_{b\,B}^{It} \rangle}{\langle C_{b\,A}^{It} \rangle + \langle C_{b\,B}^{It} \rangle + \langle C_{b\,C}^{It} \rangle}, \text{ with } \langle C_{b\,i}^{It} \rangle = \int_{0}^{t_{Step1}} C_{b\,i}^{It} dt \quad \text{(A. 16)}$$

$$PU_R = \frac{\langle C_{b\,C}^{R} \rangle}{\langle C_{b\,A}^{R} \rangle + \langle C_{b\,B}^{R} \rangle + \langle C_{b\,C}^{R} \rangle}, \text{ with } \langle C_{b\,i}^{R} \rangle = \int_{t_{Step1}}^{t_{Step2}} C_{b\,i}^{R} dt \quad \text{(A. 17)}$$

$$RE_X = \frac{\int_{t_{Step1}}^{t_{Step2}} u_X C_{b\,A}^{X} dt}{\int_{0}^{t_{Step1}} u_F C_A^F dt} \quad \text{(A. 18)}$$

$$RE_{It} = \frac{\int_{0}^{t_{Step1}} u_{It} C_{b\,B}^{It} dt}{\int_{0}^{t_{Step1}} u_F C_B^F dt} \quad \text{(A. 19)}$$

$$RE_R = \frac{\int_{t_{Step1}}^{t_{Step2}} u_R C_{b\,C}^{R} dt}{\int_{0}^{t_{Step1}} u_F C_C^F dt} \quad \text{(A. 20)}$$

As case study it is considered the separation of a ternary mixture by pseudo-simulated moving bed chromatography, according to the JO process of Japan Organo Co, (Mata and Rodrigues, 2001), caracterized by the following linear adsorption isotherms:

$$q_A^{eq} = 0.65 C_{b\,A} \quad \text{(A. 21)}$$

$$q_B^{eq} = 0.39 C_{b\,B} \quad \text{(A. 22)}$$

$$q_C^{eq} = 0.19 C_{b\,C} \quad \text{(A. 23)}$$

And the unit characteristics as model parameters in Table A. 1.

Table A. 1 – Pseudo - SMB unit characteristics and model parameters.

Model Parameters	SMB Columns
Pe_c=2000	n_j=[3 3 3 3]
ε_b=0.4;	L_c=120x10^{-2} m
k_{LDF}=0.5 s^{-1}	d_c=10.84x10^{-2} m
C_i^F=100 g.l^{-1}	t_{s1}=1090.2 s; t_{s1}=3960 s
Classic SMB Operating Conditions	
t_s=340 s;	
Q_{E_1}=422.9 ml.min^{-1}; Q_{E_2}=451.4 ml.min^{-1};	
Q_F=350.0 ml.min^{-1}; Q_{IV}^*=900.0 ml.min^{-1}	
Q_X=274.0 ml.min^{-1}; . Q_R=177.4 ml.min^{-1};	

The operating conditions during step 1 in Table A. 2.

Table A. 2 - Operating conditions in Step 1.

γ_j^1=[0.990 0.990 0.449 0.449]
Q_j^1=[772.9 772.9 350.0 350.0] ml.min^{-1}

And for the step 2 in Table A. 3.

Table A. 3 - Step 2 classic SMB and equivalent TMB section operating conditions

SMB model approach	TMB model approach
γ_j^*=[1.732 1.381 1.381 1.153]	γ_j =[0.732 0.381 0.381 0.153]
Q_j^*=[1351.5 1077.4 1077.4 900.0] ml.min^{-1}	Q_j =[571.0 297.0 297.0 119.6] ml.min^{-1}
	Q_s =1170.7 ml.min^{-1}

With the TMB model approach to step 2 it is possible to obtain a smooth profile on the outlet streams. This aspect is observed in the intermediary (B) product purge during step 1, as well as for the extract and raffinate fluxes on step 2, as can be observed in Figure A. 2.

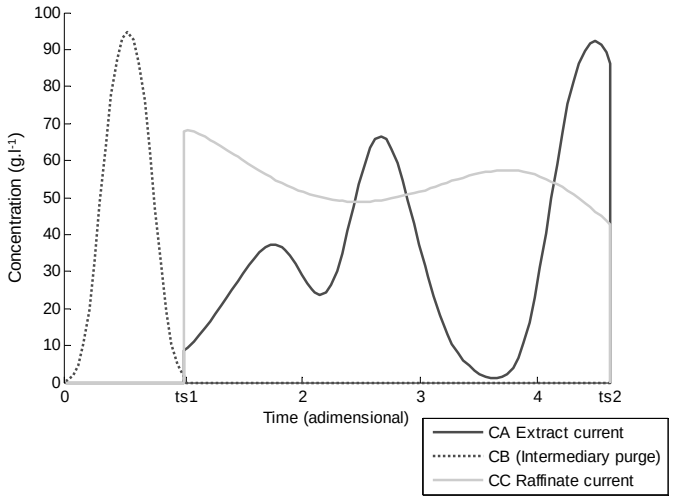

Figure A. 2 - Concentration profiles in the outlet streams, over a complete cycle at cycling steady state (CSS).

While with the SMB model approach a more oscillating history is observed in all the outlet profiles, as can be seen in Figure A. 3.

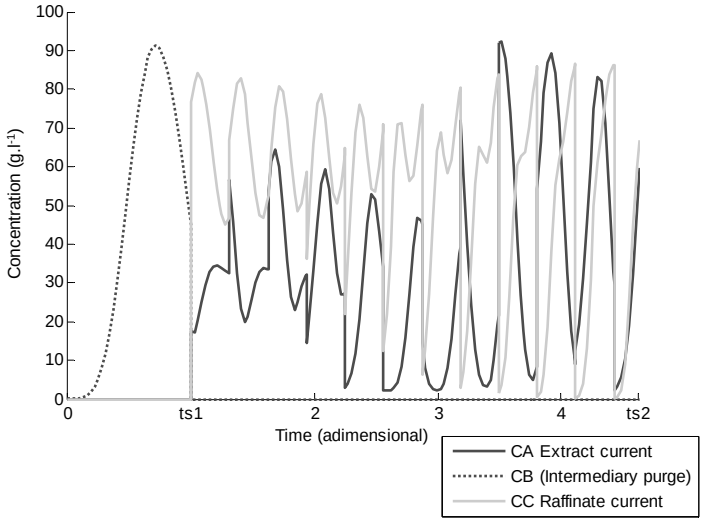

Figure A. 3 - SMB model approach concentration profiles in the outlet streams, over a complete cycle at the CSS.

From Figure A. 3 it is also possible to observe that the last switching time period in step 2 was not complete; therefore, the solid velocity was not completely simulated. One has to remind that in the Pseudo-SMB process we are in the presence of 2 major discontinuities, namely the step 1 and step 2 discontinuity and the switching time discontinuity in step 2. If these two characteristic times are coordinated, *i.e.*, the sum of switching times in step 2 divided by the step 2 time is not an integer, the simulation of the solid movement in step 2 (SMB effect) will not be well experienced.

The averaged values for the concentration profiles in the outlet streams over a complete cycle is presented in Table A.4 and for the TMB in Table A.5 for the SMB model approach.

Table A. 4 - TMB model approach concentrations at the outlet streams.

	Extract	Raffinate	Intermediary Purge
A ($g.l^{-1}$)	35.16	0.00	0.00
B ($g.l^{-1}$)	0.00	0.00	45.28
C ($g.l^{-1}$)	0.00	54.32	0.00

Table A. 5 - SMB model approach concentrations at the outlet streams.

	Extract	Raffinate	Intermediary Purge
A in Extract ($g.l^{-1}$)	33.54	1.28	1.03
B Intermediary Purge ($g.l^{-1}$)	0.16	0.00	45.06
C Raffinate ($g.l^{-1}$)	0.00	54.16	0.12

As can be observed there are some considerable differences between the two methods here-by compared. The contamination is almost inexistent in the TMB model approach while it has been proved to be quite considerable when simulated by the SMB methodology, as can be better stated by the purity and recovery values in the outlet streams, Table A.6 and Table A.7, respectively.

Table A. 6 – Purity values calculated using the Equivalent TMB and Real SMB models.

	Purity (%) TMB model approach	Purity (%) SMB model approach
A in Extract	100.00	99.53
B Intermediary Purge	100.00	97.51
C Raffinate	100.00	97.70

Table A. 7 - Recovery values calculated using the Equivalent TMB and Real SMB models.

	Recovery (%) TMB model approach	Recovery (%) SMB model approach
A in Extract	100.00	95.38
B Intermediary Purge	100.00	99.51
C Raffinate	100.00	99.71

Again it can be noted the difference between the two approaches.

INFLUENCE OF THE NUMBER OF COLUMNS

As mentioned before in Chapter 2, the TMB model approach is more accurate when a large number of columns per section is present. Here it has been shown that, for these operating conditions in this particular system, with 3 columns per section a slight difference is already noted. An additional simulation was performed, changing the number of columns in the SMB model approach from 3 to 1, a large column with length of $3L_c$, giving the possibility to infer something about the influence of the number of columns per section in the step 2.

To this new SMB simulation the same operating conditions, and model parameters, are kept constant, safe the number of columns per section, column length as the switching time, that were changed according to Table A. 8,

Table A. 8 - Values to the Real SMB 1 column per section simulation.

SMB model approach
n_j=[1 1 1 1]
L_c=3x120x10^{-2} m
t_s=3x340 s;

As for the 12 columns case, the concentration profiles in the outlet streams, presents a considerable oscillation when compared with the TMB model approach, but quite less than for the case with 3 columns per section, as can be observed in Figure A. 4.

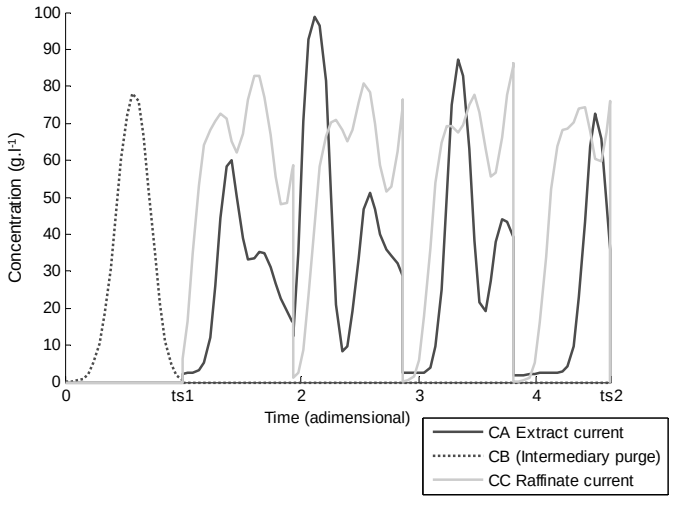

Figure A. 4 – Real SMB concentration profiles in the outlet streams, over a complete cycle at cycling steady state (CSS), in the case of 1 column, with the triple of length, per section a total of 4 columns.

Again it is quite interesting the observation of the average concentration values in the concentration outlets, as presented in Table A. 9, for purity values in Table A.10 and recovery in Table A.11.

Table A. 9 - Real SMB approach concentrations on the outlet streams, case a total of 4 columns.

	Extract	Raffinate	Intermediary Purge
A in Extract ($g.l^{-1}$)	32.22	2.26	1.84
B Intermediary Purge ($g.l^{-1}$)	15.55	0.00	27.77
C Raffinate ($g.l^{-1}$)	0.04	54.15	0.12

Table A. 10 - Purity values calculated using the Real SMB model applied to 4 and 12 columns.

	Purity (%) SMB 4 columns	Purity (%) SMB 12 columns
A in Extract	67.39	99.53
B Intermediary Purge	93.38	97.51
C Raffinate	95.99	97.70

Table A. 11 - Recovery values calculated using the Real SMB model applied to 4 and 12 columns.

	Recovery (%) SMB 4 columns	Recovery (%) SMB 12 columns
A in Extract	91.62	95.38
B Intermediary Purge	61.32	99.51
C Raffinate	99.70	99.71

CONCLUSIONS

Is easy to infer that a smaller number of columns per section will highly reduce the potential of the TMB model approach, presenting a large difference to the reality where the solid motion is being simulated by the inlet/outlet shift to fixed bed columns. As expected, in conformity to the conclusion on the classic SMB field, the TMB model approach, applied here to the second stage of the Pseudo-SMB separation process, is quite limited when a smaller number of columns per section is being used, to simulate the real operation procedure or to operative parameters optimization/studies. Additionally, this problem even get worse, based on the difficulty of the solid velocity being simulated during the step 2, if the length of step 2 is not compatible with a integer number of switching time periods.

ANNEX II – MODELLING OF SMBR UNITS OPERATING UNDER BULK CONDITIONS

In chapter 4 (section 4.4), the model used to describe an SMB for the separation of *p*-xylene from its isomers accounts for velocity variations due to the adsorption (or desorption) rate. This aspect is particularly relevant when operating under bulk (high concentration) conditions, even in liquid phase systems. However, most of the published works concerning the separation (or integrated separation-reaction) in SMB (or SMBR) units, running in liquid state conditions, do not account for this issue and usually the diluted (tracer) conditions models are used, as consequence, quite unrealistic solutions are obtained.

This aspect was detected during this thesis, and based on previous works related with fixed bed simulations either in liquid as gas phase conditions, (Morbidelli *et al.*, 1982; Morbidelli *et al.*, 1984; Malek *et al.*, 1995; Mazzotti *et al.*, 1997a; Chahbani and Tondeur, 2001), the SMB (or SMBR) modelling methodology was revised for the separation of *p*-xylene, synthesis and separation o dimethylacetal and diethylacetal as well as gas phase separation (propane/propylene).

In this annex, the same approach will now be extended for integrated separation-reaction apparatus, with the synthesis of diethylacetal by means of an SMBR unit and some pertinent observations, mainly related with the variation of intraparticle velocity, disclosed.

SYNTHESIS OF DIETHYLACETAL BY MEANS OF AN SMBR UNIT (INTRODUCTIVE NOTE)

The integrated synthesis and separation of acetals by means of the multifunctional reactor SMBR was studied in detail by Silva and Rodrigues and co-workers (Silva, 2003; Silva and Rodrigues, 2005a). These authors promoted the acetalization reaction of acetaldehyde and methanol (or ethanol) to produce dimethylacetal[*] (or diethylacetal[†]) in presence of the ion-exchange resin Amberlyst® 15-wet[‡] (acidic medium):

$$2Methanol/Ethanol\ (A) + Acetaldehyde\ (B) \overset{H^+}{\leftrightarrow} Dimethylacetal/Diethylacetal\ (C) + Water\ (D)$$

By performing such reaction in an SMBR apparatus, and making use the resin's sorption proprieties, it is possible to perform both the separation as the reaction steps in the same unit and by consequence, separate the products from the reaction mixture as they react, increasing the reactant conversion.

SMBR MODEL APPROACH

The system analysed (synthesis and separation of diethylacetal) was presented before (Silva and Rodrigues, 2005b) and is here described in terms of an SMBR model approach, and thus, with periodical shifts of nodes equations which can be represented by the following equations for the period 0 to the first switching time interval,

---

[*] also known as 1,1-dimethoxyethane or DME;

[†] also known as 1,1-diethoxyethane or DEE;

[‡] trade mark from Rohm and Haas Company, Philadelphia, USA; now a subsidiary of Dow Chemical, USA.

Desorbent node: $$C_{b\,i,\left(\sum_{j=I}^{IV} n_j, z=L_{\sum_{j=I}^{IV} n_j}\right)} = \frac{u^*_{(1,z=0)}}{u^*_{\left(\sum_{j=I}^{IV} n_j, z=L_{\sum_{j=I}^{IV} n_j}\right)}} C_{b\,i,(1,z=0)} - \frac{u_{De}}{u^*_{\left(\sum_{j=I}^{IV} n_j, z=L_{\sum_{j=I}^{IV} n_j}\right)}} C_i^{De}$$

(A. 24)

Extract, Raffinate and columns nodes: $$C_{b\,i,(k-1,z=L_k)} = C_{b\,i,(k,z=0)}$$ (A. 25)

Feed node: $$C_{b\,i,(n_I+n_{II},z=L_{n_I+n_{II}})} = \frac{u^*_{(n_I+n_{II}+1,z=0)}}{u^*_{(n_I+n_{II},z=L_{n_I+n_{II}})}} C_{b\,i,(n_I+n_{II}+1,z=0)} - \frac{u_F}{u^*_{(n_I+n_{II},z=L_{n_I+n_{II}})}} C_i^F$$

(A. 26)

and,

Desorbent (De) node: $$u^*_{(1,z=0)} = u^*_{\left(\sum_{j=I}^{IV} n_j, z=L_{\sum_{j=I}^{IV} n_j}\right)} + u_{De}$$ (A. 27)

Extract (X) node: $$u^*_{(n_I+1,z=0)} = u^*_{(n_I,z=L_{n_I})} - u_X$$ (A. 28)

Feed (F) node: $$u^*_{(n_I+n_{II}+1,z=0)} = u^*_{(n_I+n_{II},z=L_{n_I+n_{II}})} + u_F$$ (A. 29)

Raffinate (R) node: $$u^*_{(n_I+n_{II}+n_{III}+1,z=0)} = u^*_{(n_I+n_{II}+n_{III},z=L_{n_I+n_{II}+n_{III}})} - u_R$$ (A. 30)

The remaining columns: $$u^*_{(k,z=0)} = u^*_{(k-1,z=L_{k-1})}$$ (A. 31)

And then by shifting all columns in the direction of the fluid flow.

The mass balance for the component i in the bulk fluid phase in column k can then be described by:

$$\frac{\partial C_{b\,i,k}}{\partial t} = D_{b,k}\frac{\partial^2 C_{b\,i,k}}{\partial z^2} - \frac{\partial\left(C_{b\,i,k}u^*_k\right)}{\partial z} - \frac{(1-\varepsilon_b)}{\varepsilon_b}\frac{3}{r_p}k_{ov\,i}\left(C_{b\,i,k} - \langle C_{p\,i,k}\rangle\right)$$ (A. 32)

And for the particle mass balance for component i:

$$\left(1-\varepsilon_p\right)\frac{\partial q^{eq}_{i,k}}{\partial t} + \varepsilon_p\frac{\partial\langle C_{p\,i,k}\rangle}{\partial t} = \frac{3}{r_p}k_{ov\,i}\left(C_{b\,i,k} - \langle C_{p\,i,k}\rangle\right) + \nu_i\eta\rho_i\Re$$ (A. 33)

With the initial

$$\begin{cases} C_{b\,i,k}(z,0) = 0 \\ \langle C_{p\,i,k}(z,0)\rangle = 0 \\ q_{i,k}(z,0) = 0 \end{cases} \quad i = B, C, D \text{ and } \begin{cases} C_{b\,A,k}(z,0) = \rho_A \\ \langle C_{p\,A,k}(z,0)\rangle = \rho_A \\ q_{A,k}(z,0) \cong q_{m_A} \end{cases}$$ (A. 34)

.and boundary conditions:

$$z = 0: \quad C^0_{b\,i,k} = C_{b\,i,k}\Big|_{z=0} - \frac{D_{b,k}}{u^*_k}\frac{\partial C_{b\,i,k}}{\partial z}\Big|_{z=0} \tag{A. 35}$$

$$z = L_k: \quad \frac{\partial C_{b\,i,k}}{\partial z}\Big|_{z=L_k} = 0 \tag{A. 36}$$

The adsorption equilibrium isotherm defined as:

$$q^{eq}_{i,k} = \frac{q_{m\,i} K_i \langle C_{p\,i,k}\rangle}{1+\sum_{l=1}^{NC} K_l \langle C_{p\,l,k}\rangle} \tag{A. 37}$$

with $l \neq i$ for all species i and in column k, see Table A.13.

Again considering that pressure drops are negligible, $\sum_{i=1}^{NC} \frac{C_{b\,i,k}}{\rho_i} = 1$, one obtains the interstitial fluid velocity by:

$$\frac{du^*_k}{dz} = -\frac{(1-\varepsilon_b)}{\varepsilon_b}\sum_{i=1}^{NC} \frac{\frac{3}{r_p} k_{ov\,i}}{\rho_i}\left(C_{b\,i,k} - \langle C_{p\,i,k}\rangle\right) \tag{A. 38}$$

where, $C_{b\,i,j}$, $\langle C_{p\,i,j}\rangle$, $q^{eq}_{i,j}$ are the bulk, the average pore and the adsorbed concentration, respectively; t is the temporal coordinate, z is the axial coordinate, $k_{ov\,i}$ is the overal mass transfer coefficient (obtained from $\frac{1}{k_{ov\,i}} = \frac{1}{k_{ext\,i}} + \frac{1}{\varepsilon_p k_{int\,i}}$ with $k_{int\,i} = \frac{5\varepsilon_p D_{m\,i}}{\tau r_p}$ and $k_{ext\,i}$ from $Sh_i = \frac{k_{ext\,i} d_p}{D_{m\,i}} = \frac{1.09}{\varepsilon_b}(ScRe)^{\frac{1}{3}}$), ε_b and ε_p the bulk and particle porosities, respectively; r_p is the particle radius (Table A. 12), ν_i the stoichiometric coefficient, η the effectiveness factor of the catalyst, ρ_i the species i density and $\Re$ the reaction rate described in terms of activities $(a_i{}^*)$ by a two-parameters model based on a Langmuir–Hinshelwood rate expression: $\Re = k_c \frac{a_A a_B - \frac{a_C a_D}{K_{eq} a_A}}{(1+K_D a_D)^2}$, where where $k_c(mol.g^{-1}.min^{-1})$ is the reaction kinetic constant defined by $k_c = 3.3 \times 10^{11} e^{-\left(\frac{7824}{T(K)}\right)}$, K_{eq} the equilibrium constant described by $ln(K_{eq}) = \frac{1270}{T(K)} - 3.07$ and measured at the temperature range of 20-60ºC and pressure of 1 MPa, and $K_D = 6.4 \times 10^5 e^{-\left(\frac{4003}{T(K)}\right)}$; as in the literature, (Silva and Rodrigues, 2005b).

[*] Calculated from the UNIFAC method, Silva, V. M. T. M. and A. E. Rodrigues, "Novel process for diethylacetal synthesis." AIChE Journal 51(10), 2752-2768, (2005).

Table A. 12 - Characteristics of the SMB column packed with Amberlyst 15, *(Silva and Rodrigues, 2005b)*.

Length of the Packed bed (L_c)	0.23 m
Internal diameter of the column (d_c)	0.026 m
Radius of the particle (r_p)	400 μm
External void fraction (ε_b)	0.4
Internal void fraction (ε_p)	0.4
Peclet number $\left(\frac{u_j^* L_c}{D_{b_k}}\right)$	300
Bulk density (ρ_b)	390 kg.m^{-3}

Table A. 13 - Adsorption equilibrium parameters, components densities at 293.15 K, (Silva and Rodrigues, 2005b).

Component	q_{m_i} (mol.l$^{-1}_{\text{real solid}}$)	K_i (l.mol^{-1})	Density (kg.m^{-3})
Ethanol (A)	14.3	1.43	795
Acetaldehyde (B)	20.1	1.58	784
Acetal (C)	11.5	0.09	863
Water (D)	44.7	2.01	1003

Considering the following operating conditions, Table A. 14,

Table A. 14 - SMBR operating parameters, (Silva and Rodrigues, 2005b).

Columns and packing parameters			
$n_j = [3\ 3\ 3\ 3]$		C_A^F = 8.53; C_B^F = 8.96 mol.l^{-1}	
SMB operating conditions (measured)			
$Q_I^* =$	44.0 ml.min^{-1}	Eluent	23.5 ml.min^{-1}
$Q_{II}^* =$	27.1 ml.min^{-1}	Extract	16.9 ml.min^{-1}
$Q_{III}^* =$	30.1 ml.min^{-1}	Feed	3.0 ml.min^{-1}
$Q_{IV}^* =$	20.5 ml.min^{-1}	Raffinate	9.6 ml.min^{-1}
t_s =3.50 min			

SIMULATION RESULTS

Using the model, as well as, the parameters and operating conditions stated before, one obtains the following concentration profiles, Figure A. 5.

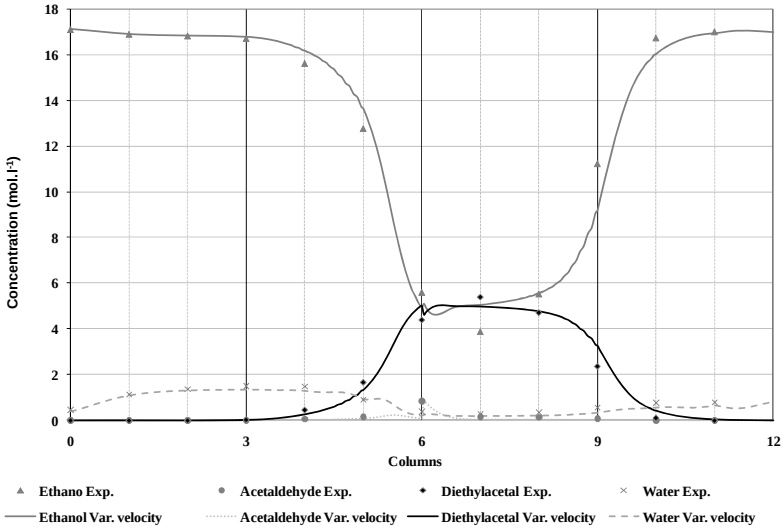

Figure A. 5 - Integrated synthesis and separation of diethylacetal by means of SMBR technology during the 10th cycle, experimental data (Exp.) from (Silva and Rodrigues, 2005b), model with variable velocity.

The experimental data and the simulation results presented in Figure A. 5 are in good agreement and just a slight variation in the velocity profiles is noted, Figure A. 6.

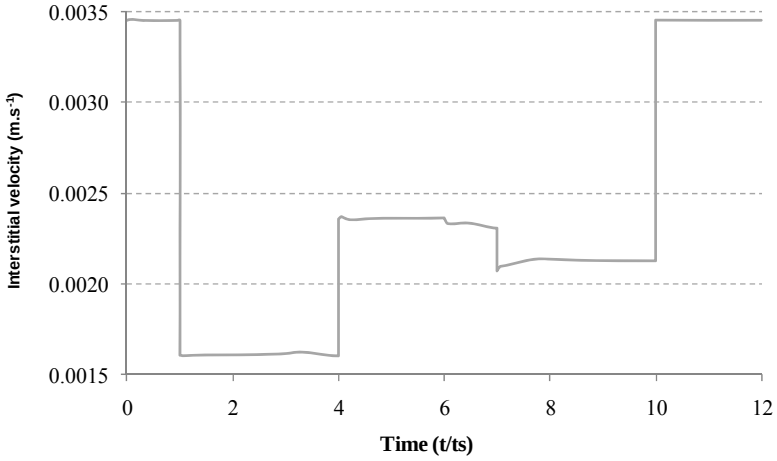

Figure A. 6 - Interstitial velocity history (during the 10th cycle) at half position of column 1.

This reduced velocity variations observed in this case, are mainly related with large amount of ethanol always present in most of the SMBR unit. In addition, one should account for the relation between the different densities that could amplify or amortize the effect of the adsorption volume variation or in this case velocity variation.

Considering a constant velocity, also a reasonable experimental data fitting can be observed, Figure A. 7.

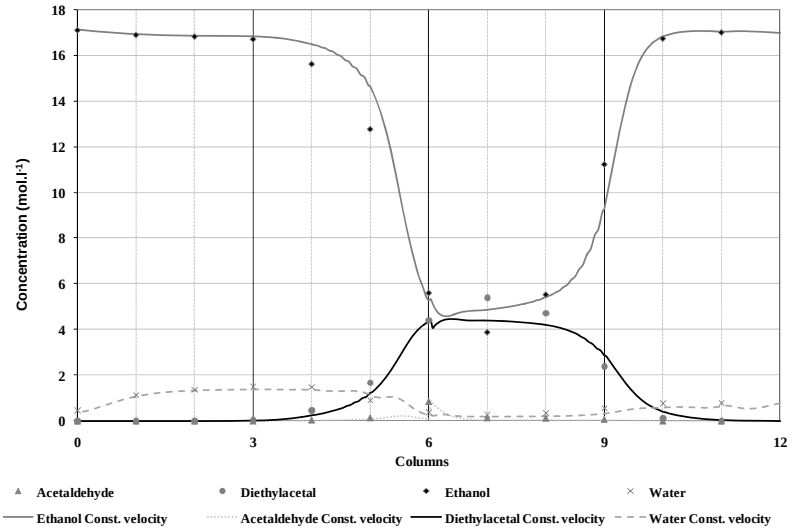

Figure A. 7 - Integrated synthesis and separation of diethylacetal by means of SMBR technology during the 10th cycle, experimental data (Exp.) from (Silva and Rodrigues, 2005b), model with constant velocity.

However, it is important to note that in the case of variable velocity model, the sum of all species concentration, divide by its respective density, at a given position in any time, always respects the Amagat derived equation stated before: $\sum_{i=1}^{NC} \frac{C_{b,i,k}}{\rho_i} = 1$. The same cannot be observed if one considers the constant velocity approach, Figure A. 8.

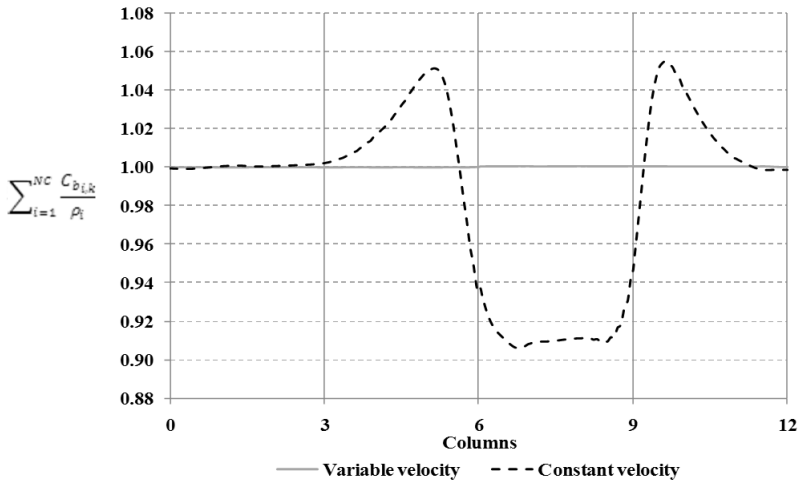

Figure A. 8 - $\sum_{i=1}^{NC} \frac{C_{b_{i,k}}}{\rho_i}$ for constant and variable velocity approaches.

In this bulk system (the integrated synthesis and separation of diethylacetal), the deviations observed from the equation $\sum_{i=1}^{NC} \frac{C_{b_{i,k}}}{\rho_i} = 1$, when using constant velocity assumptions, can go down to -10% and up to +5% of the theoretical value.

CONCLUSIONS

The use of constant velocity approaches, were term $\frac{\partial\left(C_{b_{i,k}}u_k^*\right)}{\partial z}$ is simplified by $u_k^*\frac{\partial\left(C_{b_{i,k}}\right)}{\partial z}$, is quite usual in the SMB as SMBR modelling field. However, it has been proved that this methodology lead to inaccurate results (concentrations without any physical meaning), mainly when dealing with separations (or integrated reaction and separations) processes operated in bulk conditions.

As suggestion of future work, one can think that if the interstitial velocity is changing over the time as consequence of adsorption and reaction rates, the model should in fact be extended for the intraparticle velocity profiles, and thus re-calculate the interstitial velocity in function of these ones*.

* In fact, the use of the simplified formula, $\left(1-\varepsilon_p\right)\frac{\partial q_i^{eq}}{\partial t}+\varepsilon_p\frac{\partial C_{p_i}}{\partial t}=\frac{1}{r^2}\frac{\partial}{\partial r}\left(r^2D_{pe_i}\frac{\partial C_{p_i}}{\partial r}\right)$ when using particle detailed models can lead to some inconvenient results. For instance, considering $D_{pe_{AB}}=D_{pe_{AB}}=D_{pe}$ (a binary system), and $\sum_{i=1}^{NC}\frac{C_{p_i}}{\rho_i}=1$, one will have: $\left(1-\varepsilon_p\right)\frac{\partial\left(q_A^{eq}+q_B^{eq}\right)}{\partial t}+\varepsilon_p\frac{\partial\left(C_{p_A}+\left(1-\frac{C_{p_A}}{\rho_A}\right)\rho_B\right)}{\partial t}=\frac{1}{r^2}\frac{\partial}{\partial r}\left(r^2D_{pe}\ \ \frac{\partial\left(C_{p_A}+\left(1-\frac{C_{p_A}}{\rho_A}\right)\rho_B\right)}{\partial r}\right)$ which in the case of $(\rho_A=\rho_B)$ will lead to: $\frac{\partial\left(q_A^{eq}+q_B^{eq}\right)}{\partial t}=0\ldots$

ANNEX III – VARICOL: COMPARING THE SMB AND TMB MODELING APPROACHES

In Chapter 4, was mentioned that a Varicol unit can be modeled by means of an equivalent TMB unit working with a non integer number of columns per section. In the limit, if one considers a Varicol unit with infinite number of columns and infinite number of sub-switching-intervals within the principal switching time interval, one should find the mentioned TMB unit (with non integer number of columns per section, or differentt columns length).

SMB MODEL APPROACH

To state this approach a Varicol unit was simulated by the real SMB approach (considering all Varicol discontinuities) and compared with an equivalent TMB with non integer number of columns. Thus, let us start to establish the real SMB model approach to the Varicol *modus operandi*. In this model various discontinuities are present, here classified in to categories: (i) with the principal switch, after each switching time all inlet/outlet ports suffer a synchronous shift for a "column length" in the fluid direction; and (ii) with a sub-switch, within each principal switch period selected inlet/outlet ports (located between the variable length sections) suffer an asynchronous shift, either in the fluid or solid direction.

For the nodes equations for period 0 before the first sub-switch interval it becomes:

Desorbent node: $$C_{b\,i,\left(\sum_{j=I}^{IV} n_j, z=L_{\sum_{j=I}^{IV} n_j}\right)} = \frac{u^*_{(1,z=0)}}{u^*_{\left(\sum_{j=I}^{IV} n_j, z=L_{\sum_{j=I}^{IV} n_j}\right)}} C_{b\,i,(1,z=0)} - \frac{u_{De}}{u^*_{\left(\sum_{j=I}^{IV} n_j, z=L_{\sum_{j=I}^{IV} n_j}\right)}} C_i^{De}$$

(A. 39)

Extract, Raffinate and columns nodes: $$C_{b\,i,(k-1,z=L_k)} = C_{b\,i,(k,z=0)}$$ (A. 40)

Feed node: $$C_{b\,i,(n_I+n_{II},z=L_{n_I+n_{II}})} = \frac{u^*_{(n_I+n_{II}+1,z=0)}}{u^*_{(n_I+n_{II},z=L_{n_I+n_{II}})}} C_{b\,i,(n_I+n_{II}+1,z=0)} - \frac{u_F}{u^*_{(n_I+n_{II},z=L_{n_I+n_{II}})}} C_i^F$$

(A. 41)

and,

Desorbent node: $$u^*_{(1,z=0)} = u^*_{\left(\sum_{j=I}^{IV} n_j, z=L_{\sum_{j=I}^{IV} n_j}\right)} + u_{De}$$ (A. 42)

Extract node: $$u^*_{(n_I+1,z=0)} = u^*_{(n_I,z=L_{n_I})} - u_X$$ (A. 43)

Feed node: $$u^*_{(n_I+n_{II}+1,z=0)} = u^*_{(n_I+n_{II},z=L_{n_I+n_{II}})} + u_F$$ (A. 44)

Raffinate node: $$u^*_{(n_I+n_{II}+n_{III}+1,z=0)} = u^*_{(n_I+n_{II}+n_{III},z=L_{n_I+n_{II}+n_{III}})} - u_R$$ (A. 45)

The remaining columns: $u^*_{(k,z=0)} = u^*_{(k-1,z=L_{k-1})}$ (A. 46)

In our case, a Varicol unit working with n_j=[5 7 7 5] from 0 to $0.4t_s$ and n_j=[6 6 7 5] from $0.4t_s$, there is only 1 sub-switch occurring $0.4t_s$ after the principal switch, shifting the extract port in fluid direction. In period 0 after this first sub-switch just equation (A2b) is actualized all the rest remains the ones above.

After the first principal switch Equations (A39) and (A40) become:

Desorbent node: $C_{b\,i,(1,z=L_1)} = \frac{u^*_{(2,z=0)}}{u^*_{(1,z=L_1)}} C_{b\,i,(2,z=0)} - \frac{u_{De}}{u^*_{(1,z=L_1)}} C_i^{De}$ (A. 47)

Extract, Raffinate and columns nodes: $C_{b\,i,(k-1,z=L_k)} = C_{b\,i,(k,z=0)}$ (A. 48)

Feed node:

$$C_{b\,i,\left(n_I+n_{II}+1,z=L_{n_I+n_{II}+1}\right)} = \frac{u^*_{(n_I+n_{II}+2,z=0)}}{u^*_{\left(n_I+n_{II}+1,z=L_{n_I+n_{II}+1}\right)}} C_{b\,i,(n_I+n_{II}+2,z=0)} - \frac{u_F}{u^*_{\left(n_I+n_{II}+1,z=L_{n_I+n_{II}+1}\right)}} C_i^F \quad \text{(A. 49)}$$

and,

Desorbent node: $u^*_{(2,z=0)} = u^*_{(1,z=L_1)} + u_{De}$ (A. 50)

Extract node: $u^*_{(n_I+2,z=0)} = u^*_{(n_I+1,z=L_{n_I+1})} - u_X$ (A. 51)

Feed node: $u^*_{(n_I+n_{II}+2,z=0)} = u^*_{(n_I+n_{II}+1,z=L_{n_I+n_{II}+1})} + u_F$ (A. 52)

Raffinate node: $u^*_{(n_I+n_{II}+n_{III}+2,z=0)} = u^*_{(n_I+n_{II}+n_{III}+1,z=L_{n_I+n_{II}+n_{III}}+1)} - u_R$ (A. 53)

The remaining columns: $u^*_{(k,z=0)} = u^*_{(k-1,z=L_{k-1})}$ (A. 54)

The recycle connection: $u^*_{(k,z=0)} = u^*_{\left(\sum_{j=I}^{IV} n_j, z=L_{\sum_{j=I}^{IV} n_j}\right)}$ (A. 55)

this periodical procedure continues similarly until the complete cycle and then restarts again.

Then performing the species mass balances, considering a convective axial dispersed liquid flux with variable velocity flowing, homogeneous particles with constant radius r_p, constant axial dispersion and intraparticle mass transfer resistances. Negligible pressure drops as negligible thermal effects. It becomes:

for the bulk fluid, in column k:

$$\frac{\partial C_{b\,i,k}}{\partial t} = D_{b,k}\frac{\partial^2 C_{b\,i,k}}{\partial z^2} - \frac{\partial\left(C_{b\,i,k}u_k^*\right)}{\partial z} - \frac{(1-\varepsilon_b)}{\varepsilon_b}k_{i,k}\left(C_{b\,i,k} - \langle C_{p\,i,k}\rangle\right) \quad \text{(A. 56)}$$

And for the particle mass balance for component *i*:

$$\rho_p\frac{\partial q_{i,k}^{eq}}{\partial t} + \varepsilon_p\frac{\partial\langle C_{p\,i,k}\rangle}{\partial t} = k_{i,k}\left(C_{b\,i,k} - \langle C_{p\,i,k}\rangle\right) \quad \text{(A. 57)}$$

With the initial

$$\begin{cases} C_{b\,i,k}(z,0) = 0 \\ \langle C_{p\,i,k}(z,0)\rangle = 0 \quad i = A,B,C,D \\ q_{i,k}(z,0) = 0 \end{cases} \text{ and } \begin{cases} C_{b\,E,k}(z,0) = \rho_E \\ \langle C_{p\,E,k}(z,0)\rangle = \rho_E \\ q_{E,k}(z,0) \cong q_{m_E} \end{cases} \quad \text{(A. 58)}$$

and boundary conditions:

$$z = 0: \quad C_{b\,i,k}^0 = C_{b\,i,k}\Big|_{z=0} - \frac{D_{b,k}}{u_k^*}\frac{\partial C_{b\,i,k}}{\partial z}\Big|_{z=0} \quad \text{(A. 59)}$$

$$z = L_k: \quad \frac{\partial C_{b\,i,k}}{\partial z}\Big|_{z=L_k} = 0 \quad \text{(A. 60)}$$

The adsorption equilibrium isotherm defined as:

$$q_{i,k}^{eq} = f_i\left(C_{p\,i,k}, C_{p\,l,k}\right) \quad \text{(A. 61)}$$

with $l \neq i$ and for all species *i* and in column *k*

$$\sum_{i=1}^{NC}\frac{C_{b\,i,k}}{\rho_i} = 1 \quad \text{(A. 62)}$$

to calculate the interstitial fluid velocity, u_k^*, by means of the total mass balance:

$$\frac{du_k^*}{dz} = -\frac{(1-\varepsilon_b)}{\varepsilon_b}\sum_{i=1}^{NC}\frac{k_{i,k}}{\rho_i}\left(C_{b\,i,j} - \langle C_{p\,i,j}\rangle\right) \quad \text{(A. 63)}$$

SIMULATION RESULTS

With exception to the columns distribution: n_j =[5 7 7 5] from 0 to 0.4t_s and n_j=[6 6 7 5] from 0.4t_s to t_s, and recycle flowrate (Q_{IV}^*=619.93 $m^3.h^{-1}$), the same operating conditions set on section 2.4.2 were used. The *p*-xylene concentration profile in the extract current are presented in Figure A. 23, for outlet concentration in Table A. 22 and Table A. 23.

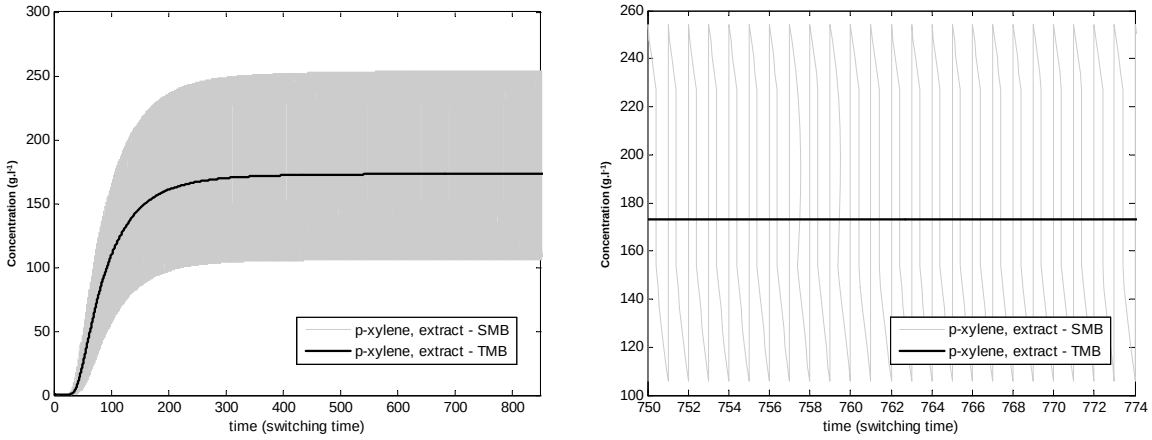

(a) (b)

Figure A. 9 – *p*-xylene concentration profiles in the extract current for Varicol *modus operandi*, modelled by SMB and the equivalent TMB, (a) until cyclic steady state, and (b) the detail over a cycle in the cyclic steady state.

by SMB and the equivalent TMB, (a) until cyclic steady state, and (b) the detail over a cycle in the cyclic steady state.

Table A. 15 - Extract concentrations for the SMB and TMB model approaches to the Varicol.

	Concentration ($g.l^{-1}$)			
	p-xylene	*o*-xylene	*m*-xylene	EB
Varicol-SMB	173.56	0.30	0.08	0.54
Varicol-TMB	173.75	0.27	0.07	0.50
$\frac{C_{b_i}^{SMB}-C_{b_i}^{TMB}}{C_{b_i}^{SMB}}$ (%)	0.11	10.00	12.50	7.41
$\frac{C_{b_i}^{SMB}-C_{b_i}^{TMB}}{C_{b_{p-xylene}}^{SMB}}$ (%)	0.11	0.02	0.01	0.02
PUX^{A}_{TMB} (%)	99.51	PUX^{A}_{SMB} (%)	99.47	

Table A. 16 - Raffinate concentrations for the SMB and TMB model approaches to the Varicol.

	Concentration ($g.l^{-1}$)			
	p-xylene	*o*-xylene	*m*-xylene	EB
Varicol-SMB	3.17	278.11	73.01	78.25
Varicol-TMB	3.02	278.16	73.02	78.28
$\frac{C_{b_i}^{SMB}-C_{b_i}^{TMB}}{C_{b_i}^{SMB}}$ (%)	4.43	-0.02	-0.01	-0.04
$\frac{C_{b_i}^{SMB}-C_{b_i}^{TMB}}{C_{b_{o-xylene}}^{SMB}+C_{b_{m-xylene}}^{SMB}+C_{b_{p-xylene}}^{SMB}}$ (%)	0.03	-0.01	<0.01	-0.01

One should take into account that the observed impurities differences (o-xylene, m-xylene, and EB in the extract current or *p*-xylene in the raffinate one) are not significant, they appear as residuals, as a result it is present a corrected deviation: $\frac{C_{b_i}^{SMB}-C_{b_i}^{TMB}}{C_{b_{p-xylene}}^{SMB}}$ in the extract and $\frac{C_{b_i}^{SMB}-C_{b_i}^{TMB}}{C_{b_{o-xylene}}^{SMB}+C_{b_{m-xylene}}^{SMB}+C_{b_{p-xylene}}^{SMB}}$ in the raffinate current, to better compare both approaches.

CONCLUSIONS

As can be noted, from Table A. 15 and Table A. 16 the results obtained from when modelling a Varicol unit by means of an equivalent TMB unit working with a non integer number of columns per section are quite similar, and in fact the relative deviations noted between the discontinuous (SMB) and continuous (TMB) modelling approaches are near to the ones obtained with classical modes of operation modelled by SMB or equivalent TMB.

ANNEX IV – DESORBENT RECOVERY ANALYSIS IN THE GAS PHASE SMB FOR PROPANE/PROPYLENE SEPARATION

As mentioned in Chapter 5, an SMB separation is only comparable with other technology if considered with its subsequent eluent/desorbent recovery units. In this Annex, one will consider the case of the propane/propylene separation presented before (Chapter 5) and compare the SMB apparatus complemented with two distillation columns (considered for desorbent recovery purposes), with a classic distillation column. In this way, it will be possible to give a brief evaluation of the potential of the SMB technology when transforming a difficult propane/propylene distillation into two easier ones (propane/desorbent and propylene/desorbent distillations).

The distillation processes were chosen for this desorbent recovery analysis, based on its large range of application and considerable number of design methodologies available. In fact, these separation process are recurrent research subjects, and over the years several simulations packages, based in strong thermodynamic database, were developed, allowing straight forward solutions in manageable time. One can make use of such tools to infer about the systems under study and obtain shortcut methodologies that can help in the process design decision making*.

AZEOTROPES SCREENING

One of the main inconvenient, when designing distillation processes, is the existence of azeotropes†. As consequence, one should be aware of this issue and not use, in the case of the SMB based separation, a desorbent that would promote azeotropes with the valuable components to be separated. One way to do it is by performing preliminary studies by means of simulations packages using different thermodynamics data. In this case, 3 desorbents are considered: isobutane, 1-butene and n-butane and using the Aspen split analysis for 1 atm and 10 atm with different thermodynamic packages (In this case, and as example: Peng Robinson and Unifac) one will have the following Aspen Spilt Analysis reports

ASPEN SPLIT ANALYSIS

AZEOTROPE SEARCH REPORT

Physical Property Model: PENG-ROB **Valid Phase:** VAP-LIQ

Mixture Investigated For Azeotropes At A Pressure Of 1 ATM

Comp ID	Component Name	Classification	Temperature
PROPA-01	PROPANE	Saddle	-42,24 C
PROPY-01	PROPYLENE	Unstable Node	-47,94 C
ISOBU-01	ISOBUTANE	Saddle	-11,62 C
1-BUT-01	1-BUTENE	Saddle	-6,36 C
N-BUT-01	N-BUTANE	Stable Node	-0,42 C

No Azeotropes Were Found

* The software Aspen Plus, 2004.1 was used to simulate most of the situations hereby analyzed;

† A composition of two or more liquids in a mixture that cannot be changed by simple distillation.

ASPEN SPLIT ANALYSIS
AZEOTROPE SEARCH REPORT

Physical Property Model: PENG-ROB Valid Phase: VAP-LIQ

Mixture Investigated For Azeotropes At A Pressure Of 10 ATM

Comp ID	Component Name	Classification	Temperature
PROPA-01	PROPANE	Saddle	27,42 C
PROPY-01	PROPYLENE	Unstable Node	19,89 C
ISOBU-01	ISOBUTANE	Saddle	66,92 C
1-BUT-01	1-BUTENE	Saddle	72,28 C
N-BUT-01	N-BUTANE	Stable Node	80,01 C

No Azeotropes Were Found

ASPEN SPLIT ANALYSIS
AZEOTROPE SEARCH REPORT

Physical Property Model: UNIFAC Valid Phase: VAP-LIQ

Mixture Investigated For Azeotropes At A Pressure Of 1 ATM

Comp ID	Component Name	Classification	Temperature
PROPA-01	PROPANE	Saddle	-42,07 C
PROPY-01	PROPYLENE	Unstable Node	-47,65 C
ISOBU-01	ISOBUTANE	Saddle	-11,91 C
1-BUT-01	1-BUTENE	Saddle	-6,28 C
N-BUT-01	N-BUTANE	Stable Node	-0,53 C

No Azeotropes Were Found

ASPEN SPLIT ANALYSIS
AZEOTROPE SEARCH REPORT

Physical Property Model: UNIFAC Valid Phase: VAP-LIQ

Mixture Investigated For Azeotropes At A Pressure Of 10 ATM

Comp ID	Component Name	Classification	Temperature
PROPA-01	PROPANE	Saddle	27,42 C
PROPY-01	PROPYLENE	Unstable Node	19,62 C
ISOBU-01	ISOBUTANE	Saddle	66,83 C
1-BUT-01	1-BUTENE	Saddle	72,40 C
N-BUT-01	N-BUTANE	Stable Node	80,01 C

No Azeotropes Were Found

As can be observed from, the answer is similar for both thermodynamic packages, stating that there are no azeotropes, and calculating similar ebullition temperatures for a given pressure condition.

DESIGN AND SIMULATION

The azeotropes reports, as pure component ebullition temperatures, can give some information on the difficulty of the separation under study, but it will not provide the all picture and thus, one should detail the analysis using short cut distillation design, which in this case was performed by means of the Aspen Plus DSTWU block design, using the Peng Robinson thermodynamic package. The Aspen Plus DSTWU design block will calculate the minimum reflux ratio (Underwood), minimum number of stages (Winn), and either the required reflux ratio for a specified number of stages or the required number of stages for a specified reflux ratio (Gilliland), for a specified recovery of light and heavy key components, feed and operational conditions. In addition, the Aspen

Plus DSTWU design block will also estimate the optimum feed stage location and the condenser and reboiler duties, which can be particularly helpful to compare the different process under study.

The optimization procedure presented before in Chapter 5, just considers the maximization of productivity for a given set of constraints. One of these constraints was in fact the desorbent consumption, Q_D=2.79 $m^3.s^{-1}$, which plays a particular role in the desorbent recovery analysis step. Thus, and at this point, one should redo the optimization procedure but now stating the minimization of the desorbent consumption as the objective function. In a way, this is in no more than a simplistic application of a two-level optimization procedure, but just performed for 2 steps for the sake of simplicity, Table A. 17.

Table A. 17 - Optimization procedure for the minimization of desorbent consumption.

$Fobj = \min(Q_D)$	Constraints	
	Q_F=1.35 $m^3.s^{-1}$	$PU_X \geq$99.50 %
Control Variables	L_c=0.52 m, d_c=1.76 m	$PU_R \geq$99.25 %
Q_{Rec}; Q_X; t_s Q_D	n_j= [2 2 2 2]	$P_1|_{z=n_1 L_c} \leq$45 kPa

Running this optimization in the gPROMS software package led to the solutions presented in Table A. 18.

Table A. 18 – Operating conditions, and column geometry results (underlined) from the optimization procedure (minimization of desorbent consumption).

Columns Geometry	Operating Conditions
L_c = 0.52 m	$T_{T,D}$ = 373 K $P_{T,D}$ = 150 kPa
d_c = 1.76 m	$\underline{t_s = 37.7\ s}$
V_c = 1.26 m^3	Q_F = 1.35 $m^3.s^{-1}$
n_j = [2 2 2 2]	$\underline{Q_X = 2.68\ m^3.s^{-1}}$
	Q_R = 1.19 $m^3.s^{-1}$
	$\underline{Q_D = 2.52\ m^3.s^{-1}}$
	$\underline{Q_{IV} = 0.27\ m^3.s^{-1}}$

From the results obtained in Table A. 18, is now possible to simulate the composition of extract and raffinate currents as their respective dilution factors.

The Aspen Plus DSTWU design block can now be used obtain the relevant parameters from each distillation considered in Figure A. 10.

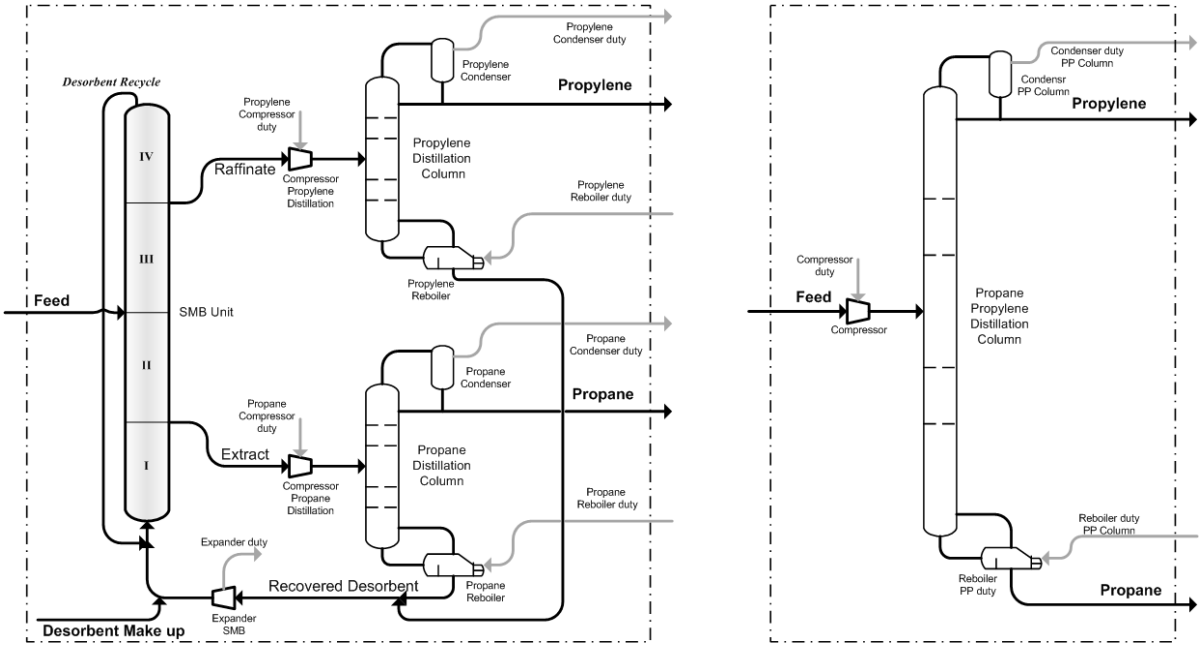

Figure A. 10 - SMB based process as its subsequent desorbent recovery unit and the classic distillation apparatus.

For each configuration (propane/propylene distillation; propane/desorbent distillation and propylene/desorbent distillation) 3 different operating pressures are considered: 1 atm; 5 atm and 10 atm, to provide different performances at different operating pressures. The distillation columns Feed is always at 150 kPa (373 K), and thus for the operation at 5 and 10 atm the compressor duty necessary to increase the feed pressure to 5 and 10 atm was calculated by means of Aspen Plus compressor design block (an efficiency value of 72 % was considered). All distillation columns were simulated for a 99.5 % propane or propylene purity and recovery specification values.

Propane/propylene distillation

Feed

Molar flow rate: 65.14 $mol.s^{-1}$;

Composition: 25 % propane and 75 % propylene, molar fraction;

Conditions: 373 K and 150 kPa.

Results (1 atm)

R_{min}=5.45; N_{min}=49

for N=120 theoretical plates

N_{Feed}=69

Reboiler (heating) required=4297.6 $kJ.s^{-1}$; Condenser (cooling) required=6138.5 $kJ.s^{-1}$

Distillate temperature=225 K; Bottom temperature=231 K

Results (5 atm)

R_{min}=7.40; N_{min}=63

for N=120 theoretical plates

N_{Feed}=68

Reboiler (heating) required=5661.5 kJ.s^{-1}; Condenser (cooling) required=7590.5 kJ.s^{-1}

Distillate temperature=269 K; Bottom temperature=275 K

Compressor duty=357.2 kJ.s^{-1}

Results (10 atm)

R_{min}=9.07; N_{min}=75

for N=120 theoretical plates

N_{Feed}=67

Reboiler (heating) required=7908.4 kJ.s^{-1}; Condenser (cooling) required=9882.0 kJ.s^{-1}

Distillate temperature=293 K; Bottom temperature=300 K

Compressor duty=577.1 kJ.s^{-1}

Propane/Isobutane distillation

Feed

Molar flow rate:57.63 mol.s^{-1};

Composition:27.86 % propane, 0.15 % propylene and 71.99 % isobutane, molar fraction;

Conditions: 373 K and 150 kPa.

Results (1 atm)

R_{min}=5.75; N_{min}=12

for N=60[*] theoretical plates

N_{Feed}=35

Reboiler (heating) required=255.7 kJ.s^{-1}; Condenser (cooling) required=2081.4 kJ.s^{-1}

Distillate temperature=231 K; Bottom temperature=262 K

Results (5 atm)

R_{min}=7.24; N_{min}=17

for N=60 theoretical plates

N_{Feed}=35

Reboiler (heating) required=486.5 kJ.s^{-1}; Condenser (cooling) required=2265.3 kJ.s^{-1}

Distillate temperature=275 K; Bottom temperature=312 K

Compressor duty=307.0 kJ.s^{-1}

Results (10 atm)

R_{min}=8.62; N_{min}=21

for N=60 theoretical plates

[*] For the propane/desorbent or propylene/desorbent distillation steps, 60 theoretical plates (half of the number of plates used for the propane/propylene distillation) were considered. This assumption will represent the worst scenario for the SMB separation approach but will allow, at this stage, a fare comparing between the propane/propylene distillation and SMB approach, by means of heating and cooling duties. A detailed analysis would consider the optimization solutions of both separation strategies.

N_{Feed}=35

Reboiler (heating) required=665.7 kJ.s^{-1}; Condenser (cooling) required=2393.7 kJ.s^{-1}

Distillate temperature=301 K; Bottom temperature=340 K

Compressor duty=488.7 kJ.s^{-1}

Propylene/isobutane distillation

Feed

Molar flow rate: 129.88 mol.s^{-1};

Composition: 0.20 % propane, 37.55 % propylene and 62.25 % isobutane, molar fraction;

Conditions: 373 K and 150 kPa.

Results (1 atm)

R_{min}=3.62; N_{min}=10

for N=60 theoretical plates

N_{Feed}=34

Reboiler (heating) required=194.6 kJ.s^{-1}; Condenser (cooling) required=4196.7 kJ.s^{-1}

Distillate temperature=225 K; Bottom temperature=261 K

Results (5 atm)

R_{min}=4.56; N_{min}=14

for N=60 theoretical plates

N_{Feed}=34

Reboiler (heating) required=569.1 kJ.s^{-1}; Condenser (cooling) required=4524.1 kJ.s^{-1}

Distillate temperature=269 K; Bottom temperature=312 K

Compressor duty=695.5 kJ.s^{-1}

Results (10 atm)

R_{min}=5.43; N_{min}=17

for N=60 theoretical plates

N_{Feed}=34

Reboiler (heating) required=866.3 kJ.s^{-1}; Condenser (cooling) required=4749.4 kJ.s^{-1}

Distillate temperature=293 K; Bottom temperature=340 K

Compressor duty=1110.6 kJ.s^{-1}

Considering now 1-butene as desorbent and the same dilution factors as for the isobutane case, one will have:

Propane/1-butene distillation

Feed

(the same as isobutane case)

Results (1 atm)

R_{min}=5.18; N_{min}=11

for N=60 theoretical plates

N_{Feed}=36

Reboiler (heating) required=107.2 kJ.s^{-1}; Condenser (cooling) required=1894.8 kJ.s^{-1}

Distillate temperature=231 K; Bottom temperature=268 K

Results (5 atm)

R_{min}=6.55; N_{min}=15

for N=60 theoretical plates

N_{Feed}=37

Reboiler (heating) required=303.7 kJ.s^{-1}; Condenser (cooling) required=2064.8 kJ.s^{-1}

Distillate temperature=275 K; Bottom temperature=317 K

Compressor duty=308.9 kJ.s^{-1}

Results (10 atm)

R_{min}=7.82; N_{min}=18

for N=60 theoretical plates

N_{Feed}=37

Reboiler (heating) required=449.0 kJ.s^{-1}; Condenser (cooling) required=2176.4 kJ.s^{-1}

Distillate temperature=301 K; Bottom temperature=345 K

Compressor duty=493.4 kJ.s^{-1}

Propylene/1-butene distillation

Feed

(the same as isobutane case)

Results (1 atm)

R_{min}=3.31; N_{min}=9

for N=60 theoretical plates

N_{Feed}=37

Reboiler (heating) required=19.0 kJ.s^{-1}; Condenser (cooling) required=3909.2 kJ.s^{-1}

Distillate temperature=225 K; Bottom temperature=267 K

Results (5 atm)

R_{min}=4.22; N_{min}=12

for N=60 theoretical plates

N_{Feed}=37

Reboiler (heating) required=303.9 kJ.s^{-1}; Condenser (cooling) required=4225.4 kJ.s^{-1}

Distillate temperature=269 K; Bottom temperature=319 K

Compressor duty=699.5 kJ.s^{-1}

Results (10 atm)

R_{min}=5.03; N_{min}=15

for N=60 theoretical plates

N_{Feed}=36

Reboiler (heating) required=549.9 kJ.s^{-1}; Condenser (cooling) required=4433.4 kJ.s^{-1}

Distillate temperature=293 K; Bottom temperature=345 K

Compressor duty=1121.0 kJ.s^{-1}

Considering now n-butane as desorbent and the same dilution factors as for the isobutane case, one will have:

Propane/n-butane distillation

Feed

(the same as isobutane case)

Results (1 atm)

R_{min}=4.98; N_{min}=9

for N=60 theoretical plates

N_{Feed}=37

Reboiler (heating) required=14.5 kJ.s^{-1}; Condenser (cooling) required=1829.2 kJ.s^{-1}

Distillate temperature=231 K; Bottom temperature=273 K

Results (5 atm)

R_{min}=6.11; N_{min}=13

for N=60 theoretical plates

N_{Feed}=37

Reboiler (heating) required=162.5 kJ.s^{-1}; Condenser (cooling) required=1937.8 kJ.s^{-1}

Distillate temperature=275 K; Bottom temperature=324 K

Compressor duty=306.4 kJ.s^{-1}

Results (10 atm)

R_{min}=7.20; N_{min}=16

for N=60 theoretical plates

N_{Feed}=36

Reboiler (heating) required=298.3 kJ.s^{-1}; Condenser (cooling) required=2010.9 kJ.s^{-1}

Distillate temperature=301 K; Bottom temperature=353 K

Compressor duty=487.4 kJ.s^{-1}

Propylene/n-butane distillation

Feed

(the same as isobutane case)

Results (1 atm)

R_{min}=3.21; N_{min}=8

for N=60 theoretical plates

N_{Feed}=36

Reboiler (heating) required=227.0 kJ.s^{-1}; Condenser (cooling) required=3811.3 kJ.s^{-1}

Distillate temperature=225 K; Bottom temperature=272 K

Results (5 atm)

R_{min}=3.96; N_{min}=11

for N=60 theoretical plates

N_{Feed}=36

Reboiler (heating) required=68.9 kJ.s^{-1}; Condenser (cooling) required=4018.1 kJ.s^{-1}

Distillate temperature=269 K; Bottom temperature=324 K

Compressor duty=694.4 kJ.s^{-1}

Results (10 atm)

R_{min}=4.68; N_{min}=13

for N=60 theoretical plates

N_{Feed}=36

Reboiler (heating) required=305.3 kJ.s^{-1}; Condenser (cooling) required=4159.4 kJ.s^{-1}

Distillate temperature=293 K; Bottom temperature=352 K

Compressor duty=1108.2 kJ.s^{-1}

The number of plates is the same in the different approaches considered, and thus it is possible to compare the reboiler (heating), condenser (cooling) and compression duties, Table A. 19.

Table A. 19 – Reboiler heating, condenser cooling and compressor duties for the distillations steps.

1 atm	distillation	SMB Isobutane	SMB 1-Butene	SMB n-Butane
Reboiler duty (kJ.s^{-1})	4297.6	450.3	126.2	241.5
Condenser duty (kJ.s^{-1})	6138.5	6278.1	5804.0	5640.5
Compressor duty (kJ.s^{-1})	-----	-----	-----	-----
5 atm	distillation	SMB Isobutane	SMB 1-Butene	SMB n-Butane
Reboiler duty (kJ.s^{-1})	5661.5	1055.6	607.6	231.4
Condenser duty (kJ.s^{-1})	7590.5	6789.4	6290.2	5955.9
Compressor duty (kJ.s^{-1})	357.2	1002.5	1008.4	1000.8
10 atm	distillation	SMB Isobutane	SMB 1-Butene	SMB n-Butane
Reboiler duty (kJ.s^{-1})	7908.4	1532.0	998.9	603.6
Condenser duty (kJ.s^{-1})	9882.0	7143.1	6609.8	6170.3
Compressor duty (kJ.s^{-1})	577.1	1599.3	1614.4	1595.6

As can be observed in Table A. 19, by means of the SMB technology it is possible to transform the difficult distillation of propane/propylene into 2 simple ones that will need less reboiler as condenser duties; however, and since the SMB approach deals with diluted streams, the compression needs (in the case of 5 and 10 atm) are considerable higher.

ANNEX V – SMB VALVES DESIGNS (REVIEW)

Usually the SMB valves design is classified according to their outline, *i.e.*, as central or distributed valves arrangement in the SMB unit, (Chin and Wang, 2004).

CENTRAL VALVE DESIGN

In terms of central valves design, the system is typically characterized by a single rotary valve (with a single stator and rotor, the rotor rotates on a single axis, aligning the various ports on the stator and rotor), with complex paths. There are mainly used two types of central rotary valves:

a) UOP single rotary valve design for SMB separations

Developed by Broughton and Gerhold (US Patent 2 985 589, 1961 and with slight differences on US Patents 3 040 777, 3 192 954 and 3 422 848) for UOP LLC (Des Plaines, IL) and earlier included under the Sorbex separation units, Figure A. 11.

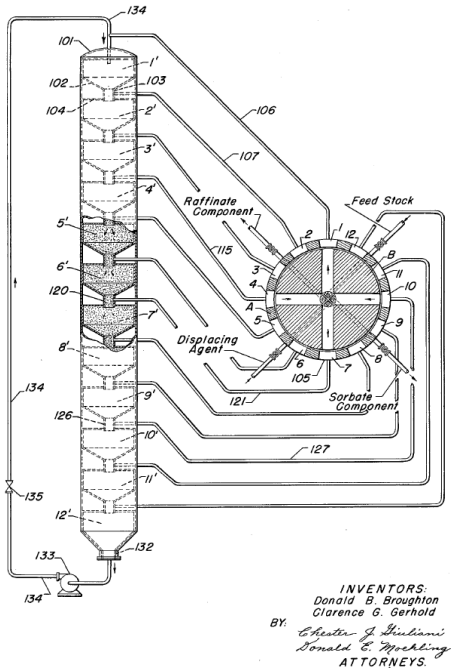

Figure A. 11 - UOP rotary valve, adapted from US Patent 2 985 589.

A system designed for large scale operations (for instance in patent 3 040 777 the rotary valve presents a 12 sq feet area with almost 10 ton weight), making use of the specialized rotary valves design from UOP with various claims on configuration flexibility, maintainability, sealing and reduced valve complexity, but almost impracticable for small scale operations. Later in 1972, de Rosset and Neuzil, also from UOP, with their US patent 3 706 812, adapted the rotary valve concept for laboratory as pilot-scale units, replacing the Broughton downcomer sections fixed for a tee connected to the rotary valve, Figure A. 12.

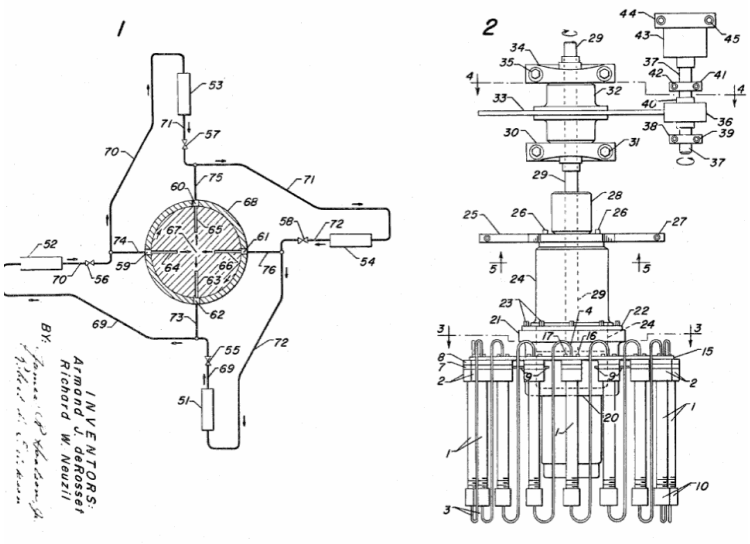

Figure A. 12 - UOP rotary valve – lab-scale use, adapted from US Patent 3 706 812.

Both arrangements results in unused connection lines that will contain solution from the previous switches. As result some flush (or rinse) procedures have been studied and implemented in the industrial units, but still dead volumes problems can be significant for small scale units. The UOP rotary valve design also requires a variable speed recycle pump. The design cannot be easily configured for different columns arrangements nor can operate the new and non-conventional SMB modes, Varicol, by-pass loop etc.

b) ISEP valve

Stands for Ion SEParator by Rossiter and Riley (US Patent 5676 826) from Advanced Separation Technology (Whippany, NJ-USA) now part of Calgon Carbon Corporation, and also sold as part of the CSEP SMB systems from Knauer (Berlin, Germany), as a similar unit sold by Torus B.V. (Haarlem, Netherlands), Figure A. 13.

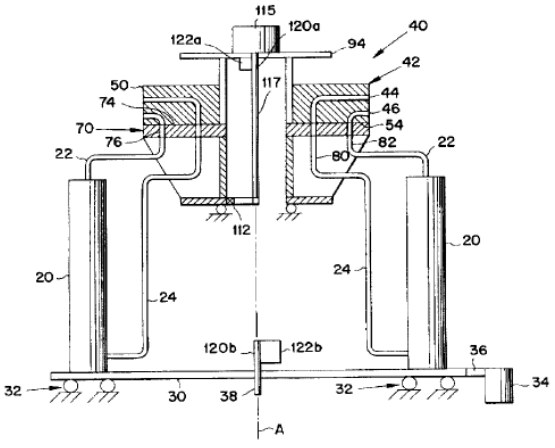

Figure A. 13 - ISEP rotary valve and columns carrousel –adapted from US Patent 5 676 826.

This valve design, uses a carrousel of columns allowing wide configurations flexibility, since any type of streams can be used at every junctions, including open-loop, by-pass and constant speed pumps. Removes the admixing in the tees and cross contamination from the connection lines. It is easy to control and, as the inventors

claim, provides easy scalability, reliability and reasonable low dead volumes. Nevertheless, it cannot perform some of the new or non-conventional SMB operating modes such as Varicol, JO, etc…

Other central valves – Several other central valves design exists (Matonte from Progress Water Technology Corp. (St. Petersburg, FL) US Patent 5 069 883; a two pieces rotary valve as in Berry US Patent 4 808317 or in Morita US Patent 5 478 475 and Oroskar et al WO/2007/038417A2), but not as significant as the previous ones described above.

DISTRIBUTED VALVES DESIGN

The distributed valves SMB configuration use a plurality of generic valves: two-way valves (on-off; with one inlet and one outlet); and/or rotary ones (multiposition valves).

The two-way valves are available in the market with different configurations: ball; gate; knife; needle; globe; butterfly or diaphragm. The rotary valves are also present in several designs: the most common one the SD (Valco Instruments Co. (Houston, TX), designation for Select-Dead-end), with one inlet/outlet and multiple outlets/inlets. A micro electric actuator (or pressure actuated) select a single stream from a number of dead-ended streams and directs it to the valve outlet or vice-versa; The SC (Select-Common-Outlet) allows the no selected streams to share a common outlet instead of being dead-ended; the ST (Select-Trapping), has a single inlet and a single outlet for the selected pair of ports, being the non selected ports dead-ended, the flow is interrupted and trapped in a line, where loops can be attached; switching between loops allow different samples to be removed and analysed. The SMB equipment can function by means of two-way valves only or a combination of rotary with two-ways valves:

a) Two-way valve design

The first publication using a primary two-ways valves switching mechanism for an SMB equipment appears also with de Rosset and Neuzil in US Patent 3 706 812, Figure A. 14,

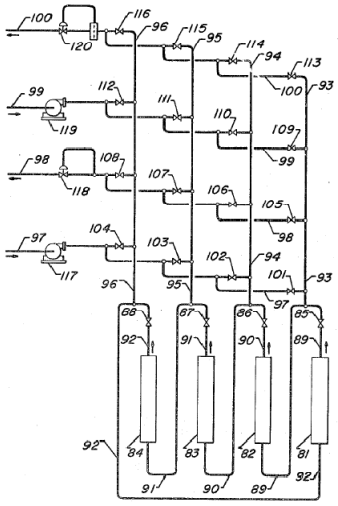

Figure A. 14 – Two-way valve SMB design –adapted from US Patent 3 706 812.

a lab scale unit to support Sorbex technology. An exclusive two-way valves design is presented in Licosep units from Novasep, France. Different designs have been used and patented under different operating modes and

designations: JO process (Masuda US Patent 5 198 120); Odawara US Patent 4 157 267; Yoritomi US Patent 4 379 051; Schoenrock US Patent 4 412 866; US Patent 5 198 120; Hyoky US Patent 5 795 398; Tanimura US Patent 5 556 546; Hotier US Patent 6 017 448; Sterling US Patent 6 375 851 and Ikeda US Patent 6 652 755) or later on in Bisschops WO/2007/043874A1. The contamination on these type of valves arrangement does not occur within the inlet or outlet manifolds, but in the lines between two-way valves and respective tees. Therefore, these lines lengths should be minimized to avoid contamination, or use of contamination rearrangements as in Golem US Patent 4 434 051, valve flushing as in Green US Patent 6 004 518 and in Hotier US Patent 6 017 448. These arrangements possibilities the use of constant speed recycle pump by the addition of two or more two-way valves per column, and the operation of Varicol, or JO processes, by means of a suitable control procedure.

b) One SD valve per stream design

Each column has its one inlet manifold, as well as outlet one, each of these manifolds are connected to the inlet/outlet SD (dead-end flow path) valve, that selects it and as result the corresponding column, Priegnitz US Patent 5 470 464 in 1995, Figure A. 15, and later with Ikeda US Patent 5 770 088, 1998.

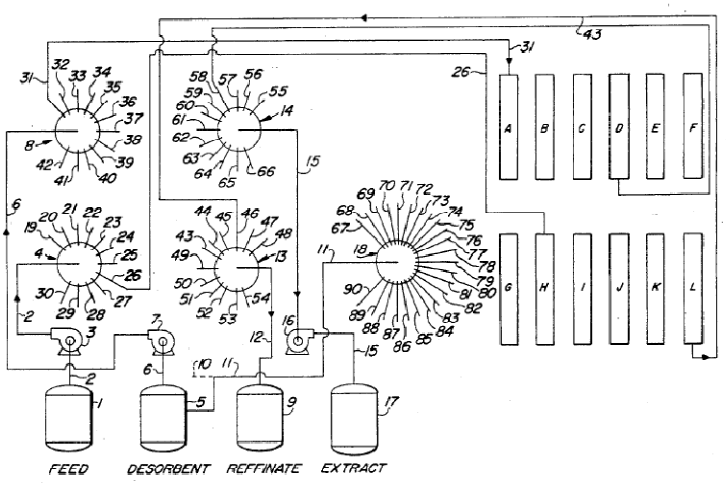

Figure A. 15 – One SD valve per stream SMB design –adapted from US Patent 5 470 464.

This type of SD valves is easy to use, has a moderate cost and is widely available in the market. For the design of SMB units with more zones than the classical operating mode, a extra valve is added for each new zone. This distributed valves design with rotary valves is the one that requires less rotary valves; nevertheless, itcannot perform bypass or open loop operation, unless a two-way is added valve between the outlet and inlet manifold as an additional SD valve per stream. There is admixing at every manifold and dead volumes from previous switching times, reduced by the use of short and thick lines. The classic design requires a variable speed pump, but with two SD valves per stream a constant speed pump can be used.

c) Two SD valve per stream design

A two SD valve per stream design has been presented by Negawa and Shoji in US Patent 5 456 825 from 1995, and Ikeda US Patent 5 770 088 both from Daicel Chemical Industries, Figure A. 16,

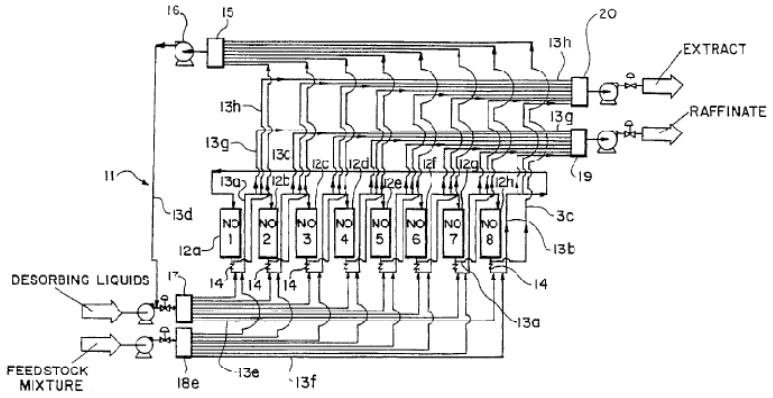

Figure A. 16 – Two SD valve per stream SMB design and constant speed pump for recycle current –adapted from US Patent 5 456 825.

Again in this two SD valve per stream design the contamination and dilution due to the stagnated fluid in the dead lines is considerable and flush procedures as the implementation of short connection lines has to be taken into account. Nevertheless, with this design it is possible to operate JO, Varicol, fast start-up and shutdown, online decoupled zones etc.

Priegnitz (US Patent 5 565 104 of 1996) introduces a variant to the one SD valve per stream, making use of an additional STF valve, that allows to interrupt the flow between columns and passing by a constant speed recycle pump, the outlet of the recycle is controlled by a pressure system to accommodate flow rate fluctuations. Again this design drawback stays in the large amount of stagnated fluid in the dead volume connections.

d) One SD valve per column design

Each SD valve is connected to a column through a tee accessory. The UOP single rotary valve operation in fragmented into multiple SD valves allowing additional columns to be added easily. The number of SMB zones is therefore limited to the number of the SD valve ports. It requires a variable speed recycle pump and is limited to closed loop systems, not being able to performed JO, fast start-up or shutdown nor on-line decoupled zone schemes.

e) One ST valve per column design

With the designation of V-SMB, that stands for Versatile-SMB, Wang *et al.* in US Patent 7 141 172, designed a flexible SMB unit by means of an ST valve per column, that can be understood by simply replacing the zone bypass and input/output lines developed for the two SD valves per column design with the ST rotary valve flow paths. By suitably coordinating the various process lines in the SMB and ST valve, and therefore using fewer valves, operational complexities and dead volumes amount, Figure A. 17.

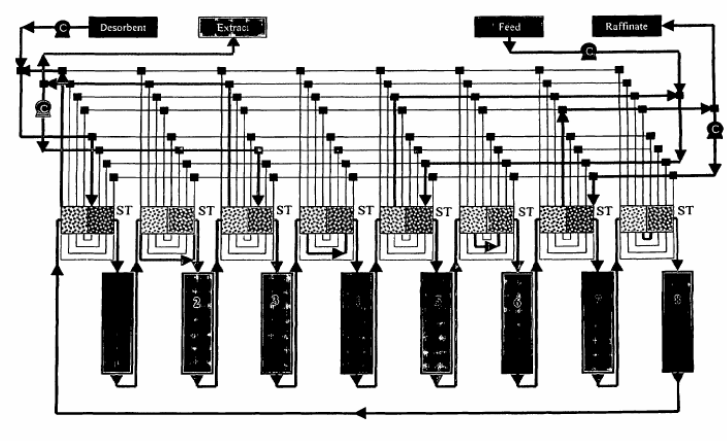

Figure A. 17 – One ST valve per Column SMB design and four constant speed pumps are used with two pumps acting as recycle pumps in section II and IV–adapted from US Patent 5 456 825.

ANNEX VI – FLEXSMB-LSRE® AUTOMATION SCHEME

PUMPS

P1 Eluent Pump

Line	channel	color	signal	function	DAQ Device	DAQ Port	DAQ channel
P1-1	1	black	DI	Stop	Dev-1	P0.0	17
P1-2	2	white	Ground	Gr Stop	Dev-1	Gr	32
P1-3	3	gray	AI	Flow	Dev-1	AO.0	14
P1-4	4	violet	Ground	Gr Flow	Dev-1	Gr	13
P1-5	5	yellow	DO	Error	Dev-1	P0.1	18
P1-6	6	orange	Ground	Gr Error	Dev-1	Gr	32
P1-7	7	red	AO	Pressure	Dev-1	AI.0	2
P1-8	8	brown	Ground	Gr Pressure	Dev-1	Gr	1

P2 Recycle Pump

Line	channel	color	signal	function	DAQ Device	DAQ Port	DAQ channel
P2-1	1	black	DI	Stop	Dev-1	P0.2	19
P2-2	2	white	Ground	Gr Stop	Dev-1	Gr	32
P2-3	3	gray	AI	Flow	Dev-1	AO.1	15
P2-4	4	violet	Ground	Gr Flow	Dev-1	Gr	16
P2-5	5	yellow	DO	Error	Dev-1	P0.3	20
P2-6	6	orange	Ground	Gr Error	Dev-1	Gr	32
P2-7	7	red	AO	Pressure	Dev-1	AI.1	5
P2-8	8	brown	Ground	Gr Pressure	Dev-1	Gr	4

P3 Feed Pump

Line	channel	color	signal	function	DAQ Device	DAQ Port	DAQ channel
P3-1	1	black	DI	Stop	Dev-2	P0.0	17
P3-2	2	white	Ground	Gr Stop	Dev-2	Gr	32
P3-3	3	gray	AI	Flow	Dev-2	AO.0	14
P3-4	4	violet	Ground	Gr Flow	Dev-2	Gr	13
P3-5	5	yellow	DO	Error	Dev-2	P0.1	18
P3-6	6	orange	Ground	Gr Error	Dev-2	Gr	32
P3-7	7	red	AO	Pressure	Dev-2	AI.0	2
P3-8	8	brown	Ground	Gr Pressure	Dev-2	Gr	1

P4 Extract Pump

Line	channel	color	signal	function	DAQ Device	DAQ Port	DAQ channel
P4-1	1	black	DI	Stop	Dev-2	P0.2	19
P4-2	2	white	Ground	Gr Stop	Dev-2	Gr	32
P4-3	3	gray	AI	Flow	Dev-2	AO.1	15
P4-4	4	violet	Ground	Gr Flow	Dev-2	Gr	16
P4-5	5	yellow	DO	Error	Dev-2	P0.3	20
P4-6	6	orange	Ground	Gr Error	Dev-2	Gr	32
P4-7	7	red	AO	Pressure	Dev-2	AI.1	5
P4-8	8	brown	Ground	Gr Pressure	Dev-2	Gr	4

TWO-WAY VALVES

T1 TW valve column 1

Line	channel	color	signal	function	DAQ Device	DAQ Port	DAQ channel
T1-1	1	red	Ground	Gr	Dev-1	Gr	7
T1-2	2	gray	+5 VDC	+5 VDC	---	---	---
T1-3	3	gray	DO	Position A	Dev-1	P0.4	21
T1-4	4	gray	DO	Position B	Dev-1	P0.5	22
T1-5	5	gray	DI	Position A	Dev-1	P0.6	23
T1-6	6	gray	DI	Position B	Dev-1	P0.7	24
---	7	gray	DO	Position A relay contact	---	---	---
---	8	gray	DO	Position A relay contact	---	---	---
---	9	gray	DO	Position B relay contact	---	---	---
---	10	gray	DO	Position B relay contact	---	---	---

T2 TW valve column 2

Line	channel	color	signal	function	DAQ Device	DAQ Port	DAQ channel
T2-1	1	red	Ground	Gr	Dev-1	Gr	7
T2-2	2	gray	+5 VDC	+5 VDC	---	---	---
T2-3	3	gray	DO	Position A	Dev-1	P1.0	21
T2-4	4	gray	DO	Position B	Dev-1	P1.1	22
T2-5	5	gray	DI	Position A	Dev-1	P1.2	23
T2-6	6	gray	DI	Position B	Dev-1	P1.3	24
---	7	gray	DO	Position A relay contact	---	---	---
---	8	gray	DO	Position A relay contact	---	---	---
---	9	gray	DO	Position B relay contact	---	---	---
---	10	gray	DO	Position B relay contact	---	---	---

T3 TW valve column 3

Line	channel	color	signal	function	DAQ Device	DAQ Port	DAQ channel
T3-1	1	red	Ground	Gr	Dev-2	Gr	7
T3-2	2	gray	+5 VDC	+5 VDC	---	---	---
T3-3	3	gray	DO	Position A	Dev-2	P0.4	21
T3-4	4	gray	DO	Position B	Dev-2	P0.5	22
T3-5	5	gray	DI	Position A	Dev-2	P0.6	23
T3-6	6	gray	DI	Position B	Dev-2	P0.7	24
---	7	gray	DO	Position A relay contact	---	---	---
---	8	gray	DO	Position A relay contact	---	---	---
---	9	gray	DO	Position B relay contact	---	---	---
---	10	gray	DO	Position B relay contact	---	---	---

T4 TW valve column 4

Line	channel	color	signal	function	DAQ Device	DAQ Port	DAQ channel
T4-1	1	red	Ground	Gr	Dev-2	Gr	7
T4-2	2	gray	+5 VDC	+5 VDC	---	---	---
T4-3	3	gray	DO	Position A	Dev-2	P1.0	21
T4-4	4	gray	DO	Position B	Dev-2	P1.1	22
T4-5	5	gray	DI	Position A	Dev-2	P1.2	23
T4-6	6	gray	DI	Position B	Dev-2	P1.3	24
---	7	gray	DO	Position A relay contact	---	---	---
---	8	gray	DO	Position A relay contact	---	---	---
---	9	gray	DO	Position B relay contact	---	---	---
---	10	gray	DO	Position B relay contact	---	---	---

T5 TW valve column 5

Line	channel	color	signal	function	DAQ Device	DAQ Port	DAQ channel
T5-1	1	red	Ground	Gr	Dev-3	Gr	25
T5-2	2	gray	+5 VDC	+5 VDC	---	---	---
T5-3	3	gray	DO	Position A	Dev-3	P0.0	17
T5-4	4	gray	DO	Position B	Dev-3	P0.1	18
T5-5	5	gray	DI	Position A	Dev-3	P0.2	19
T5-6	6	gray	DI	Position B	Dev-3	P0.3	20
---	7	gray	DO	Position A relay contact	---	---	---
---	8	gray	DO	Position A relay contact	---	---	---
---	9	gray	DO	Position B relay contact	---	---	---
---	10	gray	DO	Position B relay contact	---	---	---

T6 TW valve column 6

Line	channel	color	signal	function	DAQ Device	DAQ Port	DAQ channel
T6-1	1	red	Ground	Gr	Dev-3	Gr	25
T6-2	2	gray	+5 VDC	+5 VDC	---	---	---
T6-3	3	gray	DO	Position A	Dev-3	P0.4	21
T6-4	4	gray	DO	Position B	Dev-3	P0.5	22
T6-5	5	gray	DI	Position A	Dev-3	P0.6	23
T6-6	6	gray	DI	Position B	Dev-3	P0.7	24
---	7	gray	DO	Position A relay contact	---	---	---
---	8	gray	DO	Position A relay contact	---	---	---
---	9	gray	DO	Position B relay contact	---	---	---
---	10	gray	DO	Position B relay contact	---	---	---

SD VALVES

R1 Multiposition (12) way valve

Line	channel	color	signal	function	DAQ Device	DAQ Port	DAQ channel
R1-1	1	brown	DI	Home	Dev-3	P1.0	27
---	2	red	DO	Motor run	---	---	---
R1-3	3	orange	DI	Step	Dev-3	P1.1	28
---	4	yellow	DO	Error	---	---	---
R1-5	5	green	DI	Manual Direction	Dev-3	P1.2	29
---	6	blue	DO	Direction	---	---	---
---	7	violet	DI	Auto sdirecção	---	---	---
---	8	gray	DI	data latch	---	---	---
---	9	white	DO	+5 VDC 100 ma	---	---	---
R1-10	10	black	Ground	Gr	Dev-3	Gr	32
---	11	brown	DO	80 BCD	---	---	---
R1-12	12	red	DO	8 BCD	Dev-3	P1.3	30
---	13	orange	DO	40 BCD	---	---	---
R1-14	14	yellow	DO	4 BCD	Dev-3	P1.4	6
---	15	green	DO	20 BCD	---	---	---
R1-16	16	blue	DO	2 BCD	Dev-3	P1.5	5
R1-17	17	violet	DO	10 BCD	Dev-3	P1.7	4
R1-18	18	gray	DO	1 BCD	Dev-3	P1.6	3
---	19	white	DI	80 BCD	---	---	---
---	20	black	DI	8 BCD	---	---	---
---	21	brown	DI	40 BCD	---	---	---
---	22	red	DI	4 BCD	---	---	---
---	23	orange	DI	20 BCD	---	---	---
---	24	yellow	DI	2 BCD	---	---	---
---	25	green	DI	10 BCD	---	---	---
---	26	blue	DI	1 BCD	---	---	---

R2 Multiposition (12) way valve

Line	channel	color	signal	function	DAQ Device	DAQ Port	DAQ channel
R2-1	1	brown	DI	Home	Dev-3	P2.0	16
---	2	red	DO	Motor run	---	---	---
R2-3	3	orange	DI	Step	Dev-3	P2.1	15
---	4	yellow	DO	Error	---	---	---
R2-5	5	green	DI	Manual Direction	Dev-3	P2.2	14
---	6	blue	DO	Direction	---	---	---
---	7	violet	DI	Auto sdirecção	---	---	---
---	8	gray	DI	data latch	---	---	---
---	9	white	DO	+5 VDC 100 ma	---	---	---
R2-10	10	black	Ground	Gr	Dev-3	Gr	8
---	11	brown	DO	80 BCD	---	---	---
R2-12	12	red	DO	8 BCD	Dev-3	P2.3	13
---	13	orange	DO	40 BCD	---	---	---
R2-14	14	yellow	DO	4 BCD	Dev-3	P2.4	12
---	15	green	DO	20 BCD	---	---	---
R2-16	16	blue	DO	2 BCD	Dev-3	P2.5	11
R2-17	17	violet	DO	10 BCD	Dev-3	P2.7	9
R2-18	18	gray	DO	1 BCD	Dev-3	P2.6	10
---	19	white	DI	80 BCD	---	---	---
---	20	black	DI	8 BCD	---	---	---
---	21	brown	DI	40 BCD	---	---	---
---	22	red	DI	4 BCD	---	---	---
---	23	orange	DI	20 BCD	---	---	---
---	24	yellow	DI	2 BCD	---	---	---
---	25	green	DI	10 BCD	---	---	---
---	26	blue	DI	1 BCD	---	---	---

R3 Multiposition (12) way valve

Line	channel	color	signal	function	DAQ Device	DAQ Port	DAQ channel
R3-1	1	brown	DI	Home	Dev-4	P0.0	17
---	2	red	DO	Motor run	---	---	---
R3-3	3	orange	DI	Step	Dev-4	P0.1	18
---	4	yellow	DO	Error	---	---	---
R3-5	5	green	DI	Manual Direction	Dev-4	P0.2	19
---	6	blue	DO	Direction	---	---	---
---	7	violet	DI	Auto sdirecção	---	---	---
---	8	gray	DI	data latch	---	---	---
---	9	white	DO	+5 VDC 100 ma	---	---	---
R3-10	10	black	Ground	Gr	Dev-4	Gr	7
---	11	brown	DO	80 BCD	---	---	---
R3-12	12	red	DO	8 BCD	Dev-4	P0.3	20
---	13	orange	DO	40 BCD	---	---	---
R3-14	14	yellow	DO	4 BCD	Dev-4	P0.4	21
---	15	green	DO	20 BCD	---	---	---
R3-16	16	blue	DO	2 BCD	Dev-4	P0.5	22
R3-17	17	violet	DO	10 BCD	Dev-4	P0.7	24
R3-18	18	gray	DO	1 BCD	Dev-4	P0.6	23
---	19	white	DI	80 BCD	---	---	---
---	20	black	DI	8 BCD	---	---	---
---	21	brown	DI	40 BCD	---	---	---
---	22	red	DI	4 BCD	---	---	---
---	23	orange	DI	20 BCD	---	---	---
---	24	yellow	DI	2 BCD	---	---	---
---	25	green	DI	10 BCD	---	---	---
---	26	blue	DI	1 BCD	---	---	---

R4 Multiposition (12) way valve

Line	channel	color	signal	function	DAQ Device	DAQ Port	DAQ channel
R4-1	1	brown	DI	Home	Dev-4	P1.0	27
---	2	red	DO	Motor run	---	---	---
R4-3	3	orange	DI	Step	Dev-4	P1.1	28
---	4	yellow	DO	Error	---	---	---
R4-5	5	green	DI	Manual Direction	Dev-4	P1.2	29
---	6	blue	DO	Direction	---	---	---
---	7	violet	DI	Auto sdirecção	---	---	---
---	8	gray	DI	data latch	---	---	---
---	9	white	DO	+5 VDC 100 ma	---	---	---
R4-10	10	black	Ground	Gr	Dev-4	Gr	32
---	11	brown	DO	80 BCD	---	---	---
R4-12	12	red	DO	8 BCD	Dev-4	P1.3	30
---	13	orange	DO	40 BCD	---	---	---
R4-14	14	yellow	DO	4 BCD	Dev-4	P1.4	6
---	15	green	DO	20 BCD	---	---	---
R4-16	16	blue	DO	2 BCD	Dev-4	P1.5	5
R4-17	17	violet	DO	10 BCD	Dev-4	P1.7	4
R4-18	18	gray	DO	1 BCD	Dev-4	P1.6	3
---	19	white	DI	80 BCD	---	---	---
---	20	black	DI	8 BCD	---	---	---
---	21	brown	DI	40 BCD	---	---	---
---	22	red	DI	4 BCD	---	---	---
---	23	orange	DI	20 BCD	---	---	---
---	24	yellow	DI	2 BCD	---	---	---
---	25	green	DI	10 BCD	---	---	---
---	26	blue	DI	1 BCD	---	---	---

R5 Multiposition (12) way valve					DAQ		
Line	**channel**	**color**	**signal**	**function**	**Device**	**Port**	**channel**
R5-1	1	brown	DI	Home	Dev-4	P2.0	16
---	2	red	DO	Motor run	---	---	---
R5-3	3	orange	DI	Step	Dev-4	P2.1	15
---	4	yellow	DO	Error	---	---	---
R5-5	5	green	DI	Manual Direction	Dev-4	P2.2	14
---	6	blue	DO	Direction	---	---	---
---	7	violet	DI	Auto sdirecção	---	---	---
---	8	gray	DI	data latch	---	---	---
---	9	white	DO	+5 VDC 100 ma	---	---	---
R5-10	10	black	Ground	Gr	Dev-4	Gr	8
---	11	brown	DO	80 BCD	---	---	---
R5-12	12	red	DO	8 BCD	Dev-4	P2.3	13
---	13	orange	DO	40 BCD	---	---	---
R5-14	14	yellow	DO	4 BCD	Dev-4	P2.4	12
---	15	green	DO	20 BCD	---	---	---
R5-16	16	blue	DO	2 BCD	Dev-4	P2.5	11
R5-17	17	violet	DO	10 BCD	Dev-4	P2.7	9
R5-18	18	gray	DO	1 BCD	Dev-4	P2.6	10
---	19	white	DI	80 BCD	---	---	---
---	20	black	DI	8 BCD	---	---	---
---	21	brown	DI	40 BCD	---	---	---
---	22	red	DI	4 BCD	---	---	---
---	23	orange	DI	20 BCD	---	---	---
---	24	yellow	DI	2 BCD	---	---	---
---	25	green	DI	10 BCD	---	---	---
---	26	blue	DI	1 BCD	---	---	---

R6 Multiposition (12) way valve					DAQ		
Line	**channel**	**color**	**signal**	**function**	**Device**	**Port**	**channel**
R6-1	1	brown	DI	Home	Dev-5	P2.0	16
---	2	red	DO	Motor run	---	---	---
R6-3	3	orange	DI	Step	Dev-5	P2.1	15
---	4	yellow	DO	Error	---	---	---
R6-5	5	green	DI	Manual Direction	Dev-5	P2.2	14
---	6	blue	DO	Direction	---	---	---
---	7	violet	DI	Auto sdirecção	---	---	---
---	8	gray	DI	data latch	---	---	---
---	9	white	DO	+5 VDC 100 ma	---	---	---
R6-10	10	black	Ground	Gr	Dev-5	Gr	8
---	11	brown	DO	80 BCD	---	---	---
R6-12	12	red	DO	8 BCD	Dev-5	P2.3	13
---	13	orange	DO	40 BCD	---	---	---
R6-14	14	yellow	DO	4 BCD	Dev-5	P2.4	12
---	15	green	DO	20 BCD	---	---	---
R6-16	16	blue	DO	2 BCD	Dev-5	P2.5	11
R6-17	17	violet	DO	10 BCD	Dev-5	P2.7	9
R6-18	18	gray	DO	1 BCD	Dev-5	P2.6	10
---	19	white	DI	80 BCD	---	---	---
---	20	black	DI	8 BCD	---	---	---
---	21	brown	DI	40 BCD	---	---	---
---	22	red	DI	4 BCD	---	---	---
---	23	orange	DI	20 BCD	---	---	---
---	24	yellow	DI	2 BCD	---	---	---
---	25	green	DI	10 BCD	---	---	---
---	26	blue	DI	1 BCD	---	---	---

FLOW METERS

F1 Flow Meter

Line	channel	color	signal	function		DAQ Device	DAQ Port	DAQ channel
---	1	---	---	---		---	---	---
F1-2	2	green	AO	Flow		---	---	---
---	3	---	AI	Set Point		Dev-1	AI0.6	9
---	4	---	AO	0 VDC		---	---	---
---	5	---	AO	Valve Out		---	---	---
---	6	---	---		---	---	---	---
---	**7**	---	AO	+24 VDC		---	---	---
F1-8	8	white	Ground	Gr		Dev-1	Gr	10

F2 Flow Meter

Line	channel	color	signal	function		DAQ Device	DAQ Port	DAQ channel
---	1	---	---	---		---	---	---
F2-2	2	green	AO	Flow		---	---	---
---	3	---	AI	Set Point		Dev-2	AI0.6	9
---	4	---	AO	0 VDC		---	---	---
---	5	---	AO	Valve Out		---	---	---
---	6	---	---		---	---	---	---
---	**7**	---	AO	+24 VDC		---	---	---
F2-8	8	white	Ground	Gr		Dev-2	Gr	10

ANNEX VII – EXTENDED MODELS FOR DEAD VOLUMES AND SWITCHING TIME ASYMMETRIES: THE LICOSEP 12-26 UNIT

As mentioned before, each SMB unit design has its own particularities that will probably lead to discrepancies between the experimental results and the ones simulated by the most common models. Nevertheless, one can also extend these models by introducing the specific units' design particularities.

MODELLING STRATEGY

This methodology was developed under this thesis scope and applied to the modeling of the Licosep 12-26 unit (Zabka *et al.*, 2008b), where the tubing and equipment dead volumes were introduced in the SMB model and describe by means of an axial dispersive plug flow in a tube, as follows,

$$\frac{\partial C_{i,tb}}{\partial t} = D_{b_{tb}} \frac{\partial^2 C_{i,tb}}{\partial z^2} - v_{tb} \frac{\partial C_{i,tb}}{\partial z} \qquad \text{(A. 64)}$$

Where the $D_{b_{tb}}$ represents the axial dispersion coefficient calculated for a tube of 1 mm *i.d.*, $C_{i,tb}$ the species i concentration in tube tb and v_{tb} the velocity in tube t.

As noted before, the Licosep unit implements a compensation measure to avoid asymmetries due to the dead volume introduced by the recycle pump (Figure A. 18a). Namely, all valves passing the recycle pump are shifted with a delay of $t_D = \frac{V_{L_i}^D}{Q_j^*} t_D = \frac{V_D}{Q_j^*}$, as represented in Figure A. 21b, for the case of 8 columns SMB unit.

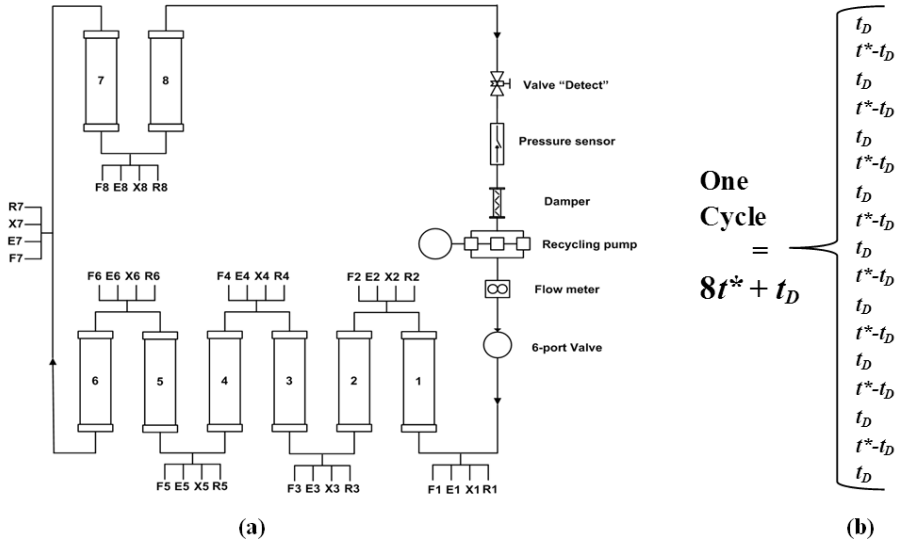

Figure A. 18 – (a) Licosep 12-26 SMB unit scheme and (b) recycle pump compensating strategy for a 8 columns configuration.

SIMULATION RESULTS

This model was applied for the simulation of an SMB chiral epoxide enantiomers separation with microcrystalline cellulose triacetate (see Chapter 2), characterized by the following multicomponent equilibrium isotherms:

$$q_A = 1.35C_A + \frac{7.32\times0.163C_A}{1+0.163C_A+0.087C_B} \quad \text{(A. 65)}$$

$$q_B = 1.35C_A + \frac{7.32\times0.087C_B}{1+0.163C_A+0.087C_B} \quad \text{(A. 66)}$$

In a unit configuration of 2 columns per section, and that run with a t_D 25 % higher than should be need (it would easy to model a unit that is compensating well the dead volumes, but it is quite more difficult to do it with one unit that is compensating more, less than it should), and by these means testing both the dead volumes as well as the compensating strategy procedure, resulting in the following concentration profiles, Figure A. 19.

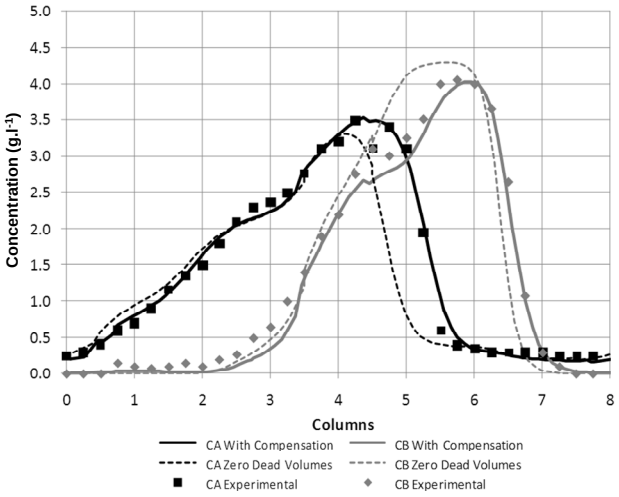

Figure A. 19 – Concentration profiles, experimental and simulated with model presented before (Zero Dead Volumes) and considering both the unit's dead volumes as compensating measure (With Compensation).

The comparison of the experimental and calculated SMB performance parameters using the detailed model, accounting for the unit's dead volumes and recycle pump dead volumes compensation is given in Table A. 20.

Table A. 20 - Purity values for experimental and simulate by mean of the detailed model, accounting for unit's dead volumes and recycle pump dead volumes compensation.

Purity	Experimental	Comp. Simulated
A Extract	90.00%	96.95%
B Raffinate	91.60%	89.08%

As can be noted from Figure A19 and Table A20 the model gives reasonable prediction of the experimental data.

From the scheme in Figure A1b, it is possible to note that the asynchronous shifting measure used to compensate the recycle pump dead volume, results in a global switching time increase, over a complete cyclic. By simulating now the Licosep SMB unit running without compensation (still with the same dead volumes as presented before), with the same operating parameters but with corrected switching time:

$$t_s|_{Licosep} = t_s|_{SMB} + \frac{V_{L_i}^D}{Q_j^*}\frac{1}{\sum_{j=I}^{IV} n_j} \qquad \text{(A. 67)}$$

The experimental and calculated SMB concentration profiles using the asynchronous and switching time compensation strategy are presented in Figure A. 20.

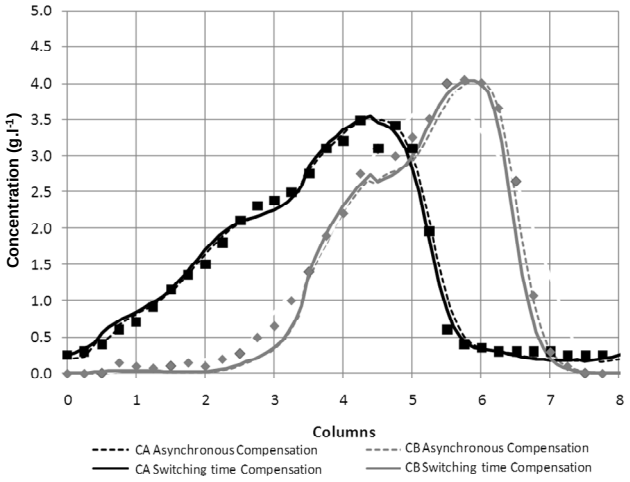

Figure A. 20 - Concentration profiles, experimental and simulated using the asynchronous and switching time compensation strategies.

The product purity values obtained by the Asynchronous and Switching time compensation strategy are presented in Table A. 21.

Table A. 21 - Purity values for simulate results obtained by the two different compensation strategies: Asynchronous and Switching time.

Purity	Switching Time	Asynchronous
A Extract	97.08%	96.95%
B Raffinate	89.61%	89.08%

As can be observed from Figure A20 and Table A21, the two strategies converged to the same, and therefore we will use the switching time compensating strategy, avoiding several problems related with the hereby-called asynchronous compensating strategy.

ANNEX VIII - SAMPLE COLLECTOR TIMES AND INTERNAL CONCENTRATION PROFILES COLLOCATION PROCEDURE

To construct the internal concentration profile for a given FlexSMB-LSRE® experiment (for instance an 18 points profile, 3 samples per column), twelve samples (1-3; 7-12; 13-15) are collected by means of a 6 ports injection valve (Knauer GmbH, Germany) installed between column 6 and column 1.

The remaining 6 points are collected directly from the extract and raffinate ports, (16-18) and (4-6) respectively; as consequence these samples can be delayed or placed with an incremental space in the abscissa profiles (dependent of the extract and raffinate flow rates, in this case is considered a 0.2 columns length delay).

These points are then related to its abscissa by the relation expressed in Table A. 22.

Table A. 22 - Relation between the times of withdraw of sample and the internal concentration profile abscissa.

No. Sample	(1)	(2)	(3)	(4)	(5)	(6)
Time in cycle	$t_s/_4$	$t_s/_2$	$3t_s/_4$	$t_s + t_s/_4$	$t_s + t_s/_2$	$t_s + 3t_s/_4$
Abscissa	0.25	6	5.75	5.25 (+0.2)	5 (+0.2)	4.75 (+0.2)
No. Sample	(7)	(8)	(9)	(10)	(11)	(12)
Time in cycle	$2t_s + t_s/_4$	$2t_s + t_s/_2$	$2t_s + 3t_s/_4$	$3t_s + t_s/_4$	$2t_s + t_s/_2$	$3t_s + 3t_s/_4$
Abscissa	4.25	4	3.75	3.25	3	2.75
No. Sample	(13)	(14)	(15)	(16)	(17)	(18)
Time in cycle	$4t_s + t_s/_4$	$4t_s + t_s/_2$	$4t_s + 3t_s/_4$	$5t_s + t_s/_4$	$5t_s + t_s/_2$	$5t_s + 3t_s/_4$
Abscissa	2.25	2	1.75	1.25 (+0.2)	1 (+0.2)	0.75 (+0.2)

ANNEX IX – OSS ANALYTICAL PROCEDURE: CALIBRATION CURVE

All the analyses concerning the OSS experiments (and similarly the Classical and asynchronous SMB experiments, see Chapter 6), were performed by means of an HPLC system, which includes a Smartline 1000 LC pump, UV detector model Smartline 2500, LPG block and degasser (Knauer, Germany). The detector was set at of 270 nm and a Rheodyne injection valve with a 10 µL sample loop was loaded manually using a syringe. Clarity (DataApex, Ltd., 2004) software was used for data acquisition and HPLC control. The analytical was column (250 mm×4.6 mm I.D.) packed with Chiralpak IB: cellulose tris (3,5 dimethylphenylcarbamate immobilized onto 5 µm silica-gel), supplied by Chiral Technologies Europe (France) was used. GC-grade organic solvents *n*-heptane and ethanol (EtOH) were obtained from Sigma-Aldrich Chemie, Germany. The antitussive drug guafeinesin was dissolved in the mobile phase which was always degassed and filtrated through a 0.2 µm, 50 mm I.D. NL 16-membrane filter (Schleicher & Schuell, Germany) before use. The mobile phase, for the OSS experiments was *n*-heptane/ethanol (85/15 %, v/v), and the standards in Table A. 23 were used to obtained the calibration curves, Figure A.21.

Table A. 23 – Measured standards and Calibration curve.

Concentration	Areas (mV.s)		Height (mV)	
($g.l^{-1}$)	P1	P2	P1	P2
0.0625	440.816	440.420	27.252	20.603
	426.126	433.927	27.007	20.405
0.125	859.361	859.972	54.519	41.191
	841.010	842.260	50.053	37.836
0.25	1835.045	1817.891	111.739	84.942
	1834.457	1829.631	113.708	86.049
0.4	2880.050	2868.954	178.920	135.328
	2655.189	*2616.189*	*173.224*	*129.370*

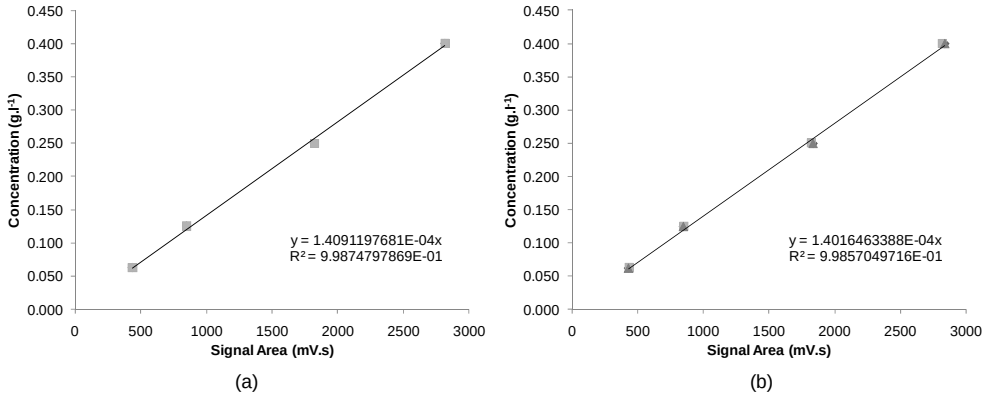

Figure A. 21 - Analytical calibration curves for the OSS guafeinesin experiments (a) more retained, (b) less retained enantiomers.

All experiments were carried at ambient temperature (approximately 25 °C).